European Commission

Optimisation of final plate flatness by set-up coordination for subsequent manufacturing process

(FinalPlateFlatness)



Research and Innovation

EUR 25852 EN

EUROPEAN COMMISSION
Directorate-General for Research and Innovation
Directorate G — Industrial Technologies
Unit G.5 — Research Fund for Coal and Steel

E-mail: rtd-steel-coal@ec.europa.eu
RTD-PUBLICATIONS@ec.europa.eu

Contact: RFCS Publications

European Commission
B-1049 Brussels

European Commission

Research Fund for Coal and Steel

Optimisation of final plate flatness by set-up coordination for subsequent manufacturing process

(FinalPlateFlatness)

U. Müller, H. Krambeer, A. Wolff
VDEh-Betriebsforschungsinstitut GmbH
Sohnstr. 65, 40237 Düsseldorf, Germany

A. Espina Viella
ArcelorMittal Espana SA
Residencia la Granda, 33418 Gozon, Asturias-Spain

A. D. Richardson
Tata Steel UK Limited, Swindon Technology Centre
Moorgate, Rotherham, South Yorkshire, S60 3AR, United Kingdom

J.-O. Perä
Swerea MEFOS
Box 812, SE-971 25 Luleå, Sweden

P. Luoto
Rautaruukki OYJ
P.O. Box 93, 92101 Raahe, Finland

W. Weber
Thyssenkrupp Steel Europe A.G.
Kaiser Wilhelm Strasse 100, 47166 Duisburg, Germany

Grant Agreement RFSR-CT-2005-00019
1 July 2005 to 30 June 2009

Final report

Directorate-General for Research and Innovation

2013

EUR 25852 EN

LEGAL NOTICE

Neither the European Commission nor any person acting on behalf of the Commission is responsible for the use which might be made of the following information.

The views expressed in this publication are the sole responsibility of the authors and do not necessarily reflect the views of the European Commission.

Europe Direct is a service to help you find answers to your questions about the European Union

Freephone number (*)**:**

00 800 6 7 8 9 10 11

(*) Certain mobile telephone operators do not allow access to 00 800 numbers or these calls may be billed.

More information on the European Union is available on the Internet (http://europa.eu).

Cataloguing data can be found at the end of this publication.

Luxembourg: Publications Office of the European Union, 2013

ISBN 978-92-79-28902-6
doi:10.2777/63845

© European Union, 2013
Reproduction is authorised provided the source is acknowledged.

Printed in Luxembourg

PRINTED ON WHITE CHLORINE-FREE PAPER

Table of content

		Page
1.	Final Summary	5
2.	Scientific and technical description of results	18
2.1	Objectives of the project	18
2.2	Comparison of initially planned activities and work accomplished.	18
2.3	Description of activities and discussion	19
WP 1:	Basic Specifications, Flatness Definition & Automatic Documentation for Through-Process Prediction and Optimization	20
Task 1.1:	Basic specifications	20
Task 1.2:	Study of current process/quality problems and definition of the relevant process-/plant variables that may influence the quality target flatness	28
Task 1.3:	Flatness characterisation	31
Task 1.4:	Definition of Systems Functionality	34
Task 1.5:	Development and implementation of an automated documentation of the flatness	36
WP 2	Analysis, Prediction and optimization of the rolling process	39
Task 2.1:	Provision of Data, Acquisition Systems and Measurement Campaigns	39
Task 2.2:	Correlation Analysis, Model Development & Validation for Prediction and Optimisation Purposes	42
Task 2.3	Rolling schedule optimisation	52
Task 2.4	Assessment of efficiency of the optimised scheduling algorithms	63
WP3:	Analysis, prediction and optimisation of the cooling and stacking process	64
Task 3.1:	Data Acquisition and Measurement Campaigns &	64
Task 3.2:	Characterisation of cooling (and stacking) conditions	64
Task 3.3:	Correlation analysis and Process Models for global prediction and optimisation use	75
Task 3.4:	Set-up optimisation to produce flatter plates	89
WP 4:	Analysis, Prediction and optimisation of levelling processes	91
Task 4.1:	Data acquisition of levelling process, component behaviour and flatness	91
Task 4.2:	Correlation analysis, first modelling approaches	98
Task 4.3:	First model validation and further extension & adaptation of models by Corus	120
Task 4.4:	Model based development of best set-up for levelling and final validation of models & set-up strategies	124
Task 4.5:	Levelling model and set-up rules for global line application	137
WP 5:	Global Through-process Flatness Predictor and Coordinated Optimiser	140
2.4	Conclusions	144
2.5	Exploitation and impact of the research results	144
	List of Tables and Figures	145

List of References 153

Appendices A1

Development, construction and installation in the plate mill of a new measuring system based on artificial vision for plate shape, flatness and turn up/down of the head end A1

Flatness measurement system, based upon an array of ultrasonic transducers A20

1. Final Summary

The core idea of this project is to combine the local optimisation of HPM process stages with a real global optimisation of the line processing by describing and tailoring main local efforts for appropriate use in a supervising coordinated prediction and optimisation system for the whole line.

The line processing comprises, **Fig. 1**, rolling, cooling, hot and cold levelling and stacking, whereas the process stages in each individual process route may differ, being product related.

The approach can be broken down into five main steps:

- Definition and establishing a flatness quality index, appropriate for modelling and optimisation use along the whole line and for each single process including additional measurement information connected with flatness.
- Determination of further correlations between processing data in terms of process signals, set-up values incoming plate data and flatness produced, developing, verifying or validating models NN based and /or physically based for prediction use in local set-up- / control systems.
- Model based development of approaches to propose optimised schedules and set-up values for the process stage in question.
- Derivation of models for local flatness prediction and local rules how to influence and optimise schedules and setup-values appropriate for use in a line through process predictor and an optimiser for subsequent process stages.
- Integration of all sub models including models of transfer conditions from process stage to process stage and establishment of a line through process flatness predictor and based on this a line set-up optimiser connecting local stage rules by a line optimisation strategy.

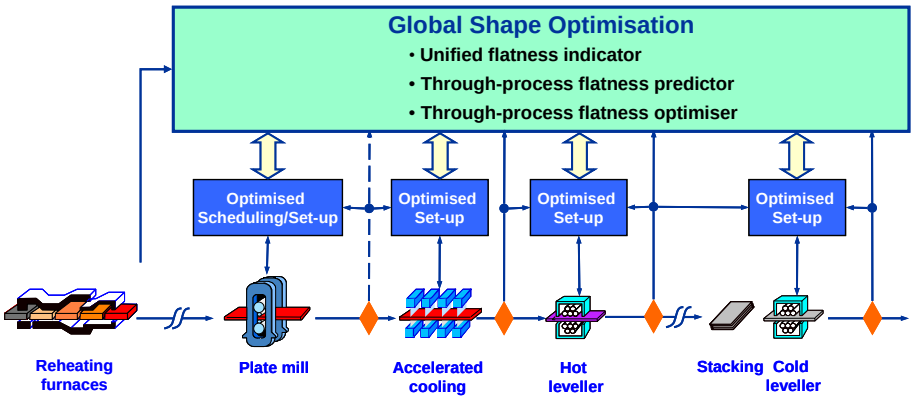


Fig. 1: Networked process stages and line coordinated approach with quality data input and the main objectives indicated

To gain the aim of the project the partners have to bring in their special expertise of the different stages of plate processing. The allocation of tasks is described in the “Technical Annex” in detail. The contribution of each partner is indicated in the chapter headlines.

- At the beginning all partners (WP 1, Leader: BFI) had to summarise the basics of plate processing and to design the system for automatic flatness documentation along the complete processing line.
- Next the optimisation of the rolling process is investigated (WP 2, Leader: AM Spain), with contributions of BFI, Corus and TKS.
- WP 3 (Leader: Rautaruukki, contributions: BFI, Corus, Mefos, TKS) is focused on the impact of plate cooling and stacking on flatness.
- The optimisation of the levelling processes is investigated in WP 4 (Leader: Corus, contributions: BFI, Mefos, Rautaruukki, TKS).

- Finally the "Global Through-process Flatness Predictor and Coordinated Optimiser" should have been developed (WP 5, Leader: BFI, contributions: AM Spain, Corus, Mefos, Rautaruukki, TKS).

WP 1: Basic Specifications, Flatness Definition & Automatic Documentation for Through-Process Prediction and Optimization

Task 1.1: Basic specifications

The concrete work objectives based on a study of each considered HPM have been specified, process/plant models available have been gathered, and the standard for data and information exchange as well as the hard- and software environments (standard software, programming languages, hardware platforms, communication standards, information flow, etc.) have been pointed out.

The rough structure of the systems to be developed under consideration of the existing data acquisition systems and process computers in each steel company have been specified.

At **ArcelorMittal Spain** a new measuring system has been developed and installed at the exit of the hot leveller to measure flatness, width, length, camber and ski effect under operating conditions. Techniques used for the development of the system are:

- Flatness and ski end effect are measured by triangulation,
- Width, camber and rectangularity are measured by conventional vision techniques.

Ruukki's plate mill is equipped with an automated flatness measurement system TopPlan®.

At the **HPM** of **TKS** two flatness measurement systems are installed:

- a TopPlan® system between the accelerated cooling device and the hot leveller (temporarily) and
- a laser-based flatness measurement system (supplier NOKRA) behind the cold leveller.

Corus relocated the prototype of a flatness measurement system, based upon an array of ultrasonic transducers, to the Light Shear Line to provide more flatness data for assessing the performance of roll pass schedules.

Task 1.2: Study of current process/quality problems and definition of the relevant process-/plant variables that may influence the quality target flatness

Flatness is manually / automatically inspected according to procedures described in the standard EN 10029. The level of rejects caused by poor flatness is significantly below 1% of production.

Task 1.3: Flatness characterisation

The final flatness is characterised according to EN 10029 classes N and S, that means, the deviations of the plate topography from a 1 or 2 m – ruler are determined. This method is mostly performed manually. A virtual ruler assessment according to DIN 10029 is carried out automatically at TKS. This kind of flatness characterisation covers no further information about the real topography of the plates.

A more sophisticated approach to characterise the flatness systematically is the decomposition of the measured height matrix into

- an "unwindable" part of the defect and
- a "non-unwindable" part of the defect.

This approach has been used to analyse the flatness by the TopPlan® system.

Task 1.4: Definition of Systems Functionality

Variations of each process conditions may contribute to essential variations to the flatness of the plates.

The general functionality of the system is schematically shown in **Fig. 2**. The main tasks of the system are:

- Monitoring / documentation of process / plant variables and
- Monitoring / documentation of quality features at each processing stage

as a basis to analyse the quality evolution and to develop a prediction model which will allow to optimise each processing step as well as to optimise the subsequent processing step to gain an optimal final flatness of the plates.

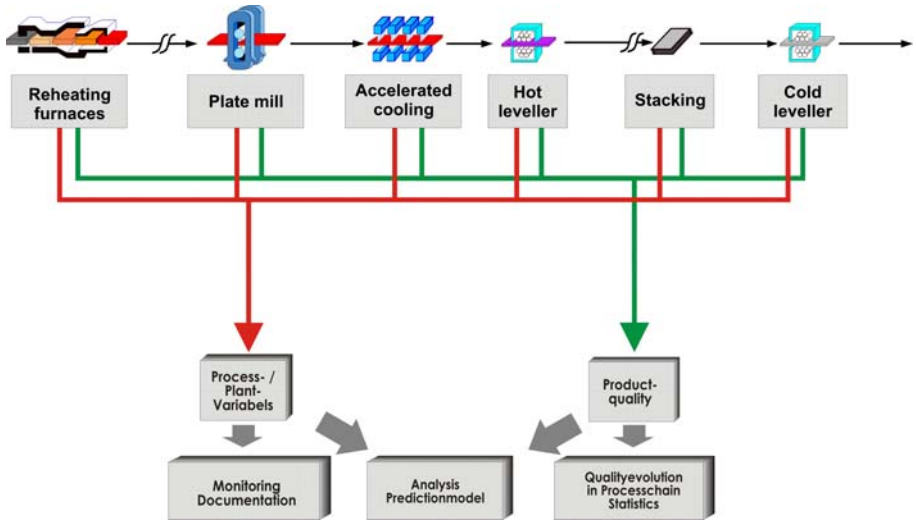


Fig. 2: Functionality of the system

Task 1.5: Development and implementation of an automated documentation of the flatness

Systems have been developed and implemented at **ArcelorMittal Spain** and **TKS**. The range of data over the whole production route includes:

- Signals from the milling shop,
- Process data of the rolling process,
- Data of the plate thickness,
- Data of the temperature profile,
- Process data of the accelerated cooling,
- Pyrometer temperatures,
- Process data of the hot levelling machine,
- Process and measuring data during heat treatment of the plates,
- D data of the ultrasonic testing facility,
- Process data of the side trimming shear,
- Data of the cross-cutting shear,
- Data of the final flatness behind the cold leveller,
- Process data of the cold leveller.

WP 2 Analysis, Prediction and optimization of the rolling process

Task 2.1: Provision of Data, Acquisition Systems and Measurement Campaigns

At the **HPM of ArcelorMittal Spain** a dataset captured from December 2006 until June 2007 was used to perform different analyses. The dataset size was initially of 89267 plates, which, after pre-processing and filtering data, gave a total of 8371 plates, with 40 attributes of each plate, suitable for the analyses.

At **HPM of TKS** a unique database that accumulates all information, available in local automation databases (furnace, rolling area, plate processing line, level 1 databases, etc.), during the complete fabrication has been developed and implemented.

As a first approach at **Scunthorpe Plate Mill** 1 m and 2 m straight edges were used together with a set of wedges, to systematically measure the wave heights of six plates as they rested on the mill floor. Thickness measurements were also taken using an ultrasonic gauge, at a number of points across the width, thus obtaining cross sectional profile of each plate.

Rolling information for specific plates had been downloaded from the process control computer. The downloads comprised speeds, rolling loads, screw positions, gauges, and temperatures among other things, on a pass by pass basis, for both the roughing and finishing stands.

Ruukki's plate mill is equipped with different mill process data systems:

- Oracle history database.

Task 2.2: Correlation Analysis, Model Development & Validation for Prediction and Optimisation Purposes

At the **HPM of ArcelorMittal Spain** different statistical techniques were applied to evaluate the characteristics of each attribute: analyses of distributions, quartile graphs and correlation analyses among attributes.

Corus examined the way the plates were rolled and assess the effectiveness of the reduction schedules by analysing the rolling load pattern over the final few passes. To confirm the flatness that was measured, Shohet and Townsend plate flatness calculations [5] were made.

At the **TKS Plate Mill** plate flatness calculations following the method of Shohet and Townsend [5] have been performed too. The calculations are based on the measured rolling forces and the stand deflection model developed. The calculation results are compared with the measured flatness at the entry of the hot leveller.

Measurements of the plate flatness confirm that the final plate has good flatness, when the calculated plate crown changes, during the last rolling passes are in the centre of the flatness dead band, according to Shohet and Townsend. A violation of the criterion of Shohet and Townsend in previous passes will be passed to the final pass.

The structure of the plate topography is often comparable to an unwindable defect characterised by wave length and amplitude. With respect to the rolling process this kind of defect is mainly influenced by

- the temperature gradient across the thickness of the plate,
- the speed behaviour of the mill (upper and lower work roll) and
- the pass-line.

Task 2.3: Rolling schedule optimisation

At the **HPM of ArcelorMittal Spain** the final stage of plate rolling could be performed following different strategies/theories. Within this project, the strategy, to maintain the relative plate crown (crown difference/thickness difference between two subsequent passes) constant, is studied.

The rolling model calculates the best pass sequence to obtain good plate flatness, additionally there is a profile adaptation introduced by the mill operator that is superimposed to the calculations. As an approach, to develop a statistical model for the estimation of the final flatness, the interventions made

by the operators were used. Statistical analyses of the interventions during several rolling campaign were performed. The correlations among different variables related to the rolls, like

- grinded roll crowns,
- tonnage rolled,
- length rolled,
- dimensions of the plates,
- working time of the rolls, etc.

have been evaluated. Amongst others these analyses showed that the interventions by the operators do not follow the corrections made by the process model. To perform a further analysis of these correlations; plates were sorted according the number of passes in different groups. This leads to 7 groups where the final rolling phase starts at the 5^{th} to the 12^{th} pass. For each plate of these groups the differences between the calculated and measured rolling forces for each pass was analyzed. As result of these analyses it can be concluded that the variable CORRFLAST influences the shape of the curves which represent the measured and calculated rolling force for the sequence of passes.

As a next step the forces distributions for similar plates, rolled with same pair of work rolls but with different values of CORRFLAST were evaluated. Main conclusions obtained were that the forces at each pass are influenced by the variable CORRFLAST, by the roll pair and the consecutive number in the roll campaign in which the plate is rolled, which is function of the roll wear and equivalent roll crown.

Based on these studies, it was found that each team of mill operators uses their own criteria of interventions, so the performance of the rolling mill is highly depending on the human factor.

At **Scunthorpe Plate Mill** the application Scheduler [7] was used to generate recommended rolling schedules for plates for which flatness measurements had been obtained. The simulations covered processing in the finishing stand, starting from the same initial plate dimensions and temperature as recorded during rolling.

Pass schedules recorded for flat plates were close to those recommended by Scheduler and the Shohet and Townsend calculations indicated good flatness for those plates.

In some cases the recorded pass sequence for the plates differed significantly from that predicted by Scheduler. This resulted in the full centre flatness defect that was measured. In contrast, the schedule calculated by Scheduler is predicted to generate a flat plate. Departure from the standard straight FLL was most likely caused by on-line corrections due to load and/or gauge errors, thus necessitating the re-computation of the schedule for the remaining passes. A sudden steepening of the FLL at the end of the schedule also led to measured (and predicted) centre buckle defects.

In another case, the recorded schedule bore no resemblance to the standard pattern, with all 13 passes rolled at a near constant load. The RD&T off-line model did generate a predicted schedule with a suitable FLL, using 17 rather than 13 passes. The consistently high load in the final passes gave rise to the edge wave defects that were measured. In contrast, the schedule calculated by “Scheduler” is predicted to generate a flat plate. As before, departure from the standard straight FLL was most likely caused by on-line corrections due to load and/or gauge errors. Strategies for optimum recalculation of schedules part way through rolling merit further investigation.

At the **TKS Plate Mill** discussions took place on how to apply the results in the mill control. BFI has proposed two measures

- the operators should have an display where on-line calculations of the plate crown change are shown that they can assess the consequences of their manual interventions with regard to the flatness,
- the results on-line calculations of the plate crown change in combination with the measured plate topography should be added to the database to be taken as basis of schedule optimizations.

Task 2.4: Assessment of efficiency of the optimised scheduling algorithms

No validation of the modified schedules has been performed. However, the off-line Scheduler model has been used to generate recommended schedules for good shape. It was noted that when the recorded schedules were close to those recommended, good flatness was measured on the plates. It was found that measured plate flatness could be successfully predicted using the off-line model, when simulating the actual recorded schedules. The off-line model therefore provides the basis for testing revised strategies for optimum recalculation of schedules partway through rolling. This is the subject of ongoing discussions with process control personnel.

WP3: Analysis, prediction and optimisation of the cooling and stacking process

Task 3.1: Data Acquisition and Measurement Campaigns &

Task 3.2: Characterisation of cooling (and stacking) conditions

Data acquisition at Scunthorpe Plate Mill

The behaviour of hot rolled plates on different types of cooling bank has been observed to determine what the effect of upstream processes has on plate flatness during cooling and what the shape of plates will be after cooling as a result. Plates were observed on both the Light Shear Line (LSL) cooling bank, usually used for plates of 20 mm gauge and lower, and the Heavy Shear Line (HSL) cooling banks, generally used for plates of 15 mm and thicker.

Plates observed on the LSL cooling banks with substantial periodic long-range shape were of the thinner gauges (<12 mm). The shape was generally of the same form as in the plate when it arrived at the hot leveller but reduced in magnitude. Centre buckle and edge wave were sometimes observed but not for consecutive plates. Thicker plates and those arriving at the hot leveller with only minor shape defects tended to exit the hot leveller in a flat condition.

Development of even minor long-range shape was not observed on any hot flat plates properly laid on the LSL cooling bank. Any long-range shape observed in plates was always present when the plate exited the hot leveller.

Plate distortion observed on the HSL cooling banks was usually transient and not a result of asymmetric cooling, but caused by a lack of support of a substantial length of the plate when it is hot (>400 °C). This distortion was seen to persist only in cases where the plate was stationary for some time and had cooled to temperatures below 300 °C in that location.

Data acquisition at TKS Plate Mill

The cooling behaviour of heavy plates in a stack is supposed to be one reason – among others – to influence the final flatness of the plates. Sometimes, stacking of the plates is inevitable due to necessary hydrogen effusion or too high temperatures for further processing.

In order to assess the impact of cooling and stacking order on the flatness of heavy plates a stack of plates was piled up under defined conditions in this experiment. Thermocouples were distributed inside the stack to get insight into the temperature distribution, since large temperature gradients might induce stress into the material and consequently lead to uneven plates.

Data acquisition at Ruukki

A thermal camera was installed after mill before accelerated cooling unit. Some tests were done in accelerated cooling device at Ruukki Heavy Plate Mill. The effect of tuning of the plate head-end cooling has been analysed. Fine tuning of new high pressure cooling equipment was carried out. At the beginning of the project it was estimated that rejection rate of high strength plates would be on the same level as flame straightening ratio for acc plates. The result has been much better. Flatness rejections (which were the ultimate fear at the beginning) have been in the level of about 1-3 % for plates depending on thickness and quality. Most difficult plates are thin and hard plates.

Task 3.3: Correlation analysis and Process Models for global prediction and optimisation use

Development of a Microsoft Excel based user interface by MEFOS

Within this project a Microsoft Excel based user interface named Plate-RQ has been developed. It is used for the pre- and post processing of data in connection with temperature simulation in the temperature calculation program Steeltemp [10]. The main application is to calculate temperature development in plate rolling and quenching. The temperature is calculated from withdrawal of slab from furnace, during rolling and during quenching after rolling. Primary descaling and secondary descaling before specified passes can be included in the calculations.

Model of buckling of heavy plates under the influence of cooling and stacking by BFI

A model and the software to simulate the phenomenon of buckling of plates after the stacking and during the cooling has been developed by BFI.

Two different cases have been simulated. For both cases air cooling of the stack has been considered.

- In the first cases natural convection with dry air is assumed,
- In the second case forced convection, with laminar flow is considered.

The results of the temperature field calculations show:

- the vertical asymmetry of the temperature field is due to the bad heat transfer caused by the ground floor (concrete) on which the stack lies and
- the increase of the temperature gradient close to the edges of the stack, which is indicated by the smaller distances between the isothermal lines.
- The upper plates on the stack are mostly threatened of the buckling phenomenon.

Model of a steel plate quenching by MEFOS

Levelling of plate is frequently applied in connection with direct quenching after rolling. A complex microstructure state is developed in the plate and the mean temperature of the plate is around 600 °C. This makes it to a challenge to achieve the desired final plate flatness. In order to get a general view of the of the deformation-, stress- and microstructure development, modelling was performed in the program Sysweld.

Task 3.4: Set-up optimisation to produce flatter plates

Scunthorpe Light shear line

There did not appear to be plate distortion problems directly associated with cooling on this type of cooling bank and it is concluded therefore that cooling was sufficiently symmetrical in combination with gravity effects to maintain rolled-in plate flatness. For the thinner gauge range of plates processed on this cooling bank, provided that they are rolled flat in the mill and are hot (>700 °C) a reasonably flat bank surface and gravity effects will ensure maintenance of flatness during cooling and the accrued strength at temperatures below 400 °C is sufficient to resist subsequent mechanical damage or thermal distortion.

Main problem on this cooling bank is rolled-in shape if the plate is cold (<600°C) prior to entry to the hot leveller. The origin of any long-range shape in plates on this bank was the finishing mill and this shape could be improved by the hot leveller but not completely removed. Poor shape was more evident in thinner colder plates generally most of this poor long-range shape was retained through the hot levelling process. The hot levellers appeared to be much less effective for thinner colder plates, probably as a result of higher strength of these plates and the limitations of the machine.

Generally push-dogs trapped under plates above 500°C were seen to cause permanent local distortion if allowed to cool further under the influence of these misaligned push-dogs; thin hot plates might be susceptible to long-range permanent distortion by the dogs lying underneath the bulk of the plates.

Dummy passes through the hot leveller would reduce the temperature of plates being pushed onto the banks and make them much less susceptible to permanent distortion and scratching by misalignment and sticking of push-dogs.

The probability of distortion and mechanical damage of plates beyond the halfway point under normal circumstances is very low because the plates are generally below 250°C and have achieved approximately 90% of their cold strength.

Scunthorpe Heavy shear line

No distortion resulting directly from cooling asymmetry was observed. All plate distortion that was observed could be attributed to mishandling or poor support of the plates whilst hot.

Permanent distortion of plate on cooling bank nos. 2, 3, and 4 is often a result of local insufficient even support when the plate is hot, and prolonged residence in these locations until the plate bulk temperature is relatively low (400 °C).

Sometimes plant localised conditions such as a slewed plate orientation between different adjacent conveying systems, cause short range plate bending when the plate is hot and weak which persists if the plate is allowed to cool in this condition.

Distortion observed at the gearbox cover between cooling banks nos. 3 and 4 is a result of insufficient support of that part of the plate whilst resident over the gearbox cover.

Plate stacking

Buckling can be avoided by influencing the temperature field e.g. the cooling behaviour of the stack by introducing the following measures:

- Reducing the air flow speed down to zero around the heavy plate stack,
  - by closing the doors in work hall or
  - putting wind shields around the stack
- Choosing the height c of heavy plate stock, so that 2c> b, whereas b is the width of the plates. In this case the asymmetry of the temperature field in vertical (height) direction will not cause buckling
- Covering the top surface of the heavy plate stack with an insulating mat to reduce the thermal gradient in the stack. The insulating mat should have the following properties

  $$\kappa_I / d_I = \kappa_B / d_B,$$

  where

  κ_I = heat conductivity of the insulting mat,

  κ_B = heat conductivity of the ground floor plate (e.g. concrete),

  dI = thickness of insulting mat and

  d = thickness of the ground floor plate.

WP 4: Analysis, Prediction and optimisation of levelling processes

Task 4.1: Data acquisition of levelling process, component behaviour and flatness

Trials on a pilot roller leveller at Corus Teesside Technology Centre

A series of trials have been conducted on a pilot roller leveller at Corus Teesside Technology Centre. The design of the pilot machine permits direct observation of the path of the plate between the rolls, allowing measurement of plate curvature and location of plate/roll contact points in each bending triangle. Position transducers indicate the deflections of the rolls under load giving the 'real' penetration settings imposed on the plate (the difference between roll penetrations in the loaded and unloaded conditions has a significant effect on outgoing plate curvature).

Deflection measurements in the hot plate leveller at Ruukki

The deflection of the frames in a hot leveller in the plate mill at Ruukki has been measured. Plates in width up to 3500 mm and thickness between 5 and 150 mm are levelled. During the trials the deflection while levelling plates of different kinds with variation in temperature, width and thickness were measured by the use of a laser triangulation system.

Hot levelling trials at MEFOS

A closer investigation of hot-levelling trials performed at the pilot-plant leveller at MEFOS has previously been done [11]. The trials were performed to study the influence of different settings on plate curvature. Straight bars were run through a flattener using two different types of settings; a one over two straightening triangle (3 rolls) and a two over three rolls set-up (5 rolls).

Pilot plant hot bending test and model validation

In order to improve the modelling of the hot levelling process, hot bending trials have been performed in the pilot-plant forging press at MEFOS [11]. Both single bending and double bending were included in the trials. In this way a reversal strain is applied, similar to regular hot levelling. The trial setup is based on the design of the hot plate leveller at Ruukki.

Task 4.2: Correlation analysis, first modelling approaches

Develop a one-dimensional levelling model capable of application to most roller leveller configurations and correlate with measured data at Corus Teesside Technology Centre

A one-dimensional levelling model, developed under previous ECSC-funded projects [14], [15], has been further developed/extended to allow simulation of operating conditions on most roller levellers used for plate and strip. The original model approximated the levelling process to a sequence of 3-point bends between evenly spaced rolls, using classical beam theory to calculate the induced strain-distribution through the strip, and hence the evolving elastic/plastic stress-distribution. It provided a useful guide to process-sensitivities and has been used successfully to identify causes of poor leveller performance (e.g. variable roll gap across the width of the plate).

The model developments / extensions concern:

- Calculation of plate path through leveller,
- Calculation of plate stresses, strains and exit bow,
- Calculation of loads and torques,
- Transverse Stresses and Crossbow,
- Consideration of Exit Breast Roll and
- Effect of Plastic Deformation on Plate Path.

Basic levelling simulations using FE-modelling by MEFOS

- Material model

Each passage over three or five rolls corresponds to a “repeated bending load case” which will generate a varying stress state over the thickness. This is a complex load case where material is subjected to almost cyclic loading and the hardening model has an impact on the final result.

- FE-simulations on 3-roll bending

The FE-analysis was done using 2D-modelling. In the initial set-up a flat bar was inserted between the upper- and the two lower levelling rolls. Then the second roll was lifted and the levelling process started. Hence, the results from the very front-end of the bar are irrelevant. The results from the simulations show good agreement with the practical trials regarding achieved geometrical curvature.

- FE-simulations on 5-roll bending

The 5-roll bending trials were analyzed. Differing settings on the second and third leveller rolls were investigated.

- Detailed investigation of stress and strain in industrial levelling

In order to achieve correct settings of industrial hot plate levellers, modelling in both 2D and 3D have been performed. The efficiency of the levelling can be evaluated by studying the strain distribution at different positions over the strip width as well as at different points over the thickness.

- Influence of varying leveller setting

The conditions in the plate after passing the leveller with different settings of cradle and gap have been evaluated.

- Varying the cradle setting

A lower value for the cradle setting will increase the amount of bending in each passage resulting in larger strains in the plate. A reduced cradle value with 2mm results in a doubling of the plastic strain on the plate surface.

- Strain history for single elements

The elongation value reached in levelling is connected to the strain level reached at each bend. For a comparison of different leveller settings the maximum strain reached in each bend for the top and bottom element was plotted vs. the time.

- Varying the gap setting

Gap setting variations have a strong impact on exit curvature. Already a gap decrease of 1mm changes the sign of the curvature.

- Comparison of shape after levelling using isotropic and kinematic hardening

An isotropic hardening and a mixed model based on 50% isotropic and 50% kinematic hardening were utilised. In these calculations the impact of isotropic hardening and the mixed hardening model gives only small differences in the shape after levelling.

- Varying the E-modulus

The results show that a higher E-module gives larger strains.

- Influence of density in the FE-simulations

FE-codes based on explicit time integration has shown to be a good method for solving complex forming simulations where high levels of deformations are present and a large number of elements are used. In these calculations the density was increased 100 times. The results were compared with calculations made using 10 times the density and showed that the influence of the change in density is very small.

Task 4.3: First model validation and further extension & adaptation of models by Corus

Verification of Plate Path/Curvature

To test the validity of the assumptions used within the '$1^{st}/2^{nd}$ order' modelling approaches outlined above, the predicted plate path has been compared with measured data generated during the trials performed.

The results indicate that the 1^{st} order analytical model is capable of accurately predicting the plate trajectory in the initial and final 2 bending triangles, but appears to underestimate the deviation of the contact points from the dead-centre position in the middle triangles. The 1^{st} order analytical model's predictions of plate curvature in each triangle show close agreement with experimental results and appear to be as accurate as those obtained using the FE approach. Application of the 2^{nd} order model did not appear to give any improvement in the accuracy of curvature/path predictions. The level of curvature generated at each bending triangle is the critical factor governing the evolving stress-condition and exit bow of the plate.

Verification of Exit Bow Predictions

The analytical models were used to simulate the levelling of all the plate samples processed in the trials, incorporating the 'real' penetration-settings recorded in the loaded condition, the measured sample gauge/length, and the appropriate yield strength data were used.

Results indicate good overall agreement between exit longbow predicted by the 1st order model and measured data, with correlation coefficients of 88% and 80% obtained for parallel nest and tilting nest leveller configurations respectively. Comparison of measurements and 2nd order model predictions gives correlation coefficients of 72% and 82% for the two leveller configurations. In general, the 1st/2nd order models appear to slightly under/overestimate the sensitivity of exit bow to product/processing conditions.

Task 4.4: Model based development of best set-up for levelling and final validation of models & set-up strategies

Assessment of the effects of variations in incoming plate condition and settings applied to leveller rolls by Corus

An assessment of the effects of variations in incoming plate condition and settings applied to leveller rolls has been undertaken, using the analytical models developed.

Roller leveller work roll configuration and settings strategy

For this study, the strategy has been to apply settings for the model runs that ensure that the plastic strain imposed by work roll #8 is more than zero so that all of the seven work roll bending triangles apply work to the plate and act to affect its unloaded curvature.

The model was run for plate of nominal gauges covering the majority of the range commonly produced in Scunthorpe Heavy Plate Mill, and for nominal yield strengths 300 N/mm^2 and 500 N/mm^2 to achieve a nominal plasticity of approximately 80% (α=8) i.e. an overstretch of 5 in the plate in process; the exit gap to achieve close to zero exit curvature (< 0.2 mm/m plate bow) was determined by iteration in the spreadsheet with the condition that the plasticity imposed at work roll 8 must be greater than zero. These base cases were then used to test the effect of changes in gauge and yield on the output bow of the plate for these base case settings. Variations in gauge up to ±1 mm and in yield strength up to ±100 N/mm^2 were tested. Arbitrarily the acceptable output plate bow was set at ±3.0 mm/m.

Pattern of plate plasticity through the roller leveller

To set the work roll gaps in a roller leveller to achieve a flat output plate the minimum information required is the plate gauge and its yield strength and some model or strategy to calculate settings appropriate for that roller leveller. The most common strategy is to set the gap in the first work roll triangle to achieve a plasticity, f in excess of 60% so that the majority of the thickness of the plate has been plastically deformed and to apply a sufficient level of strain sufficient to override inherent plate shape or curvature.

The effect of inherent plate bow on the roller levelling process

The effect of pre-existing plate bow on the output plate bow was tested. The effect was very small and insignificant especially for the settings employing higher imposed plasticity's, showing that the roller levelling process is very robust if the machine is correctly set for the processed plate gauge and yield strength.

The effect of deviations from the specified plate gauge on roller levelling performance

Although the effect of plasticity level is small especially at positive departures from base case gauge the output plate bow is very sensitive to departures from nominal gauge for all the levels of plasticity imposed at work roll #2. The effect appears worse for positive departures from the base case where the output plate bow progressively increases, but at negative departures from base case gauge the effect is smaller and oscillatory with gauge change. A deviation from the specified plate gauge of only 0.1 mm can increase the output plate bow beyond the acceptable range (±3 mm/m).

The effect of deviations from the specified plate yield strength on roller levelling performance

The change in output bow with deviation from the nominal plate yield strength followed a steady slope of constant gradient and no oscillatory pattern of behaviour was observed within the ranges of yield strength examined.

The sensitivity of output bow to last triangle setting

For a tilting nest leveller the model results show that for a given first work gap setting (work roll #2) the output plate bow is extremely sensitive to the setting of the gap in the last work roll triangle (work roll #8).

Roller levellers with independent adjustment of individual work roll heights

If a roller leveller is configured so that the upper work roll heights can be independently adjusted, then this extra degree of freedom makes it possible to rapidly decrease the bending curvatures and plasticity levels imposed in the plate as it travels towards the exit of the leveller. Thus very high levels of plastic strain necessary to override curvature or shape inherent from upstream processing can be applied in the early work roll bending triangles, whilst rapidly reducing bending curvature and plastic strain to low levels within only a few downstream work roll triangles.

Assessment of the effects of variations in incoming plate condition and settings applied to leveller rolls by Ruukki

At **Ruukki**, plates are levelled in hot conditions as previously described in a 5 over 6 leveller. Different dimensions and settings of the leveller have been investigated in industrial trials and using 3D modelling. The incoming and outgoing flatness error has been manually evaluated during the trials. Two types of defects have been studied, the first one with edge waviness and the second one with crossbow.

3D modelling of the levelling process by MEFOS

So far the levelling process has been described with 2D models assuming plain strain condition (No straining across the plate). However the deformation state is 3 dimensional and for achieving reliable results all dimensions have to be considered.

Furthermore the previous presented models had no initial defects. In the 3D models those initial defects have been taken into consideration and the models are no longer perfectly flat.

Result and discussion

The flatness measure I-unit for the simulations has been evaluated. All simulations resulted in very low I-unit values and hence the levelled plates can be considered as flat.

Task 4.5: Levelling model and set-up rules for global line application

The hot leveller at the **TKS HPM** is equipped for manual and automatic operation. Respectively, the adjustments of the leveller can be prompted by the operator or are performed by a levelling model, which requires the following input data:

- Strength of the material,
- Measured temperatures at entry and exit side of the leveller,
- Actual thickness,
- Plate width and
- Information about flatness, visually assessed by the operator.

The visual assessment of the flatness by the operator has an important significance within the above described operating procedure. Therefore the actuations of the operator were compared with the measured flatness. The comparison clarify that the actual flatness situation is not evaluated correctly by the operators which consequently leads to a non optimal adjustment of the levelling plant.

These investigations demonstrate that an installation of a flatness measuring system on levelling plants is required, in order to perform an optimal leveller adjustment carried out by the operators or by an automatic control system based on the measured flatness profile [26], [27].

WP 5: Global Through-process Flatness Predictor and Coordinated Optimiser

To predict the final flatness of a plate one has to know on which process route the plate will be passed through the different manufacturing processes. An analysis of the process route frequency has been made based on the data stored in the plant database for the **TKS HPM**.

The evaluations show that in total the peak to peak height value on an average is diminished from 4 mm to 2 mm for the unwindable part of flatness defects as well as for the non unwindable part of flatness defects. The reduction of flatness defects is nearly independent from the considered process route.

Furthermore it has to be confirmed that flatness defects are not passed through the processing chain. This is the main reason which makes it impossible to create global flatness predictions and coordinated optimisations. A fundamental prerequisite for global flatness control is that various inputs (e,g. changes of rolling process) would have a strongly correlated impact on final flatness. However, this correlations could not been identified on the basis of the comprehensive process data analysis.

Therefore the development and implementation of the “Global Through-process Flatness Predictor and Coordinated Optimiser” is obsolete by physical reasons.

Conclusions

- The development and implementation of the “Global Through-process Flatness Predictor and Coordinated Optimiser” is obsolete by physical reasons.
- Strategies to locally optimise
  - the rolling schedule,
  - the hot and cold levelling processes,
  - the cooling and stacking process inclusive quenching

  have been investigated.

2. Scientific and technical description of results

2.1 Objectives of the project

The key objectives of the project are

- development of a unified through process flatness characterisation appropriate for all process stages and all coordinated process optimisation purposes as well as for future customer demands on final flatness,
- data collection and performance of correlation analysis of flatness - process signals, - product data, - setup values of all production plants in the production chain, from rolling to levelling (model building, taking also physically based models into account),
- development, enhancement and extension of process models to predict the flatness produced at each processing stage in dependence of plate data, entry flatness, main process characteristics and set-up values, taking the above results and physically based analytical and FEM models into account
- development of best set-up strategies for each single processing stage based on the model and line production strategies
- tailoring of all single process models and single set-up strategies to through process line purposes in terms of execution-time-optimised sub-models and set-up rules appropriate to be part of an through process flatness predictor over the whole processing chain and an line set-up optimiser of the subsequent stages
- clear specification of the transfer parameters from processing stage to processing stage comprising all intermediate processes like stacking / rucking and integration of all sub-models and transfer descriptions into a global line model
- development of a line through process flatness predictor based on the global model to accompany the plate from process stage to process stage, giving the platform for set-up optimisation and process optimisation of the subsequent production steps
- development of a line set-up optimiser based on the predictor and the set-up rules developed for each stage and taking into account the line production strategy, that will propose best values for subsequent process stages during production
- industrial implementation and evaluation of the single process stage solutions and the line predictor and optimiser

2.2 Comparison of initially planned activities and work accomplished.

It has to be confirmed that flatness defects are not passed through the processing chain. This is the main reason which makes it impossible to create global flatness predictions and coordinated optimisations. A fundamental prerequisite for global flatness predictions is that various inputs (e,g. changes of rolling process) would have an strongly correlated impact on final flatness. However, this correlations could not been identified on the basis of the comprehensive process data analysis.

Therefore the development and implementation of the “Global Through-process Flatness Predictor and Coordinated Optimiser” is obsolete by physical reasons.

Nevertheless process optimisations are possible with respect to avoid especially disturbances caused by flatness defects. Using the installed flatness measurement optimisations of the rolling schedule (off-line) as well as of the hot levelling process is possible.

2.3 Description of activities and discussion

WP 1: Basic Specifications, Flatness Definition & Automatic Documentation for Through-Process Prediction and Optimization

Task 1.1: Basic specifications

Plate mill layout of ArcelorMittal Spain

The layout of the HPM of ArcelorMittal Spain at its Gijon factory is given in **Fig. 3**.

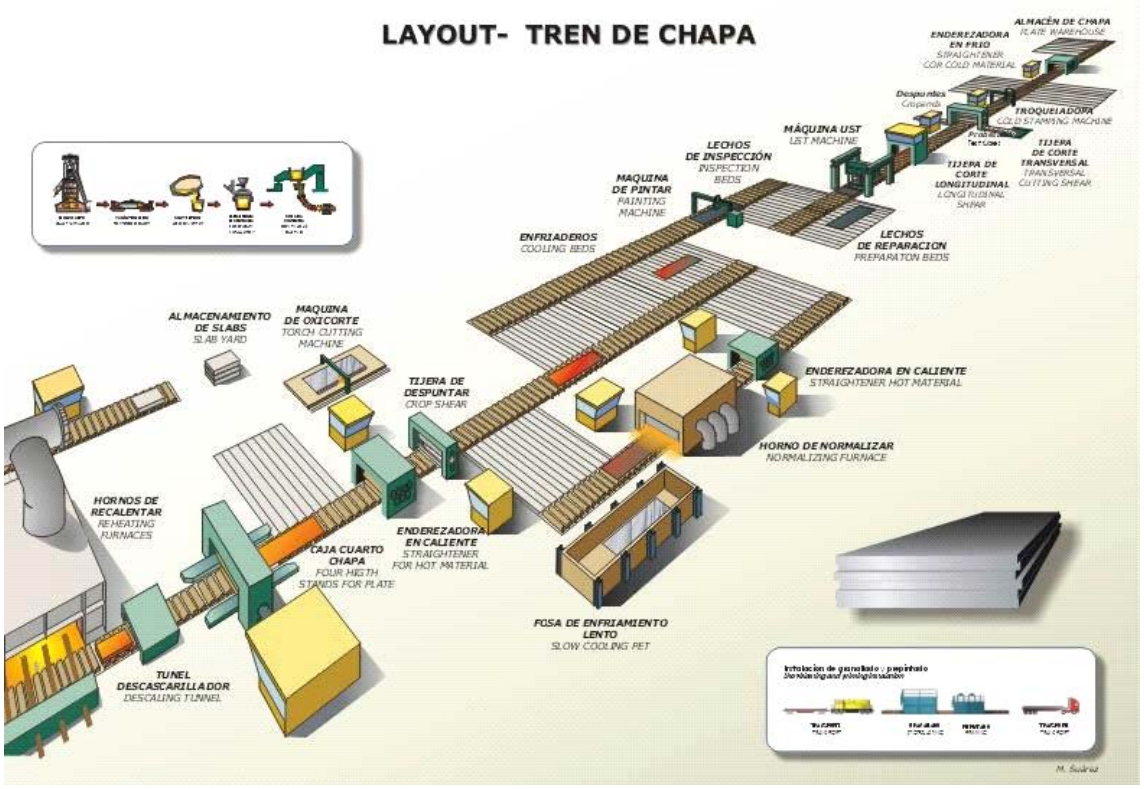


Fig. 3: ArcelorMittal's Spain HPM layout

The relevant characteristics of the rolling stand are:

- Main drive: twin drive, DC motors, 5,5 MW per motor,
- Motor speed 0/60/120 rpm,
- Maximum rolling force rated 6600 t , used 6000 t,
- Work rolls:
  - roll body: 3600 mm, roll diameter: 850 – 950 mm,
- Back up rolls:
  - roll body: 3600 mm, roll diameter: 1750 – 1900 mm.

The rolling stand is equipped with hydraulic cylinders for gap control and hydraulic automatic gage control. The mill does not have any specific equipment for profile or flatness control like roll bending. Regarding instrumentation, the mill has several pyrometers and a radio-isotope thickness gage that measures thickness in three points across the plate width and permits a rough estimate of the profile.

Plate mill layout of Ruukki

Fig. 4 and **Fig. 5** show the layout of Ruukki's plate mill.

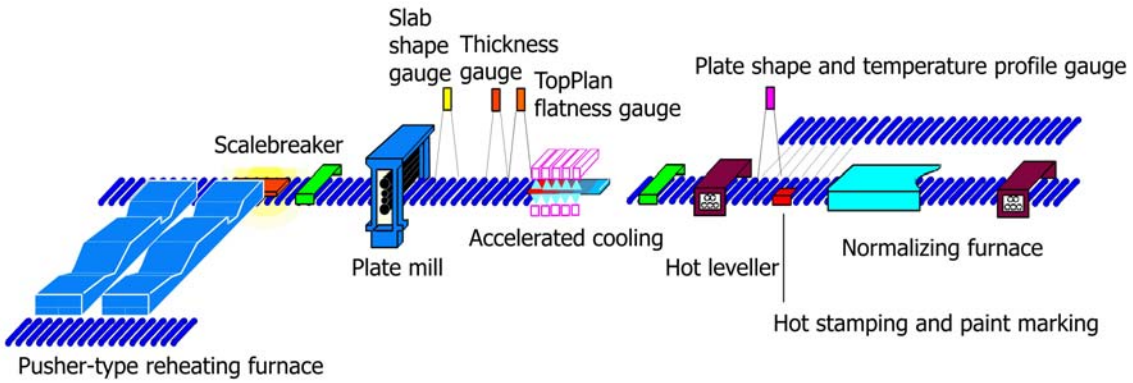


Fig. 4: Layout of the plate rolling plant, RUUKKI

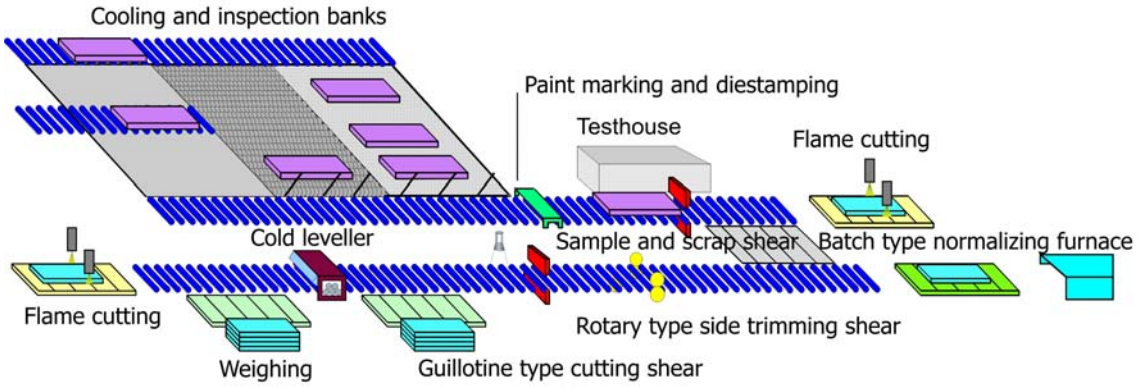


Fig. 5: Layout of the cooling and cutting, RUUKKI

The relevant characteristics of the rolling stand are:

- Main drive: twin drive, DC motors, 4,55 MW per motor,
- Motor speed 0/100 rpm,
- Maximum rolling force 53 MN,
- Work rolls:
  - roll body: 3600 mm, roll diameter: 945 – 1045 mm,
- Back up rolls:
  - roll body: 3600 mm, roll diameter: 1675 – 1825 mm.

The rolling stand is equipped with hydraulic automatic gage control (bottom) and work roll bending. Regarding instrumentation, the mill has several pyrometers and a thickness gage.

Plate mill layout of TKS

The layout of the HPM of TKS is shown in **Fig. 6**.

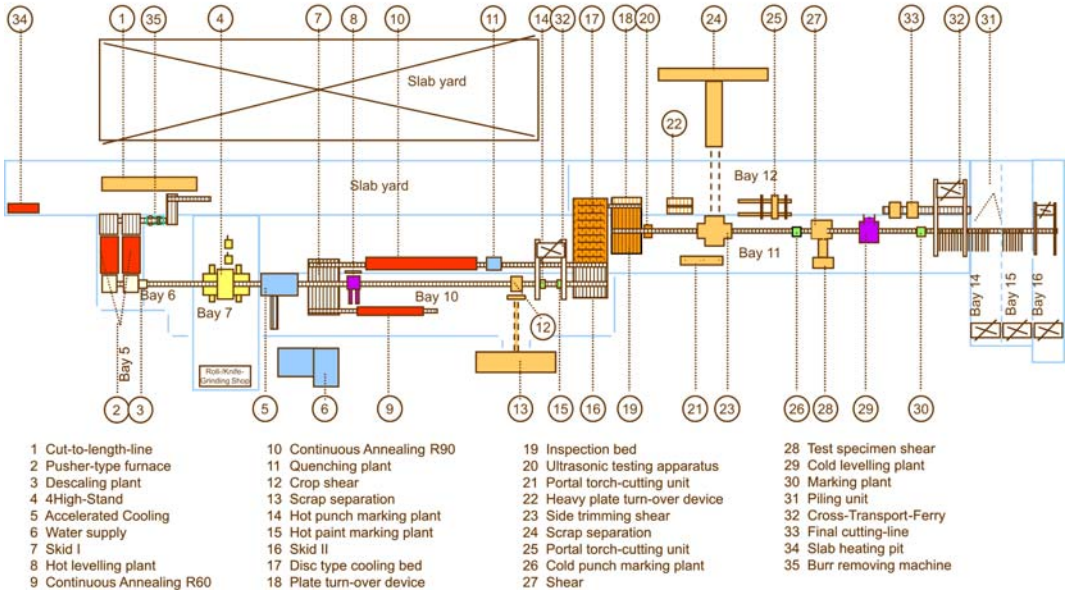


Fig. 6: HPM layout of TKS

The relevant characteristics of the rolling stand are:

- Main drive: twin drive, DC motors, 11,75 MW per motor,
- Motor speed 0/90 rpm,
- Maximum rolling force 7850 t , used 6500 t,
- Work rolls:
  - roll body: 3900 mm, roll diameter: 900 – 1000 mm,
- Back up rolls:
  - roll body: 3600 mm, roll diameter: 1950 – 2100 mm.

The rolling stand is equipped with hydraulic cylinders for gap control and hydraulic automatic gage control and work roll bending to achieve very close thickness tolerances and good flatness. Regarding instrumentation, the mill has several pyrometers and a radio-isotope thickness gage that measures thickness along the center line of the plate.

Plate mill layout of Corus Scunthorpe

The layout of the HPM of Corus Scunthorpe is shown in **Fig. 7**.

The relevant characteristics of the Roughing Mill are (1HP = 745.7 Watts):

- Main drive: twin drive, DC motors, 3000 HP per motor,
- Motor speed 0/40/80 rpm,
- Maximum rolling force ~27.5 MN,

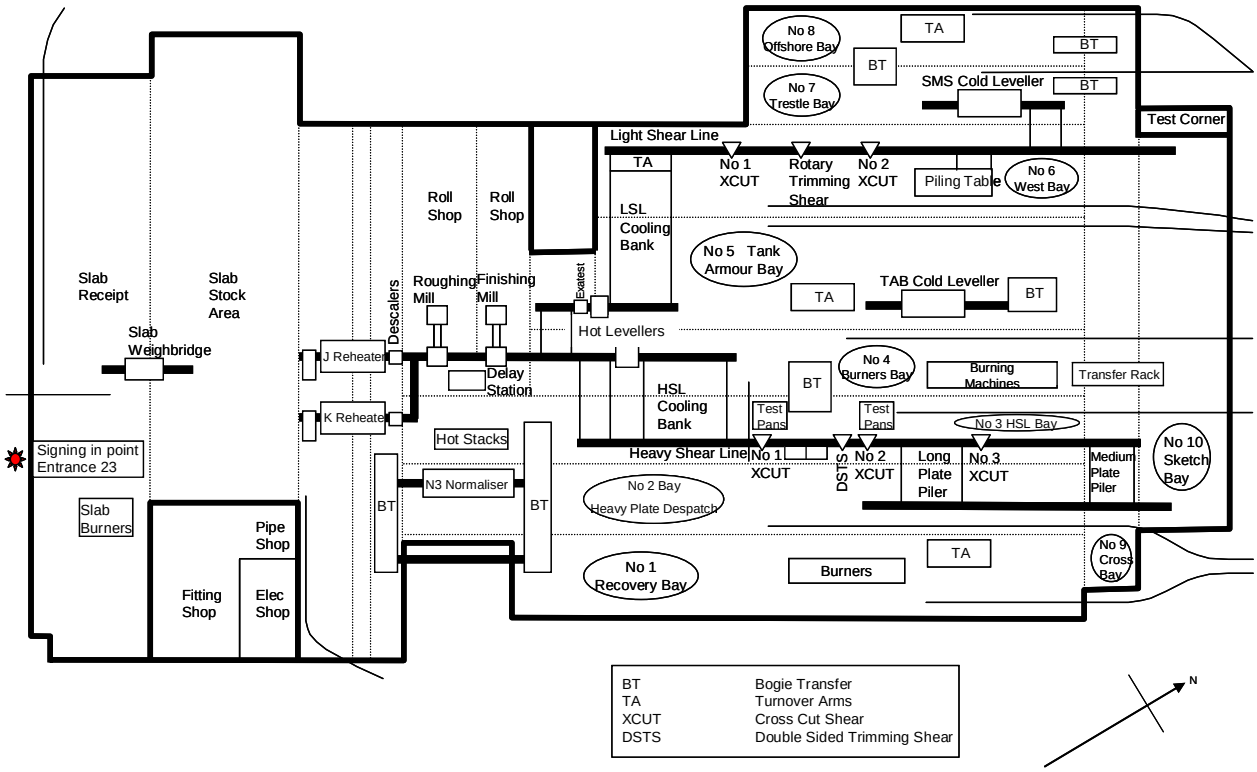


Fig. 7: HPM layout of Corus Scunthorpe

The relevant characteristics of the Finishing Mill are (1HP = 745.7 Watts):

- Main drive: twin drive, DC motors, 4000 HP per motor,
- Motor speed 0/40/80/100 rpm,
- Maximum rolling force ~38 MN,

Database & Flatness measurement system at the HPM of ArcelorMittal Spain

At the start of the project the HPM of ArcelorMittal Spain in its Gijon facilities did not have neither a unique database that accumulates all information, available in local automation databases (furnace, rolling area, plate processing line, level 1 databases, etc.), during the complete fabrication of plates nor an automated flatness measurement system. Hence the development and implementation of a new database and a flatness measurement system have been the initial tasks of the project.

A new measuring system has been developed and installed at the exit of the hot leveller to measure flatness, width, length, camber and ski effect under operating conditions, **Fig. 8**.

A detailed description of the development is given in the appendix.

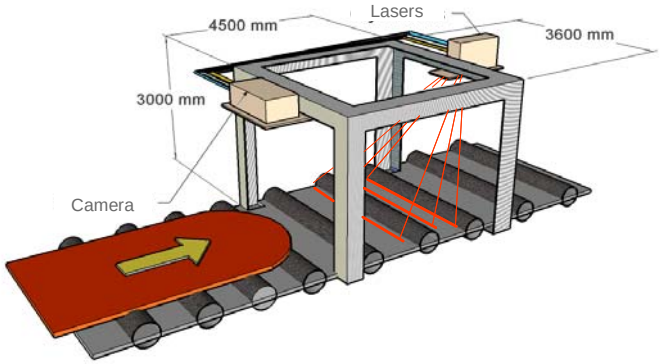


Fig. 8: Schematic installation of the measuring system at the ArcelorMittal Spain HPM

Techniques foreseen for the development of the system are:

- Flatness and ski end effect are measured by triangulation,
- Width, camber and rectangularity are measured by conventional vision techniques.

Database & Flatness measurement system at the HPM of Ruukki

Ruukki's plate mill is equipped with different mill process data systems:

- Oracle history database.

To handle plate planning values and history data how manufacturing has succeed, for example:

  - Pass data,
  - Handling time in each process phase,
  - Quality data,
  - Target temperatures and realized temperatures (heating, rolling, cooling).

- IBA data acquisition system
  - Rolling data
- Diagnostic system (Labview based)
  - Furnace measurements for example furnace temperatures, oxygen level etc.
  - Mill data.

The plate mill is equipped with an automated flatness measurement system. The TopPlan® flatness gauge, **Fig. 9**, is installed between the rolling stand and the accelerated cooling device. In addition visual flatness inspection is done on the cooling banks.

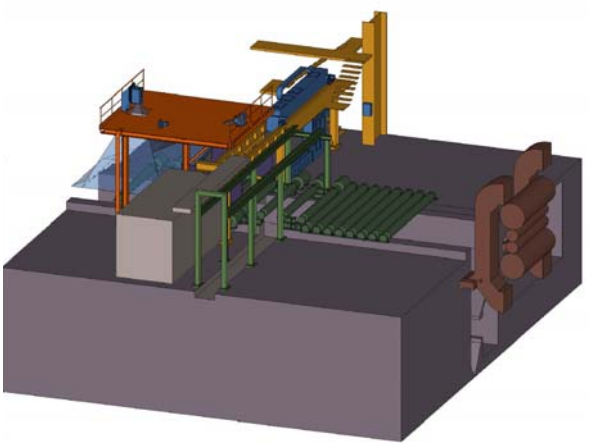


Fig. 9: TopPlan® installation at Ruukki's plate mill

Database & Flatness measurement system at the HPM of TKS

At the start of the project the **HPM TKS** did not have a unique database that accumulates all information, available in local automation databases (furnace, rolling area, plate processing line, level 1 databases, etc.), during the complete fabrication. Hence the development and implementation of a new database has been the initial tasks of the project.

Two flatness measurement systems are installed:

- a TopPlan® system between the accelerated cooling device and the hot leveller (temporarily), **Fig. 10**, and
- a laser-based flatness measurement system (supplier NOKRA) behind the cold leveller, see **Fig. 13**.

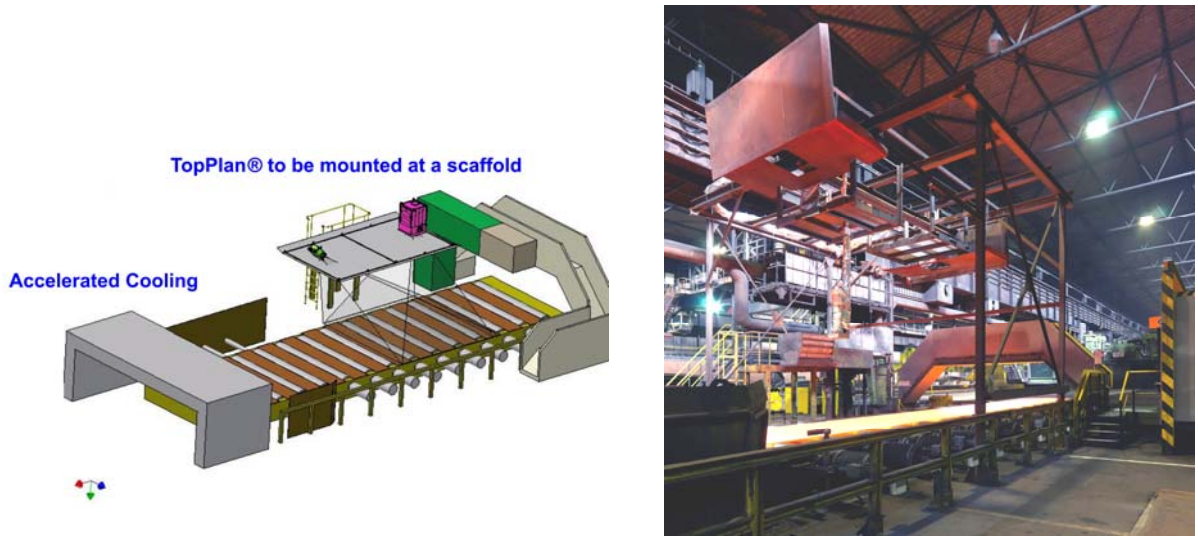


Fig. 10: TopPlan® installation at the HPM of TKS

A display screen has been installed at the pulpit of the rolling operators, **Fig. 12**.

A special feature of this TopPlan® installation is the option to lift off the entire supporting structure by a crane. The structure can be completely dismantled in less than 30 minutes. **Fig. 11** shows on the left side a photograph of the surrounding area of the plant and on the right side an image taken by the camera of the measurement system, both with visible stripe pattern on the hot plate surface.

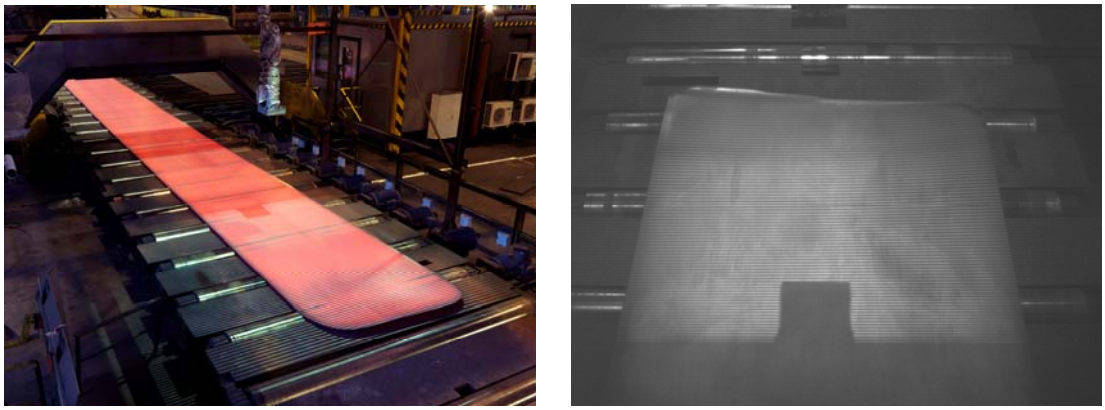


Fig. 11: Projection of the stripe pattern on the hot plate surface during the measurement

The second flatness measuring system is located downstream of the cold-levelling machine. The process of cold-levelling is the final production stage which decisively determines the quality-related plate properties. All plates with a thickness of up to 40 mm can be measured automatically by means of the flatness measuring system. Plates with thicknesses greater than 40 mm are not transported through the leveller. Therefore, the final flatness will not be automatically measured and documented for such plates.

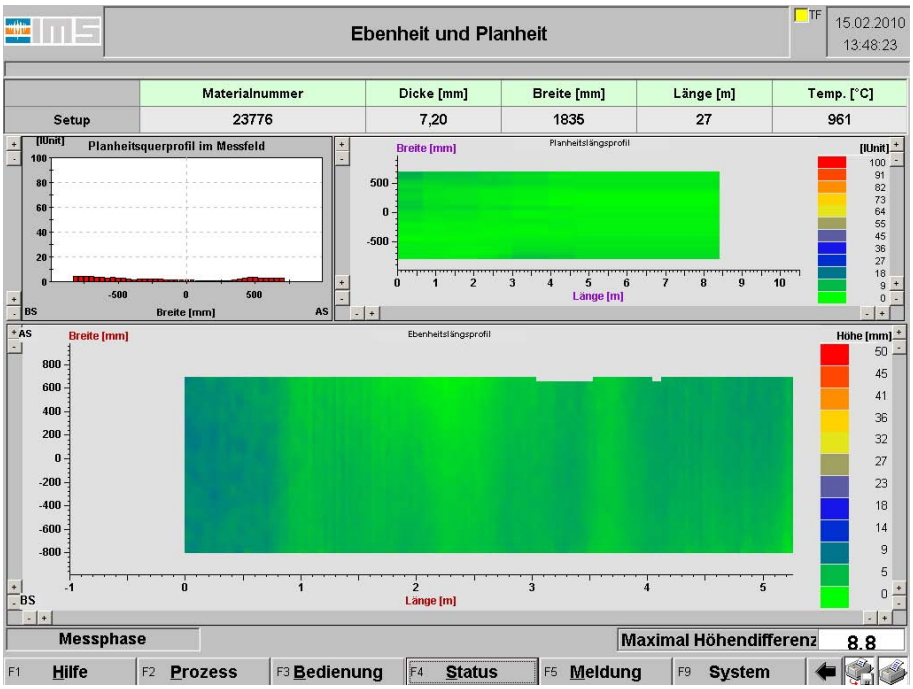


Fig. 12: TopPlan® display screen at the pulpit of the rolling operators

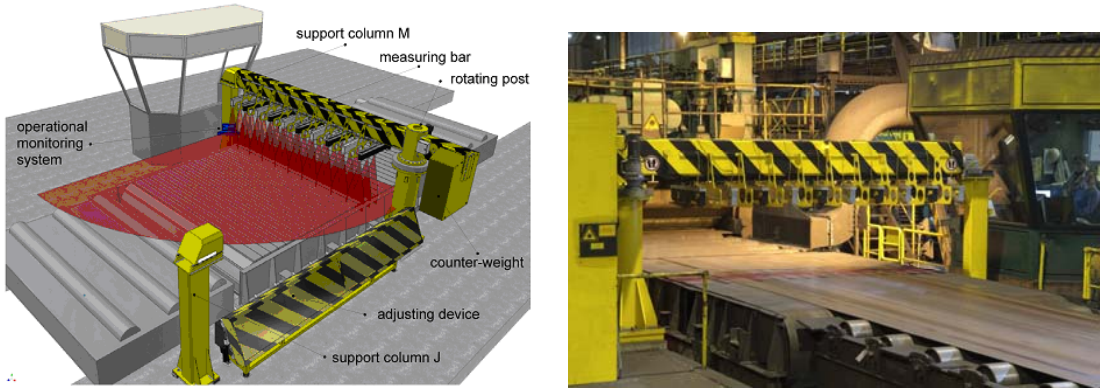


Fig. 13:Flatness measurement system (supplier NOKRA)

The plate topography is optically scanned using laser triangulation sensors. To this end, 10 individual sensors are located on the measuring bar. Each sensor here projects three parallel laser lines in plate-width-direction onto the plate surface. The optical mappings are captured by an array detector integrated into the housing of each sensor. The simultaneous input of the three laser mappings in plate-longitudinal-direction allows a co-ordinate point on the plate surface to be measured 3 times whilst the plate is being transported through the measuring system. In this way, during reconstruction of the plate topography, it is possible to compensate effectively for any interference that is due to the movement of the plate. By means of the arrangement of the individual sensors along the measuring bar, the mappings on the plate surface are input across the entire plate width. In parallel to the conveyer, there is an adjusting device with an integrated ground granite stone. Using the rotating post, the measuring bar can be swivelled across its flat surface. Here, at predefined time intervals, an adjustment and a mutual alignment of the sensors is affected on the technically flat surface. This alignment allows a surface reconstruction of the plate topography to be prepared across the plate width, using the measured data from the individual sensors.

Owing to the commissioning of the flatness measuring system TopPlan® after the accelerated cooling plant, it is possible to compare the flatness condition after the rolling directly with the final flatness obtained in the dressing and straightening shop.

Fig. 14 shows an exemplary representation of the topography of a plate after the rolling. The colour values in the illustration correspond to the height values given in the colour chart. The structure of

waviness changes from wavy edges at the left side (head end of plate) to uniform waves across the strip width on the right side.

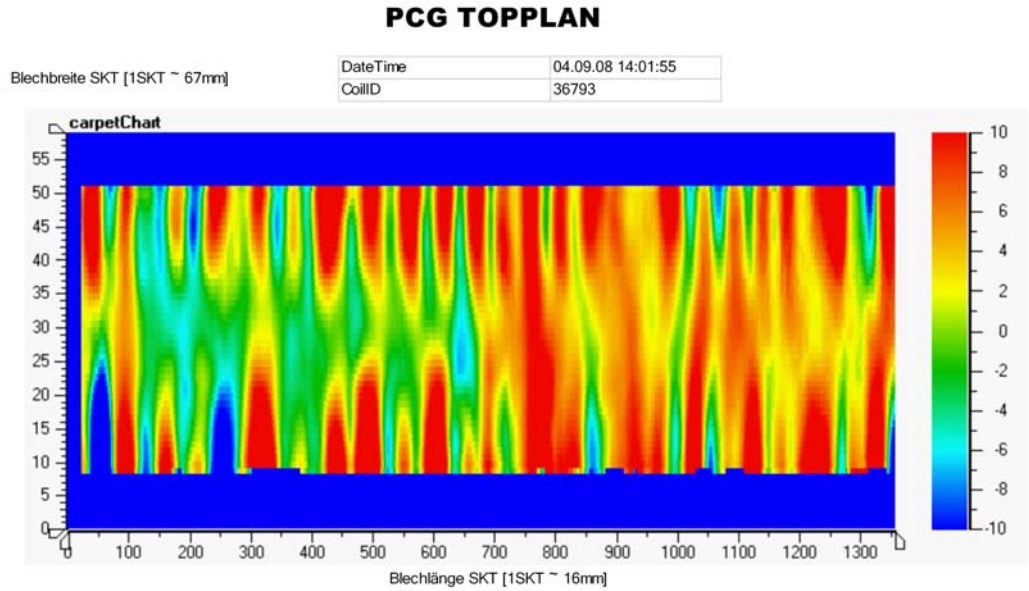


Fig. 14: Exemplary representation of the strip topography after the rolling

Plate thickness (target): 5mm; yield point Re: 350MPa;
Dimension of the mother plate (WT) - length: 24.24m; width: 2814mm

The mother plate shown in **Fig. 14** has been sheared into two plates of equal size. **Fig. 15** shows the single plates after cold levelling in the as rolled alignment. The wavy edges in the first half of the mother plate remained only on one side. The uniform waves originally present in the second half of the mother plate going have only partly been straightened. There remain centre buckles.

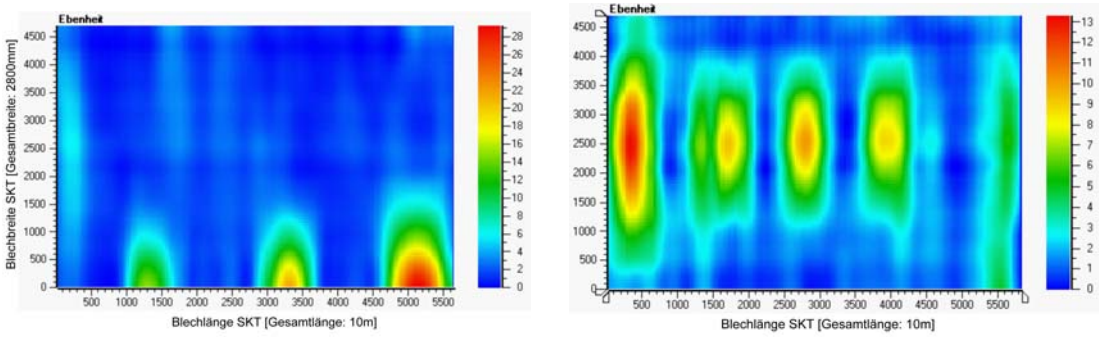


Fig. 15: Plate topography behind the cold levelling machine

Dimensions of the single plates (WTT) - length: 10m; width: 2800mm

Flatness measurement system at the Corus Scunthorpe Plate Mill

There is no on-line measurement of plate flatness carried out at the Scunthorpe Plate Mill. At the start of the project there were three possibilities for obtaining flatness measurements of rolled plates.

- A JLI Vision System flatness gauge is installed on the Heavy Shear Line, downstream of the hot leveller and cooling banks. This system is unusual in that the plate flatness is inferred by translating the measured movement of a line shadow cast across the plate, using a camera. At the time this project began, the device had only recently been installed and was not working correctly. There were ancillary issues regarding the identification of the plate being measured, and the provision of plate position information that correlated with the flatness measurements themselves. The imminent purchase and installation of a laser velocimeter was expected to solve the plate position issue.

As the project progressed, work carried out under a different project helped to make the JLI flatness gauge operational through the successful installation and commissioning of a laser velocimeter that provided plate length information. However, a number of operational issues slowed down the process of validating the actual measurements, and the fact that the system was located a long way downstream of the mill (near the end of the Heavy Shear Line), led us to dismiss this method as a way of obtaining flatness measurements on this particular project.

- Off-line manual measurement involving the use of a straight edge and ruler, on cooled plates. Initial flatness measurements were made manually, and these are described in more detail in the following section. These measurements led to the conclusion that it was not practical to carry out a large number of manual measurements and that ideally, some form of on-line flatness measurement needed to be in place.

- A prototype flatness measurement system, based upon an array of ultrasonic transducers, was tested at the entry to the SMS Cold Leveller as part of an earlier European project [1]. It is capable of measuring the variation in height of the plate on the roller table at a number of points across its width, and displays the measurements in a 2D plot on a PC.

  The prototype flatness measurement system was relocated to the Light Shear Line to provide more flatness data for assessing the performance of roll pass schedules. After being repaired and checked, the beam containing the ultrasonic gauges was fitted on the bridge just after the marking station on the Light Shear Line using purpose built brackets. Some modifications to the gauge were needed in order to clamp it into position at the desired location. An encoder was also fitted to one of the roller table motors to provide plate position information as it passed under the beam. *Details of the complete system are described in the Appendix.*

Task 1.2: Study of current process/quality problems and definition of the relevant process-/plant variables that may influence the quality target flatness

At the **HPM of ArcelorMittal Spain** the flatness is manually inspected in the plate warehouse according to procedures described in the standard EN 10029.

Plates coming from the rolling stand with thicknesses below 80 mm are passed one or more times through the hot leveller to improve their flatness. Later, after the plate is cut in the plate processing line to its final dimensions, it is passed through the cold leveller (only for plate thicknesses under 40 mm) in the own mill or sent to a subcontractor to be levelled there.

After the quality inspection, those plates with flatness problems no admitted by the customer order are re-applied to other orders directly of after removing the defective parts and/or adapted to the reapplied order. As a resume, the current situation in the HPM of ArcelorMittal Spain, regarding flatness problems, is:

- The plate mill does not have currently any equipment for automatic measurement of flatness.
- Only plates with thickness below 80 mm go through the hot leveller.
- Only thicknesses below 40 mm go through the cold leveller.
- Only about 5% of the cold plates goes through the plate cold leveller the rest is outsourced.
- Flatness is manually checked in the plate warehouse following the procedures described in EN 10029 for classes N and S.

Flatness rejects in the plate mill are all included in a single group, not being classified according to the type of flatness defect causing the reject. Flatness rejects are classified according to the plate thickness, width and length as shown in **Table 1**. These rejects represent the number of plates that were not suitable for the original order and before reparation, reapplication, to other orders, etc.

Averaged flatness rejects in year 2005, after reapplications, repairing, etc., was 0.103 % of a total production of 441578 t. No special statistical control is done regarding turn up defect. No specific guarantees are given by the mill manufacturers regarding plate flatness, shape, etc.

Table 1: Flatness rejects classified according to the plate thickness, width and length

THICKNESS	PLATES ROLLED	REJECTED	%
e<=5	898	29	3.2%
5<e<=6	10729	144	1.3%
6<e<=7	6872	18	0.3%
7<e<=8	15069	38	0.3%
8<e<=9	5007	6	0.1%
9<e<=10	17072	33	0.2%
10<e<=11	4346	4	0.1%
11<e<=12	14072	9	0.1%
12<e<=13	5005	6	0.1%
13<e<=14	6089	3	0.0%
14<e<=15	10546	5	0.0%
e>15	49686	5	0.0%

WIDTH	PLATES ROLLED	REJECTED	%
A<2000	11065	4	0.0%
2000<=A<2300	23770	27	0.1%
2300<=A<2600	71127	133	0.2%
2600<=A<2900	7716	22	0.3%
A>=2900	31713	114	0.4%

LENGTH	PLATES ROLLED	REJECTED	%
L<=10000	10552	2	0.0%
10000<L<=14000	25333	25	0.1%
14000<L<=18000	15117	50	0.3%
18000<L<=22000	22273	83	0.4%
L>22000	72116	140	0.2%

Some of the plates rolled at **Scunthorpe Plate Mill** are cold levelled as part of the customer specified process route. However, some plates are cold levelled in order to correct for poor flatness. It is this corrective cold levelling figure that provides a guide to the flatness performance of the plant in general (from hot rolling to despatch). The decision on corrective cold levelling is made either from a visual inspection of the plate (if the flatness is very poor) or from a wave height measurement made off-line at some point along the process route.

Another measure of flatness performance is the monthly level of customer complaints based upon customer feedback and from the point of view of this project, is of less use than a measure initiated before despatch. However, these data do indicate that final plate flatness and contributory factors are worthy of further investigation, particularly for relatively thin wide plates (10 mm and below and at least 3 m wide).

The biggest flatness problems at the **Ruukki Heavy Plate Mill** occur with accelerated cooled plates in thickness 5-6 mm.

The amount of flatness defects of all rolled material in 2004 has been

- • center/edge buckles 0,02 %,
- • waviness 0,04 %.

The flame straightening rate of accelerated cooled plates is approximately 34 %.

An overview of the amount of plates which have been rejected because of flatness defects is given in **Fig. 16**.

At **TKS** the result of the final flatness is transferred into a quality assurance system. Within this database, statistical evaluations about the final flatness values achieved can be effected with regard to production routes, rolling processes, heat treatment processes, steel brands, and plate dimensions.

During the period January 2006 to June 2006, the collection and evaluation of the measured final flatness values continued to be intensified, as seen in **Fig. 17**. With commissioning of the new automatic flatness measuring system, comprehensive measured flatness data are thus available to document the current final flatness. By way of example, **Fig. 18** shows the distribution of the measured maximum final flatness values for one quality group depending on the plate thickness.

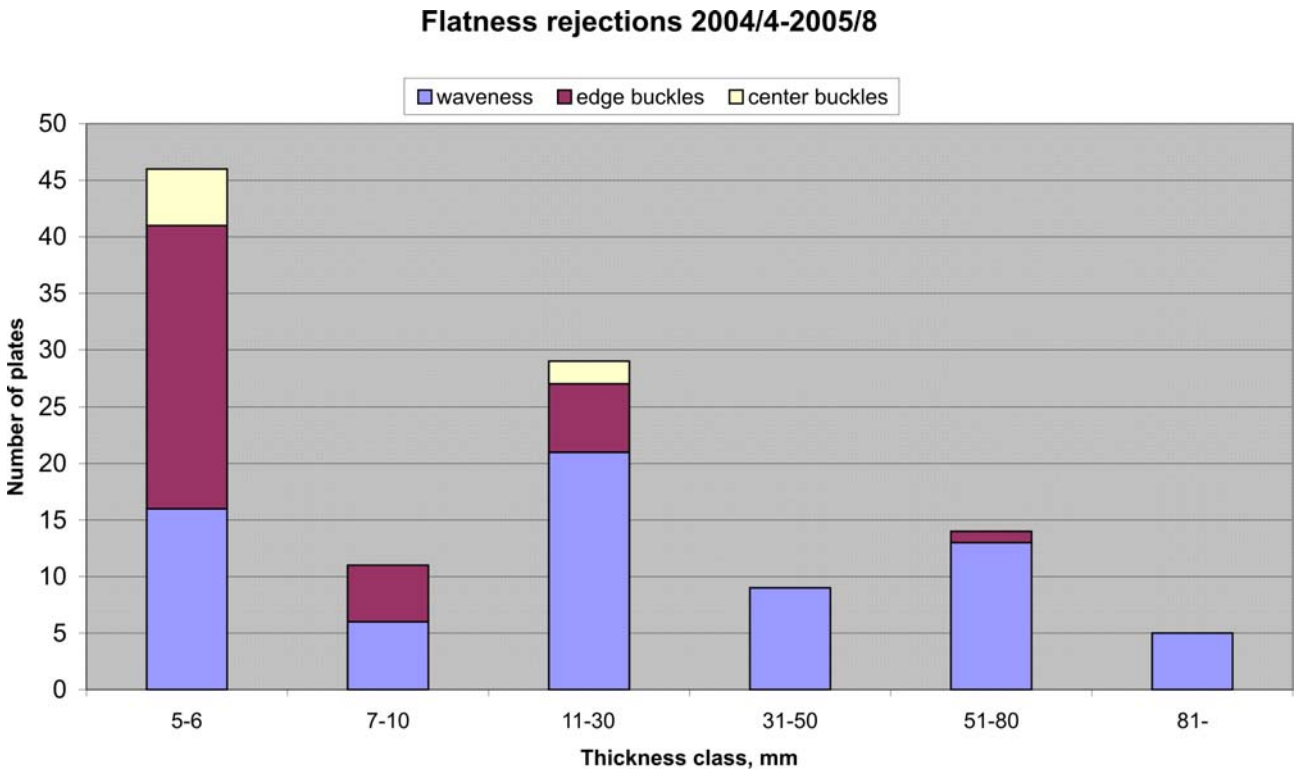
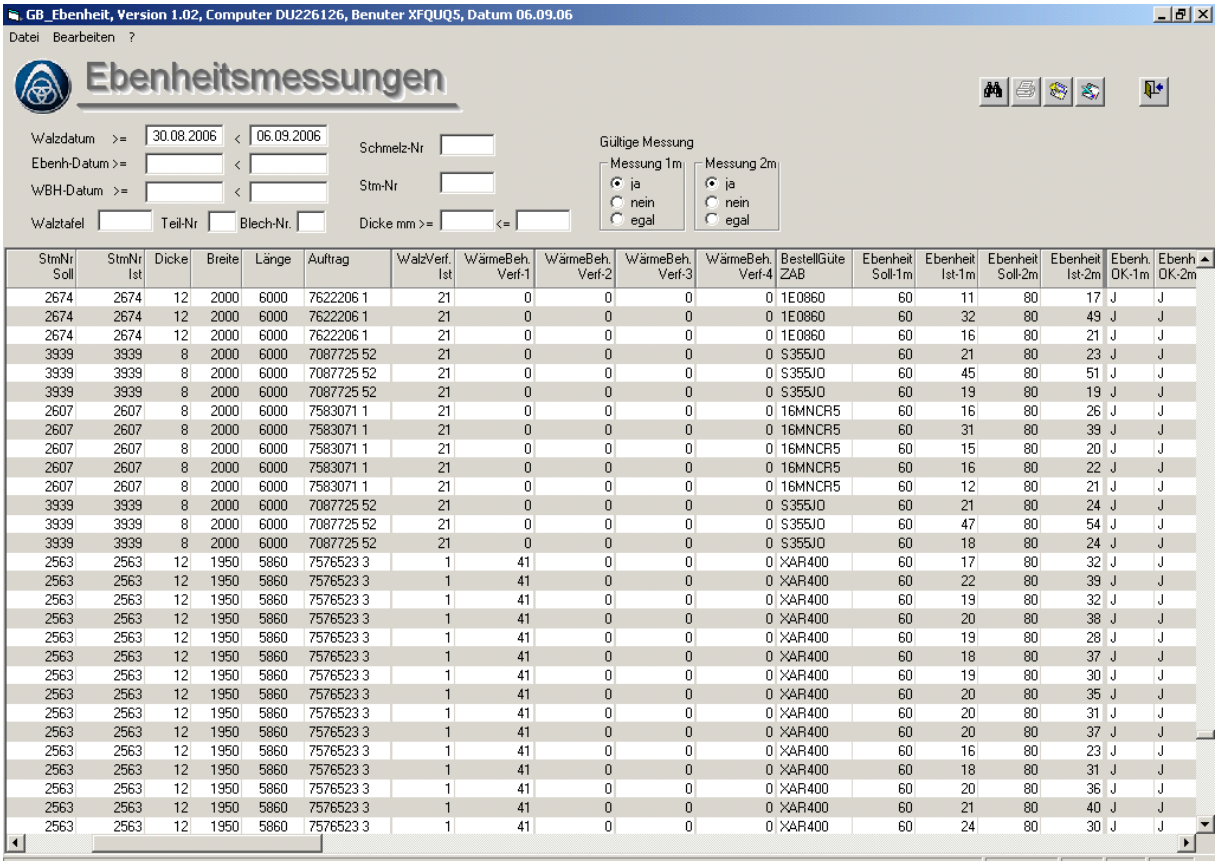


Fig. 16: Amount of flatness rejections



StmNr Soll	StmNr Ist	Dicke	Breite	Länge	Auftrag	WalzVerf. Ist	WärmeBeh. Verf-1	WärmeBeh. Verf-2	WärmeBeh. Verf-3	WärmeBeh. Verf-4	BestellGüte ZAB	Ebenheit Soll-1m	Ebenheit Ist-1m	Ebenheit Soll-2m	Ebenheit Ist-2m	Ebenh. OK-1m	Ebenh OK-2m
2674	2674	12	2000	6000	7622206 1	21	0	0	0	0	1E0860	60	11	80	17	J	J
2674	2674	12	2000	6000	7622206 1	21	0	0	0	0	1E0860	60	32	80	49	J	J
2674	2674	12	2000	6000	7622206 1	21	0	0	0	0	1E0860	60	16	80	21	J	J
3939	3939	8	2000	6000	7087725 52	21	0	0	0	0	S355J0	60	21	80	23	J	J
3939	3939	8	2000	6000	7087725 52	21	0	0	0	0	S355J0	60	45	80	51	J	J
3939	3939	8	2000	6000	7087725 52	21	0	0	0	0	S355J0	60	19	80	19	J	J
2607	2607	8	2000	6000	7583071 1	21	0	0	0	0	16MNCR5	60	16	80	26	J	J
2607	2607	8	2000	6000	7583071 1	21	0	0	0	0	16MNCR5	60	31	80	39	J	J
2607	2607	8	2000	6000	7583071 1	21	0	0	0	0	16MNCR5	60	15	80	20	J	J
2607	2607	8	2000	6000	7583071 1	21	0	0	0	0	16MNCR5	60	16	80	22	J	J
2607	2607	8	2000	6000	7583071 1	21	0	0	0	0	16MNCR5	60	12	80	21	J	J
3939	3939	8	2000	6000	7087725 52	21	0	0	0	0	S355J0	60	21	80	24	J	J
3939	3939	8	2000	6000	7087725 52	21	0	0	0	0	S355J0	60	47	80	54	J	J
3939	3939	8	2000	6000	7087725 52	21	0	0	0	0	S355J0	60	18	80	24	J	J
2563	2563	12	1950	5860	7576523 3	1	41	0	0	0	XAR400	60	17	80	32	J	J
2563	2563	12	1950	5860	7576523 3	1	41	0	0	0	XAR400	60	22	80	39	J	J
2563	2563	12	1950	5860	7576523 3	1	41	0	0	0	XAR400	60	19	80	32	J	J
2563	2563	12	1950	5860	7576523 3	1	41	0	0	0	XAR400	60	20	80	38	J	J
2563	2563	12	1950	5860	7576523 3	1	41	0	0	0	XAR400	60	19	80	28	J	J
2563	2563	12	1950	5860	7576523 3	1	41	0	0	0	XAR400	60	18	80	37	J	J
2563	2563	12	1950	5860	7576523 3	1	41	0	0	0	XAR400	60	19	80	30	J	J
2563	2563	12	1950	5860	7576523 3	1	41	0	0	0	XAR400	60	20	80	35	J	J
2563	2563	12	1950	5860	7576523 3	1	41	0	0	0	XAR400	60	20	80	31	J	J
2563	2563	12	1950	5860	7576523 3	1	41	0	0	0	XAR400	60	20	80	37	J	J
2563	2563	12	1950	5860	7576523 3	1	41	0	0	0	XAR400	60	16	80	23	J	J
2563	2563	12	1950	5860	7576523 3	1	41	0	0	0	XAR400	60	18	80	31	J	J
2563	2563	12	1950	5860	7576523 3	1	41	0	0	0	XAR400	60	20	80	36	J	J
2563	2563	12	1950	5860	7576523 3	1	41	0	0	0	XAR400	60	21	80	40	J	J
2563	2563	12	1950	5860	7576523 3	1	41	0	0	0	XAR400	60	24	80	30	J	J

Fig. 17: Quality assurance system for documenting the final flatness

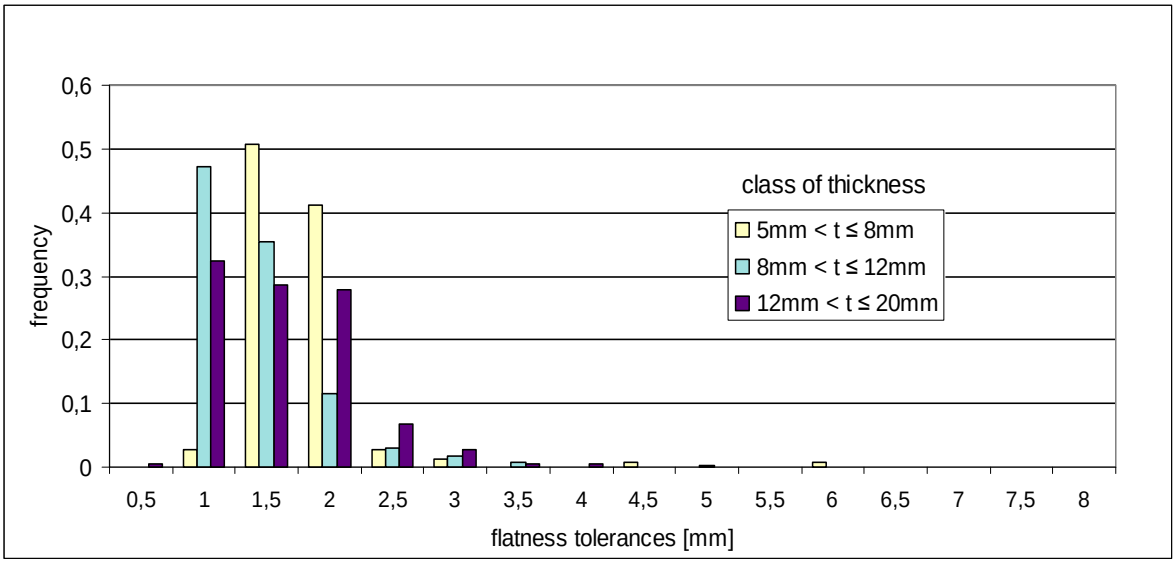


Fig. 18: Max. flatness deviation for TM-rolled plates (measuring length 1m)

This evaluation with regard to the final flatness showed that plates with a thickness >5mm meet the required flatness criteria in a sufficient manner. The specifications according to DIN EN 10029 for normally flat plates are significantly under-run by all plates, independent of the production procedure. In certain cases that the specified flatness is not reached, further repair treatments follow. This includes a further cold-levelling process as well as a repeat of heat treatment.

The process and plant parameter relevant for the final flatness were determined. The appropriate parameters of the rolling process are represented in **Table 2**. Furthermore the levelling parameters (settings) are decisive for flatness and have included in the analysis too. Beside the on-line recorded process data also further data appear of importance for the final-flatness. For example the pile conditions of the plates in the temporary storage and the allocation of the cooling bed have influence on flatness.

Table 2: Relevant process-/plant variables

Data to be sampled on-line			Data to be sampled off-line	
Stand and drive system	1	Rolling load AS	21	Material data with regard to slab ID-No.
	2	Rolling load BS	22	Work roll diameter after grinding
	3	Rolling load, Sum	23	Work roll profile after grinding
	4	Roll bending force AS	24	Work roll wear profile at the end of campaign
	5	Roll bending force BS	25	Rolling schedule
	6	Screw down position AS		
	7	Screw down position BS		
	8	Speed upper motor		
	9	Speed lower motor		
	10	Target speed difference		
	11	Switch on/off watersprays		
Slab/plate	12	Slab ID-No.		
	13	Pass ID-No.		
	14	Pass trigger		
	15	Slab position		
	16	Flatness		
	17	Ski		
	18	Thickness		
	19	Temperature top side, exit		
	20	Temperature top side, entry		

Task 1.3: Flatness characterisation

At the **HPM of ArcelorMittal Spain** flatness is defined according to EN 10029 classes N and S.

At **Scunthorpe Plate Mill** there are no formal records of flatness measurements made from hot rolling through to despatch.

Scunthorpe Plate Mill personnel determine the wave height in millimetres per metre length measurement as specified in the British Standard BS EN 10029:1991, 'Tolerances on dimensions, shape, and mass for hot rolled steel plates 3 mm thick and above. However, no formal records of flatness measurements are kept for hot rolled plates.

At the **Ruukki Heavy Plate Mill** the following criteria for good/poor flatness are used:

- Flatness error millimeter per one meter,
- Normal standard maximum allowed flatness error 6 mm/m,
- Tighter limit maximum allowed flatness error 3 mm/m.

Three flatness error classes are used:

- Center buckle error,
- Edge buckle error,
- Waviness (through whole plate) error.

At the **HPM of TKS** the flatness definition and tolerances used are according to EN 10029. Previously the flatness is measured manually after the ruler - method. The flatness deviations for the 1 and 2 m-ruler method are shown in **Fig. 19**.

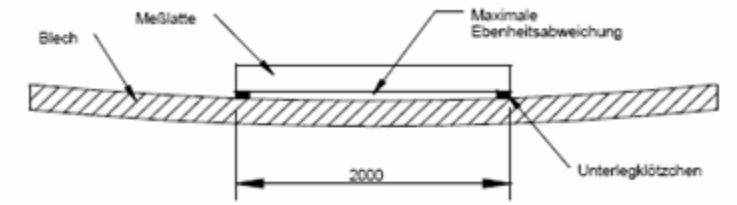


Fig. 19: Ruler assessment according to EN 10029

With the installed measuring system behind the cold levelling machine, it has become possible to measure automatically the final plate flatness of the plates which pass through the production route via the conveyer of the finishing department. The system provides a documentation of the final flatness of the plates, which is a precondition for linking the final flatness with process data during plate production.

A virtual ruler assessment according to DIN 10029 is carried out on the measured data of the plate topography. As a final result, the two values for the maximum flatness deviation are calculated in accordance with **Table 3**, using a 1 metre or 2 metre ruler.

Table 3: Flatness specifications according to EN 10029

Nominal tolerances for flatness, class N

Dimensions in mm

Nominal thickness	Steel type L		Steel type H	
	Measuring length			
	1000	2000	1000	2000
= 3 < 5	9	14	12	17
= 5 < 8	8	12	11	15
= 8 < 15	7	11	10	14
= 15 < 25	7	10	10	13
= 25 < 40	6	9	9	12
= 40 < 250	5	8	8	11

Special tolerances for flatness (class S)

Dimensions in mm

Nominal thickness	Steel type L				Steel type H	
	Plate width < 2750 mm		Plate width = 2750 mm			
	Measuring length					
	1000	2000	1000	2000	1000	2000
= 3 < 8	4	8	5	10	Shall be agreed at the time of ordering	
= 8 < 250	3	6	3	6		

Steel type L: Products with a specified minimum yield strength ≤ 460 N/mm^2, neither quenched nor quenched and tempered.

Steel type H: Products with a specified minimum yield strength > 460 N/mm^2 and < 700N/mm^2 and all grades of quenched and quenched and tempered products.

Above all, however, for the assessment of the final flatness, internal flatness specifications are relevant, and these are significantly stricter in comparison to EN 10029. In addition, particular customer specifications regarding supply and delivery must frequently be met in the assessment. By means of the automatic measurement of the plates, it is ensured that the final flatness required by the customer has demonstrably been reached.

Fig. 20 shows by way of example the operating image of the flatness measuring system and an assessed plate topography in a 3D representation with the marked ruler positions for the 1m ruler (red) and the 2m ruler (blue).

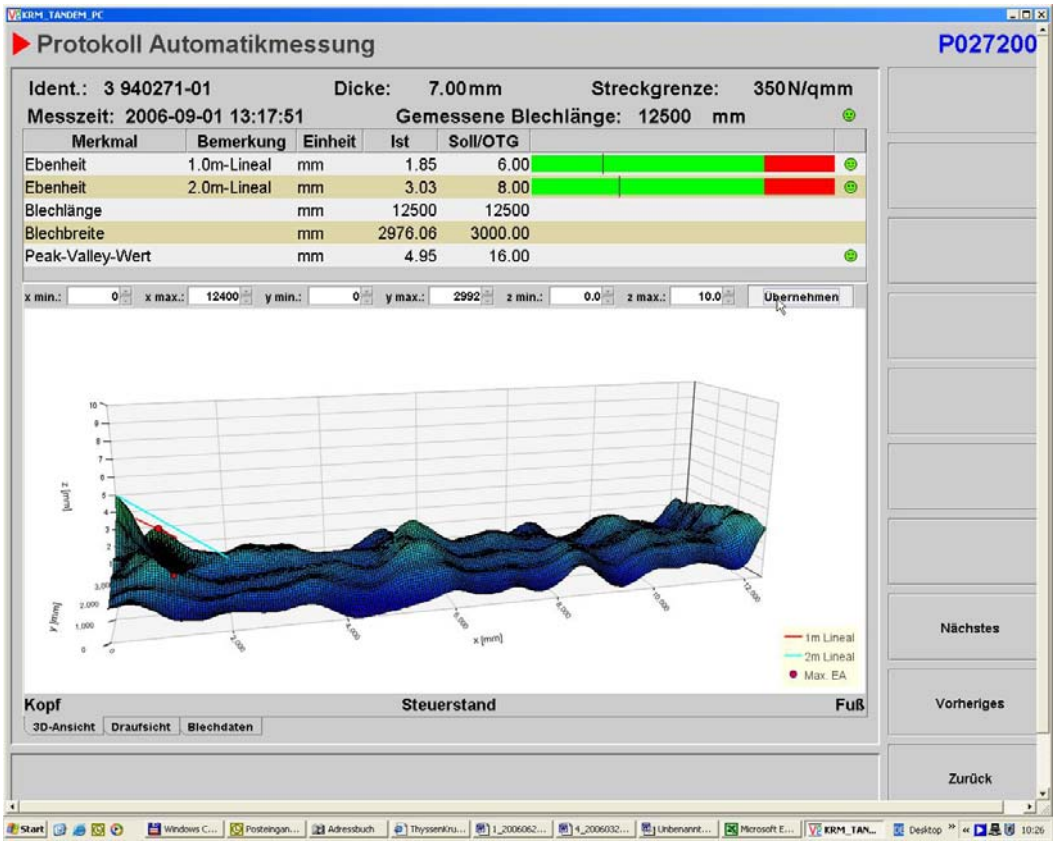


Fig. 20: Operating image of the flatness measuring system

In addition to the result of the ruler assessments, the plate length and the plate width are also determined from the measured data yielded by flatness measuring. These are used for checking purposes and to protect against any confusion when allocating the plate flatness to the respective customer plate.

For very thin plates, which are critical under aspects of flatness, a visual investigation of the flatness takes place after the warm levelling procedure and on the cooling bed apart from the measurement of the final- flatness.

An approach to characterise the flatness systematically is described schematically in **Fig. 21** [2]. Based on a measured height matrix of the whole plate in a first step decomposition should be done which differentiates between

- an “unwindable” part of the defect and
- a “non-unwindable” part of the defect.

The “unwindable” part of the defect is characterised by the amplitude and the wave length of the defect. With respect to the rolling process this part of the defect is mainly influenced by

- the temperature gradient across the thickness of the plate,
- the speed behaviour of the mill (upper and lower work roll) and
- the pass-line.

The “non-unwindable” part of the defect can be describe by the distribution of fibre length across the width of the plate which is mainly caused by the differences between

- the entry plate profile and
- the roll gap profile.

In this way a sufficient characterization of flatness throughout the production line appropriate for analyzing the influence of each single processing stage and for prediction and optimization of the final flatness can be done.

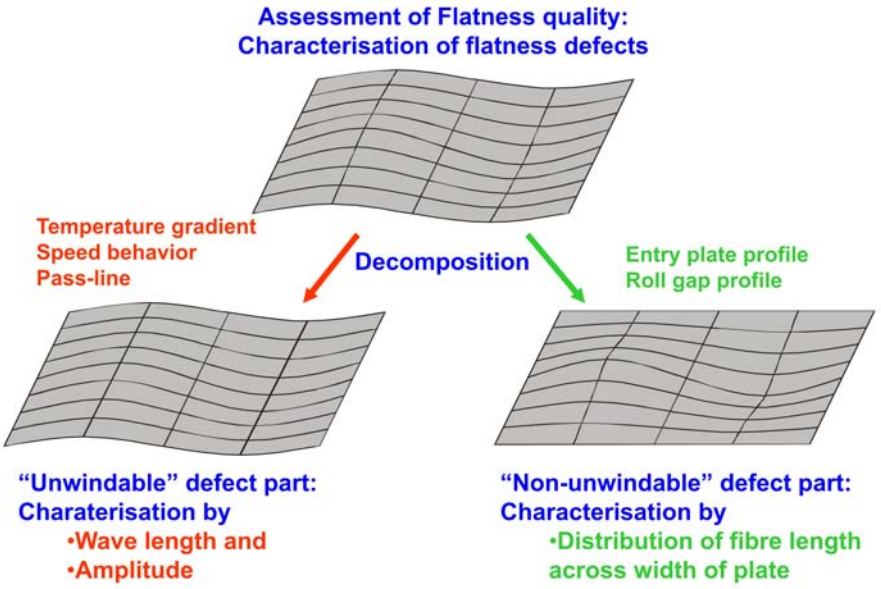


Fig. 21: Approach to characterise the plate flatness

Task 1.4: Definition of Systems Functionality

Variations of each process conditions may contribute to essential variations to the flatness of the plates as it is shown in **Fig. 22**.

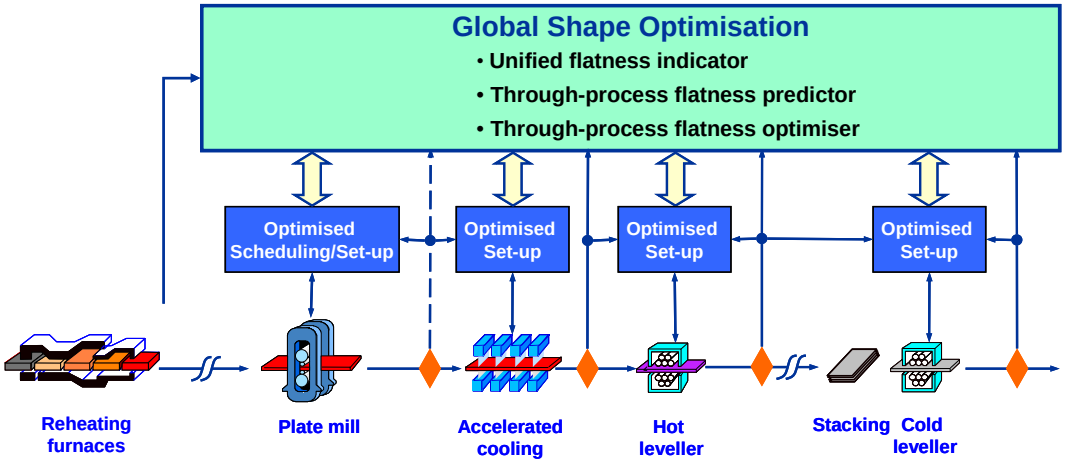


Fig. 22: Substantial process steps of rolling heavy plates

The general functionality of the system is schematically shown in **Fig. 23**. The main tasks of the system are:

- Monitoring / documentation of process / plant variables and
- Monitoring / documentation of quality features at each processing stage

as a basis to analyse the quality evolution and to develop a prediction model which will allow to optimise each processing step as well as to optimise the subsequent processing step to gain an optimal final flatness of the plates.

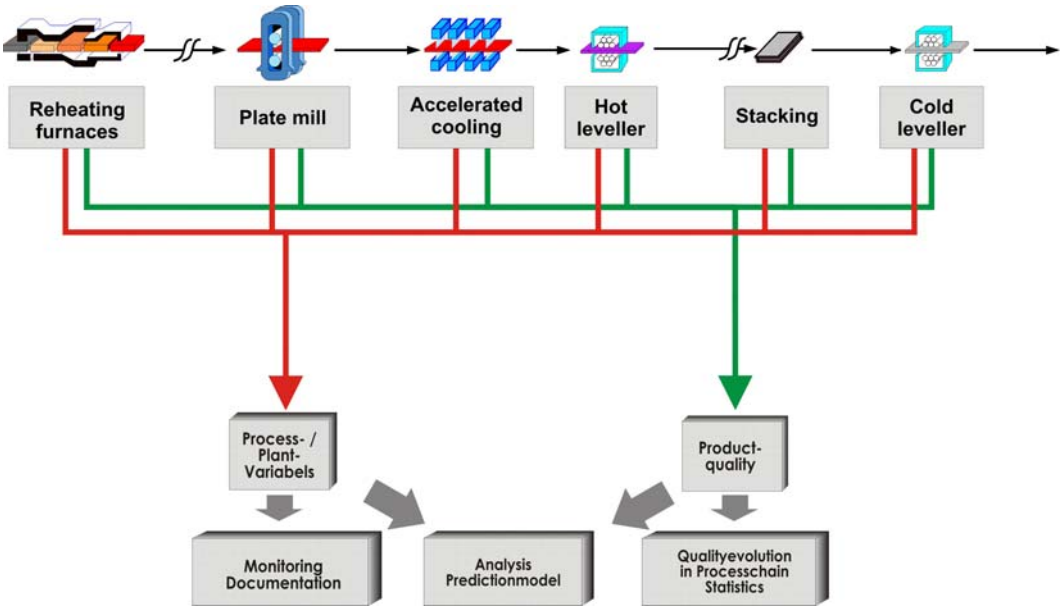


Fig. 23: General functionality of the system

The system to be developed in this project by **ArcelorMittal Spain** is oriented to improve the current situation of its HPM in aspects like: flatness, front end bending, camber and rectangularity of the plate, which will be done by developing four different models, based on data mining techniques.

Methodology to develop each one of these models will be the same:

- Large sets of data, existing in the database, corresponding to values obtained during the rolling process of large sets of plates for all the variables pre-selected, will be primarily analyzed to determine their influence over the target variable. Different techniques like principal component analysis (PCA), self-organizing maps (SOM), multivariable adaptive regression splines (MARS), statistical analysis, data visualization techniques, could be used for that task. Results at each analysis will be a weighted list of variables, from which the most influencing will be used for the model development.
- In a second step, a model based on neural network (NN) techniques will be developed using as input variables those selected from the first step, Three large sets of data of those variables will be necessary, the first set will be used for training the neural network configuration selected, and a second set will be used for testing the performances of the model. These two steps could have to be repeated by using different NN configurations. The third set of data will be used to verify the final performances of the model developed.

The models to be developed are:

1. The model for prediction of the plate rectangularity will estimate, before the slab enters the mill, the final plate shape that is going to be obtained as a function of the pass scheduling, characteristics of the slab, rolling forces, roll stack initial crowns and thermal crowns, temperature distribution, etc. Knowledge gained with this model will be useful to evaluate the pass schedule in advance to take decisions regarding accepting it or introducing some changes.
2. The model for predicting plate flatness will estimate the best rolling pass distribution to optimize flatness, especially in the last passes, since it has been demonstrated that the ratio crown change/thickness change should be maintained constant for two consecutive passes, especially in the last three passes. Hence those tools to correct the plate shape are oriented to the modification of the roll gap geometry, which can be achieved by means of an appropriated roll force distribution along the different rolling passes. The force to be applied at each pass will be a function of different variables like: plate characteristics (width, thickness, hardness, etc.), roll characteristics (stiffness, diameter, crown, etc.) and other variables.
3. The front end bending model will analyze the pass schedule for each slab rolled, estimate the front end bending obtained and generate countermeasures (like roll speeds unbalance). Studies have demonstrated that front end bending produced during rolling is a consequence of

mismatches of the speed differences of the work rolls, modulated by other factors, like the plate entry thickness (which influences on the curvature and on the position where the curvature changes its sign) or the reduction per pass.

4. The plate camber model will estimate the camber to be obtained on the exit plate before the plate enters the mill as result of the pass schedule foreseen, material characteristics and other factors.

The database of the **HPM of TKS** is accomplished to capture all important process parameters. The effort comprises the realization of a network which involves the important measurement systems recording the main process parameters of each process step linked to each plate. In addition to that, routines are developed to visualize the process parameters or to analyse the process data by statistical operations.

In the initial stage of the project it was decided in favour for the operation of the long term storage system called MEVINet-Q. Reasons for the decision were the approved functions of the quality management feature suitable for archiving and analysis the large amount of process data. A significant characteristic of the system is the logging of process data depending on the length of the plates. Furthermore, the configuration of data structures allows a continuous tracking of the plate during its path through the plate mill.

Primary measurement data, evaluation data and running data will be collected within the MEVInet Q. The running data include material identification information and specification values. These serve for the identification of the rolling material and for the comparison of nominal values with the process parameters determined during manufacture.

The presentation and evaluation of the data will take place independently of data reception and storage. The programs used will permit individual data evaluation and presentation at decentralized workplaces that will be linked via an Ethernet connection, see **Fig. 24**.

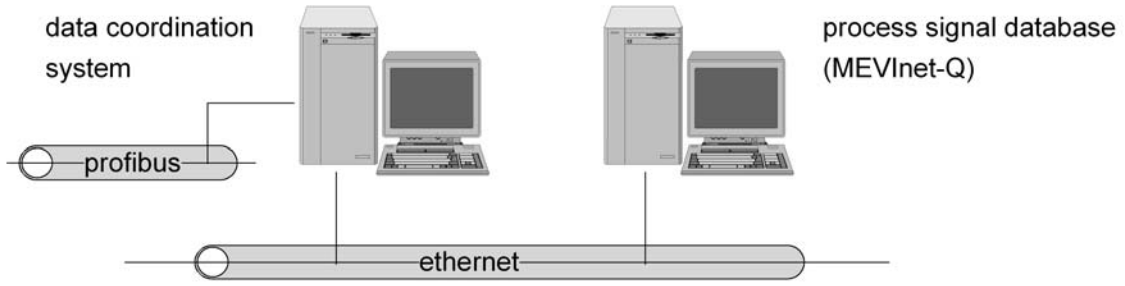


Fig. 24: Integration of the process signal data collection system into the existing network

A further option for accessing data can be set up via an HTML browser in the intranet or internet. For this purpose, the Microsoft Internet Information Server will be installed on the MEVInet Q server. This will enable the users to easily access the data, for which it will be possible to set up specific output formats using the IMS Report Generator.

Task 1.5: Development and implementation of an automated documentation of the flatness

At the **HPM of ArcelorMittal Spain** the new process database has been installed and interfaced with the mill automation data network in order to collect and centralize in a single computer all the relevant information obtained during the complete processing of each plate, from furnace entrance to finished plates at mill exit, to improve the previous situation where that information was distributed in different databases.

Main characteristics of the new database are as follows:

- Hardware
  - DELL PowerEdge 2800 with double processor Intel Xeon Dual-core 2.8 Ghz, 2x2MB cache memory, DDR2 SDRAM 4x1GB, 2x140 GB HD,
- Software
  - Operating system WINDOWS XP Professional,
  - Database ORACLE 10,
  - Custom Software for querying and tools for automatic management developed with Visual.Net and user interface base in EXCEL tools,
  - User interface direct from MS Excel.

The configuration of the database is given in **Fig. 25**.

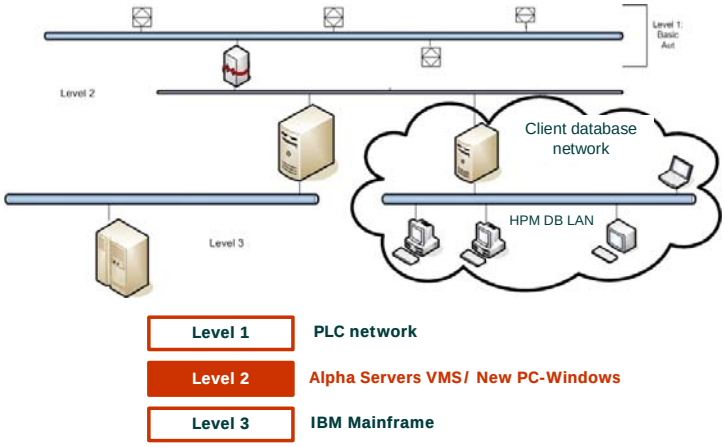


Fig. 25: Configuration for the database

At the **HPM of TKS** a central database MEVInet Q to collect flatness-relevant product and process parameters was implemented. A significant characteristic of the system is the logging of process data depending on the length of the plates. Furthermore, the configuration of data structures allows a continuous tracking of the plate during its path through the plate mill.

The range of data over the whole production route includes:

- Signals from the milling shop,
- Process data of the rolling process,
- Data of the plate thickness,
- Data of the temperature profile,
- Process data of the accelerated cooling,
- Pyrometer temperatures,
- Process data of the hot levelling machine,
- Process and measuring data during heat treatment of the plates,
- D data of the ultrasonic testing facility,
- Process data of the side trimming shear,
- Data of the cross-cutting shear,
- Data of the final flatness behind the cold leveller,
- Process data of the cold leveller.

System components

The complete process signal database system consists of the hardware and individual software modules. For the hardware, commercially available PC systems or assemblies are used. The minimum requirement for the server consists of a CPU ≥ 450 MHz with a mainframe memory of 256 MB RAM. The software modules fulfil the functions of data reception and storage in the database, of the database system itself, and of data presentation and evaluation. Additionally, various programs are available for operating and maintenance purposes.

WP 2 Analysis, Prediction and optimization of the rolling process

Task 2.1: Provision of Data, Acquisition Systems and Measurement Campaigns

At the **HPM of ArcelorMittal Spain** a dataset captured from December 2006 until June 2007 was used to perform different analyses. The dataset size was initially of 89267 plates, which, after pre-processing and filtering data, gave a total of 8371 plates, with 40 attributes of each plate, suitable for the analyses.

From that dataset, a series of attributes describing the rolling process of each plate were selected. The attributes were taken combining data from different tables within the database. The data used could be divided within two groups: input and output plate description. Input data are known or calculated before starting plate rolling and output data are measured after rolling. In **Table 4** a partial list of the 40 attributes is given.

Table 4: Variables used in the analyses (partial)

Attribute Name	Format	Comment
MATID	NUMBER(9)	Piece Identifier
ROLLINGDUR	FLOAT	Rolling duration [s]
FURDISCHTEMP	FLOAT	Furnace discharge temperature [°C]
MEASSLABWEIGHT	FLOAT	Measured slab weight [Kg]
NOOFPASSES	NUMBER(2)	Number of pass
CALCTHICKNESS	FLOAT	Plate calculated thickness [mm]
CALCWIDTH	FLOAT	Plate calculated width [mm]
CALCLENGTH	FLOAT	Plate calculated length [m]
WIDTHRATE	FLOAT	Plate width / Slab width
NOTURNS	NUMBER(2)	Number of turns during rolling
STARTTEMP	FLOAT	Start temperature [°C]
DURATIONEG (*)	FLOAT	Duration of the Egalization phase [s]
DURATIONFIRSTTURN (*)	FLOAT	Duration of the first turn [s]
DURATIONBR (*)	FLOAT	Duration of the broadsizing phase [s]
DURATIONSECTURN (*)	FLOAT	Duration of the Egalization phase [s]
MEASLENFPASS (*)	FLOAT	Length measurement before the first (AccuPlan gauge) [mm]
MEASWIDLPASSAVG (*)	FLOAT	Measured average width for the last pass by AccuPlan gauge [mm]
MEASTHICKCENTAVG (*)	FLOAT	Measured average center thickness [mm]
MEASTHICKCENTDEV (*)	FLOAT	Measured deviation center thickness [mm]
MEASCROWNAVG (*)	FLOAT	Measured average crown [mm]
CORRTGTWIDTH (*)	FLOAT	Correction term applied to the target width [mm]
CORRTGTTHICK (*)	FLOAT	Correction term applied to the target thickness [mm]

At **Scunthorpe Plate Mill** 1 m and 2 m straight edges were used together with a set of wedges, to systematically measure the wave heights of six plates as they rested on the mill floor. Thickness measurements were also taken using an ultrasonic gauge, at a number of points across the width, thus obtaining cross sectional profile of each plate.

All of the six plates were rolled as normal, both in terms of their pass reductions and their position in the rolling programme. Most of the plates were passed under the Light Shear Line hot leveller without being levelled, although one was hot levelled to provide a comparison.

Each set of measurements was in the form of a table detailing wavelengths and heights at various positions along the plate length and at three positions across the plate width. **Table 5** gives a snapshot of the measurements taken over the first 4 m of a 16 m long plate.

Table 5: Snapshot of flatness measurements for a rolled plate with no hot levelling

		Position across Plate Width		
	Distance from Plate Head End (m)	DS Edge	Centreline	OS Edge
Wavelength (mm)	2	1600	1300	1170
Height (mm)		14.2	15.2	7.6
Lift per m (mm)		8.9	11.7	6.5
Wavelength (mm)	3	810	1050	1110
Height (mm)		9.9	11.6	6.6
Lift per m (mm)		12.2	11.0	5.9
Wavelength (mm)	4	1050	1020	1080
Height (mm)		10.1	12.8	11.4
Lift per m (mm)		9.6	12.5	10.6

At each measurement point a value of lift per m (in mm) was calculated, and is shown in blue in Table 5. All the values of lift per m for each plate width position were averaged, giving three values per plate, one at the drive side edge, one at the open side edge, and one in the centre. The average arc length at each of these three cross width positions was then calculated using the formula below

$$\text{Arc length, } S = L\,[1 + (\pi h/2L)^2]$$

where L is the projected length of the arc, and h is the average wave height or lift. An I unit value of flatness was then calculated for each cross width position using the following formula

$$\text{I Units of Flatness} = (S - S_{ave})/S_{ave} \times 100000$$

Four out of five of the plates rolled and then measured without hot levelling, had full centre. For three of those four plates, the out of flatness was of the order of 15 to 20 I Units, while for the other (shown in **Fig. 26** below), the flatness was slightly worst at 24 I Units. One of the five unlevelled plates was found to be flat. Finally, the other plate that was rolled and subsequently hot levelled was found to be flat.

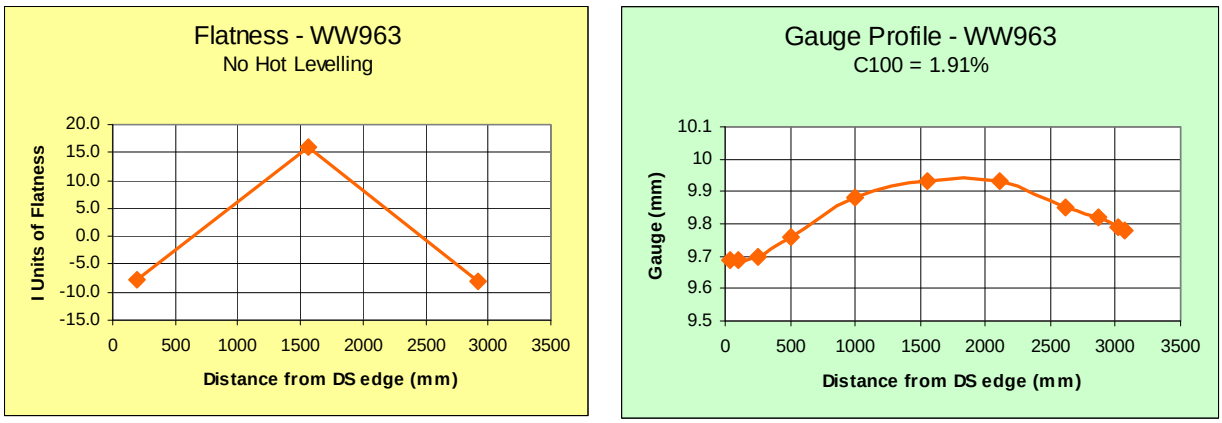


Fig. 26: Flatness and gauge profile of plate WW963 (3.15 m wide plate, 10 mm gauge)

As is implied by the way the calculations have been done, the values stated above relate only to the out of flatness caused by differential elongation of the plate across its width, in the roll gap itself. They do not account for any out of flatness caused by roll speed mismatches or instability in the rolling process, or any pass line height and roller table effects. Such effects are deliberately eliminated by the method used to calculate the flatness values quoted. In fact, a ripple effect of some degree was noted on all of the plates, which was present across the full width of the plate, and considered to not be the result of differential elongation during rolling.

It should also be noted that the accuracy of the measurements made was compromised by the fact that the plates had to be laid on the mill floor. The weight of a plate in this position will affect the measurements, although such a compromise is unavoidable as using clamps to suspend the plate vertically is not practical with plates of this size. The floor itself is very uneven, with large craters in

some areas over which the plates were laid. These also affected the flatness measurements to some degree.

To summarise these initial measurements, the flatness of these plates was fairly consistent with four out of five of the plates rolled and then measured without hot levelling, having full centre. However, the accuracy of the measurements made was compromised by the fact that the plates had to be laid on the mill floor. In addition, the few measurements made involved a good deal of time and effort and at this stage, the best option for obtaining a greater number of flatness measurements was considered to be development of the prototype on-line flatness measurement system that employed an array of ultrasonic transducers, as detailed in Appendix.

The product range that suffered the greatest number of flatness issues was perceived to be those plates from 20 mm to 25 mm thick, and between 2 m and 2.5 m wide. This was perhaps unsurprising, as these plates form a significant proportion of the total output of the Scunthorpe mill. As part of work carried out under a separate project, further manual flatness measurements of sheared plates were made during a recent flatness audit [3]. These measurements, suggested that the majority of material destined for the Heavy Shear Line (generally plates of 15 mm and thicker) was reasonably flat off the mill, with the main issue being turn up.

Comments made during the aforementioned audit also suggested that as regards flatness off the mill, the main issues were still with thin, wide plates. The manual measurement of such plates involves the removal of the plate from the cooling bank after hot levelling, before it passed down the Light Shear Line. The opportunities to do this obviously depend largely on the rolling programme and the demands of production, and also upon the space available to store plates prior to them being measured.

Over a period of weeks, flatness measurements of as rolled but hot levelled and cooled, thin, wide plates (at least 3 m wide and less than 10 mm thick) were made. A large number of such plates have good flatness, but it was possible to obtain data from a few non-flat plates. Ideally, these plates would have not been hot levelled but the logistical issues involved in missing out this process stage are obvious and would have caused further delays. In any case, it was possible to examine video footage of these non-flat plates to provide qualitative confirmation of their poor flatness off the mill. Remote access to camera views of plates at the Finishing Stand exit was obtained. The “Visimetrics” viewing software allows the plate to be observed live during rolling and also allows recently rolled plates to be viewed.

The plates were measured manually in the same way as illustrated in **Fig. 218**. **Fig. 27** shows an example of a flatness map (in mm/m) generated from manual measurements on plate RH892. This plate was 3,4 m wide and 6 mm thick, and is among the widest and thinnest rolled at Scunthorpe.

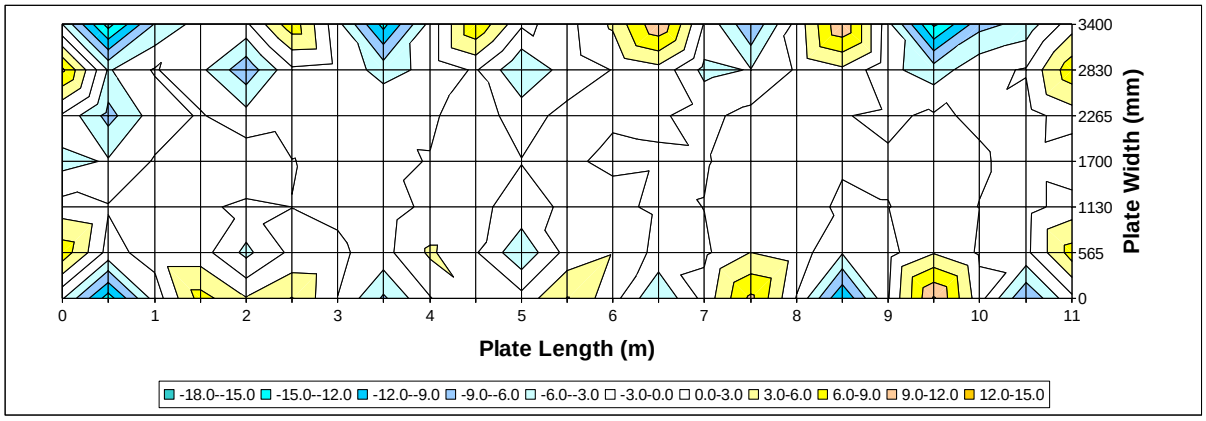


Fig. 27: Example of flatness map generated from manual measurements on 3.4 m by 6 mm plate

This map shows that the plate had wavy edges (even after hot levelling) with wave heights of up to about 20 mm/m. The video footage of this plate leaving the mill confirmed that it had poor flatness at this stage also.

In total, about 20 plates were measured, and these were often taken from a ‘ruck’ specifically created to store plates of poor flatness that had been lifted off the cooling bank. Of all the plates measured, one or two were fairly flat, but the majority either had full middle or wavy edges of various degrees. The plate

illustrated above was one of the most severe examples of wavy edge that were measured. Ideally, more plates would have been measured but time and resources were at a premium at this late stage of the project and each flatness measurement was labour intensive and time consuming.

Task 2.2: Correlation Analysis, Model Development & Validation for Prediction and Optimisation Purposes

At the **HPM of ArcelorMittal Spain** measured data were filtered to eliminate values out of range, plates where attributes are missed, etc., by using different filtering techniques. Different statistical techniques were then applied to evaluate the characteristics of each attribute: analyses of distributions (**Fig. 28**), quartile graphs (**Fig. 29**) and correlation analyses among attributes (**Table 6**).

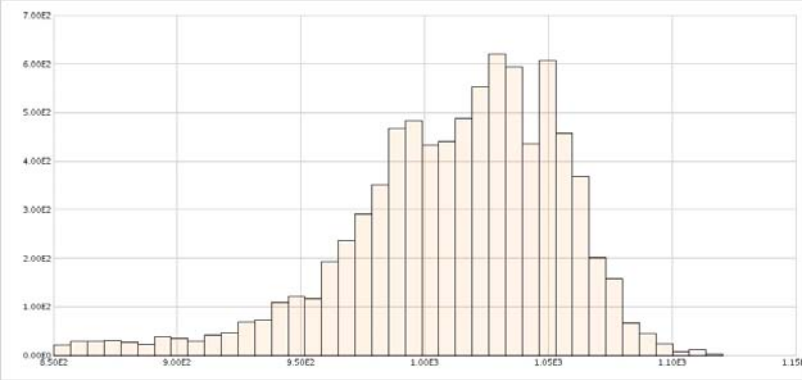


Fig. 28: Histogram STARTTEMP

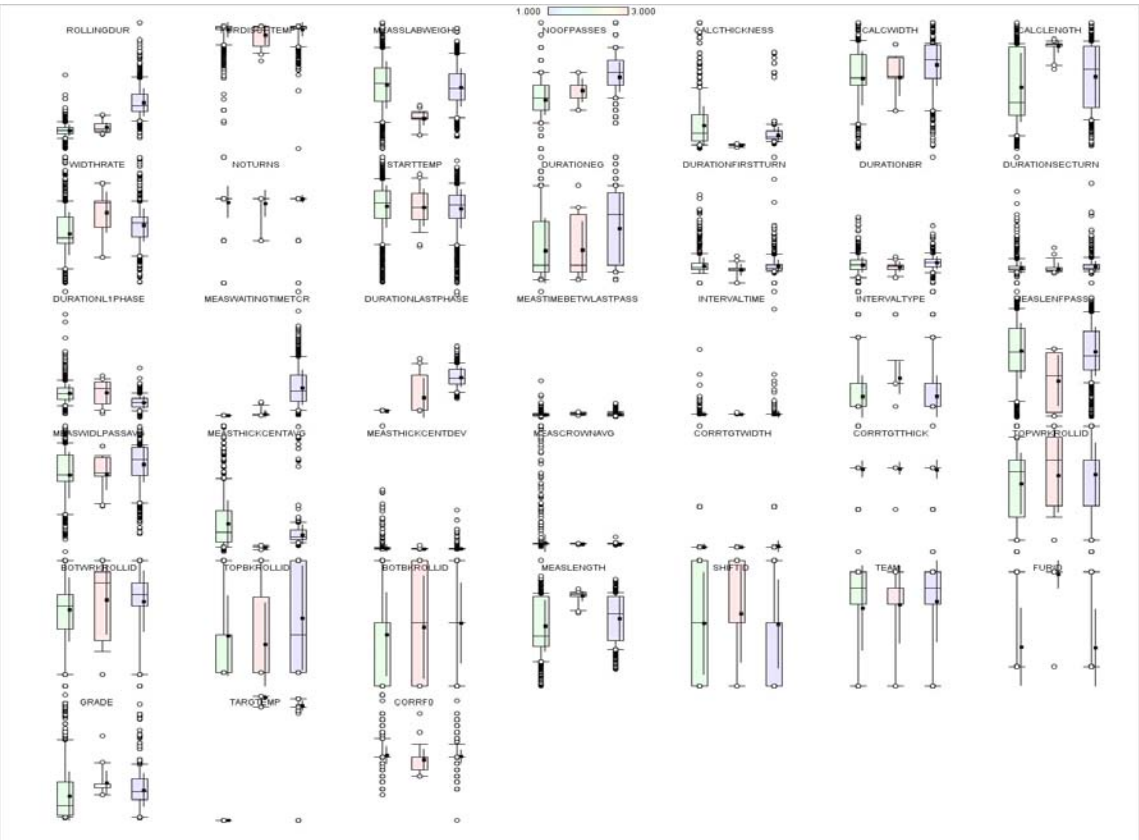


Fig. 29: Quartile matrix - ROLLMODE

Table 6: Correlation analyses (partial)

ROLLINGDUR	MEASWAITINGTIMETCR	0.9272611459808954
DURATIONLASTPHASE	TARGTEMP	0.9231256552299956
ROLLINGDUR	ROLLMODE	0.8169864055833612
ROLLINGDUR	TARGTEMP	0.800766991455627
ROLLINGDUR	DURATIONLASTPHASE	0.7790998247676988
WIDTHRATE	MEASWIDLPASSAVG	0.7733552578268424
MEASWAITINGTIMETCR	ROLLMODE	0.7724155624298087
CALCWIDTH	WIDTHRATE	0.7650053498598132
MEASWAITINGTIMETCR	TARGTEMP	0.7563780842476138
MEASSLABWEIGHT	MEASLENFPASS	0.7179441736438731
NOOFPASSES	DURATIONLASTPHASE	0.6763006555185821
MEASWAITINGTIMETCR	DURATIONLASTPHASE	0.6690941304771898

Having measured and quantified the flatness of a number of thin wide plates at **Scunthorpe Plate Mill**, the next steps were to examine the way these plates were rolled and assess the effectiveness of the reduction schedules. It was possible to download rolling information for the specific plates that had been measured which comprised speeds, rolling loads, screw positions, gauges, and temperatures among other things, on a pass by pass basis, for both the roughing and finishing stands.

Of particular interest was the rolling load pattern over the final few passes. **Fig. 30** shows an example of the rolling loads for the finishing stand for a 3.1 m wide, 10 mm thick plate. The blue line represents the load measured by the stand load cells, while the orange line is the final scheduled load for each pass. The final scheduled load may not necessarily be the original load scheduled in the process control computer, but will include any adaptations made on-line as a result of gauge deviations from the initial predictions.

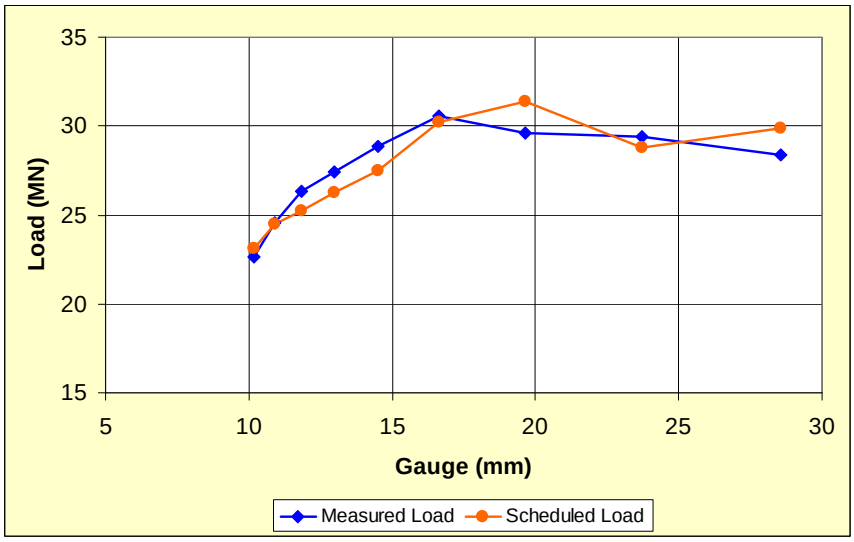


Fig. 30: Rolling loads on the finishing stand for plate number NZ653

The plate arrived at the finishing stand from the roughing stand with a gauge of about 29 mm. When the gauge reached 16.5 mm, the finishing load line was then followed (approximately) in order to produce a flat final plate at 10 mm gauge. The finishing load line can be plotted retrospectively as shown in **Fig. 31**. In this instance the measured and scheduled loads are reasonably close together, highlighted by the fact that the finishing load lines generated from the measured and scheduled loads are similar. The gradients of the two lines compare well - 1.16 for the measured loads and 1.03 for the scheduled loads. The intercepts are also in good agreement - 11.9 for the measured loads and 12.9 for the scheduled loads.

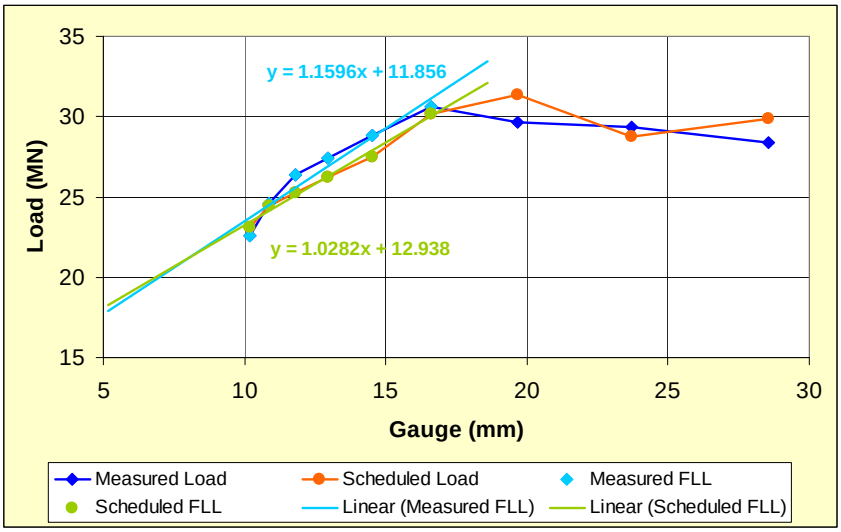


Fig. 31: Finishing load lines for plate number NZ653

The loads shown in **Fig. 30** indicate a plate that was rolled approximately as predicted and the outcome was a measured flatness that was fairly good with a maximum of ± 3 mm/m wave height. **Fig. 33** confirms the flatness that was measured. It is a construction of the Shohet and Townsend plate flatness calculation [5] where the orange line represents the difference in crown to gauge ratio between passes (crown in/gauge in - crown out/gauge out). The green line is the limit beyond which edge wave occurs, while the blue line defines the limit at which full centre will be present in the rolled plate.

Buckles or waves in a rolled plate are caused by a differential elongation of the plate across its width, see [4]. This elongation is directly related to the plate crown change during the pass reduction and is given by:

$$\delta = \frac{c_1}{h_1} - \frac{c_2}{h_2}$$

where

- δ = per-unit strip crown change
- c_1, c_2 = entry and exit plate crowns respectively
- h_1, h_2 = entry and exit plate thicknesses respectively.

When $\delta < 0$ the plate will tend to develop edge waves. Conversely, when $\delta > 0$ the plate will tend to develop center buckles. However, due to internal stresses, the deterioration of pate flatness does not occur as long as the values for the change in relative plate crown δ are within a certain range that is known as flatness dead band.

In the plate flatness model that was developed by Shohet and Townsend [5] and further studied by Somers, et a1. [6], the flatness dead band in hot rolling can be given by (**Fig. 32**):

$$-80\left(\frac{h_2}{w}\right)^a < \delta < 40\left(\frac{h_2}{w}\right)^b$$

According to Shohet and Townsend, for low carbon steel, a = b = 2, while Somers, et a1. had shown that
a = b = 1.86.

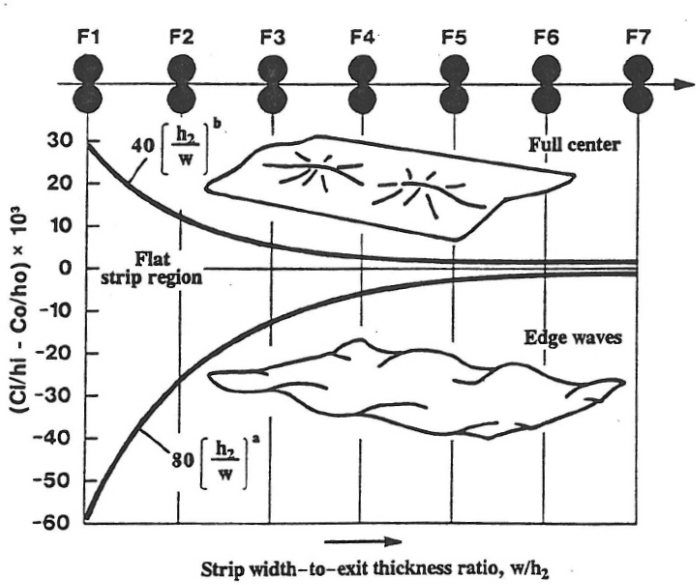


Fig. 32: Strip flatness dead band [4]

The fact that the plate finishes on pass 9 with the difference in crown to gauge ratio within the two limits, suggests that the final plate would have good flatness, **Fig. 33**.

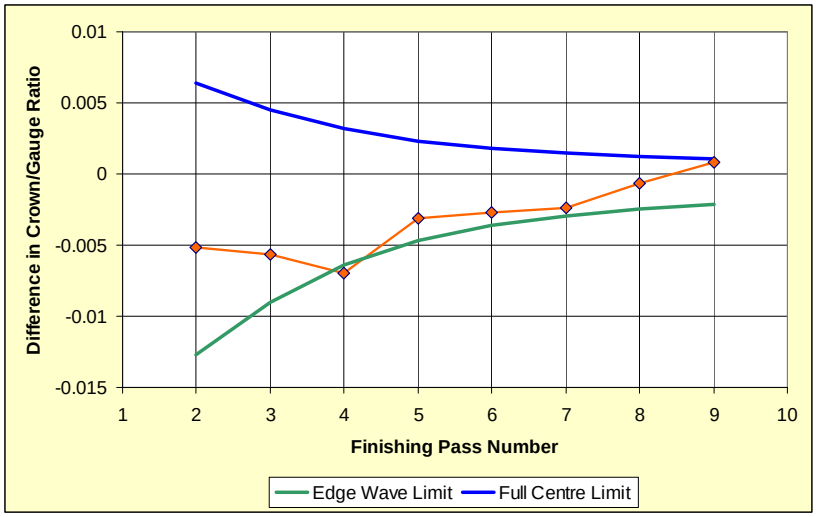


Fig. 33: Shohet and Townsend flatness calculation for plate number NZ653

An examination of the data for all the measured plates showed that the rolling load pattern for the finishing pass sequence was not always of a form that was likely to produce flat plates. For example, the load against gauge graph of **Fig. 34** for a 10 mm, 3.4 m wide plate, indicates an almost constant rolling load for the last few passes that was also relatively high. It is most unlikely that the original scheduled finishing load pattern would have been like this, although it was not possible to retrieve the original finishing load pattern in order to check. It is probable that gauge or temperature measurements made during the rolling process resulted in the scheduled load being updated on-line. However, this updated schedule would be expected to be detrimental to the flatness of the plate.

This is confirmed by the actual flatness measurements made on the plate which indicated very wavy edges of the order of 25 to 30 mm/m height, and also by **Fig. 35**, which shows that the difference in crown to gauge ratio is well outside the edge wave limit.

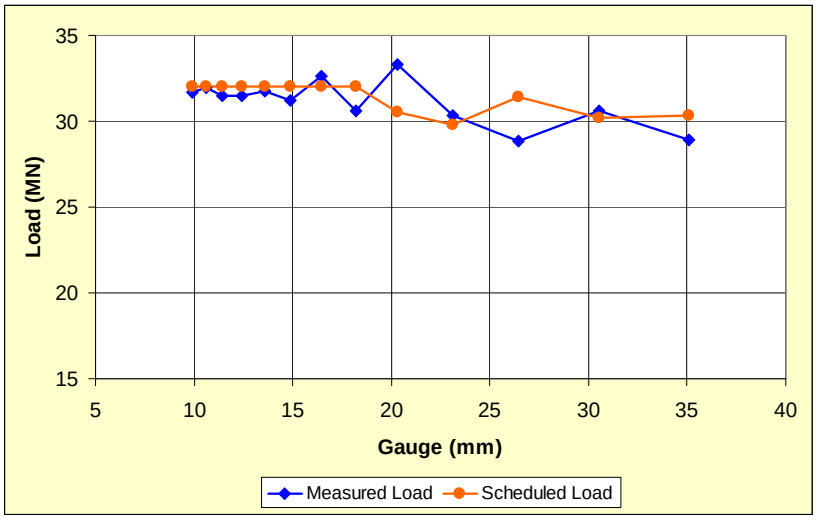


Fig. 34: Rolling loads on the finishing stand for plate number RA991



Fig. 35: Shohet and Townsend flatness calculation for plate number RA991

The loads plotted in **Fig. 36** were for an 8 mm plate that was 3 m wide, and illustrate a different pattern of finishing loads that will also tend to result in poor flatness. The loads decrease at a reasonable rate for the first part of the finishing load line down to a gauge of about 11 mm, but from that point on, the loads decrease at an increasing rate. Decreasing the load at an increasing rate is likely to cause the central region of the plate to be over rolled and result in a full centre flatness defect.

Again this is confirmed by both the actual measurement of the plate itself, with centre buckles of approximately 15 mm/m height, and by the difference in crown to gauge ratio plotted in **Fig. 37**, which finishes well outside the full centre limit.

As has already been mentioned, it has not been possible to examine the original pass reduction schedules that were generated and the scheduled loads that are presented here are those that could have been modified on-line during the rolling itself. Therefore, it is not possible to assess the effectiveness of the original schedules, but clearly, there is an opportunity to improve the way the schedules are adjusted on-line at the very least. Unfortunately, the Corus RD&T off-line model does not have the capability to simulate on-line changes to the roll pass schedules. However, it was possible to use the model with the measured data available to predict alternative pass schedules and this is described in the following section.

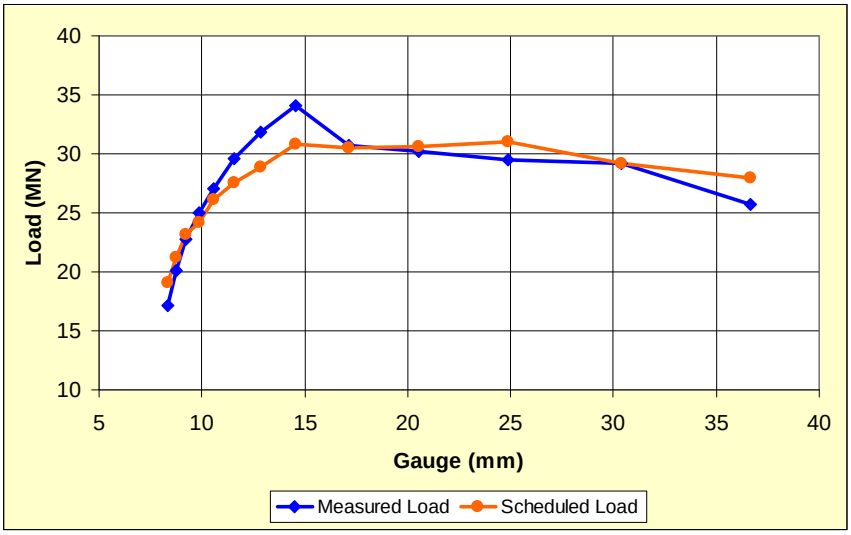


Fig. 36: Rolling loads on the finishing stand for plate number RA875

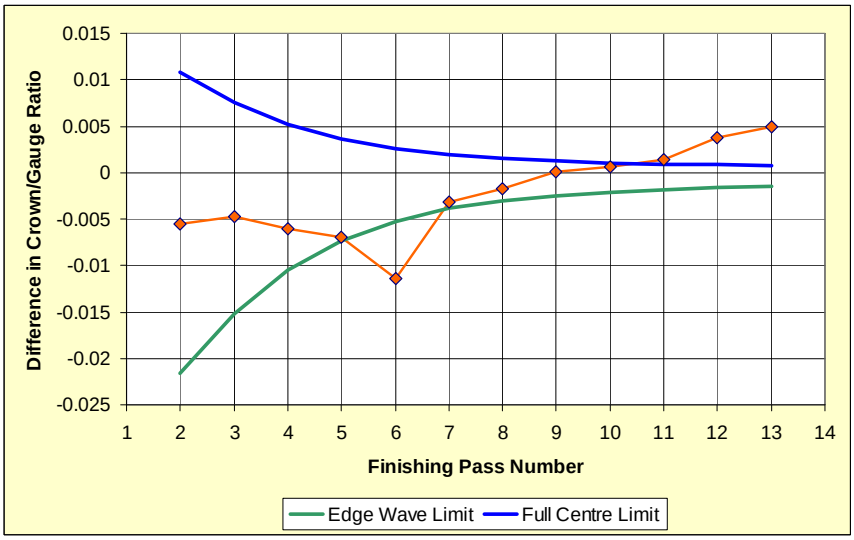


Fig. 37: Shohet and Townsend flatness calculation for plate number RA875

At the **TKS Plate Mill** plate flatness calculations following the method of Shohet and Townsend [5] have been performed too. The calculations are based on the measured rolling forces and the stand deflection model developed in [2], see **Fig. 38**. The calculation results are compared with the measured flatness at the entry of the hot leveller.

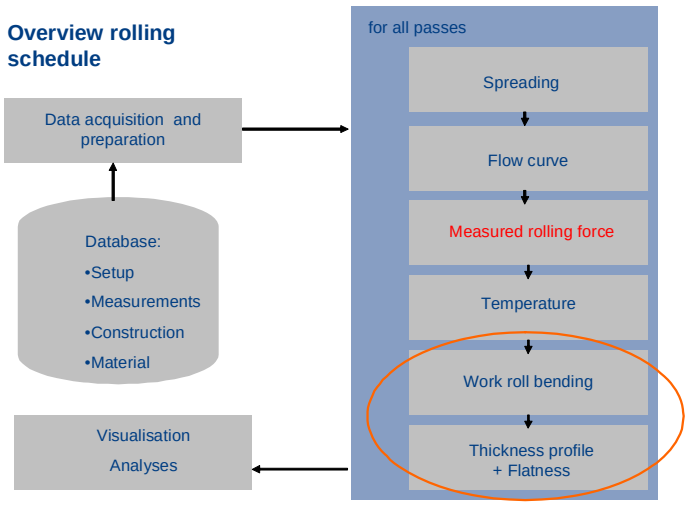


Fig. 38: Data flow and modules of the stand deflection model

Fig. 39 shows as an example the presentation of the results. The calculated plate crown changes during the pass reduction of the last 6 rolling passes is in the middle of the flatness dead band, suggesting that the final plate would have good flatness. This result of calculation fits to the measured flatness before the hot leveller, also presented. The measurements show height deviations in the range of about +/- 3 mm. The structure of the plate topography is comparable to an unwindable defect characterised by wave length and amplitude, **Fig. 21**. With respect to the rolling process this kind of defect is mainly influenced by

- the temperature gradient across the thickness of the plate,
- the speed behaviour of the mill (upper and lower work roll) and
- the pass-line.

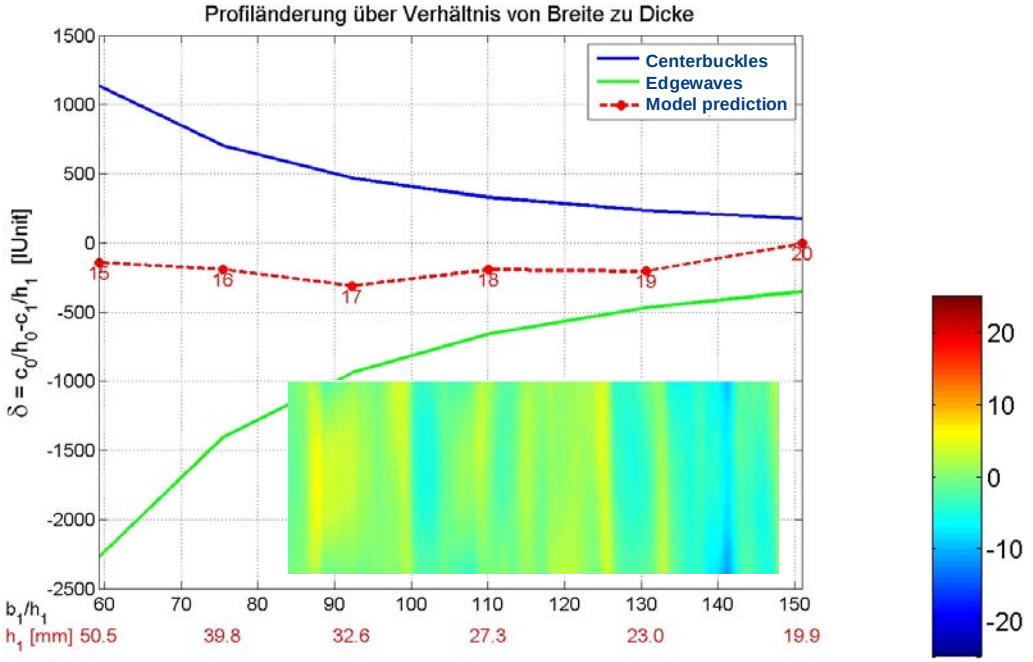


Fig. 39: Comparison of the Shohet and Townsend flatness calculation with the measured flatness before the hot leveller for plate number 70569 (scale of pseudo-colours in mm at the right)

Fig. 40 shows as another example. The calculated plate crown change during the pass reduction of passes 12, 14 and 15 is near or below the lower limit of the flatness dead band where the plate tends to develop edge waves.. This result of calculation fits to the measured flatness before the hot leveller, also presented. The measurements show edge waves in the range of about +/- 10 mm. The structure of the plate topography is comparable to a non-unwindable defect characterised by the distribution of fibre length across the width of the plate, **Fig. 21**. With respect to the rolling process this kind of defect is mainly influenced by the differences between

- the entry plate profile and
- the roll gap profile.

Fig. 41, **Fig. 42** show similar results as **Fig. 40**.

Fig. 43 shows a similar result as **Fig. 39**. The calculated plate crown change during the pass reduction of the last 6 rolling passes is in the middle of the flatness dead band, except the final pass, where the calculated plate crown change is above the upper limit of the flatness dead band, suggesting that the final plate would have center buckles. The measurements show continuous change of the height from the head end to the tail end of the plate in the range of about 10 mm, which may be caused by temperature differences. These “macro”-structure of the plate topography is superimposed by slight center buckles.

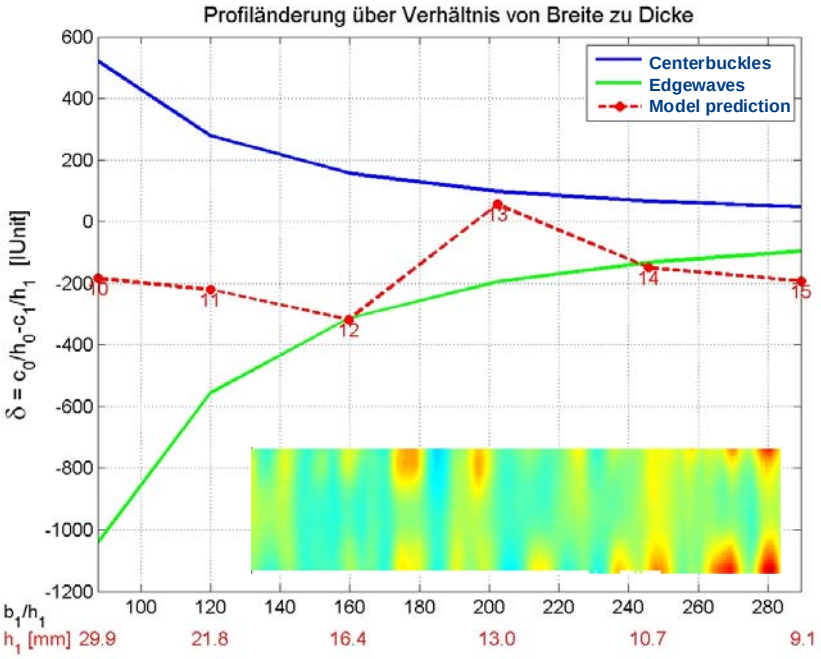


Fig. 40: Comparison of the Shohet and Townsend flatness calculation with the measured flatness before the hot leveller for plate number 82487

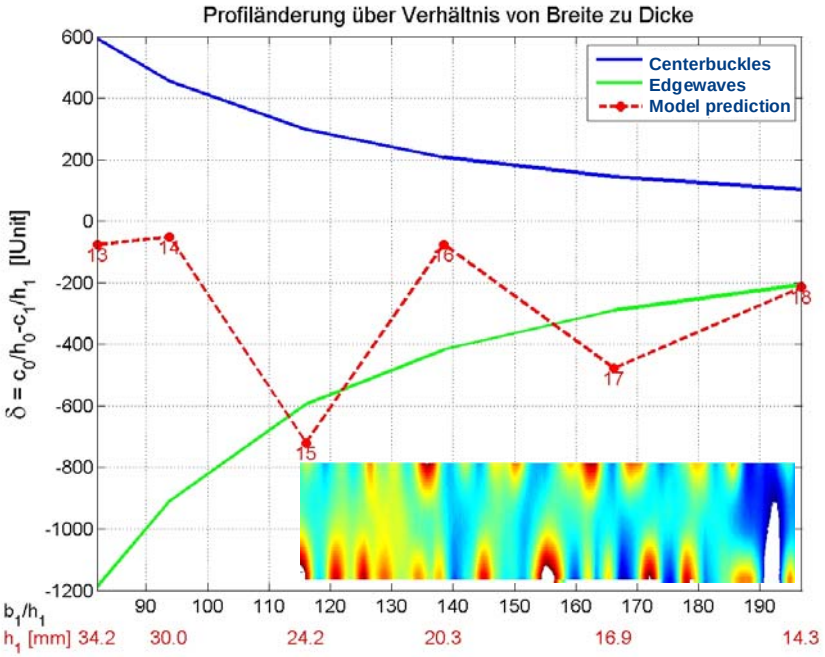


Fig. 41: Comparison of the Shohet and Townsend flatness calculation with the measured flatness before the hot leveller for plate number 86606

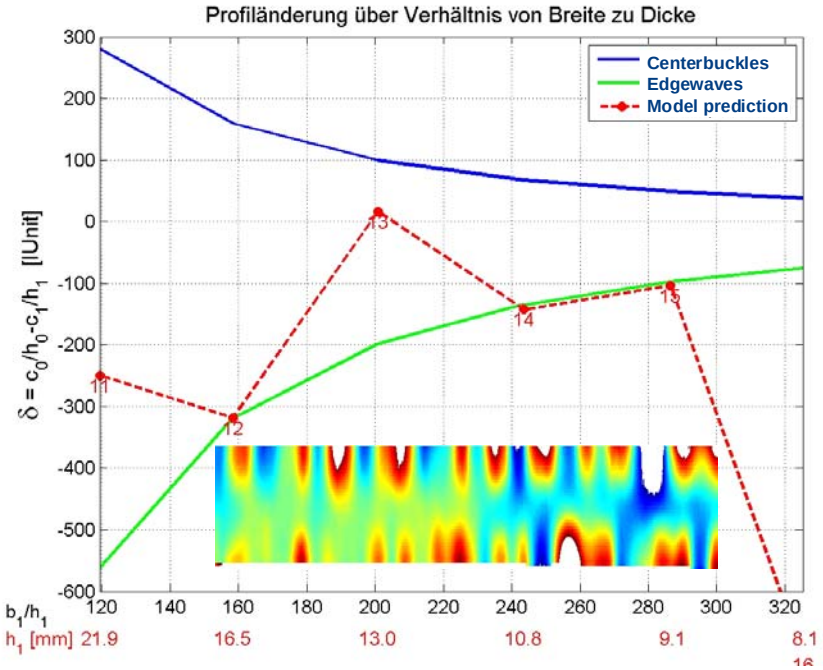


Fig. 42: Comparison of the Shohet and Townsend flatness calculation with the measured flatness before the hot leveller for plate number 82475

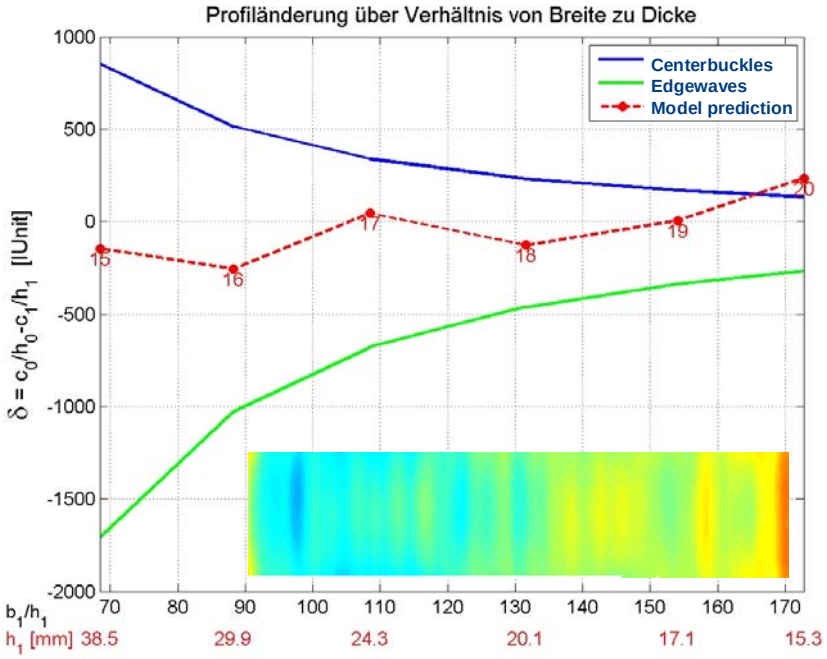


Fig. 43: Comparison of the Shohet and Townsend flatness calculation with the measured flatness before the hot leveller for plate number 84487

Fig. 44 shows similar results as **Fig. 43**.

Fig. 45 shows a remarkable behaviour. The calculated plate crown change is in the passes 13, 14, 15 to some extend significantly below the lower limit of the flatness dead band, only in the final pass the plate crown change is above the upper limit. The tendency to generate wavy edges is determined in the passes 13 and 14 passed on to the final pass.

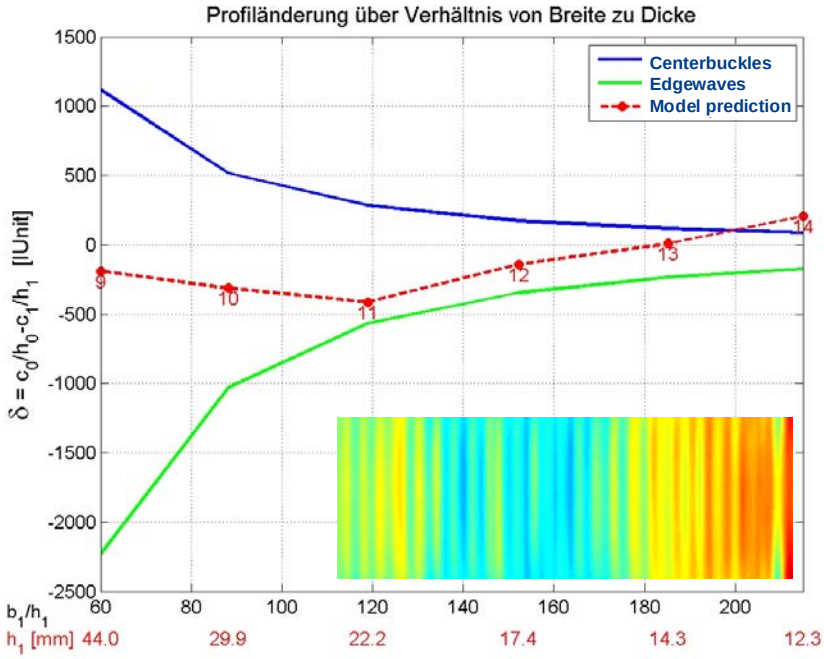


Fig. 44: Comparison of the Shohet and Townsend flatness calculation with the measured flatness before the hot leveller for plate number 82393

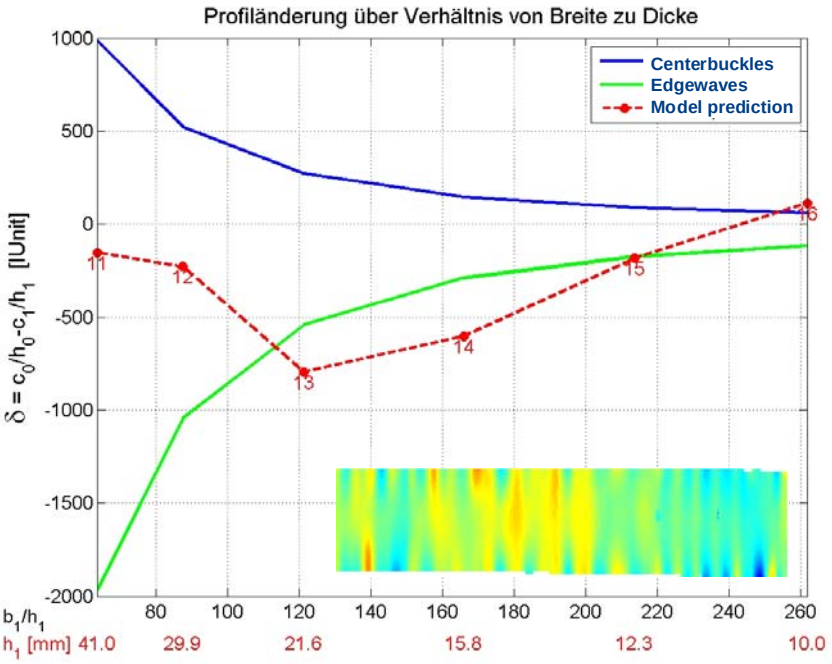


Fig. 45: Comparison of the Shohet and Townsend flatness calculation with the measured flatness before the hot leveller for plate number 85149

Fig. 46 shows extreme oscillation of the calculated plate crown change in the passes 16, 17 and 18, where the huge amount of the calculated plate crown change in the final pass is responsible for the generated center buckles.

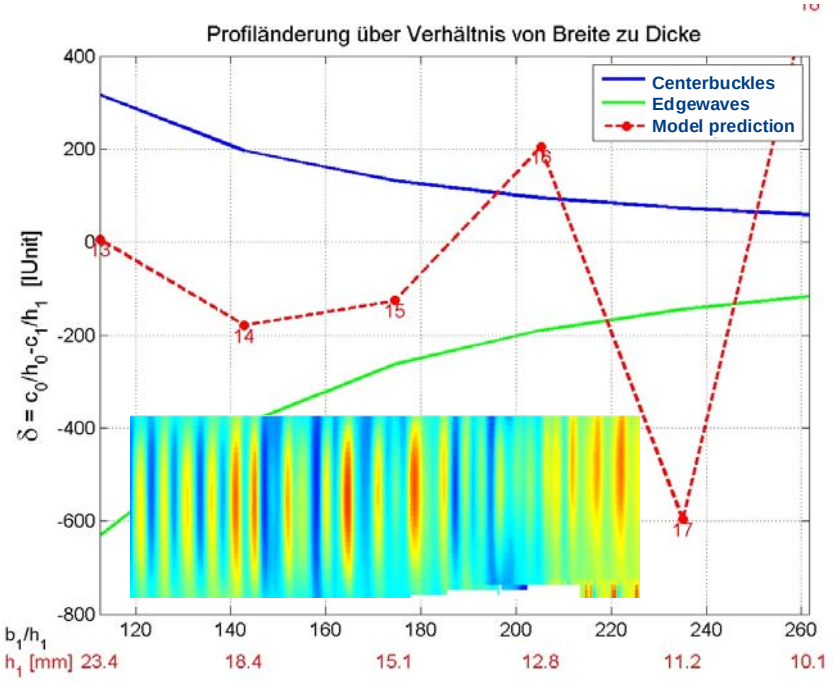


Fig. 46: Comparison of the Shohet and Townsend flatness calculation with the measured flatness before the hot leveller for plate number 85145

Task 2.3 Rolling schedule optimisation

At the **HPM of ArcelorMittal Spain** the final stage of plate rolling could be performed following different strategies/theories. Within this project, the targeting for constant relative plate crown is studied, because it's the more related with the plate flatness. To fabricate a plate free of flatness defects depends on the application of a correct pass schedule. It was demonstrated by several authors that a good plate shape can be achieved through the maintenance of a constant crown difference/thickness difference ratio between two subsequent passes, that is, when the relative shape does not change from pass to pass. Nowadays, most pass scheduling models still follow this principle. The plate mill facility of ArcelorMittal at Veriña has implemented four years ago a new rolling model from Siemens/VAI. This model includes different strategies for the last rolling phase, being the more interesting from the flatness point of view, the maintenance of the constant relative plate crown.

According to this model, for rolling a flat plate the relative plate crown (p=P/h) should be kept constant during the last final passes (where P is the absolute crown and h is the plate thickness). The absolute crown P depends on the roll force and the roll contour and can be calculated as P=α*(F-F0), being F0 the force required to get zero crown over the plate width and α describing the stiffness of the roll stack.

Keeping the relative plate crown p constant means p= α*(F-F0)/h which is equivalent to F=h*p/α+F0, thus the final passes have to lie on a straight line passing through F0 at h=0. (see **Fig. 47**). So, the final plate crown is determined by P=α*(F-F0). According to this model, a high roll crown causes a high F0 and low plate crown. In case F0 exceeds the maximum possible force the calculated schedule will have rising roll force at the end and the plate will have negative crown. The force F0 at which the roll gap crown over the plate width gets zero depends on several variables like: Work and back-up roll grinding crowns, rolls thermal crowns, Work roll wear, Plate width, etc.

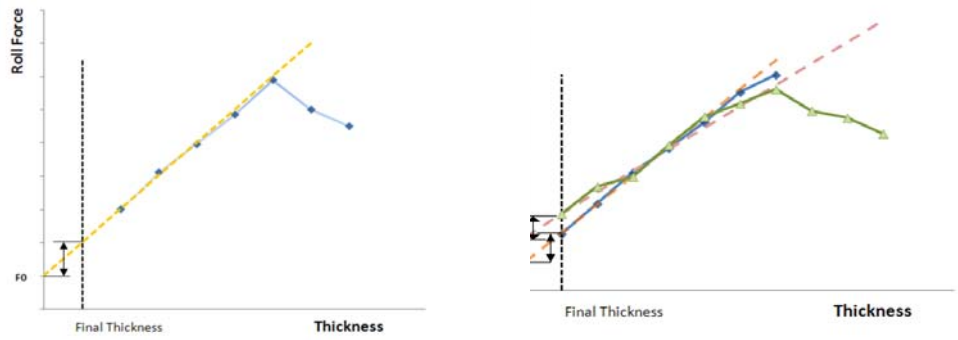


Figure a

Figure b

Fig. 47: Pass schedule philosophy and influence of CORRF0

The rolling model calculates the best pass distribution to obtain good plate flatness, additionally there is a profile adaptation introduced by the mill operator, via the user interface (variable CORRF0), that is superimposed to the calculation and thus directly influences F0. By changing F0 the passes will be distributed in a different way (different slope, different last pass force), see **Fig. 47 b**. This will also affect the final plate crown. This correction represents the subjective opinion of the mill operator respect the plate flatness being obtained, according to his experience and can be therefore considered as a subjective measurement of the flatness.

The approach followed to try to develop a statistical model for the estimate of flatness to be obtained is to use the flatness corrections made by the operators in those cases where the strategy followed by the process model is to keep the relative crown constant (this strategy is called “Strategy 32” in the model) and discarding for the analysis plates rolled following other strategies. The strategy 32 is schematically shown in **Fig. 48**.

After selecting a large group of plates rolled under strategy 32, different hybrid techniques were tested in order to develop a model that can input a corrective reference for the next pass set-up emulating the corrections that the operator would have tried to introduce. The great advantage of using hybrid techniques is the fact that there is no need to develop an algorithm to calculate the parameters being modelled, in this case, the F0 and FLAST corrections. These techniques can extract the necessary knowledge from different process variables and the manual actuations of the operators. They can "learn" the specific rules automatically from a data set containing the association of the real applied rolling process parameters and the real plate characteristics obtained. Additionally, these techniques should be able to perform an automatic retuning on-line, using a continuous learning strategy, without the need of periodical re-training the model. Intelligent modelling techniques are quite usual nowadays (Neural Networks, Fuzzy Logic, Genetic Algorithms, …) and they have demonstrated their benefits over manufacturing process lot of times, but the real challenge is avoiding of periodical training to be the model fitted.

A significant part of the work done was devoted to analyze the influence of the roll stack characteristics on the corrections introduced in the target variables CORRF0 and CORRFLAST. Analyses of the corrections introduced during several rolling campaign (number of plates rolled by a given pair of work rolls since they were installed in the mill until they were replaced by a new set) were performed and graphics like the one showed in **Fig. 49** were obtained.

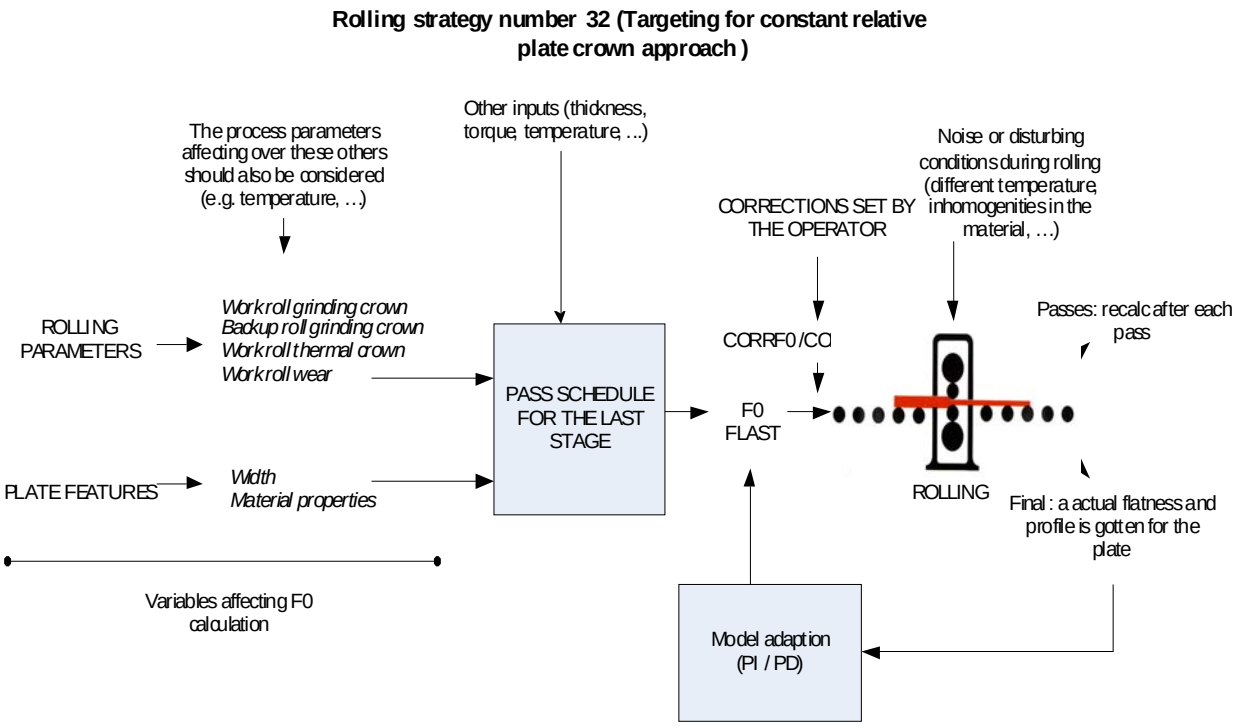


Fig. 48: Schematic functionality of rolling strategy 32

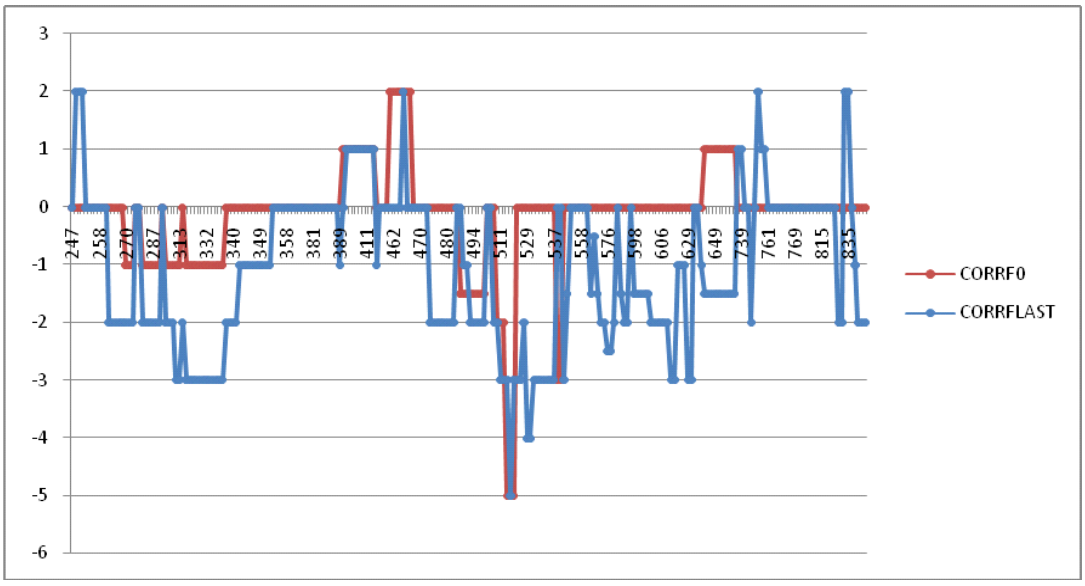


Fig. 49: Corrections on CORRF0 and CORRFLAST Vs plate number for the work roll pair

Also, matrix of correlations, like the one showed in **Fig. 50** were done in order to evaluate correlations among different variables related to the rolls, like grinded roll crowns, tonnage rolled, length rolled, dimensions of the plates, time the rolls were installed and removed from the mill, etc. Using this technique allows a quick visualization of which variables should be used in further analyses or discarded.

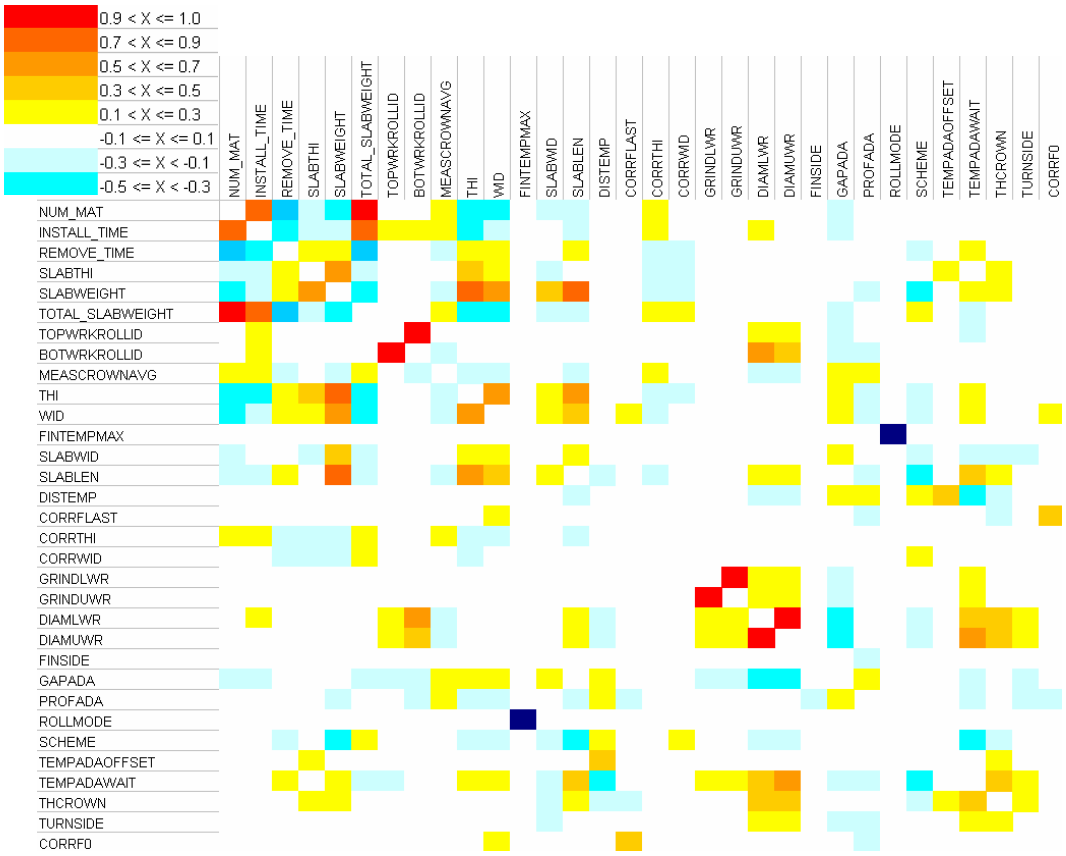


Fig. 50: Correlation matrix

In this matrix, it can be seen the correlation existing between CORRF0, CORRFLAST and WID, and the inverse correlation between CORRF0 and PROFADA, which means that corrections introduced by the operators do not follow corrections made by the process model, among other interesting correlations.

Similar analyses done for other variables showed the correlation among CORRF0 and CORRFLAST with the number of passes given to each plate NOOFPASSES. To perform a deeper analysis of these correlations; plates were sorted according the number of passes in different group ranging from 8 to 24 passes. Among these groups those that gave more interesting results were 8, 10, 12, 14, 16 and 18 passes.

The following analyses for this group of plates (16 passes) were oriented to determine in which of the 16 passes the fourth rolling phase start, where flatness constraints are applied. This lead to sort these plates in new 7 groups corresponding to plates where the 4th rolling phase starts at the 5 th to the 12th pass. For each plate of these groups was graphically analyzed the differences among the calculated and measured rolling forces for each pass. **Fig. 51** shows two different plates.

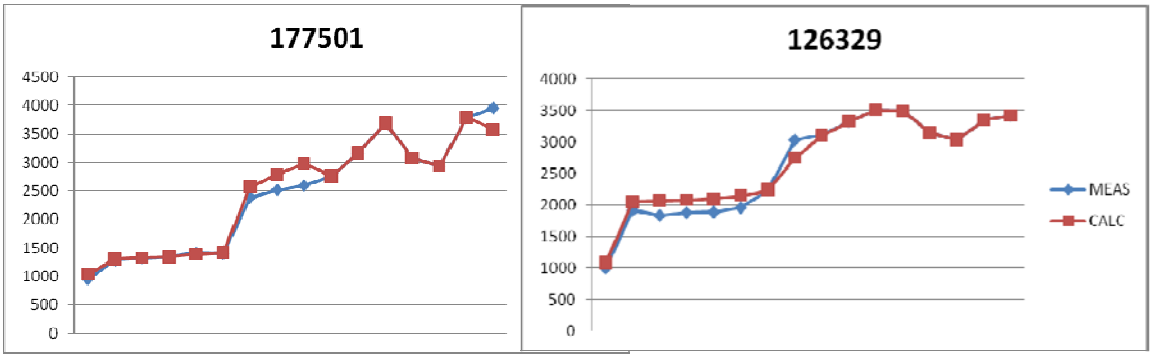


Fig. 51: Measured Vs predicted rolling forces at each pass

As result of these analyses arose the conclusion that the value of the variable CORRFLAST influences the shape of the curve that represents the average rolling force measured and calculated by the rolling model for the passes of each piece.

The next step was to evaluate the behaviour of the forces distribution for similar plates, rolled with same pair of work rolls but with different values of CORRFLAST. The analyses were done for several groups of plates being each group constituted by plates rolled in the same number of passes and where in each group the last rolling phase started at same pass number. As an example of the analyses done, the results for plates rolled in 16 passes (612 plates), where the fourth rolling stage started at pass 8 will be shown.

Fig. 52 shows a group of 11 plates rolled with the pair of work rolls 224-225, with values of CORRFLAST= 3 and CORRF0=5. As it can be seen, the averaged forces of each pass are quite similar for all plates, but for two of them 168297 and 168298 that were rolled near 40 plates later than the last of the homogeneous group.

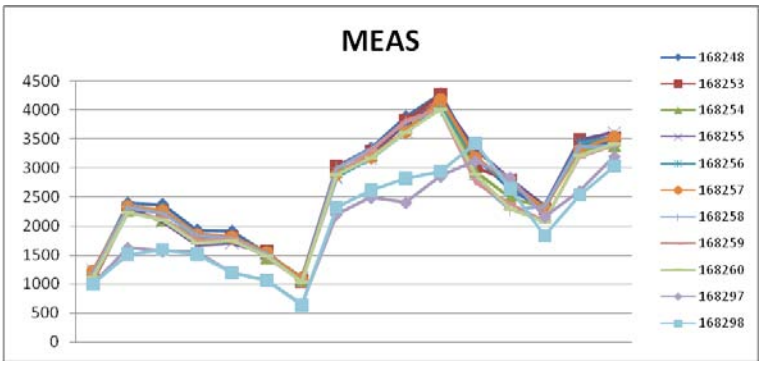


Fig. 52: Plates rolled with the work roll pair 224-225 and CORRFLAST=3

When analyzing the curves that compare the calculated forces and real forces for each pass it was found, that both forces were quite similar as seen here for plate 168297, **Fig. 53**.

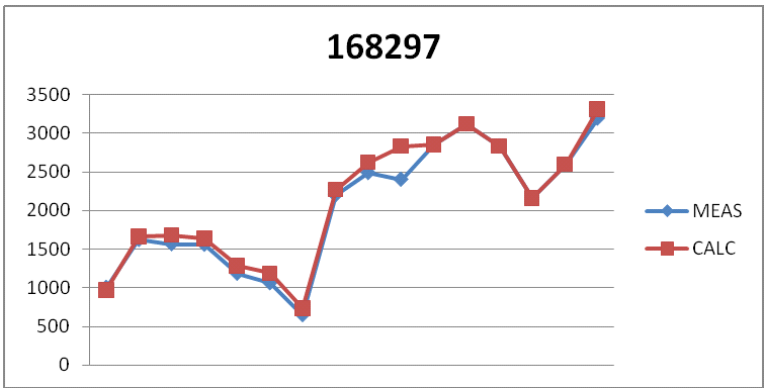


Fig. 53: Calculated and real forces for the 16 passes of plate 168297

Fig. 54 shows another group of plates of same characteristics but where CORRFLAST took values among 9 - 9.5. As it can be seen the curves are very different to those showed previously.

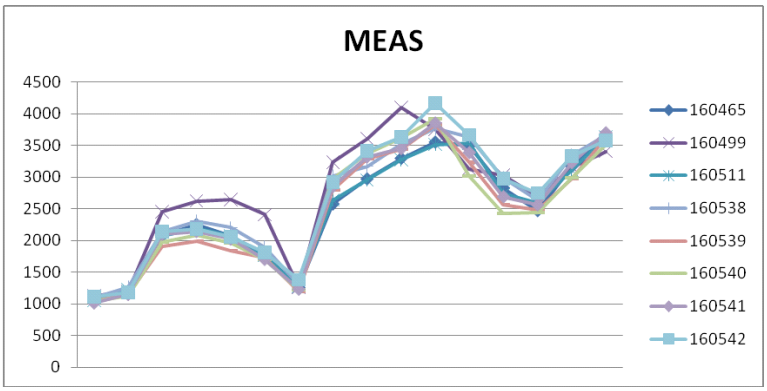


Fig. 54: Plates rolled with the work roll pair 224-225 and CORRFLAST=9 to 9.5

For another group of plates rolled with the work roll pair 280-281, values of CORRF0=4-5 and CORRFLAST=3, the results doing the same analyses are shown in **Fig. 55**.

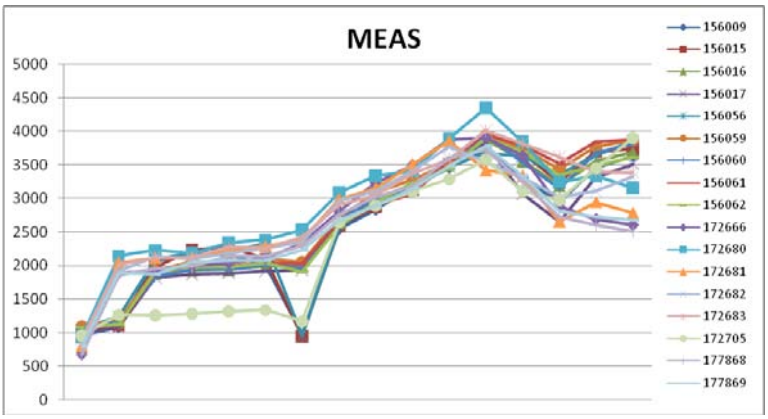
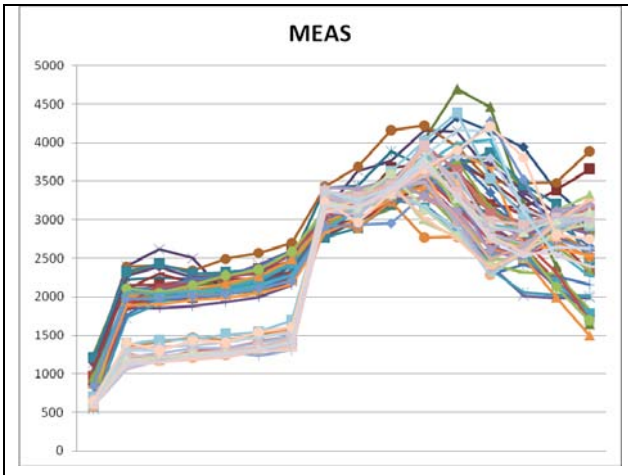
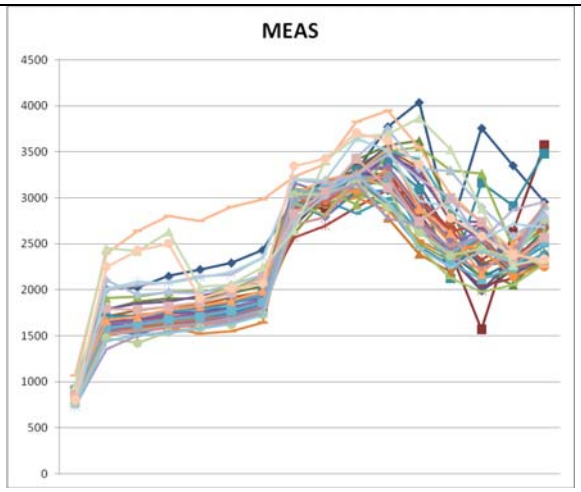


Fig. 55: Plates rolled with the work roll pair 280-281 and CORRFLAST=3

In order to evaluate the influence of the work rolls on forces distribution in the rolling passes, all plates of similar characteristics rolled by each pair of work rolls during its campaign were represented together. **Fig. 56** shows the results obtained for roll pair 224-225 and those obtained for the roll pair 278-279.



Similar plates rolled with rolls 224-225



Similar plates rolled with rolls 278-279

Fig. 56: Influence of the work rolls on forces distribution

Some correlation has been found among the plates with lower rolling forces correspond to plates rolled closer to the end of the campaign. Main conclusions obtained till this moment were that the values of forces at each pass are influenced by the variable CORRFLAST and by the roll pair and the moment in the roll campaign in which the plate is rolled, which is function of the roll wear and equivalent roll crown.

Based on these studies, it was found that each team uses their own criteria, so the operation of the rolling mill is highly dependent of the human factor (As represented within the quartile graph for the correction applied by each team). Therefore, the plate flatness is also very influenced by the human factor.

Due to the importance of rolls more variables were introduced including diameters and roll crown as well as more variables related to the steel composition, **Table 7**.

Data were filtered and some attributes were eliminated obtaining a new data set with 8717 plates and 66 attributes. In the correlation graph it is evident the important relationship of some variables, **Fig. 57**.

Table 7: Extended set of variables

Attribute Name	Comment	Attribute Name	Comment
STARTPRODTIM	Date of first pass	**PB**	Percent of Pb in the alloy
INSTALLTIME	Data/time of installation	**MG**	Percent of Mg in the alloy
REMOVETIME	Data/time of removal	**MN**	Percent of Mn in the alloy
TOPCENTERDIA	Diameter at half of the barrel	**MO**	Percent of Mo in the alloy
TOPCOREDIA	Diameter of core = inner roll	**N**	Percent of N in the alloy
TOPCROWN	Crown at the centre of roll [µm]	**NB**	Percent of Nb in the alloy
BOTCENTERDIA	Diameter at half of the barrel	**NI**	Percent of Nil in the alloy
BOTCOREDIA	Diameter of core = inner roll	**O**	Percent of O in the alloy
BOTCROWN	Crown at the centre of roll [µm]	**P**	Percent of P in the alloy
AL	Percent of Al in the alloy	**S**	Percent of S in the alloy
ARS	Percent of Arsl in the alloy	**SI**	Percent of Si in the alloy
B	Percent of B in the alloy	**SB**	Percent of Sb in the alloy
BI	Percent of Bl in the alloy	**SN**	Percent of Sn in the alloy
C	Percent of C in the alloy	**TA**	Percent of Ta in the alloy
CA	Percent of Ca in the alloy	**TI**	Percent of Ti in the alloy
CR	Percent of Cr in the alloy	**W**	Percent of W in the alloy
CO	Percent of Co in the alloy	**V**	Percent of V in the alloy
CU	Percent of Cu in the alloy	**ZN**	Percent of Zn in the alloy
H	Percent of H in the alloy	**ZR**	Percent of Zr in the alloy

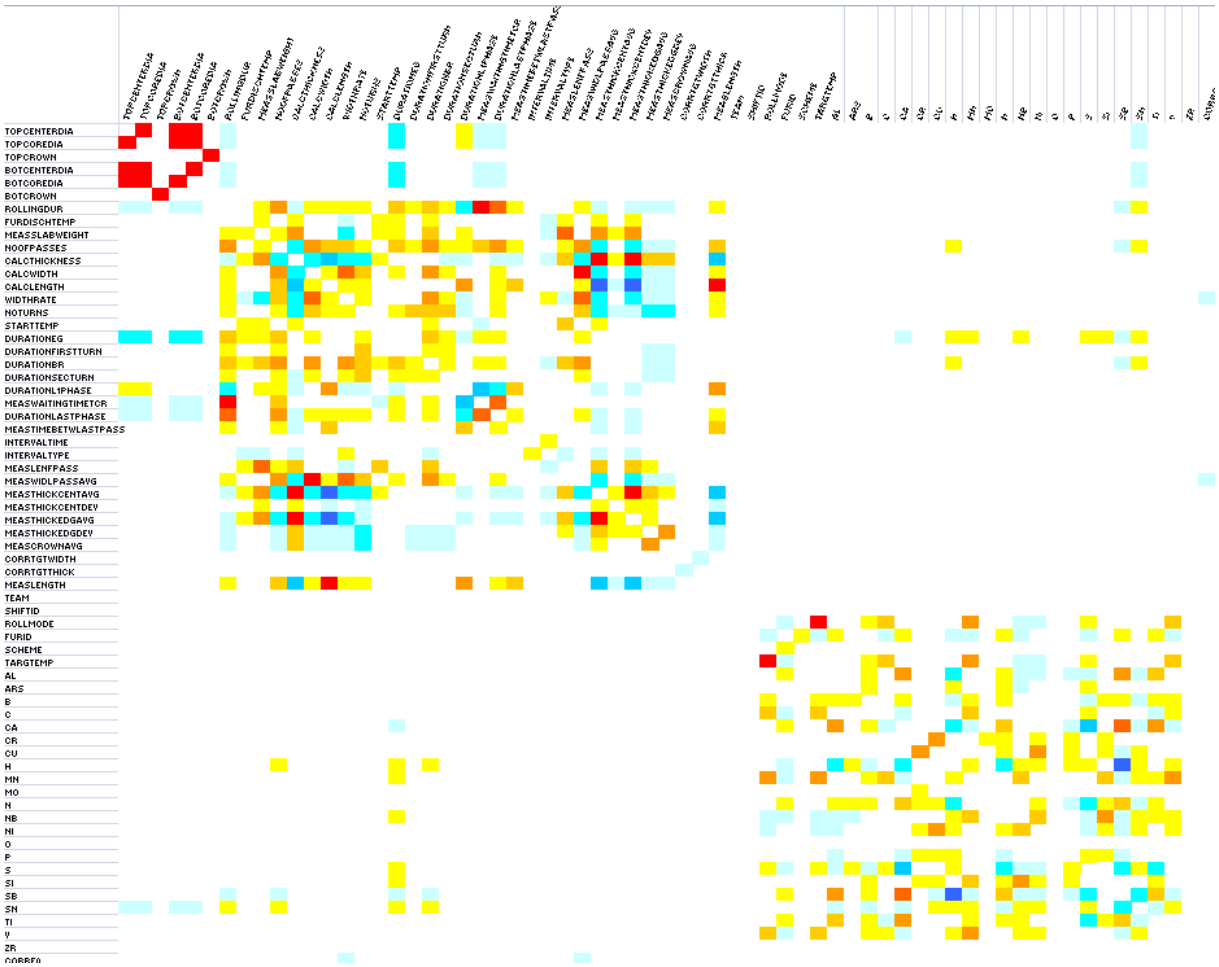


Fig. 57: Correlation matrix

The most significant correlations are presented in **Table 8**. Results show that the relationship between the data of upper and lower rolls is so high that it is not necessary to introduce them all, especially considering the negative effect of the increment of the dimension of the input space on the model performance.

Table 8: Highest correlations

ATTRIBUTE1	ATTRIBUTE2	CORRELATION	ATTRIBUTE1	ATTRIBUTE2	CORRELATION
TOPCROWN	BOTCROWN	1.00000	CALCWIDTH	WIDTHRATE	0.73005
BOTCENTERDIA	BOTCOREDIA	0.99982	MEASWAITINGTIMETCR	DURATIONLASTPHASE	0.72251
TOPCENTERDIA	TOPCOREDIA	0.99966	MEASSLABWEIGHT	MEASLENFPASS	0.71880
CALCTHICKNESS	MEASTHICKCENTAVG	0.99638	CU	NI	0.68432
CALCWIDTH	MEASWIDLPASSAVG	0.99518	NOOFPASSES	DURATIONBR	0.66660
ROLLMODE	TARGTEMP	0.98697	ROLLINGDUR	NOOFPASSES	0.66467
CALCLENGTH	MEASLENGTH	0.98599	NOOFPASSES	DURATIONLASTPHASE	0.63739
TOPCENTERDIA	BOTCENTERDIA	0.98440	CALCWIDTH	DURATIONBR	0.63691
TOPCOREDIA	BOTCOREDIA	0.98426	DURATIONBR	MEASWIDLPASSAVG	0.63215
TOPCOREDIA	BOTCENTERDIA	0.98418	MN	V	0.61211
TOPCENTERDIA	BOTCOREDIA	0.98399	CALCTHICKNESS	MEASLENGTH	-0.69116
MEASTHICKCENTAVG	MEASTHICKEDGAVG	0.95269	MEASTHICKCENTAVG	MEASLENGTH	-0.69542
CALCTHICKNESS	MEASTHICKEDGAVG	0.95083	MEASTHICKEDGAVG	MEASLENGTH	-0.69542
ROLLINGDUR	MEASWAITINGTIMETCR	0.93610	CALCTHICKNESS	CALCLENGTH	-0.69740
CA	SB	0.80110	CALCLENGTH	MEASTHICKCENTAVG	-0.70150
ROLLINGDUR	DURATIONLASTPHASE	0.79753	CALCLENGTH	MEASTHICKEDGAVG	-0.70266
WIDTHRATE	MEASWIDLPASSAVG	0.74135	H	SB	-0.71579

At **Scunthorpe Plate Mill** the application Scheduler [7] was used to generate recommended rolling schedules for plates for which flatness measurements had been obtained. The simulations covered processing in the finishing stand, starting from the same initial plate dimensions and temperature as recorded during rolling. Examples are given below.

Pass schedules recorded for flat plates RA300 and NZ653 were close to those recommended by Scheduler and are shown in **Fig. 58** and **Fig. 59**. The Shohet and Townsend calculations indicated good flatness for both plates.

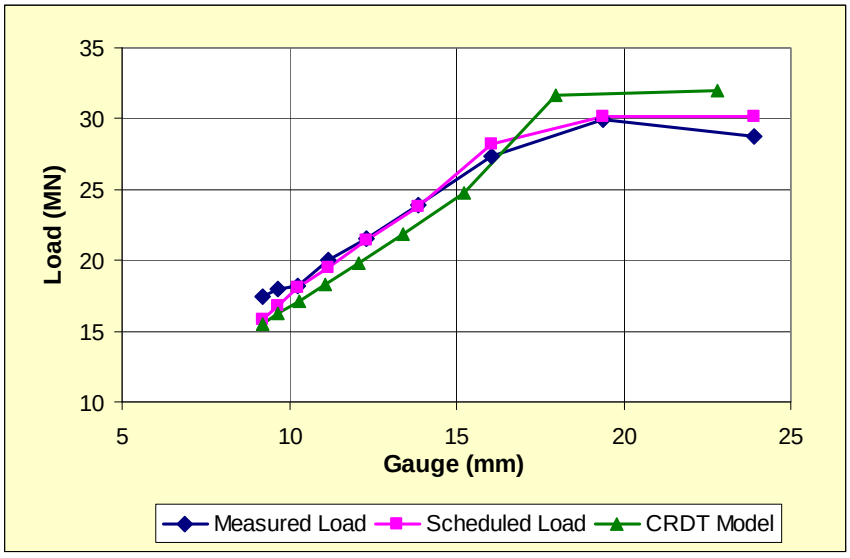


Fig. 58: Comparison of actual pass sequence with Scheduler prediction for plate RA300 [Plate dimensions: gauge 9 mm, width 3.2 m, CMn grade]

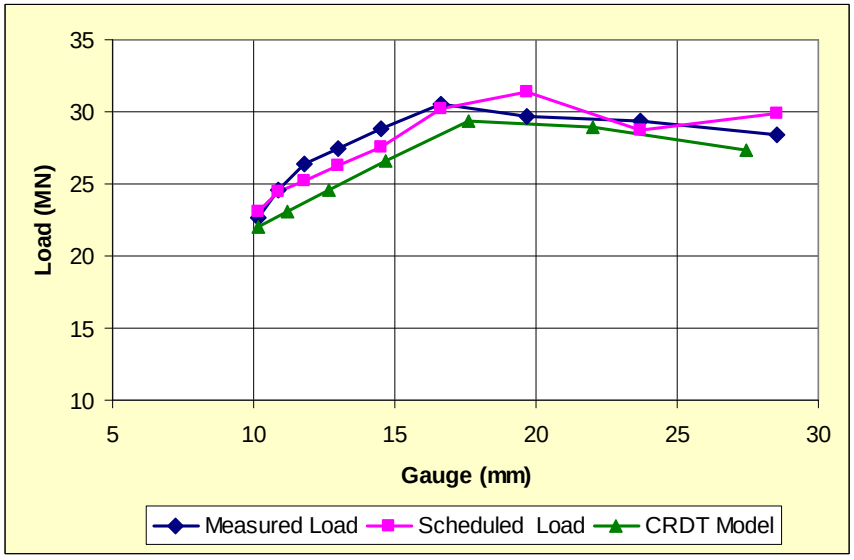


Fig. 59: Comparison of actual pass sequence with Scheduler prediction for plate NZ653 [Plate dimensions: gauge 10 mm, width 3.15 m, CMnNb grade]

The recorded pass sequence for plate RA875 differed significantly from that predicted by Scheduler, in that the gradient of the FLL increased continually in the later passes, as shown in **Fig. 60**. As reported previously, this resulted in the full centre flatness defect that was measured. In contrast, the schedule calculated by Scheduler is predicted to generate a flat plate, as shown in **Fig. 61**. Departure from the standard straight FLL was most likely caused by on-line corrections due to load and/or gauge errors, thus necessitating the re-computation of the schedule for the remaining passes. A sudden steepening of the FLL at the end of the schedule also led to measured (and predicted) centre buckle defects on plate RA703, as shown in **Fig. 62** and **Fig. 63**.

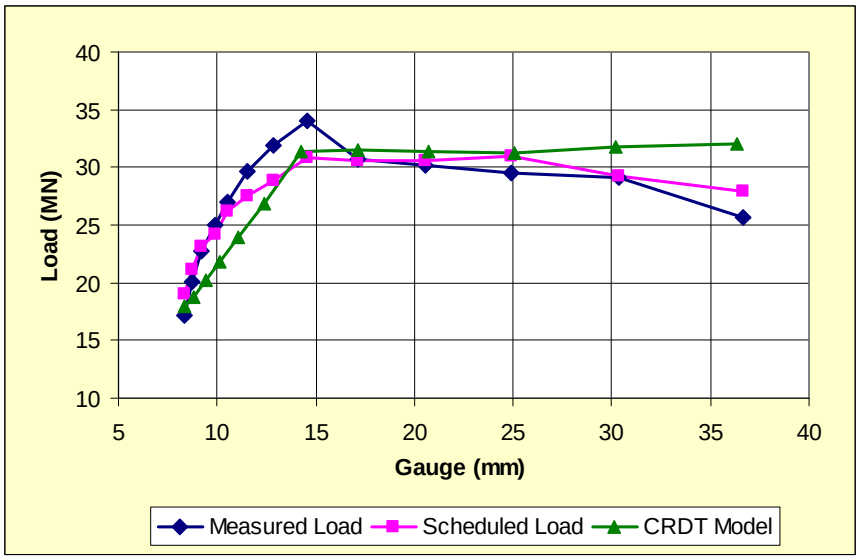


Fig. 60: Comparison of actual pass sequence with Scheduler prediction for plate RA875 [Plate dimensions: gauge 8 mm, width 3 m]

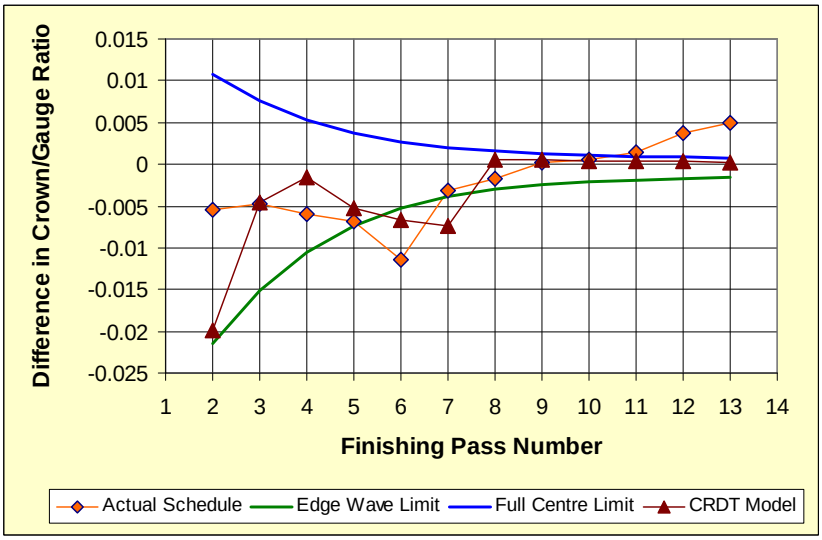


Fig. 61: Comparison of Shohet and Townsend flatness calculations for plate RA875

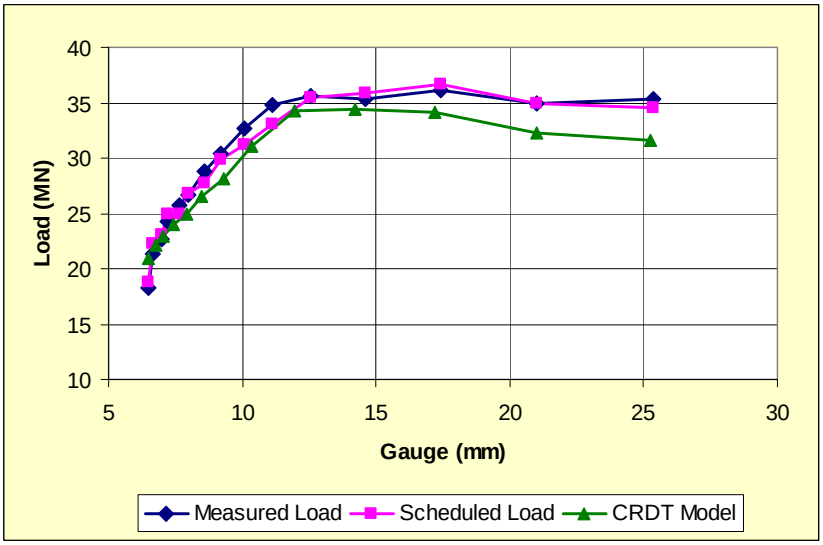


Fig. 62: Comparison of actual pass sequence with Scheduler prediction for plate RA703 [Plate dimensions: gauge 6.5 mm, width 3.2 m]

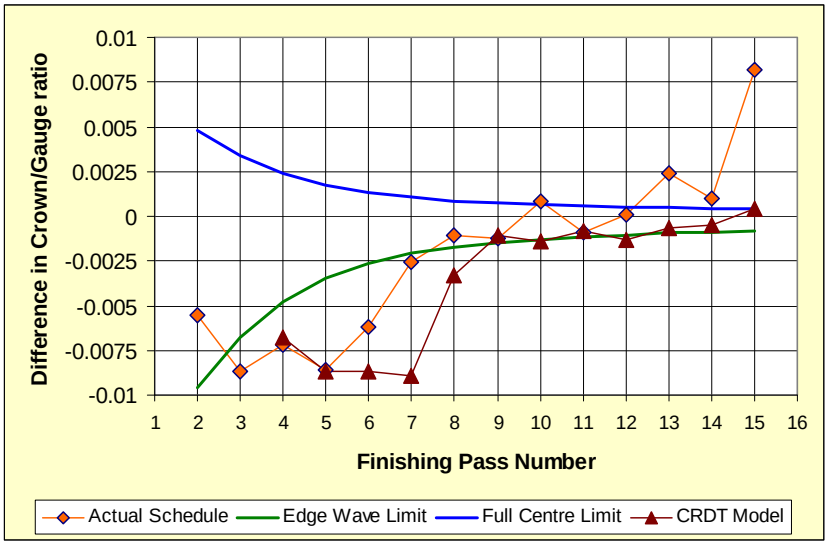


Fig. 63: Comparison of Shohet and Townsend flatness calculations for plate RA703

For plate RA991, the recorded schedule bore no resemblance to the standard pattern, with all 13 passes rolled at a near constant load. The RD&T off-line model did generate a predicted schedule with a suitable FLL, using 17 rather than 13 passes, a shown in **Fig. 64**. As reported in the previous section, the consistently high load in the final passes gave rise to the edge wave defects that were measured. In contrast, the schedule calculated by "Scheduler" is predicted to generate a flat plate, as illustrated in **Fig. 65**. Note that for ease of comparison, only the final 12 RD&T predicted finishing passes are shown. As before, departure from the standard straight FLL was most likely caused by on-line corrections due to load and/or gauge errors. Strategies for optimum recalculation of schedules part way through rolling merit further investigation.

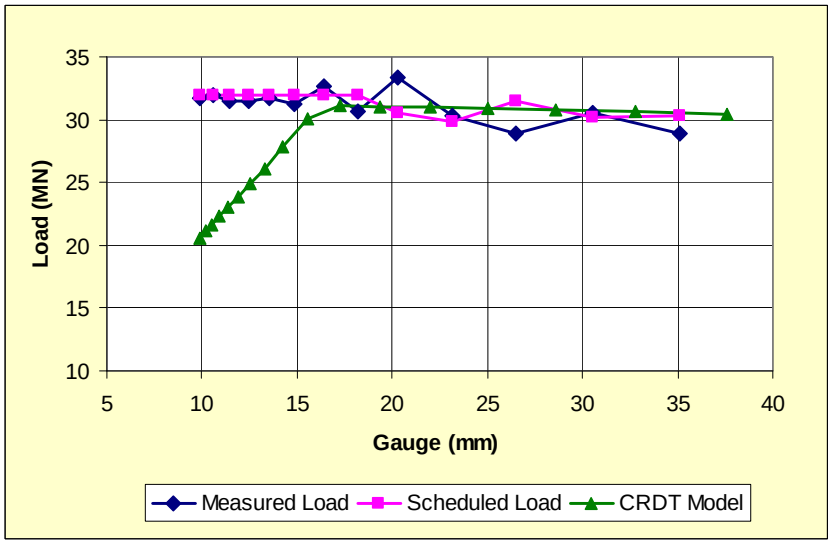


Fig. 64: Comparison of actual pass sequence with Scheduler prediction for plate RA991
[Plate dimensions: gauge 10 mm, width 3.4 m]

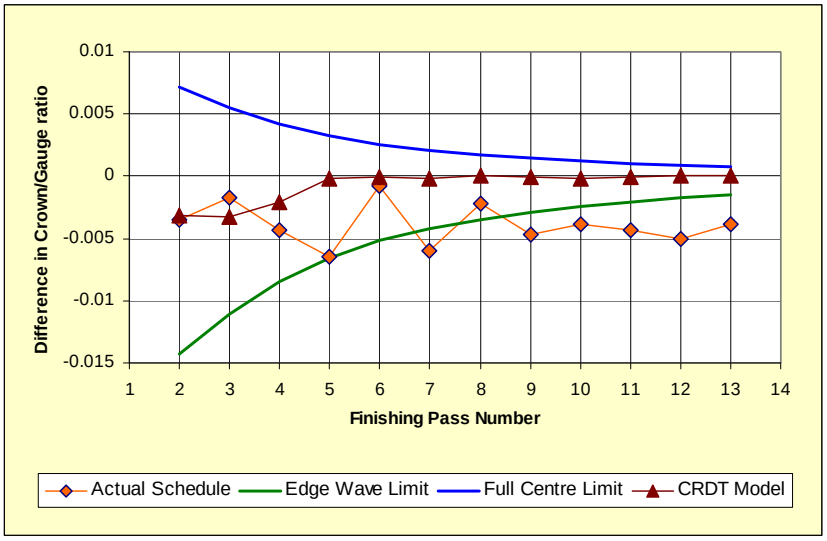


Fig. 65: Comparison of Shohet and Townsend flatness calculations for plate RA991

At the **TKS Plate Mill** discussions took place on how to apply the results in the mill control. BFI has proposed two measures

- the operators should have an display where on-line calculations of the plate crown change are shown that they can assess the consequences of their manual interventions with regard to the flatness,
- the results on-line calculations of the plate crown change in combination with the measured plate topography should be added to the database to be taken as basis of schedule optimizations.

Task 2.4 Assessment of efficiency of the optimised scheduling algorithms

No validation of the modified schedules has been performed. However, the off-line Scheduler model has been used to generate recommended schedules for good shape. It was noted that when the recorded schedules were close to those recommended, good flatness was measured on the plates. It was found that measured plate flatness could be successfully predicted using the off-line model, when simulating the actual recorded schedules. The off-line model therefore provides the basis for testing revised strategies for optimum recalculation of schedules partway through rolling. This is the subject of ongoing discussions with process control personnel.

WP3: Analysis, prediction and optimisation of the cooling and stacking process

Task 3.1: Data Acquisition and Measurement Campaigns &

Task 3.2: Characterisation of cooling (and stacking) conditions

Data acquisition at Scunthorpe Plate Mill

The behaviour of hot rolled plates on different types of cooling bank has been observed to determine what the effect of upstream processes has on plate flatness during cooling and what the shape of plates will be after cooling as a result. Plates were observed on both the Light Shear Line (LSL) cooling bank, usually used for plates of 20 mm gauge and lower, and the Heavy Shear Line (HSL) cooling banks, generally used for plates of 15 mm and thicker.

Observations of the light shear line (LSL) cooling bank (Bank no. 1)

The LSL cooling bank (**Fig. 66**) is a skid bank employing dogs on chains to pull plates from the hot leveller exit roller table onto the bank; shuffle bars and dogs convey plates down the banks to the turn over arms and first cross cut entry and marking roller table. The floor of the bank comprises cast iron grids to a position past half way down the bank. The cast iron grids provide closely spaced support of hot, potentially very weak plates. These grids have been replaced in places by wrought steel plate but they are largely intact across the full width of the hot end of the cooling bank. The plates are conveyed across skid rails at the cold end of the bank towards the turn over arms and cross cut shear entry roller table.

The LSL bank is approximately one metre above ground level and viewing the rolled plates by an observer standing at ground level allows a good appreciation of plate shape, especially if viewed from the south side of the LSL cooling bank where advantage can be taken of the low angle incident daylight from the open doors at the north end of the plant.

Regular transverse marks of approximately 1.5 m pitch in the surface scale on some of the plates going to both shear lines (thinner plates on the HSL), which could only be seen when the plates were viewed at a low angle were thought to be mill exit roller table chill marks.

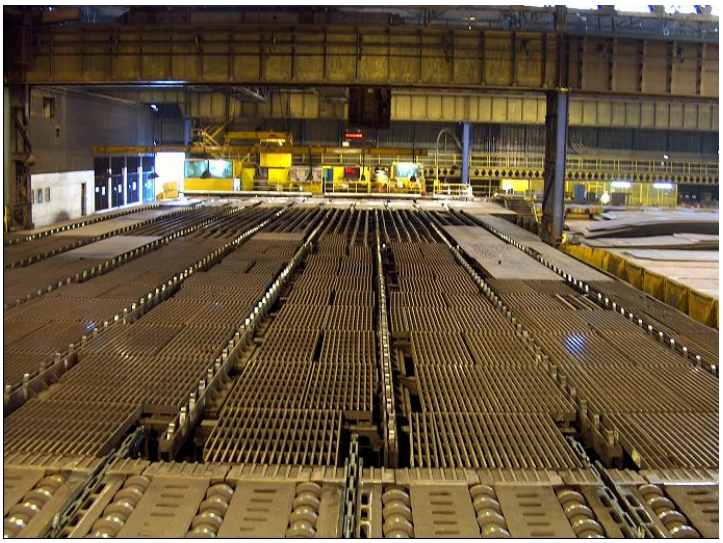


Fig. 66: View from the hot leveller exit roller table of the LSL cooling bank

Low angle viewing (50 - 300 mm above plate surface) of some plates which had appeared flat when viewed from more than about 2 m height revealed 14 to 15 low amplitude full cross width ripples along the length of plates covering about three-quarters of the bank width. These ripples were present as the plates emerged from the hot leveller and because of their pitch it is suspected that they are the remnants of the effect of the Finishing Mill pass line and plate end collision with the exit roller table rolls.

Plates observed on the LSL cooling banks with substantial periodic long-range shape were of the thinner gauges (<12 mm). The shape was generally of the same form as in the plate when it arrived at the hot leveller but reduced in magnitude. Centre buckle and edge wave were sometimes observed but

not for consecutive plates. Thicker plates and those arriving at the hot leveller with only minor shape defects tended to exit the hot leveller in a flat condition. The hot leveller seemed incapable of completely removing substantial long-range shape on thin/cold plates.

Development of even minor long-range shape was not observed on any hot flat plates properly laid on the LSL cooling bank. Any long-range shape observed in plates was always present when the plate exited the hot leveller.

Thinner plates on the LSL are below 400 °C within about 10 minutes of emerging from the hot leveller. **Fig. 67** shows the fall in surface temperature with time for a 12.1 mm gauge plate on the LSL cooling bank (no. 1). The start temperature shown is the temperature of the plate as it arrived on the hot leveller exit roller table.

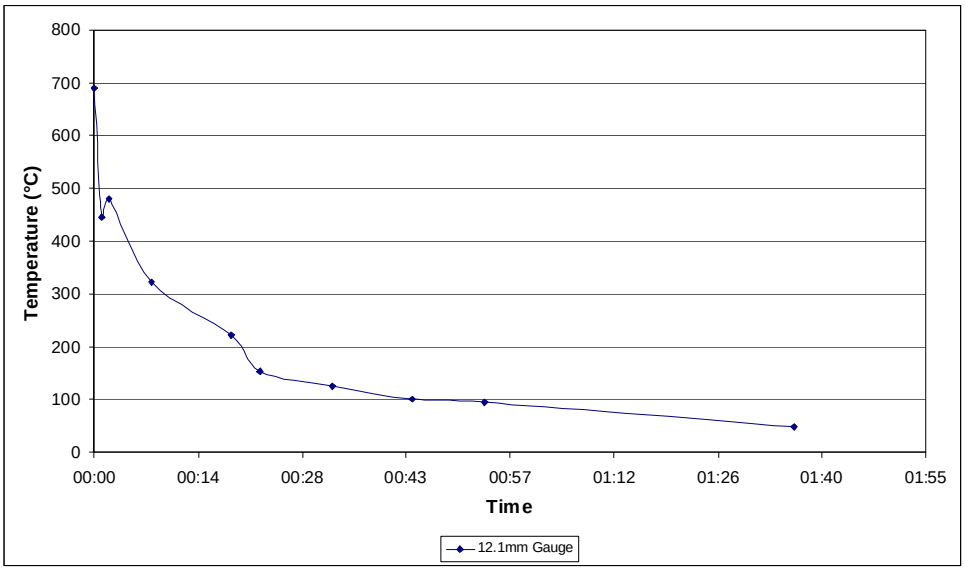


Fig. 67: Temperature-time trace of a 12 mm gauge plate in the LSL after hot levelling

Fig. 68 shows the development of yield strength with temperature for common plain carbon steel grades. It can be seen that as the steel cools there is a steep rise in its yield strength with temperature decrease from only 25% of its cold yield strength at 700 °C to 70% of its cold strength at approximately 500 °C and 85% of its cold yield strength at 400 °C.

The thinner plates rolled and cooled on the LSL cooling bank are therefore mechanically weak for relatively short periods of time. Observed distortion of plates during residence on the LSL cooling banks was always short range, due to mechanical damage to the plates by the banks equipment whilst they were hot and usually when the cause of the damage had endured until the plate had cooled to relatively low temperatures (<400 °C).

A common cause of mechanical damage was the sticking of the push dogs underneath the trailing edge of plates on the LSL cooling bank.

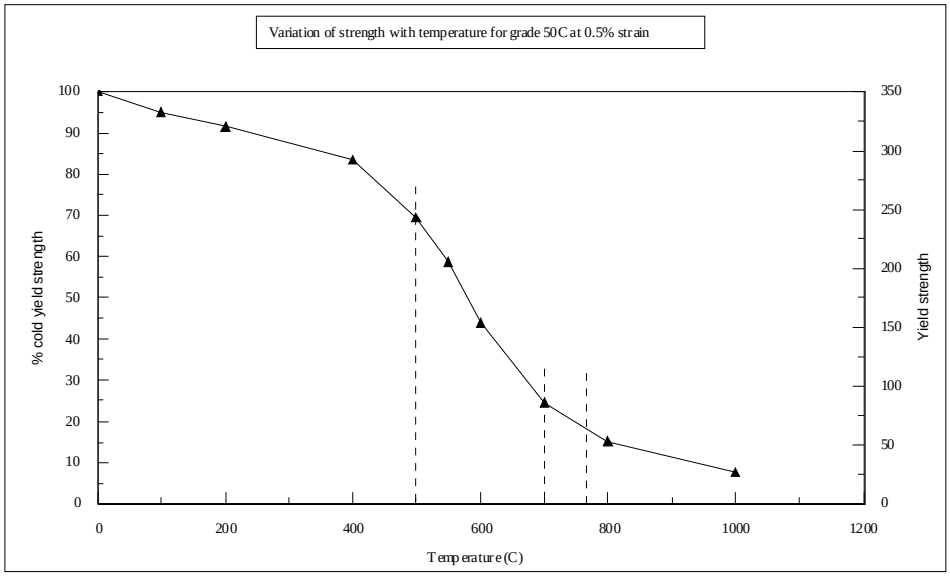


Fig. 68: Yield strength variation with temperature for common grades of plain carbon structural steel

One plate, which had slight camber and a slight plan view curvature of its trailing edge at its head end, had been pushed onto the banks at a temperature in excess of 500 °C and permanent deformation of the plate resulted when a dog standing proud underneath the plate at the head end lifted it causing severe local distortion. The plate remained in this location until its temperature had fallen to below 400 °C and it was then passed quickly down the bank and piled at a temperature in excess of 250 °C. The local distortion caused by the trapped dog remained unchanged when the plate had cooled to below 70 °C even though flat plates above it in the pile had pressed it. See **Fig. 69**.



(a) (b)

Fig. 69: Local distortion retained in a cold plate caused by a misplaced push-dog whilst the plate was hot and allowed to cooled to temperatures below 400 °C
(a) Damaged plate on skid rails; (b) Damaged plate on the top of the pile

Other instances of dogs trapped under the trailing edge of plates were observed but in most cases the plates were substantially below 400 °C and the local distortion dissipated when the plates were pushed further down the bank.

The hot leveller exit roller table provides level parking space for plates. It was observed that plates were prone to mechanical damage when pushed from this roller table onto the banks when still hot and when the push gear on the hot end of the cooling bank was in poor condition.

Plates approaching the turn-over arms were 10 °C hotter at their south end (65 °C), where they had been passing over a substantial length of bank where the skid rail supports (55 °C) had been replaced by plates, but there was no apparent distortion. Substitution of floor grids or skid rails by plates did affect the plate surface temperatures, but beyond the shop columns (west end of the bank) the effect was small and it did not appear to cause distortion. Uneven skid rails caused only temporary elastic distortion of plates at this (west) end of the bank. At the hot (east) end of the cooling bank substitution of grids by plates might result in plate temperature profiles likely to cause thermal distortion in plates if, when hot, they are slewed across areas of adjacent floor grids and floor plates. Floor grids are important at the hot (east) end of the cooling bank to ensure rapid cooling and strength development in the hot rolled plates

and thereby reduce the probability of permanent distortion by mechanical damage at high temperatures when the plates are weak.

Plates are most vulnerable to thermal distortion when they are piled at high temperatures; this is sometimes done to clear the cooling banks for engineering maintenance access. It has been reported elsewhere that in piles of plates with varying width, gauge and length, thermal distortion can occur at moderate temperatures (>250 °C) [9], however this work refers mainly to effects when plates are piled at high temperatures (>600 °C).

Observations of the heavy shear line (HSL) cooling banks (banks no. 2, 3 and 4)

Plates sent to the HSL are generally of heavier gauge and are therefore inherently stronger than their thinner counterparts at the same temperature. The second moment of area (I) of a rectangular beam is proportional to the cube power of gauge (h),

$$\text{i.e.} \quad I = wh^3/12, \text{ where w is the beam width}$$

Therefore, generally, wider spaced support can be tolerated for thicker plates at a given temperature, but thicker plates remain hot for much longer periods of time and must therefore be maintained in a level attitude for longer periods of time. The higher temperatures of the thicker plates might, however make them more susceptible to scratching by plant equipment and therefore a wheel bank after hot levelling is much preferred to a skid bank for these plate gauges.

Cooling bank no. 2

Cooling bank no. 2 (**Fig. 70**) is a narrow bank adjacent the HSL hot leveller entry roller table (mill side of the hot leveller) and is generally used for shorter heavier plates. It comprises a short wheel bank, leading to a chain conveyor across a skid bank to the first cross cut shear entry and marking roller table.

One plate (gauge 61.2 mm) slewed during pull-off from the leveller entry roller table because of faulty pull-off chains and rested for a considerable time at the junction of the pull-off chains and wheel bank. It bent as a result of uneven support and the self-weight of the plate and this distortion remained in the plate as it passed further down the bank.

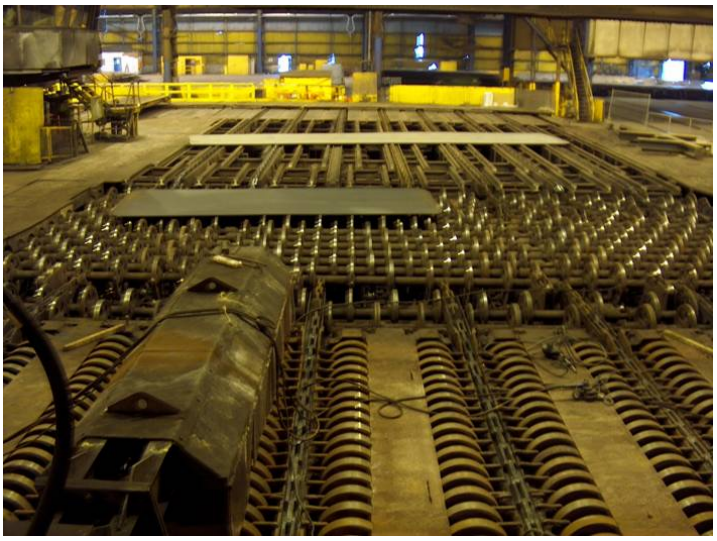


Fig. 70: View of cooling bank no. 2 from the hot leveller entry/exit roller table

Plastic bending under self-weight of thick plates has been observed on No. 2 bank when the plates were slewed during pull-off from the hot leveller roller table and allowed to rest between the wheel bank and the chain bank whilst hot, relatively weak and not supported in a level attitude. If allowed to cool for some time at this location the bend in the plate will become permanent.

When this cooling bank's transport mechanisms were working properly no problems of plate distortion were observed.

Cooling banks no. 3 and 4

Cooling banks no. 3 and 4 (**Fig. 71**) are parallel to each other and adjacent the HSL hot leveller exit roller table (shears side of the hot leveller). They are wheel banks continuous with each other across their width, allowing them to be used as one wide cooling bank and they run parallel to no. 2 bank, being separated from it by a wide walkway. They appear to be a single bank but originally plates were transported side by side down these banks. Cooling banks no. 3 and 4 are used for heavy gauge plates (>13 mm), long plates of heavy gauges and very long plates of lighter gauges (>10 mm), which might otherwise be processed through the LSL. They convey plates to the first cross cut shear entry and marking roller table. Longer plates straddle both banks during cooling and transport towards the cross cut shear. Adjacent the halfway point of the hot leveller exit roller table, a gearbox cover plate runs down the junction of these two banks for a few metres. Operators are instructed to avoid resting hot rolled plates over the gearbox cover if possible.

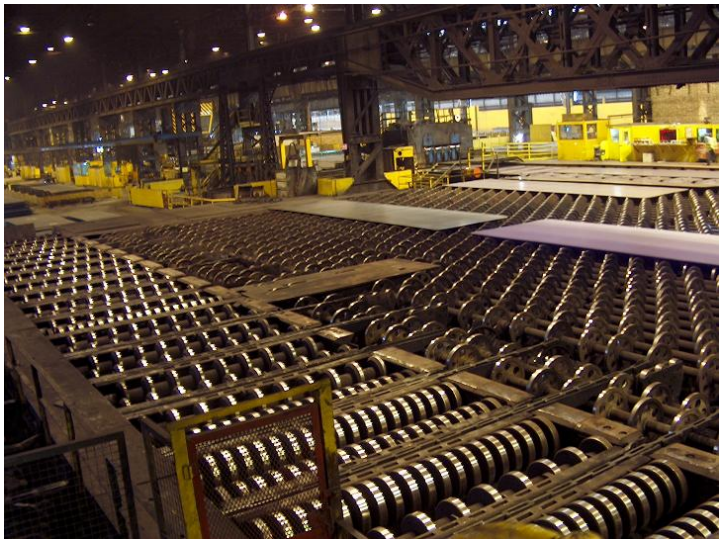


Fig. 71: View of the HSL hot leveller exit roller table, and cooling banks no. 3 and no. 4

One plate observed was rested on the leveller exit roller table and the two plates ahead of it were rested on the gearbox cover. These two plates (both gauge 20 mm) were seen to dip at the gearbox cover when their top surface temperature was between 500 °C and 350 °C. Top surface temperatures along the plate from the north end, over the gearbox and south of the gearbox were fairly constant. This dip was no longer detectable later when the plates had been pushed further east and had cooled to less than 100 °C. The HSL hot leveller operators claim that distortion becomes more obvious and persistent for thinner gauge plates (<15 mm). This is probably because of their inherent weakness at high temperatures, faster bulk cooling rate to temperatures below 500 °C and permanent set because of developed yield strength.

Other examples of plate distortion at high temperatures due to local unevenness of the cooling bank were observed. Such distortion healed provided the plates were moved to a level area whilst their bulk temperature was still high (>500 °C) which was usually the case.

Plate distortion observed on the HSL cooling banks was usually transient and not a result of asymmetric cooling, but caused by a lack of support of a substantial length of the plate when it is hot (>400 °C). This distortion was seen to persist only in cases where the plate was stationary for some time and had cooled to temperatures below 300 °C in that location.

Data acquisition at TKS Plate Mill

The cooling behaviour of heavy plates in a stack is supposed to be one reason – among others – to influence the final flatness of the plates. Sometimes, stacking of the plates is inevitable due to necessary hydrogen effusion or too high temperatures for further processing.

In order to assess the impact of cooling and stacking order on the flatness of heavy plates a stack of plates was piled up under defined conditions in this experiment. Thermocouples were distributed inside the stack to get insight into the temperature distribution, since large temperature gradients might induce stress into the material and consequently lead to uneven plates.

The stack consists of 49 heavy plates in a thickness range from 20 to 40 mm and has a final height of around 1,6 m. The lengths of the plates vary from about 6 to 12 m and it took about 4 hours to build up the stack. One side of the stack is flush with the foot end of the plates as can be seen in **Fig. 72**.



Fig. 72: Photograph of the final stack. In front one can see the aligned edges of the heavy plates (foot end of the plates)

The stacking temperature of each plate was measured at head, middle and foot position with values between 300 and 600°C.

Fig. 73 sketches the position of the thermocouples which were implemented into 5 mm thick sheet metal strips for protection (see **Fig. 74**).

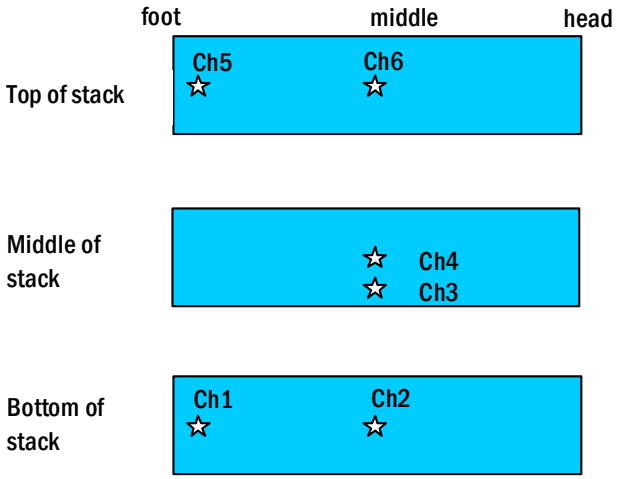


Fig. 73: Thermocouple position (top view)



Fig. 74: Photograph of the stack with thermocouples

The first two thermocouples (channel 1 and 2) were installed on top of the fifth plate according to **Fig. 73**. The distance of the thermocouple channel 1 was about 30 cm from the edge. After 14 more plates the second layer of thermocouples was placed. Once more the distance from the side of thermocouple channel 3 was around 30 cm. Near completion of the stack, the top layer of thermocouples is inserted (channel 5 and 6) and three more plates were put on top. To protect the thermocouples from the weight of the plates they were embedded into metal sheet strips as it is shown in **Fig. 74**. After the last thermocouples were placed three more plates were positioned on top.

Fig. 75 shows a thermograph image of the top plate with edges of underlying plates. The image was taken after the sixth plate was piled on top of the first layer of thermocouples and shows the temperature gradients at the edges.

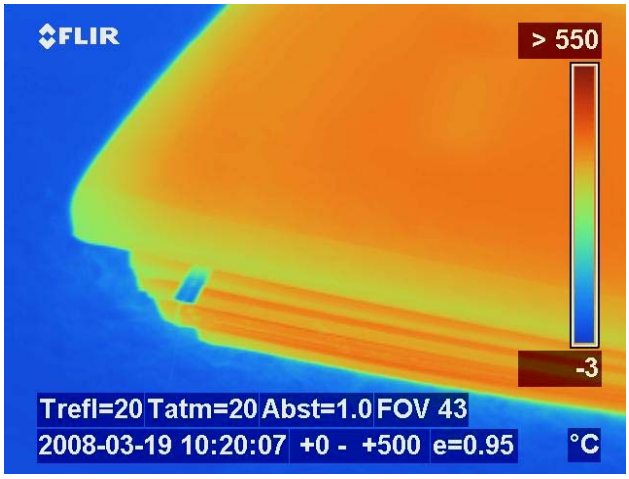


Fig. 75: Thermograph image of the foot end of the stack after positioning of heavy plate No. 6 on top the first layer of thermocouples

Fig. 76 shows a thermograph image of the final stack, and corresponds to the photography of **Fig. 72**. The cold sites at the stack edge originate from emission characteristics of the edges and do not represent correct temperatures.

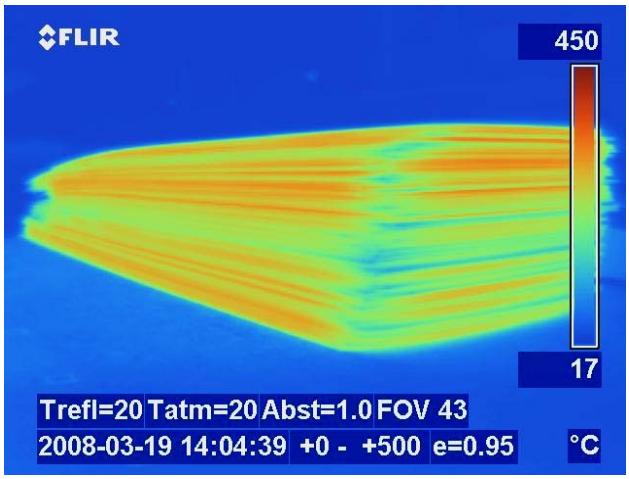


Fig. 76: Thermograph image of the completed stack from the same angle of view as in Fig. 72

Fig. 77 indicates the difference of edge temperatures which arise from different stacking temperatures and unequal cooling conditions of protruding plates.

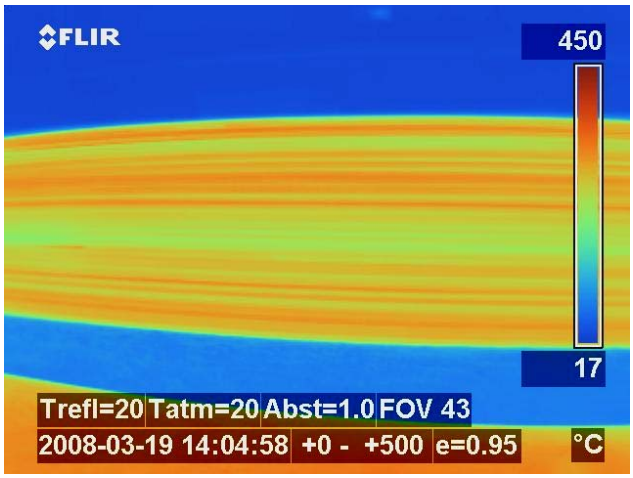


Fig. 77: Thermograph image of the long side of the completed stack

The temperature measurement has been performed during three days. **Fig. 78** shows the course of temperature, which can be described by

$$T(t) = Ae^{Bt}$$

with A = 425°C and B = 0,37 1/day

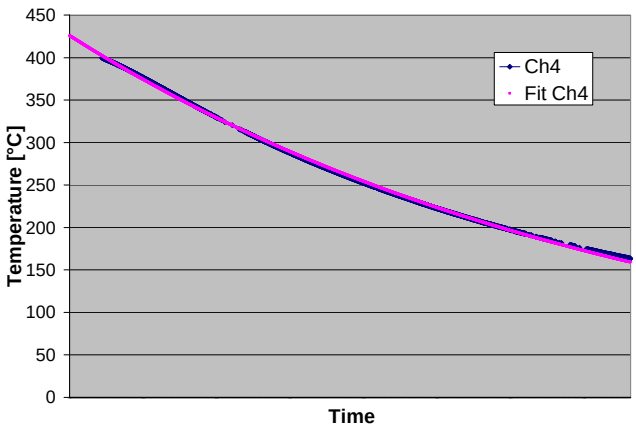


Fig. 78: Measured temperature vs. time
(Ch 4, middle of the stack)

Data acquisition at Ruukki

A thermal camera was installed after mill before accelerated cooling unit. An example of measurement is shown in **Fig. 79**.

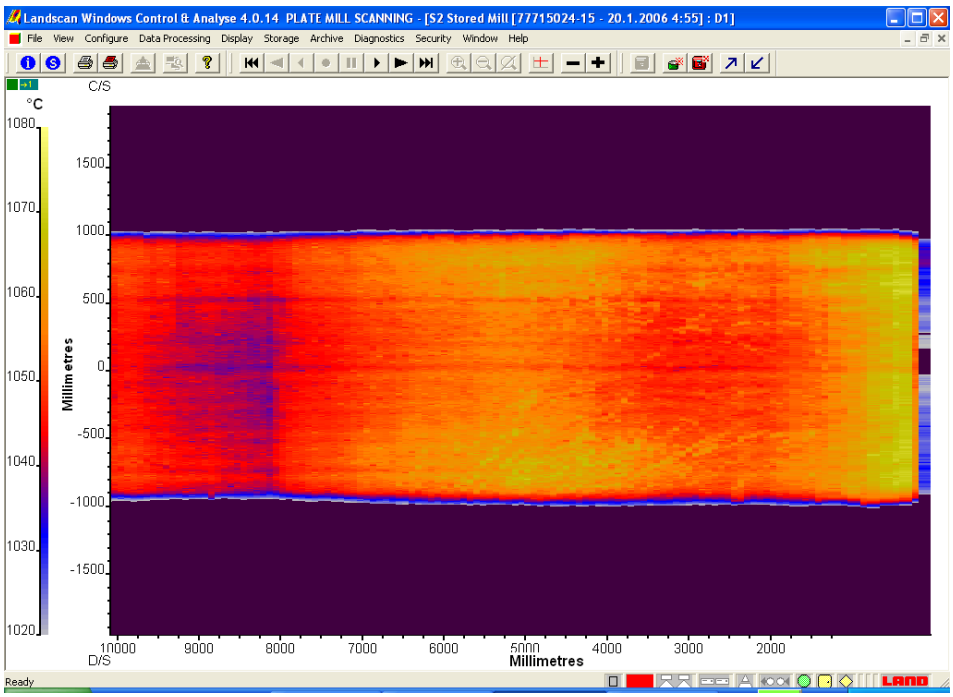


Fig. 79: Example of plate temperature measurement after mill

The varying reheating time can give different plate temperature uniformity especially the soaking time has a strong effect. As seen in thermal camera picture in **Fig. 80** very big skidmarks can occur if reheating time is too short. The skidmarks in finished plate are smaller for thinner gauges than for thicker gauges, starting with the same slab size and having the same furnace conditions and total heating time. The effect of soaking time could not yet be analysed, because soaking time was missing in the data base.

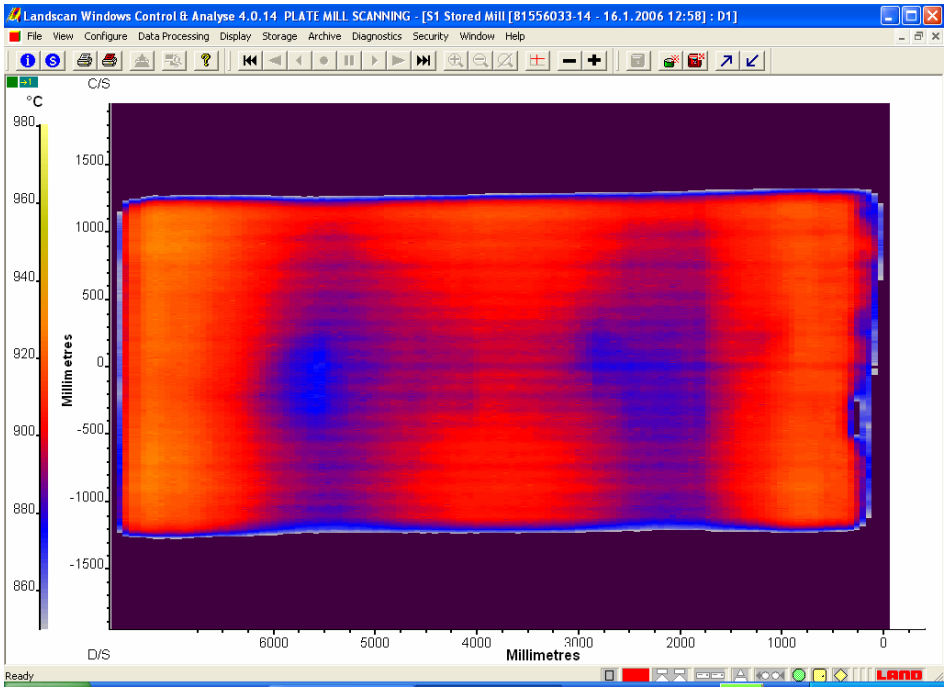


Fig. 80: Example of plate temperature measurement after mill when there are big skidmarks in the plate

Skidmarks can be removed by increasing reheating time and soaking time, **Fig. 81**. Longer reheating time can affect productivity.

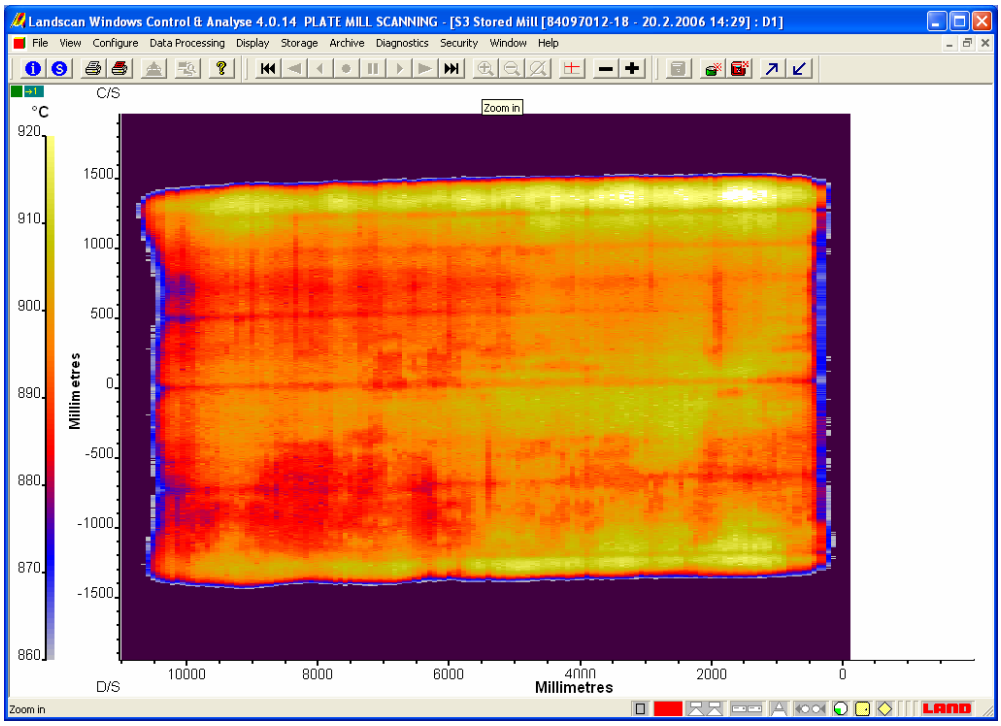


Fig. 81: Example of plate temperature measurement after mill when there is no skidmarks in the plate

Some tests were done in accelerated cooling device at Ruukki Heavy Plate Mill. The effect of tuning of the plate head-end cooling has been analysed. Tests included 330 plates with tuned head-end cooling and 200 plates without tuned head-end cooling. Tuning length was 500 mm or 700 mm. Temperature difference dT between plate head-end and main plate was analysed. The result was that temperature difference dT decreased when tuning was used. The effect increased when plate thickness increased, but the tuning length does not affect the temperature difference. When tuning was used, dT was 15 °C and without tuning dT was 30 °C. The effect on flatness was negative. The head-end flatness was poor and more transversal flatness error was seen than without using tuned head-end cooling. The effect on flatness was bigger with thinner plates than thicker plates, no negative effect with thick plates.

Fine tuning of new high pressure cooling equipment was carried out. Mostly things proceeded well. A functional problem in the new cooling system has been that control valves are not operating at the optimal opening angles. This is due to mismatch of the flow capacity of top/bottom -water feeding pipes compared to used top to bottom -ratios.

At the beginning of the project it was estimated that rejection rate of high strength plates would be on the same level as flame straightening ratio for acc plates. That estimation was done based on the assumption that cold leveller would not be available.

The result has been much better. Flatness rejections (which were the ultimate fear at the beginning) have been in the level of about 1-3 % for plates depending on thickness and quality. Most difficult plates are thin and hard plates.

The cooling stop temperature accuracy of new cooling system is quite good. About 80 % of measured stop temperature values have been within +/- 25 ºC to target. With laminar cooling one problem has been hot tail end occuring sometimes even if plate was pre-levelled (**Fig. 82** and **Fig. 83**). The temperature spike in those pictures is more than 100 ºC. This problem has practically disappeared with high pressure unit.

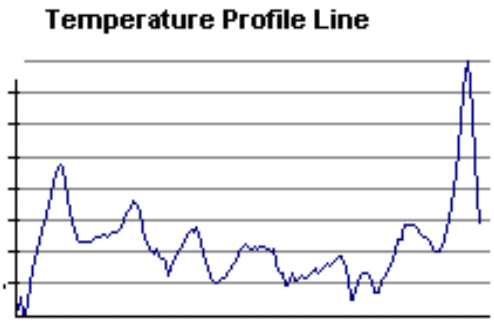


Fig. 82: Longitudinal temperature profile of 15 mm plate cooled with laminar cooling system

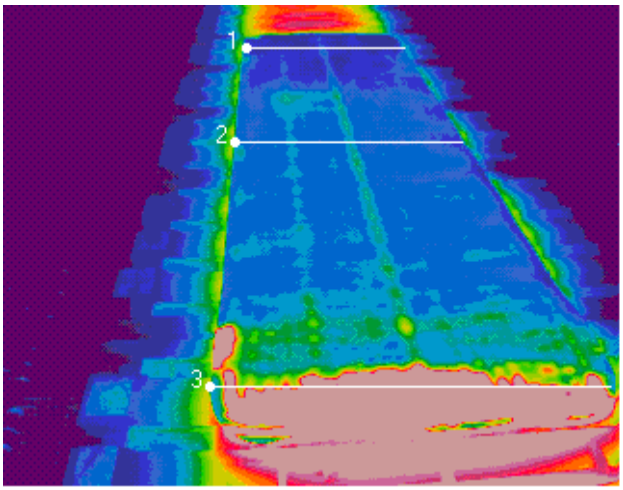


Fig. 83: Thermal camera picture of 15 mm plate cooled with laminar cooling system (same plate)

The flatness of plates has been very good after high pressure unit. Pinch rolls have been used slightly open and by pressing them to plate surfaces. No differences in flatness point of view have been discovered between these two strategies. In **Fig. 84** and **Fig. 85** two different 15 mm plates after cooling and hot levelling are shown.

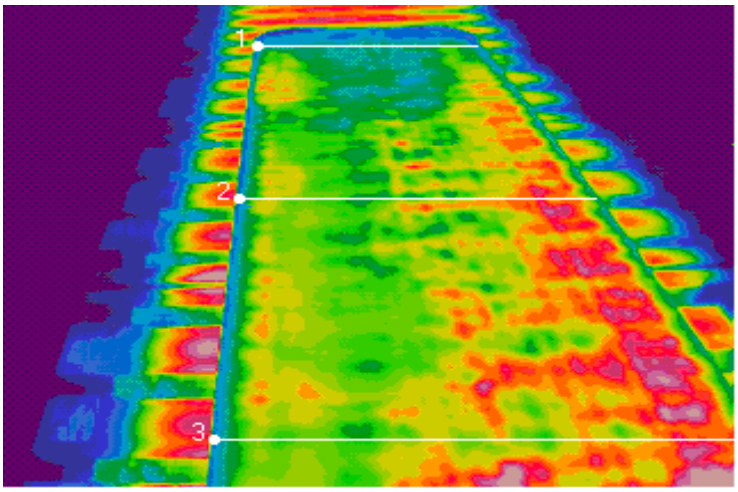


Fig. 84:15 mm plate after cooling and hot levelling
Transversal flatness avg 1,8 mm/m
Longitudinal flatness avg 1,7 mm/m

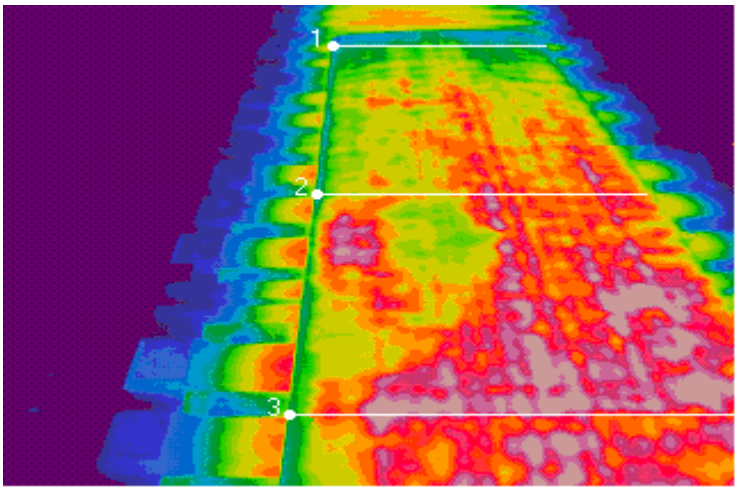


Fig. 85: Another 15 mm plate after cooling and hot levelling
Transversal flatness avg 2,3 mm/m
Longitudinal flatness avg 1,9 mm/m

The controllability of intermediate cooling has been under development. Possibility to control stop temperature based on plate waiting thickness and starting temperature of intermediate cooling has been implemented. There are still some practical problems in the function of intermediate cooling for thin water cooled plates but they will be solved.

With new pre-leveller the operator has to be careful with gap settings. The temperature of rolls increases when plates to be pre-levelled are produced which closes the gap a little bit. This has caused up lifting heads especially with thin plates. Operator makes slight offset corrections on gap values based on the behaviour of the plate heads. Pre-leveller has been calibrated every second week.

Task 3.3: Correlation analysis and Process Models for global prediction and optimisation use

Development of a Microsoft Excel based user interface by MEFOS

Within this project a Microsoft Excel based user interface named Plate-RQ has been developed. It is used for the pre- and post processing of data in connection with temperature simulation in the temperature calculation program Steeltemp [10]. The main application is to calculate temperature development in plate rolling and quenching. The temperature is calculated from withdrawal of slab from furnace, during rolling and during quenching after rolling. Primary descaling and secondary descaling before specified passes can be included in the calculations.

Plate_RQ uses a number of spreadsheets in Excel where the user can enter process data and process conditions. An input file formatted to be read by Steeltemp is created. After running the calculation in Steeltemp the results are transferred back to Plate-RQ and presented in diagrams and data tables. In **Fig. 86**, the main spreadsheet for input of rolling parameters is presented. **Fig. 87** shows the spreadsheet for input of descaling and quenching parameters. The results from the calculations are presented in **Fig. 88**.

STEELTEMP® 2D is a finite-difference program for temperature and heat-transfer analysis during teeming or continuous casting, cooling, stripping, heating, flat rolling and open die forging. Temperatures and densities of heat flow rate are calculated in a cross section of the steel. Various heat balances, time and isothermal plots can be printed out.

In the material database of the program thermal data (ρ, cp and λ) of steels, moulds, oxide scale, air, flue gases etc. are stored. For low alloy steels phase transformations and re-crystallization during rolling and water cooling on the run-out table can be calculated.

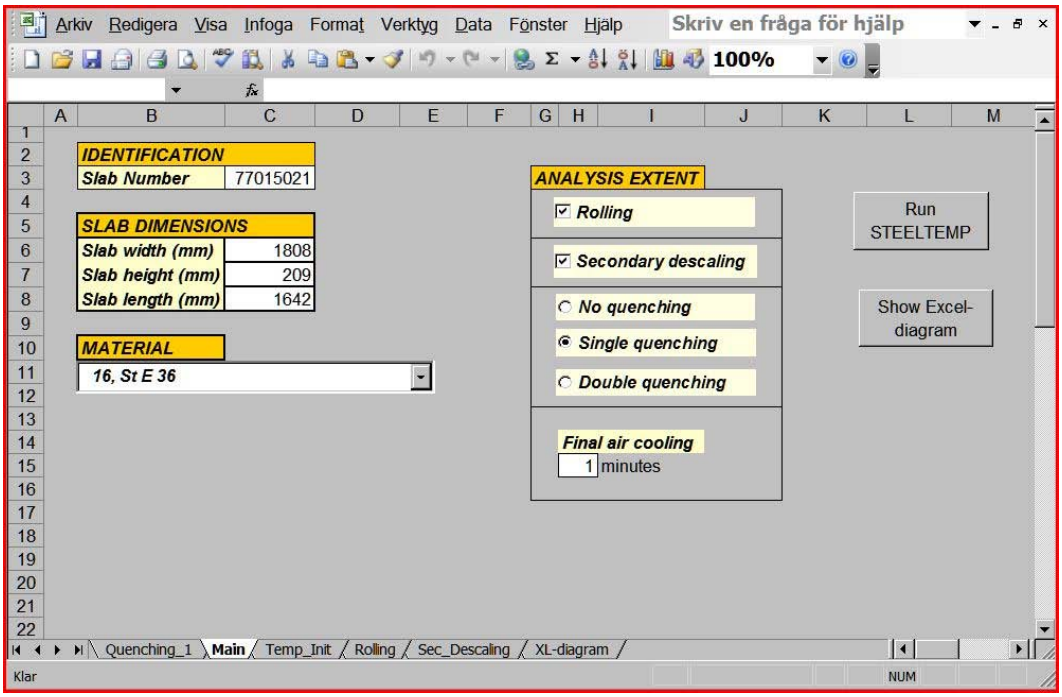


Fig. 86: Main menu of the user interface

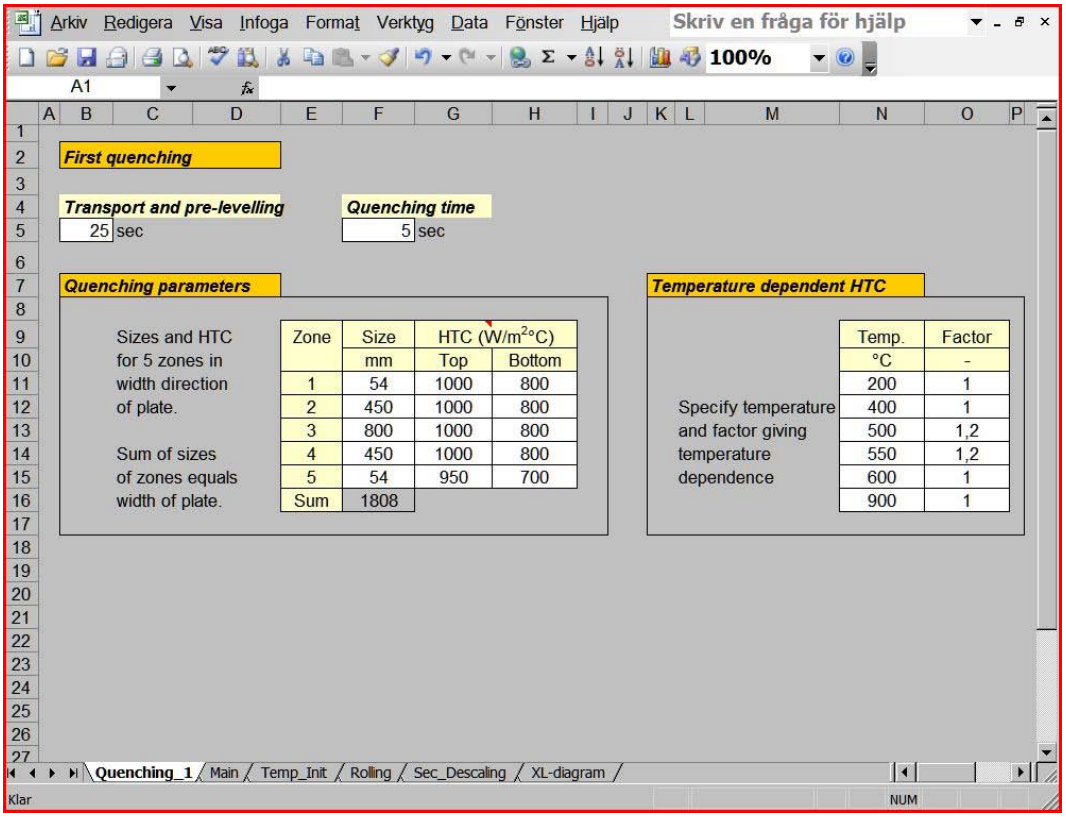


Fig. 87: Data input section for the quenching part

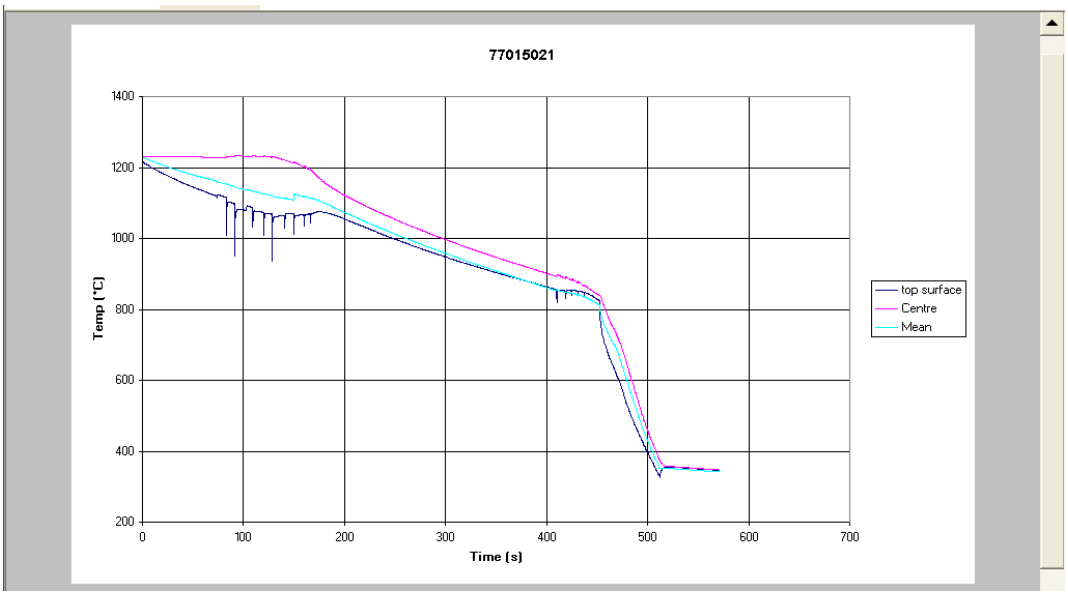


Fig. 88: Presentation of results calculated with Steeltemp.

Model of buckling of heavy plates under the influence of cooling and stacking by BFI

In the production process of heavy plates often the phenomenon of buckling of plates arises after the stacking and during the cooling of plates. The deformation connected with buckling have to be corrected in the subsequent treatment of the heavy plates. Therefore the occurrence of buckling should be avoided if possible.

As shown below, the main cause of buckling of heavy plates is the occurrence of self-equilibrating stresses, which result from thermal tensions during the cooling process. Therefore, for better understanding, first the cooling process is described briefly from the view of thermodynamics.

Thermodynamic basics of the cooling process of heavy plates

From the view of thermodynamics the cooling process of heavy plates is a special case of the heat transmission, i.e. the transport of heat of a place of higher temperature to a place of lower temperature.

Generally heat transmission can take place via thermal conduction, heat convection and heat radiation, as well as via combination of these three fundamental kinds of the heat transport:

- The thermal conduction arises in solids, liquids and gases. It is based on the energy transfer by the unordered thermal motion of the atoms and molecules. Thereby the body which can be cooled down (or warmed up) is brought in contact with a colder (and/or warmer) one, so that the on average faster particles of the warmer area pass kinetic energy by impacts on to the on average slower particles of the colder area. In same way the thermal conduction between different warm areas within the body takes place.
- In contrast to the thermal conduction the heat convection, at which the heat is transported by flowing liquids or gases, is connected to the shifting of matter (convection). Here substantially larger amounts of heat can be transferred than of resting media by thermal conduction. With the heat convection the liquids and gases involved are subjected to the regularities of hydrodynamics.
- The heat transport by emission and absorption of electromagnetic radiation without matter as transmitting medium is called radiant heat.

At the cooling process of heavy plates all three kinds of the heat transport arise. The physical treatment of this cooling process is thus based on the application of the laws of thermodynamics and hydrodynamics to a two-phase medium, consisting of the stack of the heavy plates and the cooling down air (V2 viscous fluid).

The temperature distribution in general is based on the law of heat conduction. It states that the time rate of heat transfer through a material is proportional to the negative gradient in the temperature and to the area, through which the heat is flowing:

$$\vec{q} = -k\nabla T$$

where $\vec{q}$ is the local heat flux [$W \bullet m^{-2}$],

k is the material's conductivity [$W \bullet m^{-1} \bullet K^{-1}$] and

∇T is the temperature gradient [$K \bullet m^{-1}$].

This equation is called Fourier differential equation of the thermal conduction. It was deduced for the first time 1822 by the French mathematician and physicist Jean Baptiste Joseph, Baron de Fourier (1768-1830).

The temperature distribution of a stack of heavy plates is modelled by

$$\frac{\partial T}{\partial t} - \chi_0 \Delta T = f \quad \text{with} \quad -\frac{a}{2} \le x \le \frac{a}{2} \wedge -\frac{b}{2} \le y \le \frac{b}{2} \wedge -\frac{c}{2} \le z \le \frac{c}{2}$$

with **a** = length of stack,

b = width of stack,

c = height of stack and

χ_0 = function of material density, heat capacity and thermal conductivity.

The initial temperature

$$T(x,y,z,0) = T_{\max}\left(1-\left(\frac{x}{\xi}\right)^2\right)\left(1-\left(\frac{y}{\eta}\right)^2\right)\left(1-\left(\frac{z}{\zeta}\right)^2\right)$$

is describing a realistic situation. Because the initial temperature gradient of the stack will have an influence on the later computed buckling of the plates.

Second the boundary conditions for the surfaces of the plate stack are

$$\pm\frac{\partial T}{\partial x} = -\frac{T - T_f}{\kappa_0}\alpha(T, T_f, \cdots)$$

$$\pm\frac{\partial T}{\partial y} = -\frac{T - T_f}{\kappa_0}\alpha(T, T_f, \cdots)$$

$$\pm\frac{\partial T}{\partial z} = -\frac{T - T_f}{\kappa_0}\alpha(T, T_f, \cdots)$$

with the heat transmission coefficient

$$\alpha(T, T_f, \cdots) := (\alpha_0 + \beta_0\upsilon)(H(\upsilon) - H(\upsilon - \upsilon_0)) + (\alpha_0 + \beta_0\upsilon_0)\left(\frac{\upsilon}{\upsilon^0}\right)^{\gamma_0} H(\upsilon - \upsilon_0) + \varepsilon\sigma(T + T_f)(T^2 + T_f^2)$$

where υ = air flow viscosity around the stack,

H = the Heaviside function and

T_f = the temperature of the surrounding far away form the stack.

They are now also considering free and forced convection and radiation.

The resulting partial differential equation (PDE) is inhomogeneous and has inhomogeneous boundary conditions and an inhomogeneous start condition. In order to get an analytical solution, the PDE will be transformed in to a homogenous PDE.

Next the calculation of the heat transmission will be simplified by inducing an average value **υ** of the air flow velocity. Θ within calculation of heat transmission coefficient will be defined by

$$\theta(x,y,z,t) := T(x,y,z,t) - T_f$$

The previous equation is now transformed to:

$$\frac{\partial \Theta}{\partial t} - \chi_0 \Delta \Theta = f \quad \text{with} \quad -\frac{a}{2} \le x \le \frac{a}{2} \wedge -\frac{b}{2} \le y \le \frac{b}{2} \wedge -\frac{c}{2} \le z \le \frac{c}{2}$$

The initial temperature profile Θ is given by

$$\Theta(x,y,z,0) = T_{\max}\left(1-\left(\frac{x}{\xi}\right)^2\right)\left(1-\left(\frac{y}{\eta}\right)^2\right)\left(1-\left(\frac{z}{\zeta}\right)^2\right) - T_f$$

The PDE can be simplified to:

$$\pm\frac{\partial \Theta}{\partial x} = -\frac{\Theta}{\kappa_0}\overline{\alpha}$$
$$\pm\frac{\partial \Theta}{\partial y} = -\frac{\Theta}{\kappa_0}\overline{\alpha}$$
$$\pm\frac{\partial \Theta}{\partial z} = -\frac{\Theta}{\kappa_0}\overline{\alpha}$$

whereas the heat transmission coefficient is κ_0 constant and α depends on (Θ_0,T_f ,v, ε; α_0, β_0, γ_0,v_0).

This special case for the surfaces of the plate stack is now a homogeneous PDE but the boundary conditions and the start condition are still inhomogeneous. To get an analytical solution we make use of the symmetrical knowledge of the problem. The PDE is separated into four isolated linear homogeneous differential equations and so it is now analytically solvable. The solution is given by

$$\hbar = 1{,}054\ 571\ 628\ 10^{-34}\ Js \quad \wedge \quad k = 1{,}380\ 6504\ 10^{-23}\ JK^{-1} \quad \wedge \quad c_0 = 299\ 792\ 458\ ms^{-1} \quad \wedge$$

$$\sigma = \frac{\pi^2 k^4}{60\hbar^3 c_0^2} = 5{,}670400 \cdot 10^{-8}\ Wm^{-2}K^{-4} \quad \wedge$$

$$\alpha_0 = 5{,}8 Wm^{-2}K^{-1} \quad \wedge \quad \beta_0 = 3{,}85 Jm^{-3}K^{-1} \quad \wedge \quad \gamma_0 = 0{,}78 \quad \wedge \quad v_0 = 5 ms^{-1} \quad \wedge$$

$$\overline{\alpha_{12}}\left(T_0^{(0)}, T_f, \overline{v}, \varepsilon; \alpha_0, \beta_0, \gamma_0, v_0\right) = \left(\alpha_0 + \beta_0\overline{v}\right)\left(H\left(\overline{v}\right) - H\left(\overline{v} - v_0\right)\right) + \left(\alpha_0 + \beta_0 v_0\right)\left(\frac{\overline{v}}{v_0}\right)^{\gamma_0} H\left(\overline{v} - v_0\right) + \varepsilon\sigma\left(T_0^{(0)} + T_f\right)\left(T_0^{(0)2} + T_f^2\right) \quad \wedge$$

$$\alpha_{13}\left(d;\kappa_B\right) = \frac{\kappa_B}{d} \quad \wedge \quad C_1\left(a, \kappa_0, T_0^{(0)}, T_f, \overline{v}, \varepsilon; \alpha_0, \beta_0, \gamma_0, v_0\right) = \frac{\overline{\alpha_{12}}\left(T_0^{(0)}, T_f, \overline{v}, \varepsilon; \alpha_0, \beta_0, \gamma_0, v_0\right)a}{2\kappa_0} \quad \wedge$$

$$C_2\left(b, \kappa_0, T_0^{(0)}, T_f, \overline{v}, \varepsilon; \alpha_0, \beta_0, \gamma_0, v_0\right) = \frac{\overline{\alpha_{12}}\left(T_0^{(0)}, T_f, \overline{v}, \varepsilon; \alpha_0, \beta_0, \gamma_0, v_0\right)b}{2\kappa_0} \quad \wedge$$

$$C_3\left(c, \kappa_0, T_0^{(0)}, T_f, \overline{v}, \varepsilon; \alpha_0, \beta_0, \gamma_0, v_0\right) = \frac{\overline{\alpha_{12}}\left(T_0^{(0)}, T_f, \overline{v}, \varepsilon; \alpha_0, \beta_0, \gamma_0, v_0\right)c}{2\kappa_0} \quad \wedge$$

$$D_3\left(c, d, \kappa_0, \kappa_B\right) = \frac{\kappa_B c}{2\kappa_0 d} \quad \wedge \quad \delta\left(d, \kappa_B, T_0^{(0)}, T_f, \overline{v}, \varepsilon; \alpha_0, \beta_0, \gamma_0, v_0\right) = \frac{D_3\left(c, d, \kappa_0, \kappa_B\right)}{C_3\left(c, \kappa_0, T_0^{(0)}, T_f, \overline{v}, \varepsilon; \alpha_0, \beta_0, \gamma_0, v_0\right)} \quad \wedge$$

and

$$
\left(
\begin{array}{c}
\gamma_{1,n}^{(1)}(C_1) = \dfrac{\pi\left(8\left(8\left(4-\pi\right)n-3\pi+10\right)C_1+\left(8-\pi\right)\pi^2 n+\sqrt{64\left(6-\pi\right)^2 C_1^2-16\left(8-\pi\right)\pi^2\left(\left(10-3\pi\right)n+2-\pi\right)C_1+\left(8-\pi\right)^2\pi^4 n^2}\right)}{2\left(32\left(4-\pi\right)C_1+\left(8-\pi\right)\pi^2\right)} \\
\gamma_{2,n}^{(1)}(C_2) = \dfrac{\pi\left(8\left(8\left(4-\pi\right)n-3\pi+10\right)C_2+\left(8-\pi\right)\pi^2 n+\sqrt{64\left(6-\pi\right)^2 C_2^2-16\left(8-\pi\right)\pi^2\left(\left(10-3\pi\right)n+2-\pi\right)C_2+\left(8-\pi\right)^2\pi^4 n^2}\right)}{2\left(32\left(4-\pi\right)C_2+\left(8-\pi\right)\pi^2\right)} \\
\gamma_{3,n}^{(1)}(C_3,\delta) = \dfrac{C_3\left(\left(4n+1\right)\pi\left(1+\delta\right)+\sqrt{16\delta\left(2C_3\left(1+\delta\right)+1\right)+\left(4n+1\right)^2\pi^2\left(1+\delta\right)^2}\right)}{4\left(2C_3\left(1+\delta\right)+1\right)} \\
\gamma_{1,n}^{(2)}(C_1) = \dfrac{2\left(\left(\gamma_{1,n}^{(1)}(C_1)\right)^2+C_1\cos^2\left(\gamma_{1,n}^{(1)}(C_1)\right)\right)}{\sin\left(2\gamma_{1,n}^{(1)}(C_1)\right)+2\gamma_{1,n}^{(1)}(C_1)} \\
\gamma_{2,n}^{(2)}(C_2) = \dfrac{2\left(\left(\gamma_{2,n}^{(1)}(C_2)\right)^2+C_2\cos^2\left(\gamma_{2,n}^{(1)}(C_2)\right)\right)}{\sin\left(2\gamma_{2,n}^{(1)}(C_2)\right)+2\gamma_{2,n}^{(1)}(C_2)} \\
\gamma_{3,n}^{(2)}(C_3,\delta) = \dfrac{2\left(2C_3\left(1+\delta\right)\gamma_{3,n}^{(1)2}(C_3,\delta)+\left(\gamma_{3,n}^{(1)2}(C_3,\delta)+C_3^2\delta\right)\sin^2\left(2\gamma_{3,n}^{(1)}(C_3,\delta)\right)\right)}{2\gamma_{3,n}^{(1)}(C_3,\delta)\left(2C_3\left(1+\delta\right)+1\right)-2\gamma_{3,n}^{(1)}(C_3,\delta)\cos\left(4\gamma_{3,n}^{(1)}(C_3,\delta)\right)-C_3\left(1+\delta\right)\sin\left(4\gamma_{3,n}^{(1)}(C_3,\delta)\right)} \\
\gamma_{1,n}(C_1) = \dfrac{2\left(\left(\gamma_{1,n}^{(2)}(C_1)\right)^2+C_1\cos^2\left(\gamma_{1,n}^{(2)}(C_1)\right)\right)}{\sin\left(2\gamma_{1,n}^{(2)}(C_1)\right)+2\gamma_{1,n}^{(2)}(C_1)} \\
\gamma_{2,n}(C_2) = \dfrac{2\left(\left(\gamma_{2,n}^{(2)}(C_2)\right)^2+C_2\cos^2\left(\gamma_{2,n}^{(2)}(C_2)\right)\right)}{\sin\left(2\gamma_{2,n}^{(2)}(C_2)\right)+2\gamma_{2,n}^{(2)}(C_2)} \\
\gamma_{3,n}(C_3,\delta) = \dfrac{2\left(2C_3\left(1+\delta\right)\gamma_{3,n}^{(2)2}(C_3,\delta)+\left(\gamma_{3,n}^{(2)2}(C_3,\delta)+C_3^2\delta\right)\sin^2\left(2\gamma_{3,n}^{(2)}(C_3,\delta)\right)\right)}{2\gamma_{3,n}^{(2)}(C_3,\delta)\left(2C_3\left(1+\delta\right)+1\right)-2\gamma_{3,n}^{(2)}(C_3,\delta)\cos\left(4\gamma_{3,n}^{(2)}(C_3,\delta)\right)-C_3\left(1+\delta\right)\sin\left(4\gamma_{3,n}^{(2)}(C_3,\delta)\right)} \\
A_n = \dfrac{8C_1C_2C_3\sqrt{C_1^2+\gamma_{1,n}^2}\sqrt{C_2^2+\gamma_{2,n}^2}\left(C_3\tan\left(\gamma_{3,n}\right)+\gamma_{3,n}\right)\left(C_3^2\delta^2+\gamma_{3,n}^2\right)\left(1+\delta\right)\left(T_0^{(0)}-T_f\right)}{\gamma_{1,n}\gamma_{2,n}\left(C_1^2+C_1+\gamma_{1,n}^2\right)\left(C_2^2+C_2+\gamma_{2,n}^2\right)\left(2C_3^4\delta^2+C_3^3\delta\left(1+\delta\right)+2C_3^2\left(1+\delta^2\right)\gamma_{3,n}^2+C_3\left(1+\delta\right)\gamma_{3,n}^2+2\gamma_{3,n}^4\right)\sqrt{C_3^2\gamma_{3,n}^2\left(1+\delta\right)^2+\left(\gamma_{3,n}^2-C_3^2\delta\right)^2}} \\
\textit{für} \\
n\in\mathbb{N}_0
\end{array}
\right)
$$

and

$$
\left(
\begin{array}{c}
T\left(x,y,z,t\right) = T_f+\sum_{n=0}^{\infty}\left(A_n e^{-4\gamma_0 t\left(\frac{\gamma_{1,n}^2}{a^2}+\frac{\gamma_{2,n}^2}{b^2}+\frac{\gamma_{3,n}^2}{c^2}\right)}\cos\left(\frac{2\gamma_{1,n}x}{a}\right)\cos\left(\frac{2\gamma_{2,n}y}{b}\right)\left(C_3\sin\left(\gamma_{3,n}-\frac{2\gamma_{3,n}z}{c}\right)+\gamma_{3,n}\cos\left(\gamma_{3,n}-\frac{2\gamma_{3,n}z}{c}\right)\right)\right) \\
\textit{für} \\
-\frac{a}{2}\le x\le\frac{a}{2}\quad\wedge\quad-\frac{b}{2}\le y\le\frac{b}{2}\quad\wedge\quad-\frac{c}{2}\le z\le\frac{c}{2}
\end{array}
\right)
$$

This solution can be easily implemented online.

Simulation Results

In order to document the effectiveness of the above presented analytical solution, two different cases have been simulated. For both cases air cooling of the stack will be considered.

- In the first cases natural convection with dry air is assumed,
- In the second case forced convection, with laminar flow is considered.

The average value of air flow speed v relative to the stack is assumed to be zero in the first case and in the second case 4 m/s. The set of parameters is shown in **Table 9**.

Table 9: Set of parameters

Meaning	Value	Unit	
Length of stack	12,7	m	
Width of stack	2,438	m	
Height of stack	0,8925	m	
Density	7850,0	kg/m3	material dependent
Specific heat capacity	475,0	J/K/kg	material dependent
Thermal conductivity material	51,6	W/K/m	material dependent
Temperature conductivity	1,3838E-05	m2/s	calculated
Stefan-Boltzmann constant	5,67E-08	W/m2/K4	constant
Start temperature stack	538	° C	process dependent
Air flow	4,00	m/s	process dependent
Air flow average	5,00	m/s	average
Room temperature	32	° C	average
Thermal conductivity concrete	2,1	W/K/m	literature
Size concrete	0,80	m	estimated
Start temperature difference inside -outside stack	150	° C	estimated
Hemispherical total emissivity	0,8		estimated
Time since start cooling	3600	s	user input
Crtitical temperature gradient	490	° C	

Case 1: Natural convection with dry air (air flow speed: 0 m/s)

Fig. 89 shows the calculated temperature field across width and height in the middle of the stack and the corresponding temperature gradient at the start of cooling.

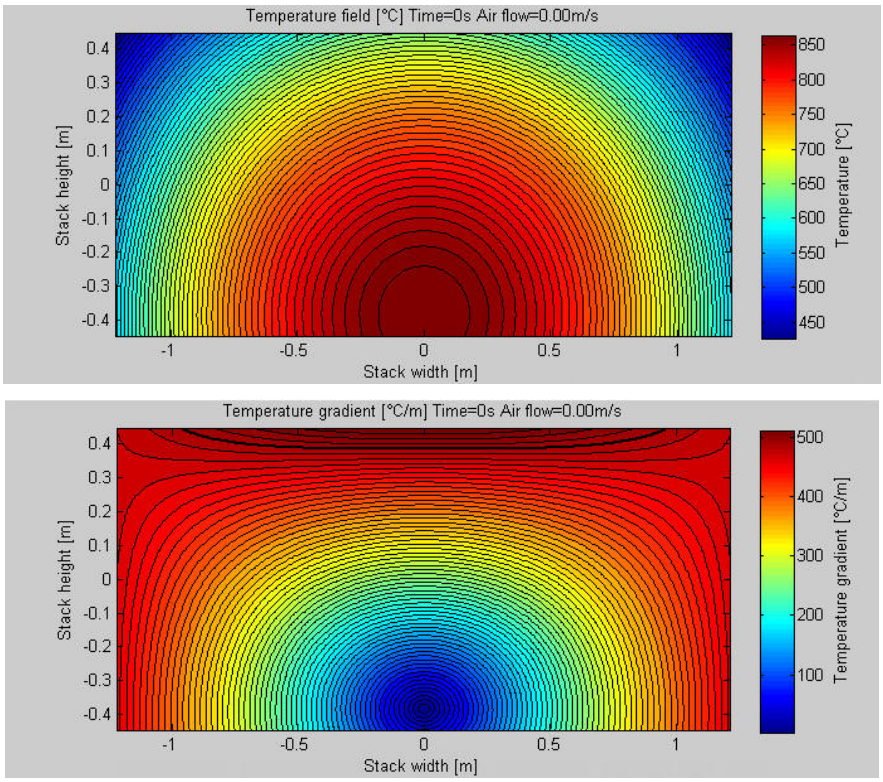


Fig. 89: Temperature field (top) and the temperature gradient (bottom)

Fig. 90 shows the calculated temperature field across width and height in the middle of the stack and the corresponding temperature gradient after 1 hour of cooling.

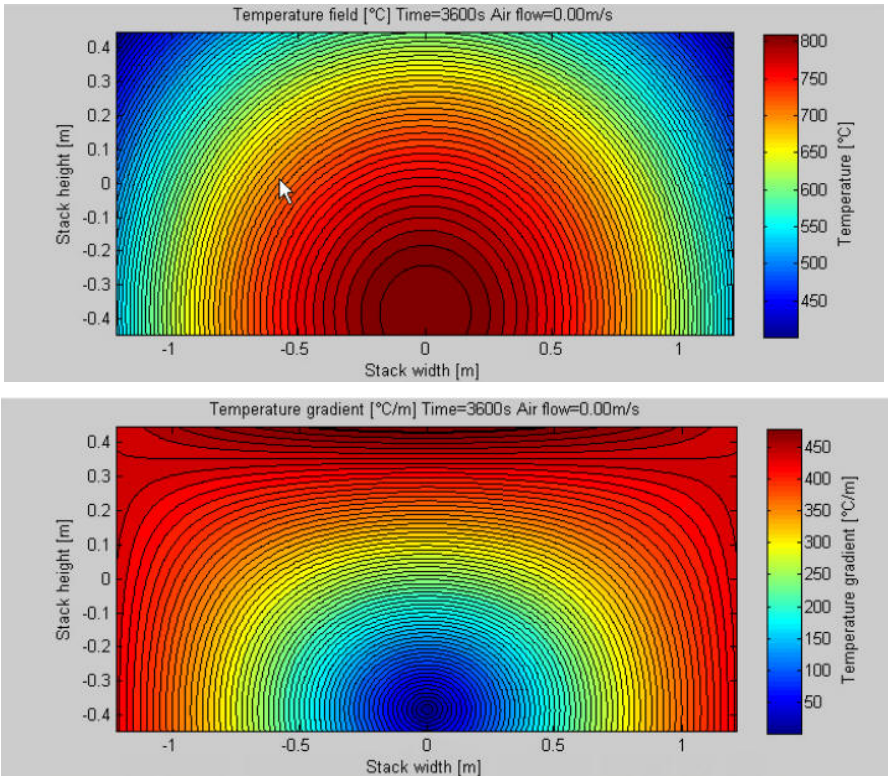


Fig. 90:Temperature field (top) and the temperature gradient (bottom)

Case 2: Forced convection (air flow speed: 4 m/s)

Fig. 91 shows the calculated temperature field across width and height in the middle of the stack and the corresponding temperature gradient at the start of cooling.

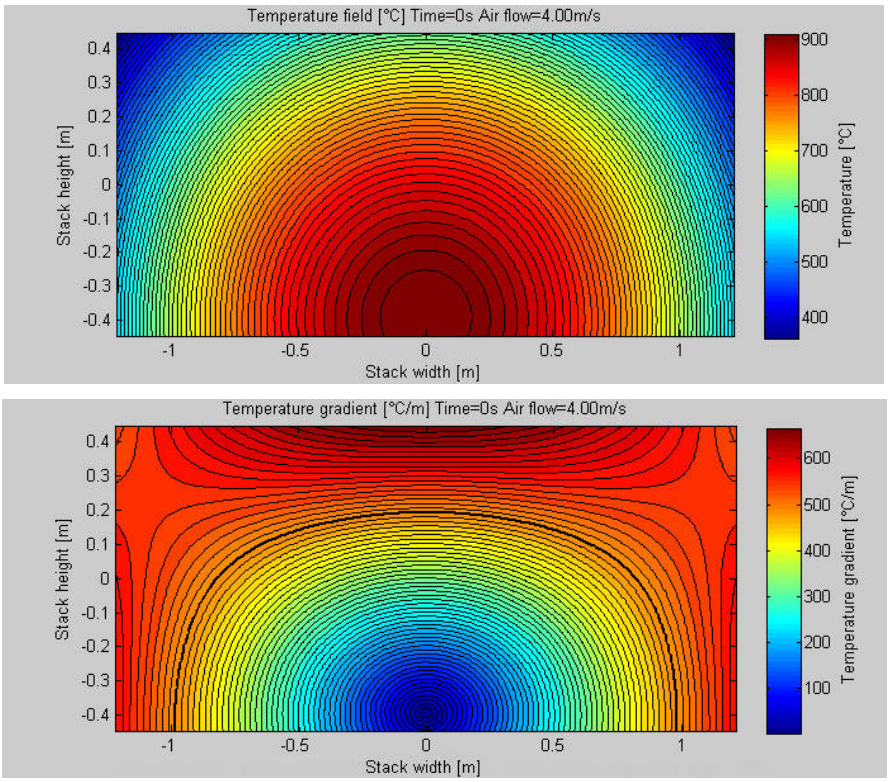


Fig. 91: Temperature field (top) and the temperature gradient (bottom)

Fig. 92 shows the calculated temperature field across width and height in the middle of the stack and the corresponding temperature gradient after 1 hour of cooling.

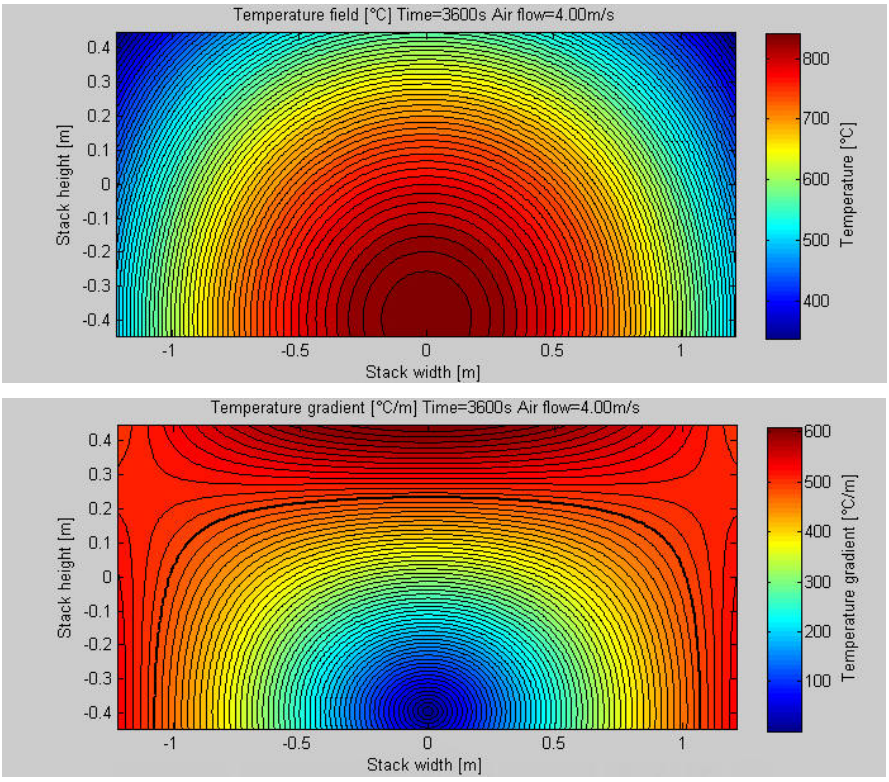


Fig. 92: Temperature field (top) and the temperature gradient (bottom)

The results of the temperature field calculations show:

- the vertical asymmetry of the temperature field is due to the bad heat transfer caused by the ground floor (concrete) on which the stack lies and
- the increase of the temperature gradient close to the edges of the stack, which is indicated by the smaller distances between the isothermal lines.
- The upper plates on the stack are mostly threatened of the buckling phenomenon.

In order to perform cooling simulations with various parameters an user interface has been created as shown in **Fig. 93**.

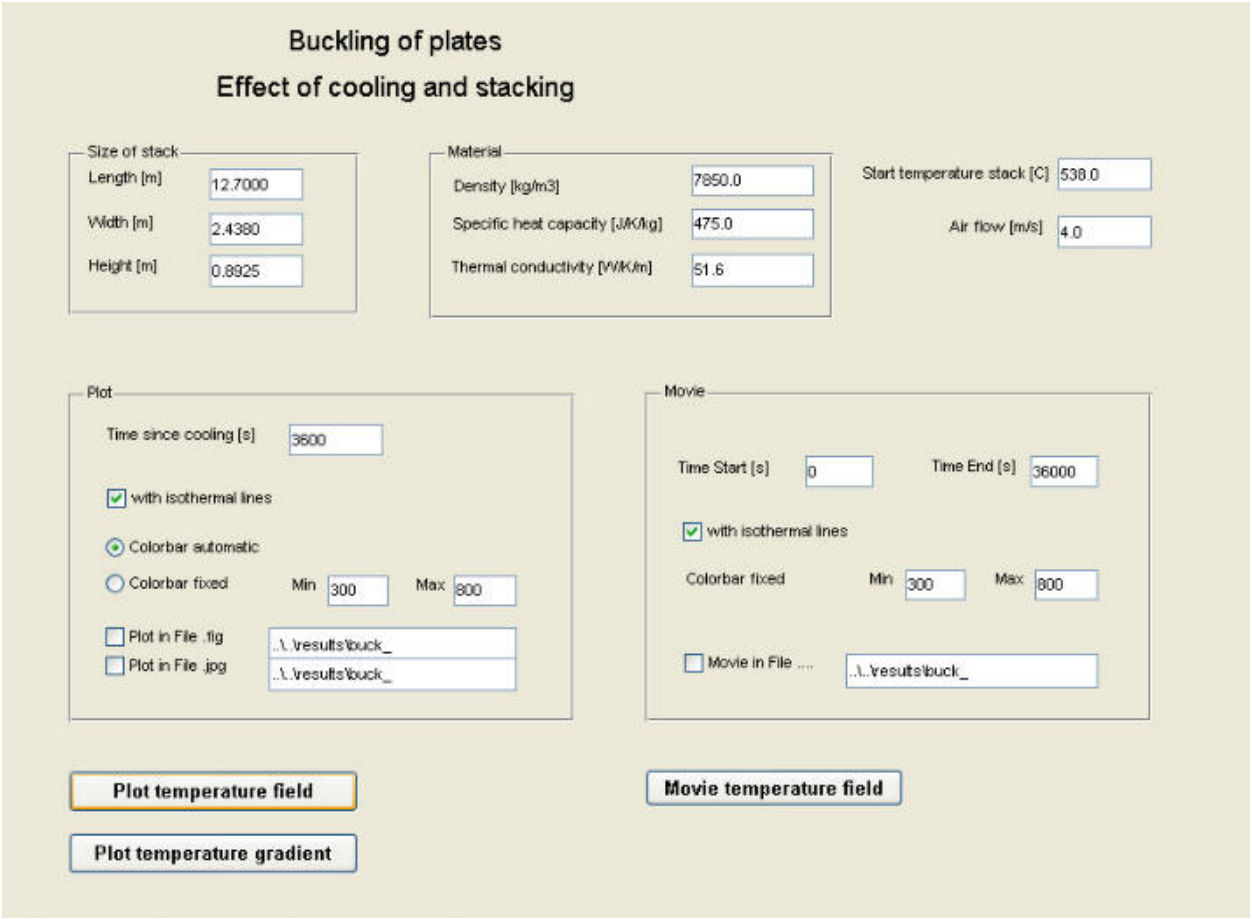


Fig. 93: User Interface of the cooling simulation module

Quenching of a steel plate (Mefos)

Levelling of plate is frequently applied in connection with direct quenching after rolling. A complex microstructure state is developed in the plate and the mean temperature of the plate is around 600 °C. This makes it to a challenge to achieve the desired final plate flatness. In order to get a general view of the of the deformation-, stress- and microstructure development, modelling was performed in the program Sysweld. The plate-model was placed standing on the length-wise edge as shown in **Fig. 94**. In this way, gravitational force was not needed to be counted upon. The analysis was based on the following conditions:

- Steel grade selected is 18CD4 with a nominal analysis of 0,2%C 0,7%Mn and 1%Cr.
- The initial temperature is homogenous and set to 900 °C
- 100% initial austenitic structure is assumed.

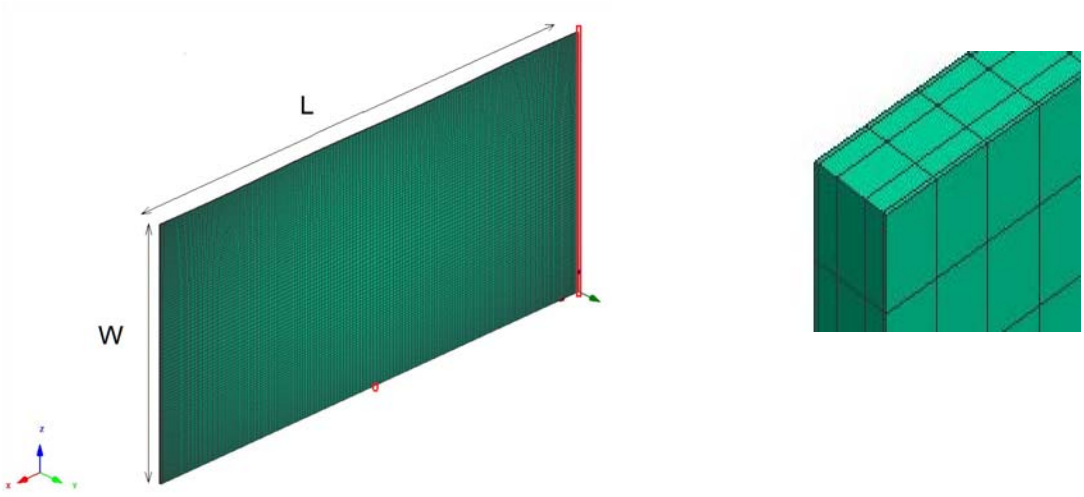


Fig. 94: Model with locked displacements (left) and close-up showing element-structure (right)

The model is generated using a dedicated meshing-program for temperature analysis. In total around 100.000 elements are used for this model. The elements on the surface are made very thin in order to catch the effect of cooling on temperature development. Locking of nodes are applied on the edge and in y-direction in the middle of the plate according to **Fig. 94**. A model in 3D is used in order to study the development of the geometrical deformation of the plate.

Quenching is done on both sides of the plate. For this analysis example the quenching applied is unsymmetrical as illustrated in **Fig. 95** where the heat exchange coefficient for the upper and lower side is plotted as a function of temperature. The difference between upper and lower side is set in order to illustrate the effect of eventual excess water on the upper side caused by unflatness of the plates, water pools etc.

Based on a CCT-diagram for the steel grade 18CD4 a metallurgical diagram suited to be used in Sysweld-calculations can be derived, see **Fig. 96**. The blue lines show the development of the martensitic region and the green lines the development of bainitic regions with cooling speed as parameter.

The temperature part of the calculation is obviously very fast. Resulting temperature, microstructure and stress distribution is shown for the upper left corner of the plate while calculated displacement is shown for the whole plate. The extent of the analysis is 22 seconds and intermediate results after 5,5 seconds are also presented.

The results from the temperature calculation are shown in **Fig. 97**. After 5,5 seconds of quenching the main part of the plate is between 500 – 750°C and after 22 seconds the main part is between 125 – 185°C.

The calculated microstructure evaluation is shown in **Fig. 98** - **Fig. 99**. After 5,5 seconds the bainite content is around 1% and the martensite content is around 13% on 75% of the thickness. About 25% over the thickness (on the upper surface) is however a mixture of bainite and, up to 90%, martensite. 5,5 seconds is also a common point of time where pre-levelling is performed. Obviously this high martensite content on only one side of the plate affects the levelling process as it results in varying tensile properties over the thickness.

After 22 seconds of quenching the microstructure is more homogenous through the thickness. The martensite content is between 81 and 92%. The properties over the thickness are thus more uniform, but this hard material is more difficult to level and the higher levelling force needed results in a higher deflection in the leveller as discussed earlier.

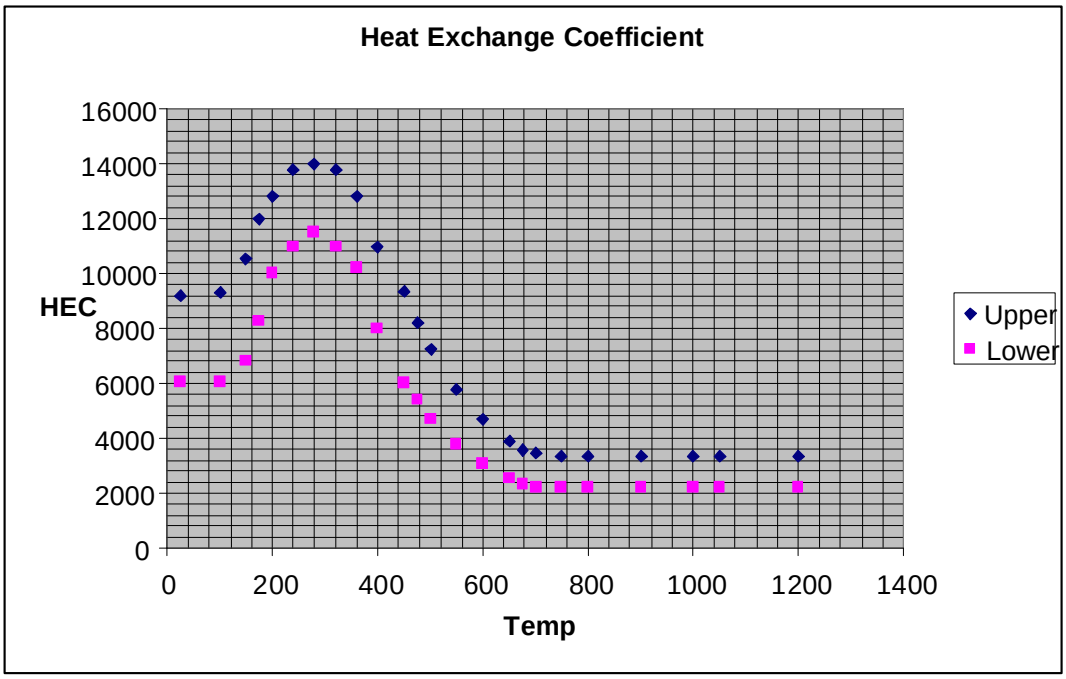


Fig. 95: Heat exchange coefficient as applied in the analysis

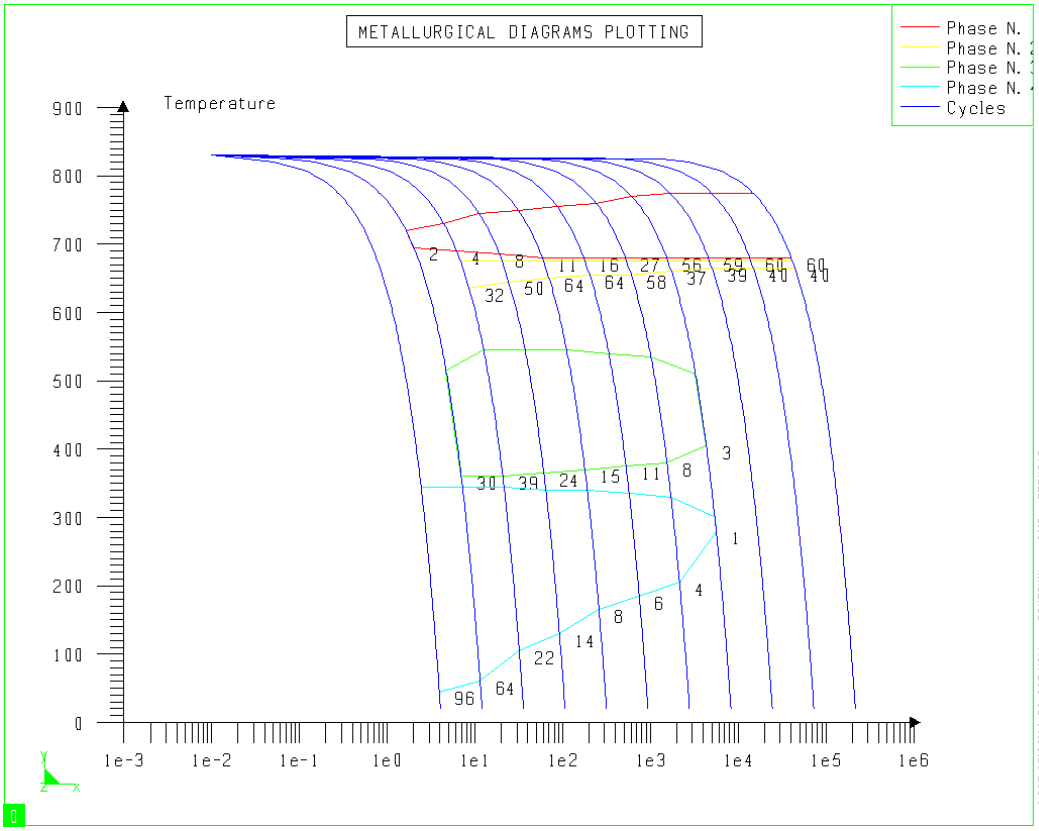


Fig. 96: Metallurgical diagram derived from the CCT-diagram for steel grade 18CD4

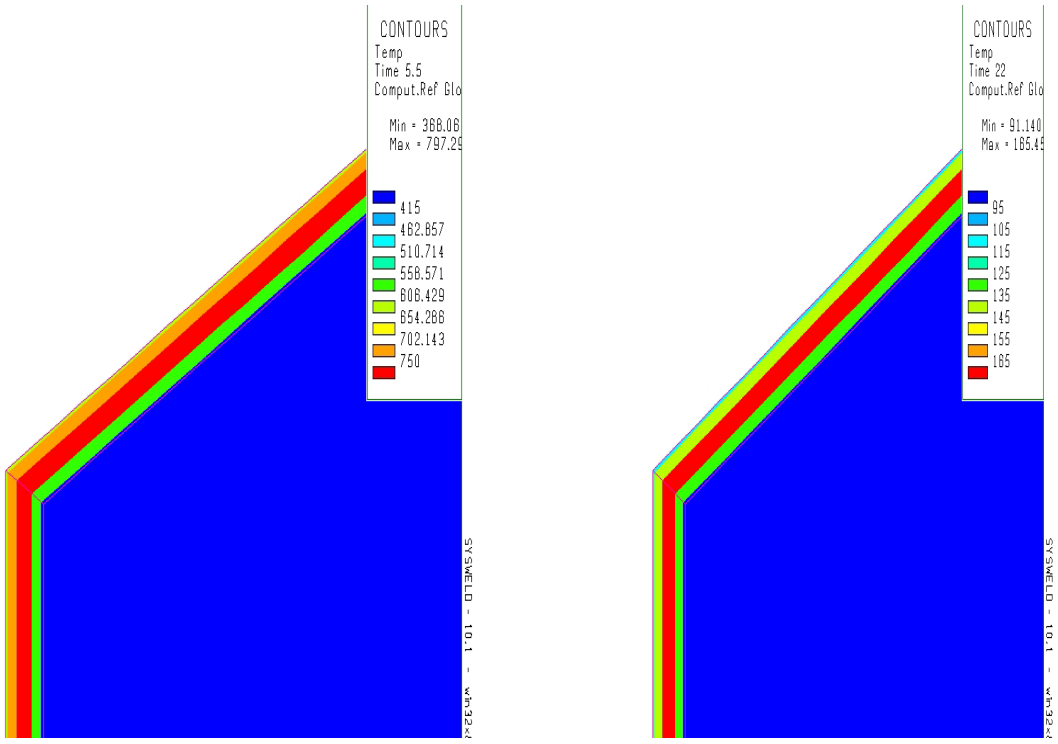


Fig. 97: Temperature in the cross-section of the plate after 5,5sec and 22sec respectively (upper left corner)

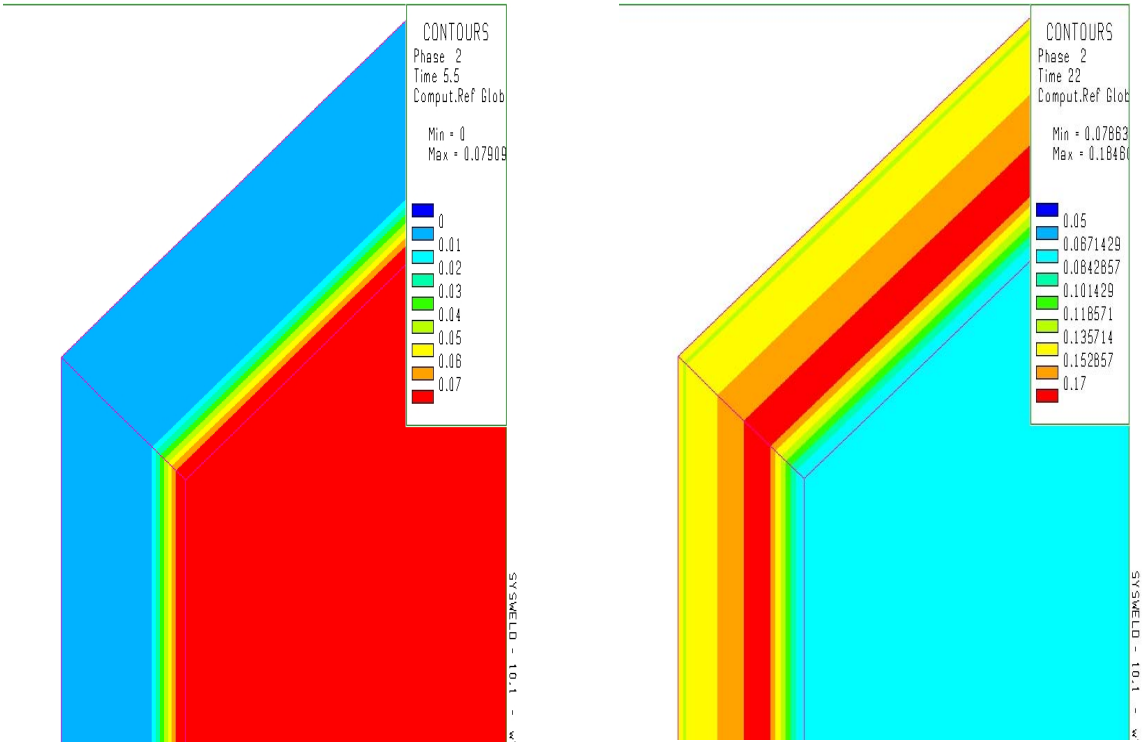


Fig. 98: Bainite content after 5,5sec and 22sec respectively

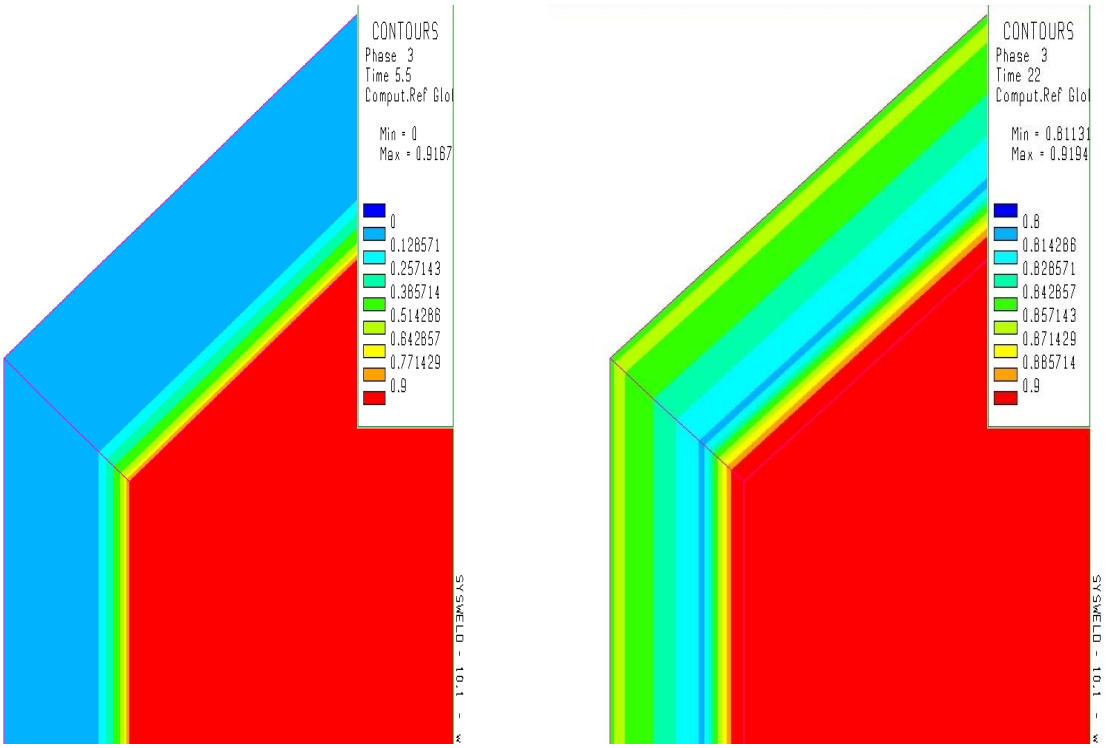


Fig. 99: Martensite content after 5,5sec and 22sec respectively

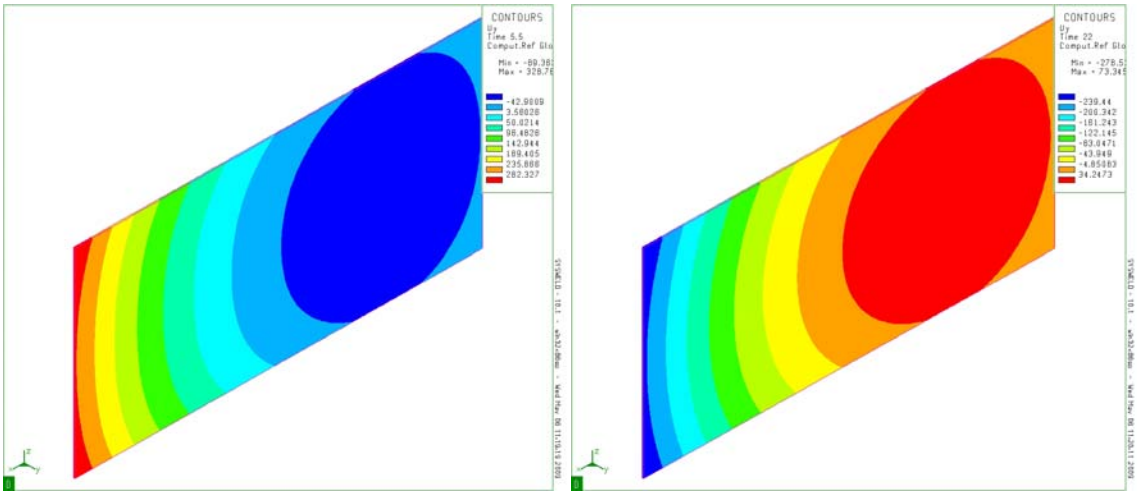


Fig. 100: Displacement in thickness direction after 5,5 sec and 22 sec respectively

In **Fig. 100** the displacement in thickness direction after 5,5 sec and 22 sec are shown. As stated earlier, fictive boundary conditions according to **Fig. 94** are applied. Clearly, there is a change in displacement direction and high displacements throughout the cooling process.

Calculated lengthwise stress development during quenching is shown in **Fig. 101**. Initially the stress state is compressive in the center of the plate. After completed quenching the stress state on the surface is tensile. This is also verified from industrial experience.

With the plate in correct position and gravity forces included a modified residual stress pattern could be anticipated.

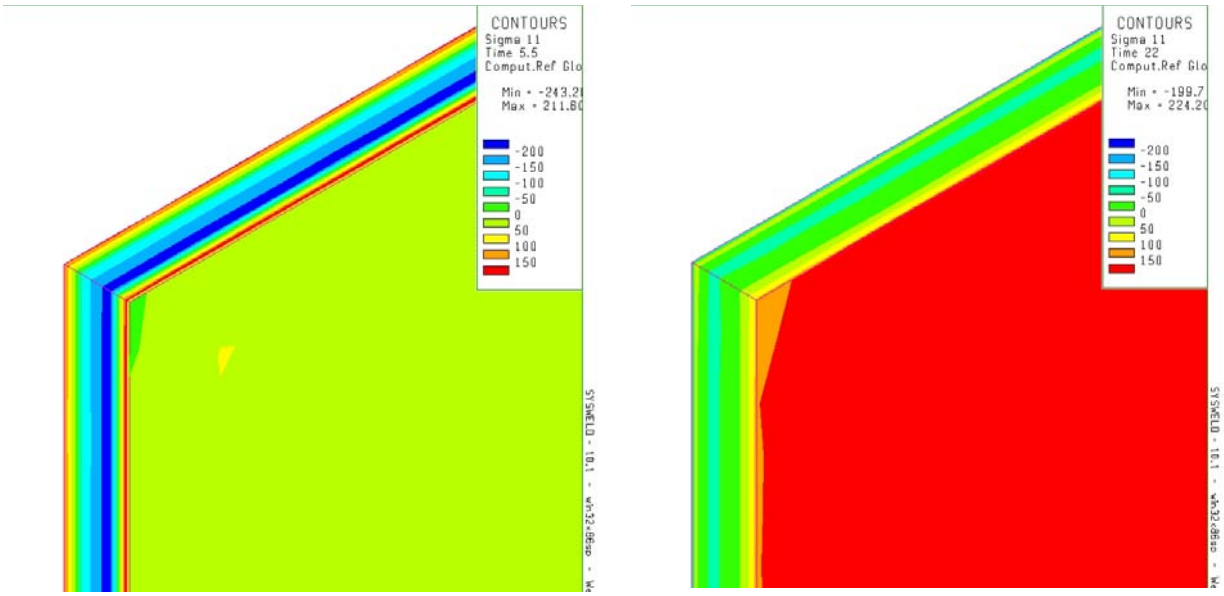


Fig. 101: Stress in the x-direction (lengthwise) after 5,5sec and 22sec respectively
Stresses with positive sign are tensile.

Task 3.4: Set-up optimisation to produce flatter plates

Scunthorpe Light shear line

There did not appear to be plate distortion problems directly associated with cooling on this type of cooling bank and it is concluded therefore that cooling was sufficiently symmetrical in combination with gravity effects to maintain rolled-in plate flatness. For the thinner gauge range of plates processed on this cooling bank, provided that they are rolled flat in the mill and are hot (>700 °C) a reasonably flat bank surface and gravity effects will ensure maintenance of flatness during cooling and the accrued strength at temperatures below 400 °C is sufficient to resist subsequent mechanical damage or thermal distortion.

Main problem on this cooling bank is rolled-in shape if the plate is cold (<600°C) prior to entry to the hot leveller. The origin of any long-range shape in plates on this bank was the finishing mill and this shape could be improved by the hot leveller but not completely removed. Poor shape was more evident in thinner colder plates generally most of this poor long-range shape was retained through the hot levelling process. The hot levellers appeared to be much less effective for thinner colder plates, probably as a result of higher strength of these plates and the limitations of the machine.

Generally push-dogs trapped under plates above 500°C were seen to cause permanent local distortion if allowed to cool further under the influence of these misaligned push-dogs; thin hot plates might be susceptible to long-range permanent distortion by the dogs lying underneath the bulk of the plates.

Dummy passes through the hot leveller would reduce the temperature of plates being pushed onto the banks and make them much less susceptible to permanent distortion and scratching by misalignment and sticking of push-dogs.

The probability of distortion and mechanical damage of plates beyond the halfway point under normal circumstances is very low because the plates are generally below 250°C and have achieved approximately 90% of their cold strength.

Scunthorpe Heavy shear line

No distortion resulting directly from cooling asymmetry was observed. All plate distortion that was observed could be attributed to mishandling or poor support of the plates whilst hot.

Permanent distortion of plate on cooling bank nos. 2, 3, and 4 is often a result of local insufficient even support when the plate is hot, and prolonged residence in these locations until the plate bulk temperature is relatively low (400 °C).

Sometimes plant localised conditions such as a slewed plate orientation between different adjacent conveying systems, cause short range plate bending when the plate is hot and weak which persists if the plate is allowed to cool in this condition.

Distortion observed at the gearbox cover between cooling banks nos. 3 and 4 is a result of insufficient support of that part of the plate whilst resident over the gearbox cover.

Plate stacking

According to the above analyse buckling can be avoided by influencing the temperature field e.g. the cooling behaviour of the stack by introducing the following measures:

- Reducing the air flow speed down to zero around the heavy plate stack,
  - by closing the doors in work hall or
  - putting wind shields around the stack
- Choosing the height c of heavy plate stock, so that 2c> b, whereas b is the width of the plates. In this case the asymmetry of the temperature field in vertical (height) direction will not cause buckling
- Covering the top surface of the heavy plate stack with an insulating mat to reduce the thermal gradient in the stack. The insulating mat should have the following properties

  $$\kappa_I / d_I = \kappa_B / d_B,$$

  where

  κ_I = heat conductivity of the insulting mat,

  κ_B = heat conductivity of the ground floor plate (e.g. concrete),

  dI = thickness of insulting mat and

  d = thickness of the ground floor plate.

WP 4: Analysis, Prediction and optimisation of levelling processes

Task 4.1: Data acquisition of levelling process, component behaviour and flatness

Trials on a pilot roller leveller at Corus Teesside Technology Centre

A series of trials have been conducted on a pilot roller leveller at Corus Teesside Technology Centre. The pilot leveller can use up to 9 rolls of up to 270 mm in diameter (pitch 310 mm), arranged in alternative 'tilting nest' or 'parallel nest plus exit breast roll' configurations (**Fig. 102** and **Fig. 103**).

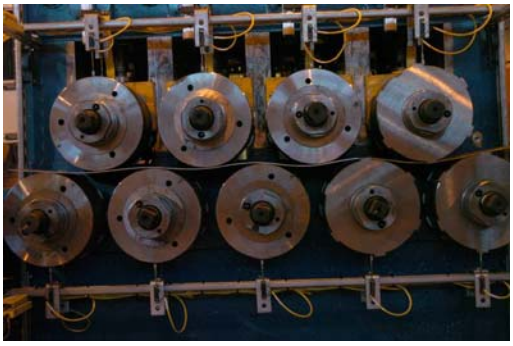


Fig. 102: Pilot leveller with rolls arranged in the 'tilting nest' configuration



Fig. 103: Rearrangement of pilot leveller rolls to simulate conditions in a parallel-nested leveller equipped with an exit breast roll.

[Final bottom roll (9) removed; constant penetration imposed at main top roll (2, 4 & 6)
Final top roll (8) raised above the level of the other top rolls to act as breast roll.
Breast roll offset = height of base of breast roll above base of other top rolls]

In contrast with levellers located on steel mills, the design of the pilot machine permits direct observation of the path of the plate between the rolls, allowing measurement of plate curvature and location of plate/roll contact points in each bending triangle. Position transducers indicate the deflections of the rolls under load (**Fig. 104**) giving the 'real' penetration settings imposed on the plate (the difference between roll penetrations in the loaded and unloaded conditions has a significant effect on outgoing plate curvature).

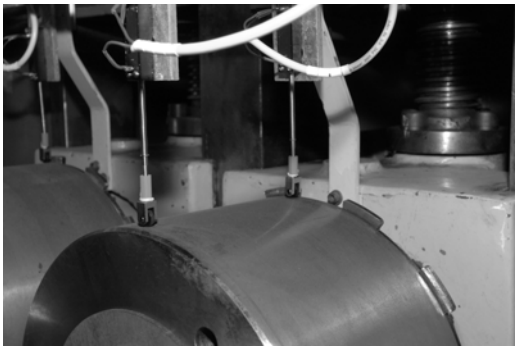


Fig. 104: Position transducers monitoring deflection of rolls under load

A wide range of samples of coil sourced laser cut strip have been processed within the pilot leveller (grades S275, S355 and S460, gauge 3 to 10 mm, length 2 to 3 m), using both 'tilting nest' and 'parallel nest' roll configurations. Nominal/loaded penetrations, and measured entry/exit bow (measured in length direction, see **Fig. 105**), were recorded in each case (**Table 10** and **Table 11**). Leveller settings were varied systematically for each distinct sample grade/size, so as to study the sensitivity of exit bow to roll penetrations and to exit breast roll position.

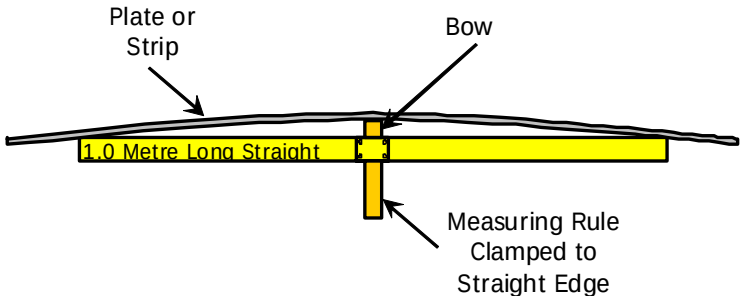


Fig. 105: Measurement of plate bow

[Long/cross bow is measured as the maximum deflection over a fixed distance (normally 1 m) in the strip length/transverse direction (units mm/m). Bow is defined to be positive/negative if the ends of this 1 m length are above/below the mid-length position (the bow illustrated is negative)]

Digital photographs of plates within the leveller allowed measurement (by pixel count) of curvature and plate/roll contact points in each bending triangle (**Fig. 106**). In general, the contact points are close to/slightly before the roll centre positions, with the turning points (peaks/troughs) in the plate trajectory a short distance (10 to 40 mm) beyond the roll centres.

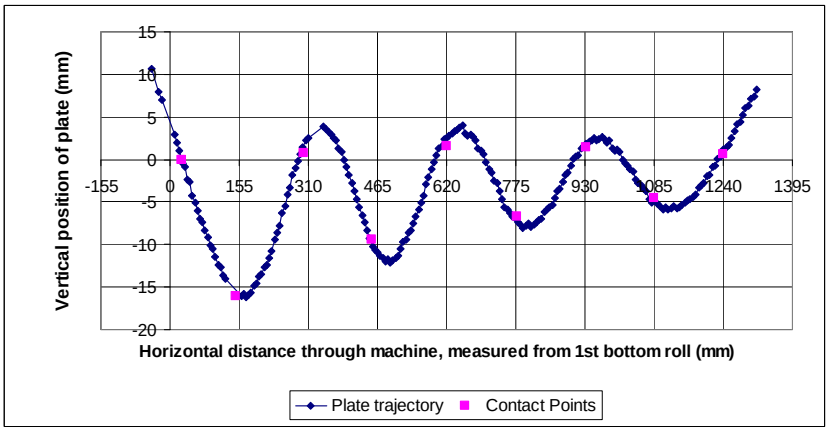


Fig. 106: Path of plate (sample 'SH20') through leveller, with 9 roll contact points indicated

[Plate path and contact points obtained by analysing pixels in digital photograph
Roll centres located at x=0, 155, 310, ... 1240 mm]

Table 10: Leveller-settings and measured exit bow for strip samples processed using the standard '4 over 5 roll' configuration

				Effective Loaded Penetrations (mm)			
Sample I.D.	Gauge (mm)	Grade	Post-bow (mm/m)	Roll T2	Roll T4	Roll T6	Roll T8
SH5	10	S275	-5	8.4	5.8	3.1	0.4
SH6	10	S275	-4	8.6	5.9	3.4	0.0
SH7	10	S275	-5	8.5	5.6	2.9	0.5
SH12	6	S275	-6	10.6	8.0	4.9	1.3
SH13	6	S275	6	10.7	8.2	4.9	2.8
SH14	6	S275	3.3	10.9	8.2	5.0	2.6
SH18	3	S275	30	16.5	13.5	9.7	5.7
SH19	3	S275	21	16.4	13.5	9.6	5.2
SH20	3	S275	39	16.7	13.5	9.5	6.2
SH21	3	S275	42	18.9	13.4	9.4	6.3
ADR08	3	S275	-2	13.4	13.4	13.4	1.7
ADR09	3	S275	0.5	16.6	16.6	16.6	1.7
ADR10	3	S355	-35	15.3	15.3	15.3	0.0
ADR11	3	S355	-41	18.4	18.4	18.4	0.0
ADR12	3	S355	15.5	18.2	18.2	18.2	4.1
ADR13	3	S355	59	18.4	18.4	18.4	8.9
ADR50	10	S460	-8.0	4.9	1.8	1.5	1.5
ADR51	10	S460	-6.0	5.1	2.3	1.2	0.6
ADR52	10	S460	15.0	4.8	2.4	2.4	1.9
ADR53	10	S460	8.5	6.0	3.4	1.9	1.6
ADR54	10	S355	7.0	3.5	1.4	1.2	0.5
ADR55	10	S355	3.0	3.9	0.9	0.9	-0.2
ADR56	10	S355	3.5	3.7	1.1	1.0	0.1
ADR57	10	S355	17.0	4.6	2.2	1.8	2.1
ADR58	6	S355	0.0	9.6	6.3	4.5	2.1
ADR59	6	S355	21.5	9.3	6.5	5.2	3.7
ADR60	6	S355	-6.0	9.5	5.6	3.2	0.8
ADR61	6	S355	71.0	11.3	8.3	7.5	5.6
ADR62	3	S355	73.0	21.6	16.9	13.2	9.1
ADR63	3	S355	29.0	21.5	15.7	10.6	6.5
ADR64	3	S355	-2.5	21.3	15.0	9.0	3.5
ADR65	3	S355	187.0	21.5	19.3	16.9	15.2

Table 11: Leveller-settings and measured exit bow for strip samples processed using the '3 over 4 plus exit breast roll' configuration

[Pilot leveller rolls arranged to simulate conditions in a parallel-nested leveller equipped with an exit breast roll.
Breast roll offset = height of base of breast roll above base of other top rolls]

				Effective Loaded Penetrations (mm)			Breast Roll Offset
Sample I.D.	Gauge (mm)	Grade	Post-bow (mm/m)	Roll T2	Roll T4	Roll T6	(mm)
ADR02	3	S355	290	18.5	18.5	18.5	119
ADR03	3	S355	195	16.5	16.5	16.5	119
ADR04	3	S355	192	16.5	16.5	16.5	119
ADR05	3	S275	203	14.6	14.6	14.6	119
ADR06	6	S275	75.5	7	7	7	119
ADR07	10	S275	6.5	3.5	3.5	3.5	119
ADR14	3	S355	-75	18.4	18.4	18.4	18.4
ADR15	3	S355	-32	14.1	14.1	14.1	14.1
ADR16	6	S275	-22.5	8.2	8.2	8.2	8.2
ADR17	10	S275	5	3.7	3.7	3.7	3.7
ADR18	10	S460	43.5	5.8	4.7	5.8	21.3
ADR19	10	S460	31.5	5.8	4.8	5.3	15.9
ADR20	10	S460	10.5	5.4	4.6	5.0	7.1
ADR21	10	S460	-6.5	5.5	4.6	4.8	3.1
ADR22	10	S460	-13.0	5.6	4.7	5.0	5.0
ADR23	10	S355	6.0	4.6	3.8	4.3	24.7
ADR24	10	S355	6.0	4.6	3.8	4.1	14.5
ADR25	10	S355	7.5	4.7	3.9	4.1	10.8
ADR26	10	S355	-6.5	4.6	3.7	3.8	6.1
ADR27	10	S275	3.0	3.2	2.4	2.8	23.3
ADR28	10	S275	3.0	3.2	2.5	3.0	13.3
ADR29	10	S275	5.0	3.2	2.6	2.7	7.2
ADR30	10	S275	2.0	3.4	2.8	2.9	4.2
ADR31	10	S275	-8.0	3.4	2.8	2.7	-0.3
ADR40	3	S355	<<0	15.8	15.8	15.8	13.2
ADR41	3	S355	-6	16.1	16.1	16.1	24.9
ADR42	3	S355	47.5	18.2	16.3	16.9	35.6
ADR43	3	S355	21.5	18.4	16.8	16.6	30.3
ADR44	3	S355	0	17.9	15.7	16.3	26.7
ADR45	3	S355	8	17.5	16.2	15.9	28.3
ADR46	6	S355	-11	7.9	5.8	5.9	8.3
ADR47	6	S355	-1	7.9	5.9	6.1	10.5
ADR48	6	S355	7	8.2	5.9	5.9	12.4
ADR49	6	S355	15	7.7	5.7	6.1	14.4

Deflection measurements in the hot plate leveller at Ruukki

The deflection of the frames in a hot leveller in the plate mill at Ruukki has been measured. Plates in width up to 3500 mm and thickness between 5 and 150 mm are levelled. The leveller is mainly constructed as two frames, each carrying a set of rolls as can bee seen in **Fig. 107**. The lower frame can only be transverse tilted while the upper frame can be transverse as well as lengthwise tilted which is done in the so-called cradle setup. During these trials the deflection while levelling plates of different kinds with variation in temperature, width and thickness were measured by the use of a laser triangulation system.

Measurements

The measurement was performed by mounting two laser units on the leveller upper frame, one on the entry side and the other on the exit side. Reflecting steel sheets were welded on the lower frame directly under the position of the lasers. A close-up of the left side of the leveller shows where the laser unit and the reflecting surface were mounted, see **Fig. 108**. The laser units were held in place with three strong magnets.

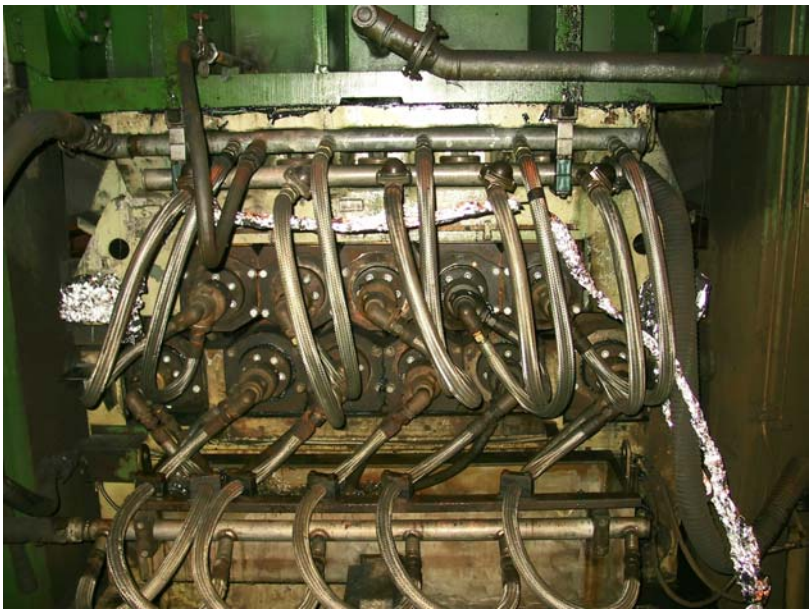


Fig. 107: Hot levelling machine at Ruukki heavy plate mill



Fig. 108: Left side of leveller with laser unit mounted on the upper frame and the reflecting surface on the lower frame

The measuring range for the used laser unit is ±35 mm at a stand-off distance of 200 mm meaning that the measurements are to be performed between 165 and 235 mm away from the laser unit. The deflection measured was on the roll change side of the leveller.

Measurements were performed during production. Deflection during levelling of plates with variation in steel grade, width, thickness and temperature at the leveller was collected. The variation in plate thickness was between 8 and 60 mm and the width variation was between 1945 and 3223 mm. The steel grades were all plain C-Mn steels with small variation in yield point.

Evaluation of measured deflection

The average deflection for the first pass in the leveller was extracted from the measured data. One example of measured deflection during levelling is presented in **Fig. 109**. The figure shows the deflection at the entry side and the exit side of the plate leveller at Ruukki Raahe during 5 consecutive levelling passes with the same plate. Depending on the material properties, rolling conditions and plate dimensions the deflection varies between 0,04-0,26 mm.

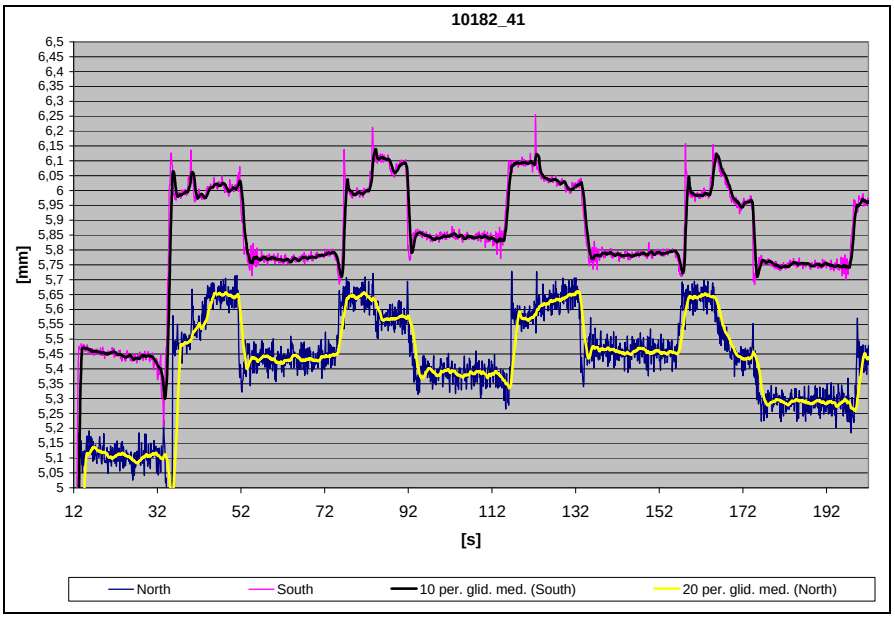


Fig. 109: Deflection at the entry- and exit side of the leveller

The measured deflection together with selected parameters from the process data were analysed using multivariate data analysis. The results show that the average deflection in the leveller is a function of thickness, width and temperature after rolling. The variable importance plot for the model gives at hand that the plate temperature is very important since the hot yield strength is strongly linked to the temperature. The plate thickness has more importance than the plate width as an increase in plate width with one millimetre increases the cross section area more than an increase in thickness with one mm. The resulting expression for the deflection is the following:

$$\mathbf{D = 0{,}2055 + 0{,}003028*Thickness + 1{,}46E\text{-}05*Width - 0{,}0002137*Temperature.}$$

The model is valid for plates with a thickness range of $8 \leq t < 40$ mm.

Hot levelling trials at MEFOS

A closer investigation of hot-levelling trials performed at the pilot-plant leveller at MEFOS has previously been done [11]. The trials were performed to study the influence of different settings on plate curvature. Straight bars were run through a flattener using two different types of settings; a one over two straightening triangle (3 rolls) and a two over three rolls set-up (5 rolls), see **Fig. 110**. The material used was Weldox 960, which is a high strength construction steel. The temperature range was between 850 – 1000 °C. Experimental data is shown in **Table 12**.

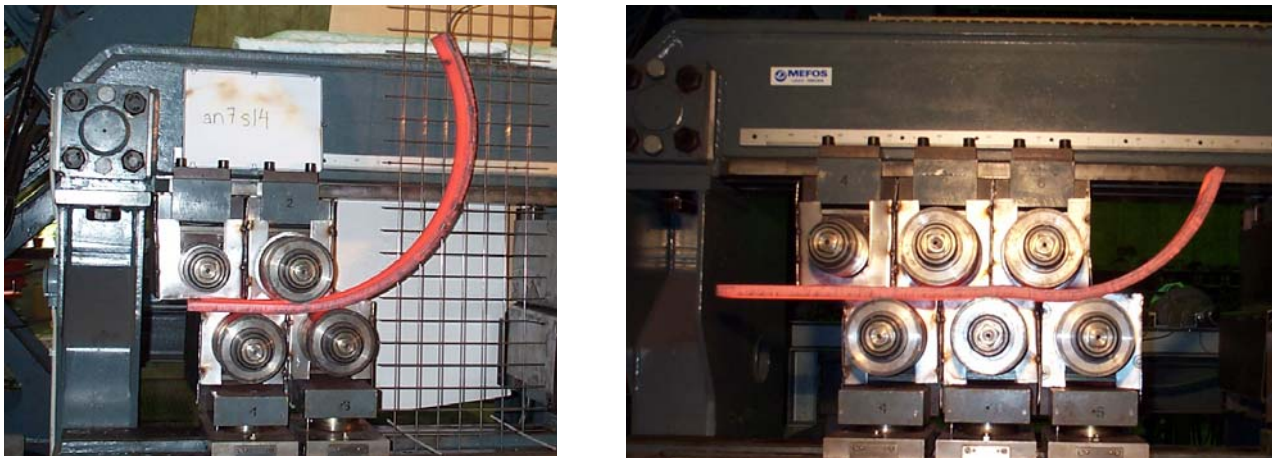


Fig. 110: Hot levelling trials: 3-roll levelling (left) and 5-roll levelling (right).

Table 12: Experimental data

Roll diameter	140 mm
Speed	0.07 m/s
Material	Weldox 960
Bar dimension h x w x l	20.2 x 78.5 x 1000 mm

The 3-roll bending results in a one-way bending with compressive strain on the upper side of the bar and tensile strain on the lower side. The 5-roll bending results in repeated compressive and tensile loading on both sides of the bar. In order to evaluate different material modelling, FE-simulations using the program MSC Marc were performed on both of the trial types.

Pilot plant hot bending test and model validation

In order to improve the modelling of the hot levelling process, hot bending trials have been performed in the pilot-plant forging press at MEFOS [11]. Both single bending and double bending were included in the trials. In this way a reversal strain is applied, similar to regular hot levelling. The trial setup is based on the design of the hot plate leveller at Ruukki. This design is basically a conventional leveller with a roll radius of 130mm and a c-c distance of 260mm for the 5 over 4 rolls in the centre. For the pilot-plant trials, tools were designed to cover the contact area and c-c distance in the leveller, see Fig. 111. The trial pieces were cut out from regular rolled plates at Ruukki. Three different cross-section geometries were tried: 20x80mm, 30x120 and 40x160mm. The length of all pieces is 1000mm. The analysis is 0,18%C and 1,5%Mn with additions of Si, Nb and V.

The pieces were heated to 600 °C in an electrically heated bell-type furnace. Then they were transported to the forging-press and placed in the manipulator grip. The trial pieces were bent over the lower tool as showed in **Fig. 111**. The trial schedule was designed to cover both single bending and double bending where the trial piece is turned 180° before the second bending. In this way a reversal strain was applied, similar to regular hot levelling.

Resulting deflections and bending radii together with measured bending forces is presented in **Fig. 112**.

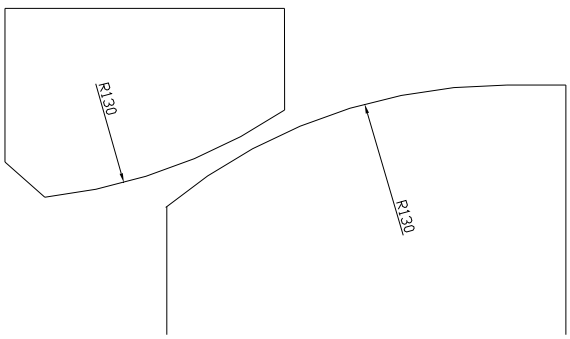


Fig. 111: Design of tools for hot bending trials. The left tool is moving vertically and the right tool is fixed



Fig. 112: Hot bending trials in the pilot-plant forging press at MEFOS

Table 13: Trial schedule and measured values

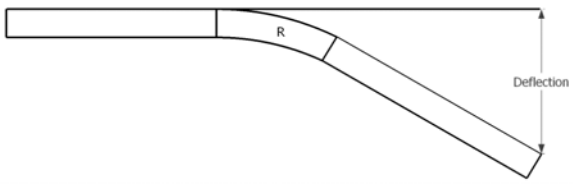
Trial No	Bar-height	Bar-width	Ben-dings	Deflection (mm)	R (mm)	Force 1 (kN)	Force 2 (kN)	Remark
4	40	160	1	59	6900	344		
5	40	160	2	52	6120	340	391	
6	30	120	2	194	823	430	584	r6
7	30	120	1	182	1753	480		
9	30	120	1	54	5350	295		
10	30	120	2	24	8570	286	286	
13	20	80	1	120	1300	216		
14	20	80	2	63	4980	276	325	
15	20	80	2	66,5	5930	213	274	r15

Remarks:

Measured surface temp 600-610C before first stroke (trial 4-5, 7-15)

r6 Furnace temp 625C

r15 Surface temp 515C before second stroke



Task 4.2: Correlation analysis, first modelling approaches

Develop a one-dimensional levelling model capable of application to most roller leveller configurations and correlate with measured data at Corus Teesside Technology Centre

A one-dimensional levelling model, developed under previous ECSC-funded projects [14], [15], has been further developed/extended to allow simulation of operating conditions on most roller levellers used for plate and strip. The original model approximated the levelling process to a sequence of 3-point bends between evenly spaced rolls, using classical beam theory to calculate the induced strain-distribution through the strip, and hence the evolving elastic/plastic stress-distribution. It provided a useful guide to process-sensitivities and has been used successfully to identify causes of poor leveller performance (e.g. variable roll gap across the width of the plate). However, analyses were limited by:

- a restriction to consideration of uniformly-spaced rolls (some levellers have a non-uniform roll spacing close to the front and rear ends of the machine),
- no facility for considering the effect of breast rolls on exit bow,
- an absence of detailed experimental data to confirm assumptions made concerning the path/curvature of the plate through the leveller (most roller levellers are poorly instrumented), and verify exit bow predictions.

The plate/strip is now modelled as a continuous beam subject to displacements, at the leveller roll contact points, determined by the penetration settings (**Fig. 113**). Use of continuous beam theory allows consideration of the combined effect/mutual interactions of all the rolls. The resultant cyclic reverse-bending is used to calculate induced stress- and strain-histories, and hence the final residual stress-distribution and curvature. A spreadsheet-based user interface allows input of arbitrary roll configurations and spacings, and product geometry and properties (**Fig. 114**), the model being accessed via a command button. Calculated contact forces, plate/strip curvature, levels of induced plasticity, and torques at each roll position are given in tabular form and the final residual stress distribution is presented graphically.

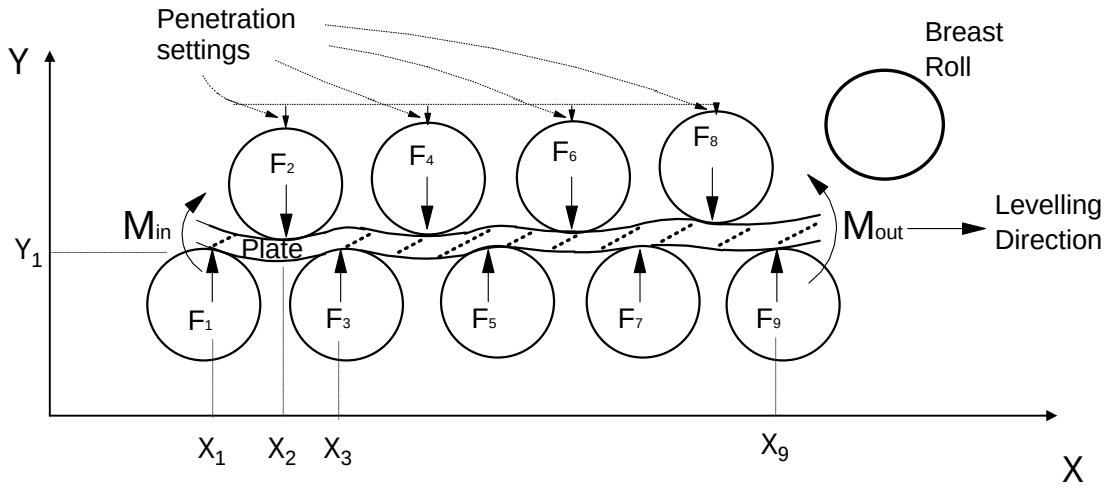


Fig. 113: Forces and bending moments acting on a plate during levelling
[Force F_i exerted on plate by work roll i, at contact points (X_i,Y_i).
Breast roll acts as an additional roll if plate significantly turned up at exit]

Referring to **Fig. 113**, the plate can be considered as a continuous beam, in contact with a series of supports at the roll positions. The external bending moments M_{in} and M_{out} at the first/last roll positions are a function of the constraint/support conditions before and after the leveller. For the tension-free conditions encountered in roller levelling, the end moments will be largely determined by the length and weight of unsupported beam immediately upstream/downstream of the leveller (**Fig. 115**). If weight per unit length = and unsupported length = dl, then the external moment is given by:

$$M_{out} = -0.5 * \rho g . dl^2 \qquad (1)$$

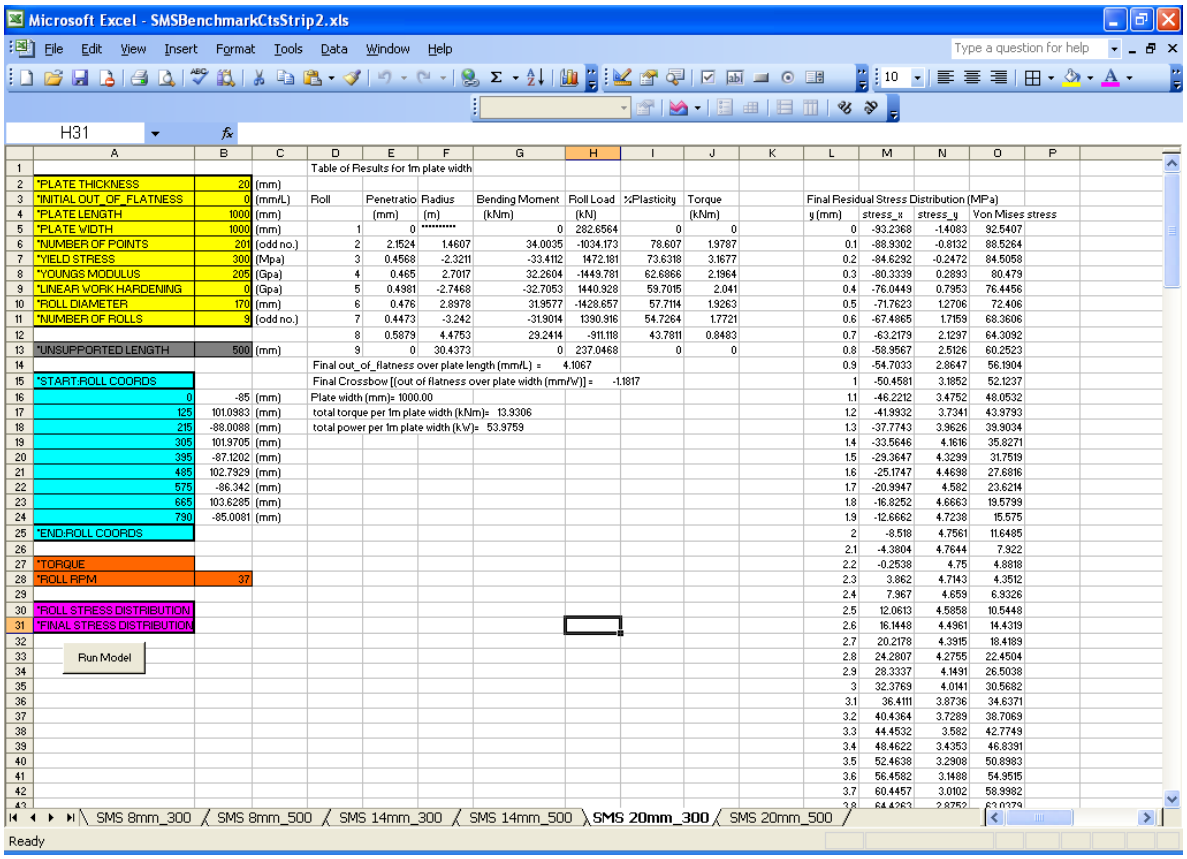


Fig. 114: Spreadsheet-based user interface for analytical levelling model

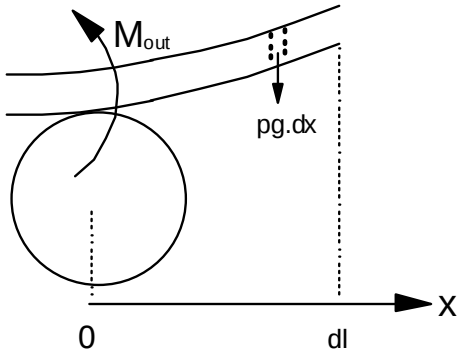


Fig. 115: External moment Mout due to unsupported length of beam downstream of leveller

Values of M_{in}/M_{out} close to zero will generate simply-supported boundary conditions at the first/last roll positions, whereas differing conditions could develop if the external bending moments are sufficiently high. The external moments at each end will vary as the plate passes through the leveller, and will depend on the gauge and length of the plate.

Calculation of plate path through leveller

In order to calculate the path of the plate through the leveller, estimating the contact point locations and plate curvatures at each roll, the model makes the following assumptions [16], [17]:

1. the plate contacts each roll tangentially, and does not penetrate its surface [i.e. at each roll contact point, the gradient of the plate trajectory is tangential to the roll surface at that point],
2. the internal bending moment within the plate, due to the longitudinal stress distribution, varies linearly between successive roll contact points,
3. at the first and last roll contact points, the bending of the plate is insufficient to generate plastic deformation. The curvature of the plate at these points can therefore be obtained directly from the end bending moments M_{in}/M_{out},

4. the path of the plate exhibits continuity of both deflection and gradient [i.e. plate curvature is always finite – there are no 'kinks' in the plate].

The implications of assumption (1.) are illustrated in **Fig. 116**. The location of the contact point on roll i is determined by the local gradient of the plate path.

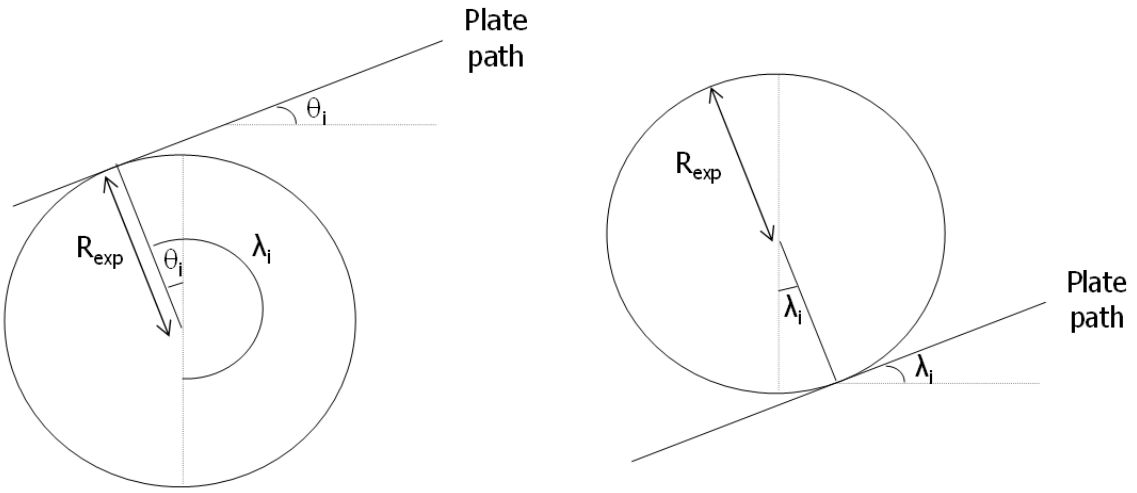


Fig. 116: Contact conditions between plate and top/bottom rolls
[R_{exp}='Expanded roll radius' = roll radius + 0.5*plate gauge]

For top rolls, the local gradient of the plate is given by:

$$\frac{dy}{dx}\left(X^{i}\right) = \tan\left(\lambda_i\right) \tag{2a}$$

and for bottom rolls by:

$$\frac{dy}{dx}\left(X^{i}\right) = \tan\left(\theta_i\right) = \tan(\lambda_i) \tag{2b}$$

For a roll centre located at (xc_i,yc_i), the location of the contact point can be written:

$$X^{i} = xc_i + R_{\exp}\sin\left(\lambda_i\right), \qquad Y^{i} = yc_i - R_{\exp}\cos\left(\lambda_i\right) \tag{2c}$$

From assumption (2.), the variation in strip curvature between pairs of adjacent contact points is approximately linear (exactly linear if deformation is purely elastic), giving a piecewise cubic plate trajectory through the leveller.

For a leveller with N rolls, the plate curvatures at rolls 1 and N are given (assumption (3.)) by:

$$C^{1} = {M_{in}}/{EI}, \qquad C^{N} = {M_{out}}/{EI} \tag{3}$$

where:

- E = Young's modulus of plate
- I = plate's second moment of area.

If the contact points are known then an approximate solution for the plate path, satisfying conditions (1.) to (4.), is obtainable by treating the plate as a continuous beam, simply supported by the rolls (at $X^{i} = \eta_i L;\ \ i \in [1, N]$), and overhanging the end rolls (**Fig. 117**).

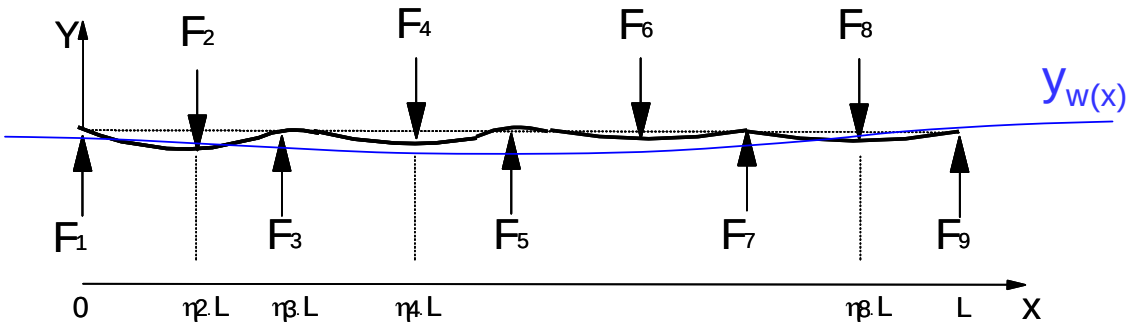


Fig. 117: Initial estimation of plate path through 9-roll leveller.

[Plate idealised as an elastic continuous beam, simply-supported at roll positions, and overhanging end rolls.
$y_w(x)$ = deflection of plate subject due to self-weight when only supported at rolls 1 & 9.
Actual plate path $y(x) = y_w(x)$ + deflection due to point loads F1 ,…,F9.]

The plate deflection y(X) is given by

$$y(X) = y_W(X) + y_{SUP}(X) \tag{4}$$

where:

- $y_w(X)$ = deflection of plate under self-weight when only supported at first/last roll-positions,
- $y_{sup}(X)$ = plate deflection generated by point loads F_1 ,…,F_N

loads/deflections defined as positive in the upward direction.

Using standard beam-bending theory/notation [18], the components of deflection are given by:

$$y_w(X) = \frac{-\rho g}{2EI}\left\{\frac{X^4}{12} - \frac{L}{6}X^3 + \frac{dl^2}{2}X^2 + X\left[L\left(\frac{L^2}{12} - \frac{dl^2}{2}\right)\right]\right\} + \frac{\left[X.Y^N + (L-X).Y^1\right]}{L};\ X \in [0, L]$$

$$y_{SUP}(X) = \sum_{i=2}^{N-1} F_i y_{ss}(\eta_i, \theta);\ \theta = \frac{X}{L};\ \eta, \theta \in [0,1]$$

$$y_{ss}(\eta, \theta) = \frac{L^3}{6EI}\left\{(1-\eta)\theta^3 - \langle\theta - \eta\rangle^3 - \theta(1-\eta)\left[1-(1-\eta)^2\right]\right\} \tag{5}$$

where:

- $yss(\eta, \theta) =$ deflection at X= θ L, due to unit load at X= ηL
- $L = X^N - X^1,\ \eta_1 = 0,\ \eta_N = 1;\ L >> \left(Y^N - Y^1\right)$

and the term $\langle\theta - \eta\rangle$ is omitted if $\theta < \eta$.

The point loads F_i are obtained from the requirement that the plate must pass through the contact points $\left(X^i, Y^i\right)$ at each roll. This gives the linear system:

$$\sum_{j=2}^{N-1} F_j y_{ss}(\eta_j, \eta_i) = Y^i - y_w(\eta_i L);\ \ i \in [2, N-1] \tag{6}$$

Loads at first/final rolls are obtained by imposition of force and torque equilibrium on the plate. Assuming plate overhangs both first and last rollers by length dl then:

$$M_{out} = -0.5\rho g.dl^2$$

$$= -0.5\rho g(L + dl)^2 + L\sum_{i=2}^{N-1} F_i(1-\eta_i) + LF_1 \tag{7a}$$

and

$$\sum_{i=1}^{N} F_i = \rho g\left(L + 2.dl\right) \tag{7b}$$

The curvatures C^i at each contact point can then be estimated using

$$C^i = \frac{L}{EI}\sum_{j=1}^{i-1} F_j\left(\eta_i - \eta_j\right);\ \text{(i=2,3,…,N-1).} \tag{8}$$

For assumed contact points $\left(X^i, Y^i\right)$, equations (4-8) give the plate path $y(x)$ and associated curvatures through the leveller. A revised estimate of the contact point coordinates can then be obtained at each roll from the local path gradient $dy/dx\left(X^i\right)$ using equations (2a-c).

In summary, the model adopts the following procedure for calculation of the plate path:

An initial estimation for the plate path is made, in which the contact points (X^i, Y^i) are assumed to be directly above or below the roll centres (i.e. $\lambda_i = \pi$ or 0), and equations (4-8) are used to calculate the plate path $y(x)$ and curvatures C^i.

The local path gradients $dy/dx\left(X^i\right)$ are input to equations (2a-c) to obtain revised estimates for λ_i, and hence modified contact point coordinates (X^i, Y^i) at each roll.

Equations (4-8) are re-applied, using the latest values for (X^i, Y^i), to obtain a revised calculation of plate path and curvatures.

Changes in estimated plate curvatures and/or contact positions are compared with predefined tolerance-values to establish whether the prediction for plate path has converged. If not then program returns to step 2 for a further iteration.

Following convergence, the calculated plate-path satisfies the conditions (1.) to (4.), including deflection/gradient continuity and tangential roll surface contact.

Calculation of plate stresses, strains and exit bow

The model uses the calculated curvatures C^i at each roll position to impose a series of reverse bends on the plate, calculating the evolution of through-thickness stress and strain distributions generated by elastic-plastic deformation [15], [14]. The plate's internal bending moment at each roll position is calculated from the through-thickness stress-distribution using

$$M_i = w\int_{-h/2}^{h/2} \sigma.y.dy \tag{9}$$

Where

- h = plate gauge,
- w = plate width,
- y = distance from neutral axis, and
- σ = longitudinal stress.

The residual plate curvature (out-of-flatness) is then obtained by relaxing the internal bending moment after the last bending triangle (iteratively adjust estimated residual curvature until the associated change in internal stress distribution gives the required zero bending moment).

Calculation of loads and torques

Assuming that the plate overhangs the 1st and last rollers by a length dl (**Fig. 113**), a final estimate of the forces acting at the plate/roll contact points can then be obtained from the internal bending moments using the linear system:

$$M_i = \frac{-\rho g}{2}\left(dl + L\eta_i\right)^2 + L\sum_{j=1}^{i-1} F_j\left(\eta_i - \eta_j\right);(\text{i=2,3,…,N})$$

$$M_{N-1} = \frac{-\rho g}{2}\left(dl + L\left(1-\eta_{N-1}\right)\right)^2 + F_N L\left(1-\eta_{N-1}\right) \qquad (10)$$

Predictions of total power-usage by the leveller, and hence total levelling torque, are generated by consideration of the total work done to the plate, and the speed at which the plate passes through the leveller [19], [20]. The work done to a unit length of plate is obtained from the area traced out by the graph of bending moment plotted against curvature during successive bending triangles (**Fig. 118**).

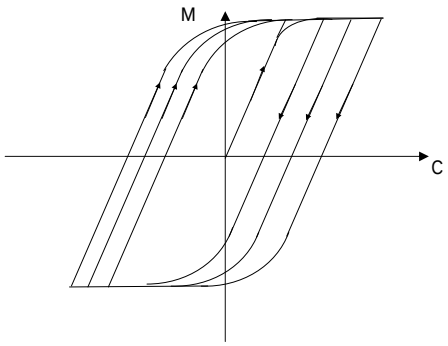


Fig. 118: Evaluation of work done to plate by calculation of area traced out by bending moment-curvature graph during successive bending triangles

[M=Bending Moment, C=Curvature
Power-usage = work per unit plate length multiplied by plate speed
Total torque = power-usage divided by the angular velocity of the leveller rolls.]

Transverse Stresses and Crossbow

Two versions of the analytical model have been developed. The first considers only longitudinal stresses/strains, calculating exit bow in the length direction as described above. A second model takes account of both longitudinal and transverse stress components, using the following assumptions [21]:

- stress components in the thickness direction are neglected
- shear stress components may be ignored
- cross-sections perpendicular to the central or mid-thickness plane remain perpendicular
- strain in the transverse direction may be ignored
- the Von Mises yield criterion is used.

Both versions of the model assume that the steel undergoes linear elastic deformation up to the yield point, and then exhibits either perfect-plasticity, or linear (isotropic or kinematic) work hardening. Within the two-dimensional model, the Prandtl-Reuss equations [22], [23] are used to relate increments in stress and strain components during plastic deformation.

Consideration of Exit Breast Roll

The models have the facility to consider parallel nested levellers. These are normally equipped with exit breast rolls, to eliminate excessive positive exit bow. An initial simulation is performed ignoring the breast roll. If the predicted exit longbow is sufficiently positive to generate contact with the breast roll then a repeat-simulation is performed, in which an additional bending triangle is generated around the final work roll (**Fig. 119**). The exit longbow can be decreased/increased by lowering/raising the breast roll.

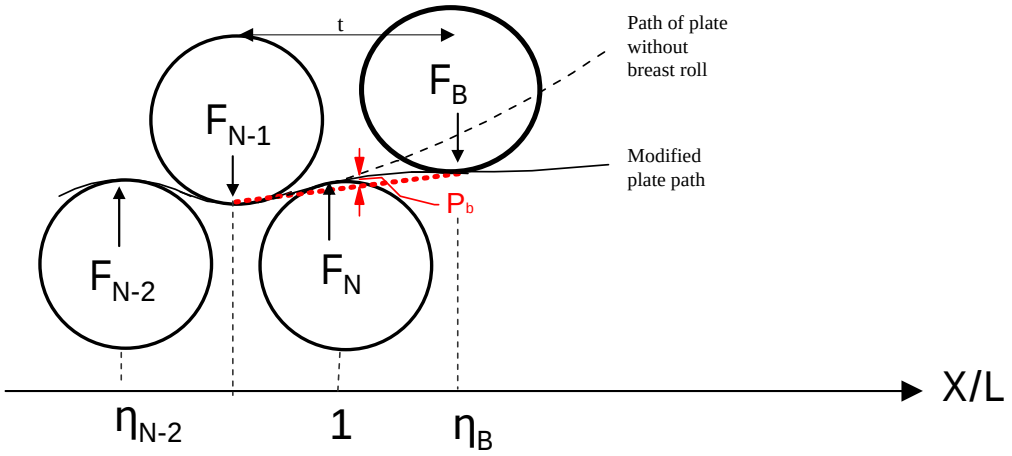


Fig. 119: Reduction in plate longbow using exit breast roll

[Breast roll creates extra bending triangle with penetration Pb]

With breast roll contact, calculation of the plate path through the leveller is modified. The plate now contacts N+1 rolls. Equation above giving the (elastic) bending at first and final contact points now becomes:

$$C^1 = \frac{-0.5 * \rho g.dl^2}{EI}, \quad C^{N+1} = \frac{-0.5 * \rho g.[dl - (\eta_B - 1)L]^2}{EI} \tag{11}$$

Replaced by:

$$\sum_{j=2}^{N-1} F_j y_{ss}(\eta_j, \eta_i) + F_B G(\eta_B, \eta_i) = Y^i - y_w(\eta_i L); \quad i \in [2, N-1] \tag{12a}$$

$$\sum_{j=2}^{N-1} F_j B(\eta_j, \eta_B) + F_B \left[\frac{L^3 \eta_B (\eta_B - 1)^2}{3EI} \right] = Y^B - y_w(\eta_B L) \tag{12b}$$

where:

$\eta_i, \eta_j \in (0,1); \ \eta_B > 1$

$y_w(X)$ is defined for X<L

$$y_w(L+z) = \frac{-\rho g}{24EI}\{(z-dl)^4 - dl^4\} + \frac{\rho g z}{6EI}\left\{\frac{L^3}{4} - \frac{3dl^2 L}{2} - dl^3\right\} + Y^N + (Y^N - Y^1)\left(z/L\right)$$

breast roll contact point is at $(\eta_B L, Y^B)$

$$G(\eta_B, \eta_i) = \frac{(\eta_B - 1)\eta_i L^3}{6EI}(\eta_i^2 - 1)$$

$$B(\eta_j, \eta_B) = -\frac{L^3(\eta_B - 1)}{6EI}(1 - \eta_i)[2 - 3.(1 - \eta_i) + (1 - \eta_i)^2].$$

Having solved equation for $F_2, \ldots, F_{N-1}$, and F_B, loads at first/final rolls of the main leveller unit (F_1, F_N) are obtained by imposition of modified force/torque equilibrium equations (equations modified to include breast roll contact force):

$$M_{out} = -0.5\rho g.dl^2 + F_B(\eta_B - 1)L$$

$$= -0.5\rho g\left(L+dl\right)^2 + L\sum_{i=2}^{N-1} F_i\left(1-\eta_i\right) + LF_1 \tag{13a}$$

and

$$F_B + \sum_{i=1}^{N} F_i = \rho g\left(L+2.dl\right) \tag{13b}$$

Calculation of plate-path proceeds following the iterative scheme outlined earlier, with equations (3), (6), and (7a-b) replaced by (11), (12a-b), and (13a-b) respectively, and an additional equation giving the plate curvature around roll N:

$$C^N = \frac{-0.5 * \rho g.dl^2 + F_B\left(\eta_B - 1\right)L}{EI} \tag{14}$$

Once a converged set of curvature-values has been obtained, the model calculates evolution of through-thickness stress/strain distributions, final exit bow, and loads/torques as before (imposing an extra bending triangle around roll N).

Effect of Plastic Deformation on Plate Path

The modelling technique outlined above offers a fast analytical solution (1D model CPU times in the range 0.01 to 0.05 s, 2D model CPU time up to 0.5 s, spreadsheet user interface takes 1-2 s to refresh), but requires the simplifying assumption that the plate trajectory through the leveller can be approximated by a series of cubic curves between successive roll contact points (linear variation in bending moment between each successive pair of contact points giving rise to a linear variation in curvature). In reality, plastic deformation of the plate will yield a non-linear relationship between bending moment and curvature, and hence a departure from the assumed cubic plate trajectory. To investigate this effect, an alternative '2nd order' version of the analytical model was developed, in which the modified plate path under plastic deformation is calculated iteratively [15], [17], using the 'elastic' path as a starting point.

For an initially straight/stress-free plate, the maximum curvature C0 for which elastic conditions hold is:

$$C_0 = \frac{2\varepsilon_0}{h} \tag{15}$$

where ε_0 is the yield strain. The associated bending moment M_0 can be written

$$M_0 = EIC_0 = wE\varepsilon_0 h^2/6 \tag{16}$$

Higher curvatures will cause yielding over fraction f of the plate thickness, given by:

$$C = \frac{C_0}{\left(1-f\right)} \tag{17}$$

The associated bending moment for elastic-plastic bending M_f can be obtained from equation (9). For perfect plasticity (no work hardening), we have:

$$M_f = M_0\left[1.5 - 0.5\left(1-f\right)^2\right] \tag{18}$$

Equivalent expressions for the case of work hardening can be derived straightforwardly. Equations (17-18) define a non-linear relationship between bending moment and curvature for the case of elastic-plastic deformation. Assuming that the gradient of the plate path is small, the curvature C(x) is given in terms of plate deflection y(x) as

$$C(x) = \frac{1}{\left[1 + \left(\frac{dy}{dx}\right)^2\right]^{\frac{3}{2}}} \cdot \frac{d^2y}{dx^2} \approx \frac{d^2y}{dx^2} \tag{19}$$

For an initial estimated plate path with roll contact points/angles $(X^i,Y^i)/\lambda_i$, and curvatures C^i, for which the internal plate bending moments Mi, and roll forces F_i have been calculated, and assuming that the bending moment varies linearly between contact points (assumption (2.) above), the bending moment M(x) is a known piecewise linear function of x, given by:

$$M(x) = M_i + \frac{(x - X^i)}{(X^{i+1} - X^i)}(M_{i+1} - M_i) \tag{20}$$

Curvature C(x) can then be obtained by combining equations (16-18 & 20), and equation (19) is integrated numerically to obtain a revised estimate for plate path y(x). Between successive pairs of roll contact points i and i+1, integration proceeds as follows [17]:

1. subdivide the distance between the two contact points into a series of short intervals over which the change in curvature/bending moment is small
2. assuming that the curvature changes linearly over each interval, calculate the local (cubic) plate path, imposing displacement- and gradient-continuity at the intermediate points between adjacent intervals, together with the boundary conditions $y(X^i)=Y^i$, $y(X^{i+1})= Y^{i+1}$
3. note the gradient of the local paths at the start of the 1st interval (roll i contact point) and at the end of the final interval (roll i+1 contact point). Calculate the differences r^{2i-1}, r^{2i} between the local path gradient and the roll surface gradient at these 2 points, given by:

$$r^{2i-1} = \frac{dy}{dx}(X^i) - \tan(\lambda_i) \tag{21a}$$

$$r^{2i} = \frac{dy}{dx}(X^i) - \tan(\lambda_{i+1}) \tag{21b}$$

Steps 1-3 are repeated for each pair of successive roll contact points, giving a revised estimated plate path y(x) through the leveller (assuming the previously-calculated set of contact point locations λ_i and curvatures C^i). The extent to which the revised path fails to satisfy the condition of tangential contact at the roll surfaces [assumption (i)/equation (2) above] is governed by the values r^j (j = 1 to 2N-2), which are a function of the contact point locations λ_i and curvatures C^i. Calculation of the correct plate path essentially involves finding a set of values for λ_i and C^i such that the calculated plate path satisfies the condition of tangential roll contact ($r^j \approx 0$). This is achieved by Newton's iteration method, in which Jacobian matrix components $\frac{\partial r^k}{\partial C_m}, \frac{\partial r^l}{\partial \lambda_n}$ are obtained by numerical differencing. As with the '1st order' analytical model, iteration continues until plate curvatures and contact positions have converged to predefined tolerance values, and then evaluation of stress/strain-history, loads, torques and exit bow proceeds as outlined above. Use of the '2nd order' approach increased the CPU time by a factor of about 4.

Basic levelling simulations using FE-modelling by MEFOS

Material model

Each passage over three or five rolls corresponds to a "repeated bending load case" which will generate a varying stress state over the thickness. This is a complex load case where material is subjected to almost cyclic loading and the hardening model has an impact on the final result.

Modelling with various work-hardening rules has been applied. The default model in MSC.Marc is a piecewise linear plasticity model with isotropic hardening as illustrated in **Fig. 120**.

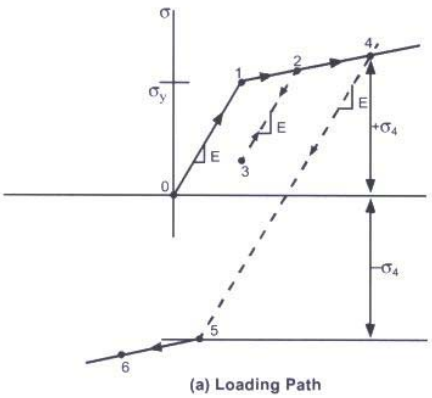


Fig. 120: Isotropic hardening rule, uniaxial test

For the kinematic hardening yield criterion the yield surface does not change in size but the centre of the yield surface can move in the stress space. The use of this model is motivated because most metals experience a change in hardening properties in cyclic loadings.

The combined hardening yield criterion, as described in [12], describes a material with nonlinear hardening. Initially the hardening is isotropic but after some straining, the elastic range attains a constant value (i.e. kinematic hardening). This is illustrated in **Fig. 121**. A variable proportion between isotropic and kinematic hardening can be applied. In this context a value of 0.5 is used.

The Chaboche model [13] combines isotropic hardening and nonlinear kinematic hardening for describing cyclic hardening behaviour such as the Bauschinger effect (**Fig. 122**). The model is also capable to handle effects like ratcheting, mean-stress relaxation effect and plastic strain range memorization. Also, strain rate dependency and kinematic hardening is specified together with corresponding material constants.

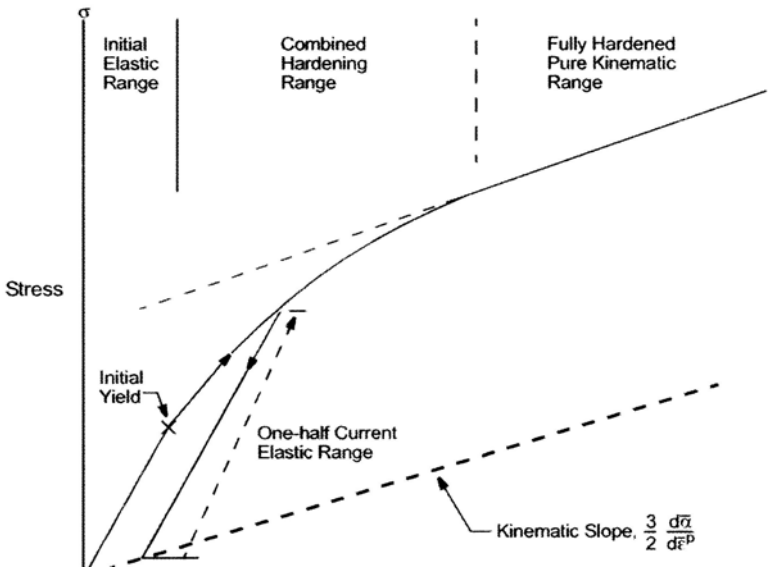


Fig. 121: Combined hardening model - uniaxial tension

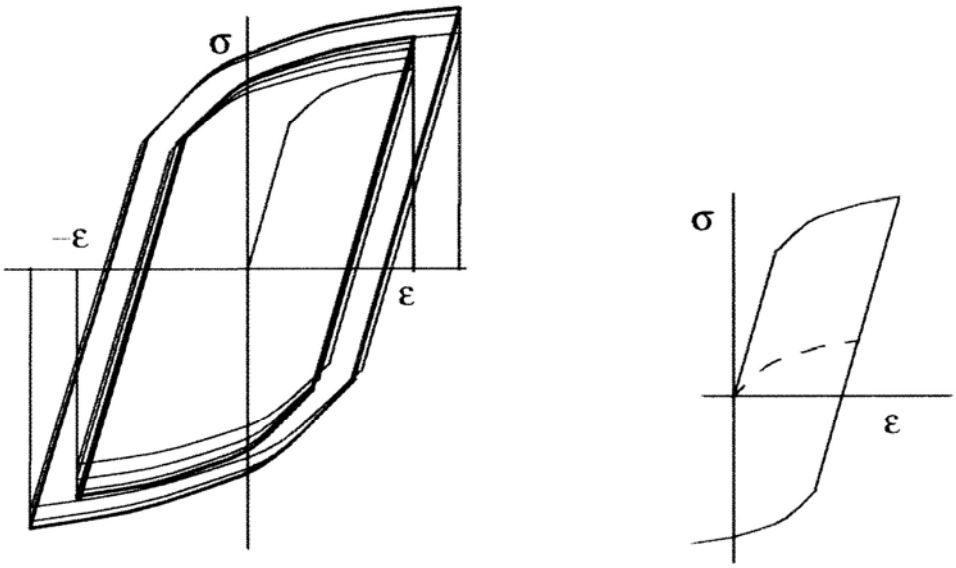


Fig. 122: Application of the Chaboche model.
Cyclic hardening under multiple cyclic loading (left) and Bauschinger effect (right)

FE-simulations on 3-roll bending

The FE-analysis was done using 2D-modelling. In the initial set-up a flat bar was inserted between the upper- and the two lower levelling rolls. Then the second roll was lifted and the levelling process started. Hence, the results from the very front-end of the bar are irrelevant.

The results from the simulations (see **Fig. 123**) show good agreement with the practical trials regarding achieved geometrical curvature. The material model used was an isotropic piecewise linear model for a low carbon steel grade (MSC.Marc default data). The simulations show the plastification level achieved. The calculated radius is clearly a function of the introduced plastic straining, see **Table 14**. Experimental data are for 850 °C and a corresponding analysis is made for 600 °C.

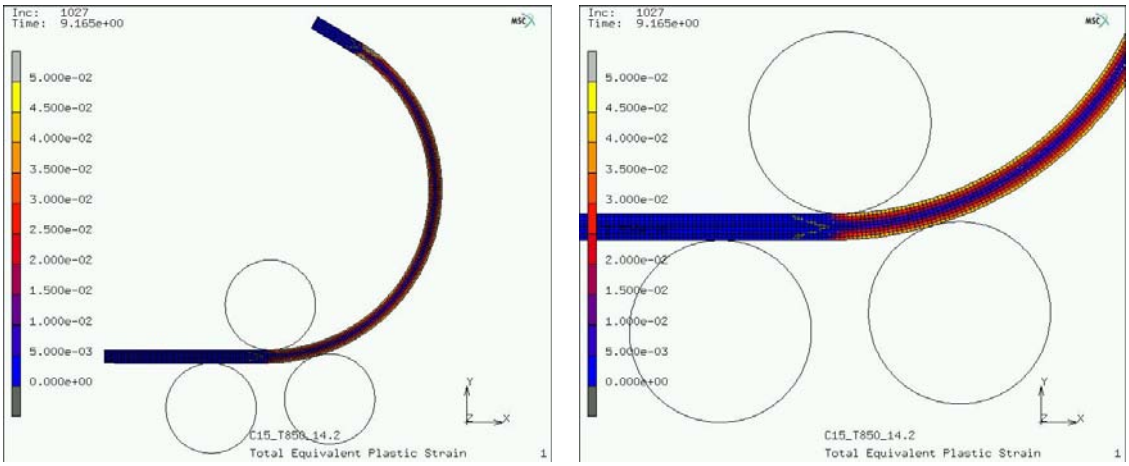


Fig. 123: FE-simulations 3-roll bending. 850 °C

Table 14: Results from FE-simulations on 3-roll bending. Marc default data.

Temp	Measured radius	Calculated radius	Calculated upper surface strain	Calcululated lower surface strain	Calculated center strain
600	-	290	0.042	0.038	0.003
850	315	266	0.049	0.043	0.0037

FE-simulations on 5-roll bending

The 5-roll bending trials were analyzed in a similar way. Differing settings on the second and third leveller rolls were investigated. The results from the analysis are shown in **Fig. 124** and **Fig. 125** and in **Table 15**.

In **Fig. 124** the analysis is done using the default isotropic piecewise linear material model for a low carbon steel grade (MSC.Marc default data). The deviation from the neutral line is the same in the second and third roll. Plastification starts at the second lower roll and results in a continuous radius from the second upper roll and onward.

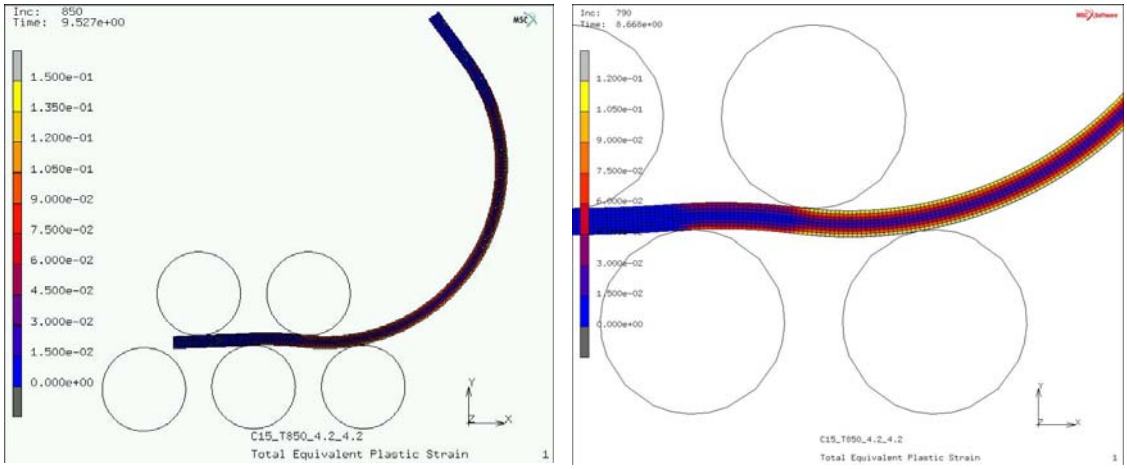


Fig. 124: Results from FE-simulation of 5-roll bending. Isotropic material model. Temperature 850 °C

In order to investigate the appearance of cycling hardening the yield criterion according to Chaboche [13] was applied. This criterion combines isotropic hardening and nonlinear kinematic hardening for describing cyclic hardening behaviour such as the Baushinger effect, ratcheting and mean-stress relaxation

In **Fig. 125** the flow stress as function of temperature and strain obtained from uniaxial compression tests were used to describe the work hardening behaviour. Isotropic hardening determines the size of the elastic region and cyclic hardening is defined by two material constants. For modelling of kinematic hardening additional material constants are needed, one of them controls the portion between linear and nonlinear kinematic hardening. Strain-rate dependency and strain-range memorization are not included in these calculations.

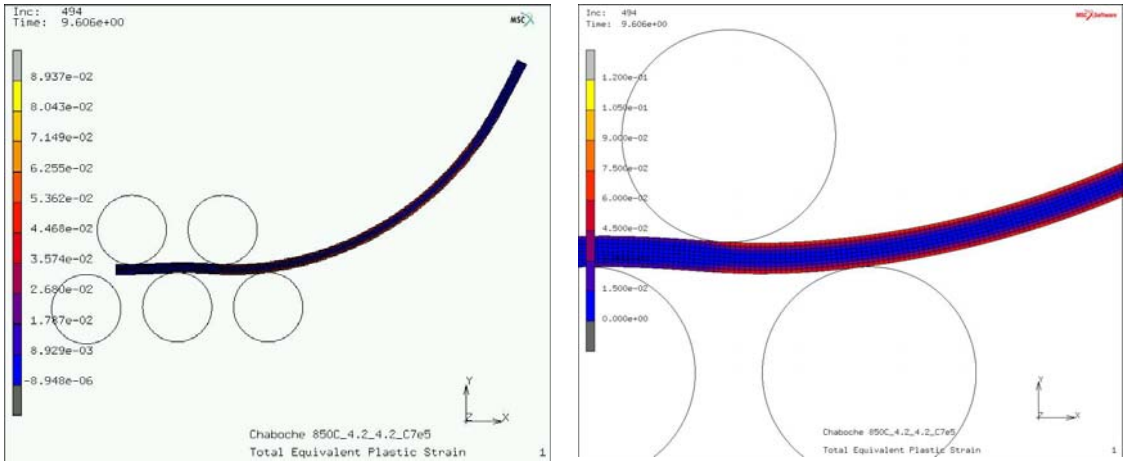


Fig. 125: Results from FE-simulation of 5-roll bending. Yield criterion according to Chaboche. Temperature 850 °C

Also in **Fig. 125** the deviation from the neutral line is the same in the second and third roll. The calculated plastification pattern is similar to the simulation with the isotropic hardening material model in **Fig. 124**. The calculated plastic strain level is however lower both at the surface and in the centre.

Table 15: Results from FE-simulations on 5-roll bending.

Roll-setting	Mea-sured radius	Calculated radius. (Marc-default)	Calc surface strain. (Marc-default)	Calc. center strain. (Marc-default)	Calculated radius. (Chaboche)	Calculated surface strain. (Chaboche)	Calculated center strain. (Chaboche)
4.2, 4.2	547	292	0.130	0.014	614	0.042	0.0013

A 2-dimensional FE-model of the bending case was modelled in MSC.MARC. **Fig. 126** shows the single bending model of trial No 4 and the corresponding model for trial No 5 when reverse bending was applied. The material was described by the default piecewise linear plasticity model with isotropic hardening.

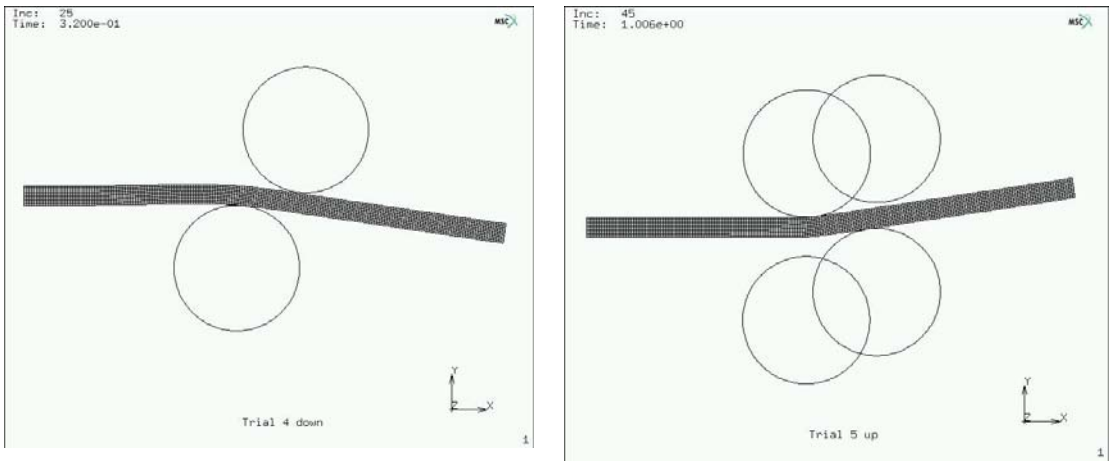


Fig. 126: Single bending model of trial No 4 (left) and when reverse bending was applied in trial No 5 (right)

After the completion of each bending the tool movement was reversed. After unloading and simultaneous springback in the work piece the remaining deflection and plastic straining can be evaluated, see **Fig. 127**.

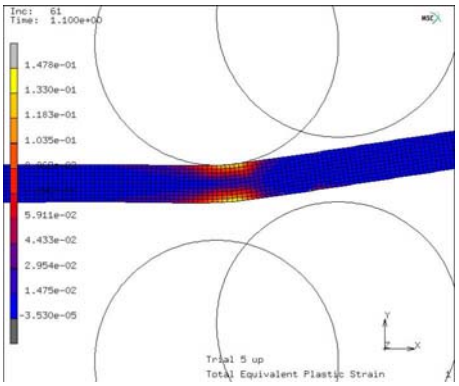


Fig. 127: Calculated plastic strain for the second bend

The results from the analyses are shown in **Table 16**. Measured tip deflections in the bending trials, as illustrated in the figure of table 1, and corresponding results from the FE-analysis are presented. Two of the trials could not be calculated when using the kinematic hardening criterion. None of the models catch the deflection in trial no 10. This is also when the measured deflection is smallest. The tendency is that the Chaboche model gives results closer to the measured ones. It should be remembered that the resulting deflections after bending were measured in cold state. Some geometrical change due to thermal shrinking is taking place during the cooling process. This is due to thermal asymmetries originating from cold tools etc.

Table 16: Measured and calculated tip deflection

Trial No	Thick-ness	Ben-dings	Mea-sured	Isotropic	Kinematic	Combined	Chaboche
4	40	1	59	84,3	58,1	78,2	52,2
5	40	2	52	75,8	66,8	76	46,6
6	30	2	194	194,3	185	184	190,5
7	30	1	182	194,1	187	194	182
9	30	1	54	64,3	66,1	74,5	63,3
10	30	2	24	38	46,8	39,5	33,8
13	20	1	120	88,6	84,1	104,8	106,5
14	20	2	63	74,1	-	52,2	65,7
15	20	2	66,5	65,6	-	67,0	65,3

Detailed investigation of stress and strain in industrial levelling

In order to achieve correct settings of industrial hot plate levellers, modelling in both 2D and 3D have been performed.

The efficiency of the levelling can be evaluated by studying the strain distribution at different positions over the strip width as well as at different points over the thickness.

A 2D FE-model of hot levelling on the Ruukki leveller was made using LS-Dyna. The motivation for using LS-Dyna instead of continuing to use MSC.Marc is that LS-Dyna solves large models, which will be present when going from 2D to 3D, with less computational time.

The flow stress curve, see **Fig. 128**, is taken from a Gleeble test at 900°C for a low strain rate of 0,1 /s. The chosen value for Young´s modulus applied in the simulations was E=1.04E11 N/m^2.

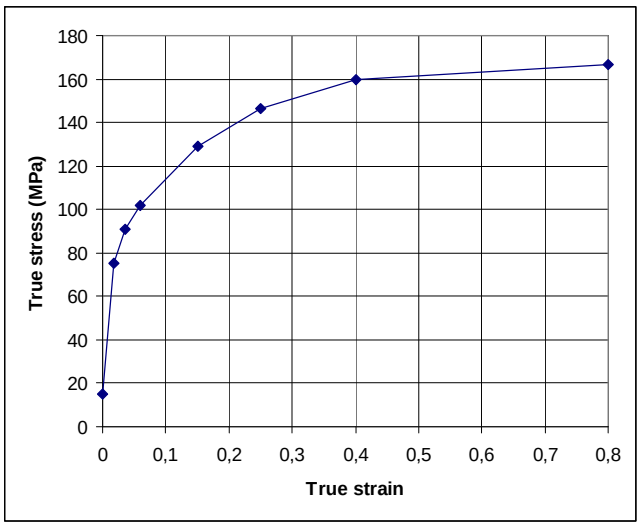


Fig. 128: Flow stress curve used in the simulations

In order to get detailed information regarding stress and strain distribution ten solid brick elements were used through the thickness. The cradle setting was set to 3 mm, see **Fig. 129**.

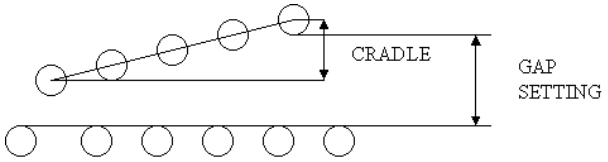


Fig. 129: Hot plate leveller at Ruukki. Definitions of cradle and gap settings

In **Fig. 130** the complete model of the 11 roll Ruukki leveller is shown. The development of stresses and strains was investigated at positions A-E. A mixed model based on 50% isotropic and 50% kinematic hardening was used for this simulation.

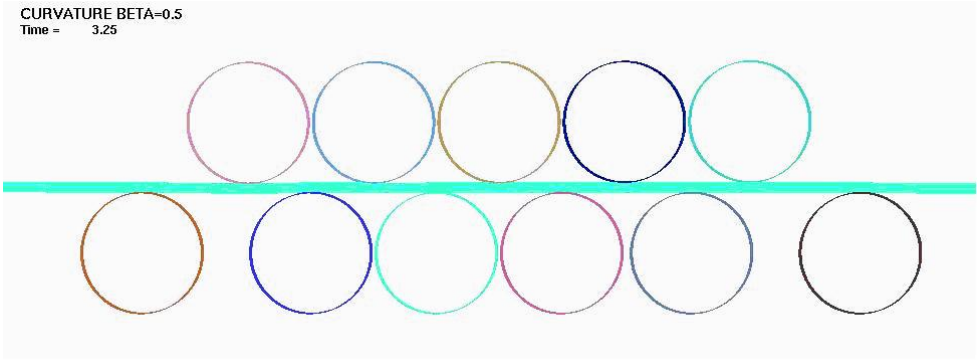


Fig. 130: FE-Model of the Ruukki leveller. Ten solid brick elements over the plate thickness

In **Fig. 131** the stress in the longitudinal direction during passage in the leveller is shown and **Fig. 132** shows the stress distribution through the plate thickness during levelling. It can be seen that the stress is compressive on the side of the plate that is in contact with the roll and tensile on the opposite side. The stress distribution through the plate thickness is constant from position C and onwards.

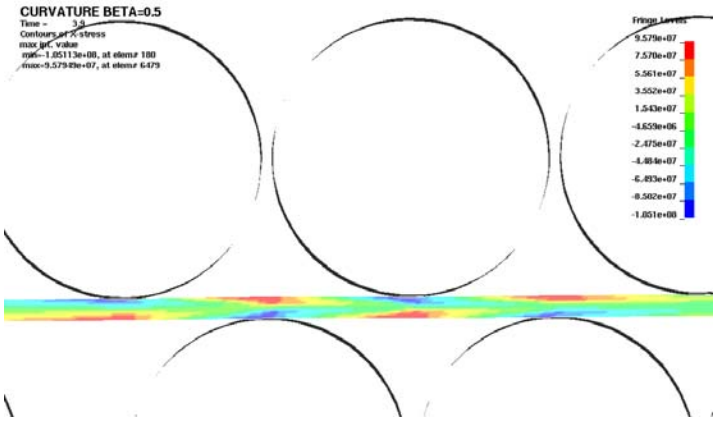


Fig. 131: Stress in the longitudinal direction

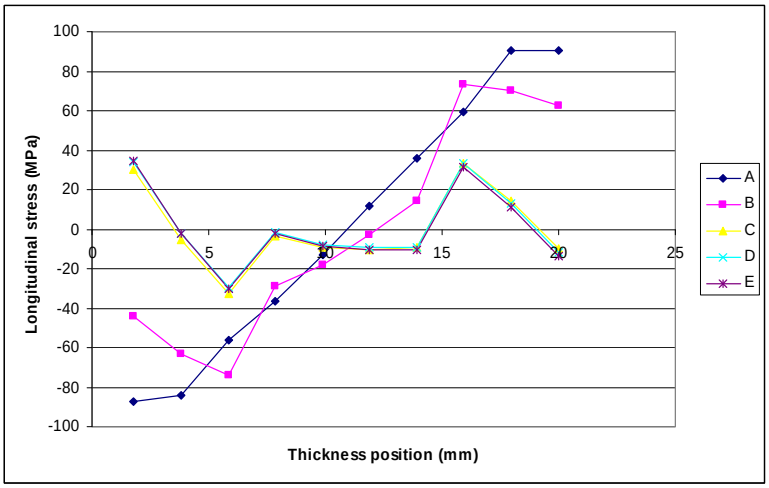


Fig. 132: Stress distribution through the plate thickness

In **Fig. 133** the effective plastic strain development during passage in the leveller is shown and **Fig. 134** shows the strain distribution through the plate thickness after levelling. After the first bending about 30% of the cross-section have a plastic deformation increasing to about 70% from the third bending (pos B) and onwards. Also, for these leveller settings, the plastic deformation is not increased for bending in position C and onwards where the straining is elastic.

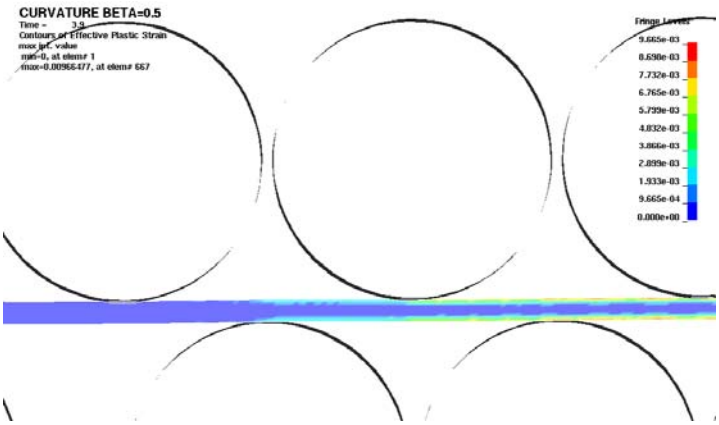


Fig. 133: Development of effective plastic strain during levelling

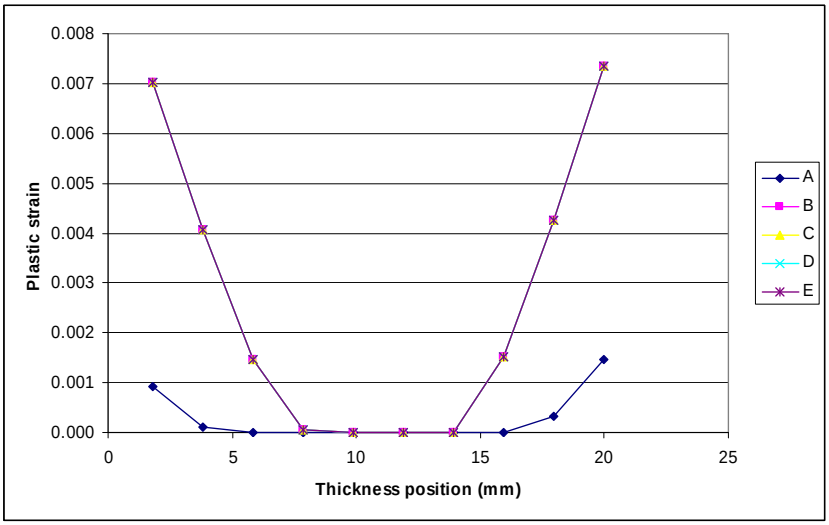


Fig. 134: Strain distribution through the plate thickness at different positions during levelling

Influence of varying leveller setting

The conditions in the plate after passing the leveller with different settings of cradle and gap have been evaluated. The influence of varying the density and E-modulus was also investigated.

Cradle and gap setting

Two values were used for the description of leveller setting, see **Fig. 129**. The cradle is measured in millimetres as the distance between the centre of the first roll and the last roll in the upper part of the leveller. In the simulation this value was varied between 2 and 4 mm. The gap setting determines the largest gap in the leveller. The plate thickness was 20.2 mm, the normal gap setting for this plate is 22 mm.

Varying the cradle setting

In the simulation the tilting of the upper frame of the leveller was changed. The cradle setting was changed +/- 1 mm. A lower value for the cradle setting will increase the amount of bending in each passage resulting in larger strains in the plate. A reduced cradle value with 2mm results in a doubling of the plastic strain on the plate surface. This is shown in **Fig. 135**.

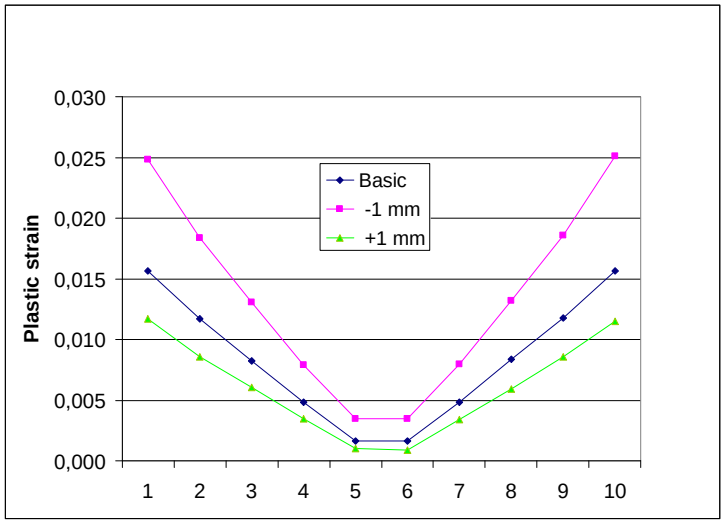


Fig. 135: Distribution of accumulated plastic strains for different cradle settings. Plate thickness 20.2 mm

Strain history for single elements

The strain history shows the effect of bending at different positions over the thickness. The outer layers of the plate experiences the highest amount of total strain and the top and bottom surface experience alternating compressive and tensile straining depending on the direction of the bend. This is shown in **Fig. 136**.

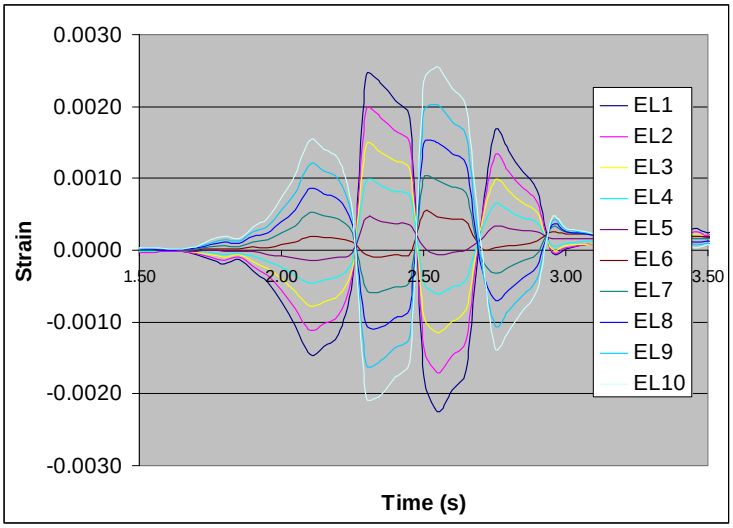


Fig. 136: Strain history for all elements cross the plate thickness as the plate passes through the leveller

The elongation value reached in levelling is connected to the strain level reached at each bend. For a comparison of different leveller settings the maximum strain reached in each bend for the top and bottom element was plotted vs. the time. When the tilt of the upper roll bridle was changed the strain at the top and bottom element changed as shown below, see **Fig. 137**. Here only the maximum strain is plotted for a more simple presentation of the results.

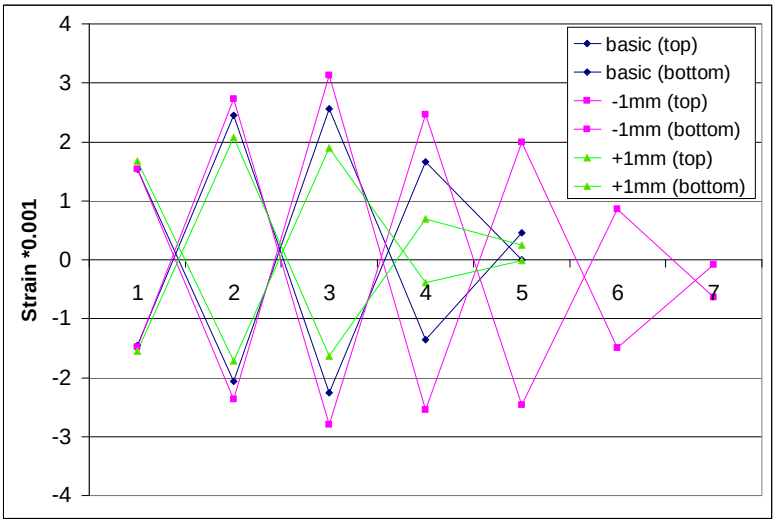


Fig. 137: Maximum total strain reached in each bend for different cradle settings for elements on the top and bottom surface in the plate

A practically used way to measure curvature is to measure the deviation from an assumed 0,5 m long ruler. **Table 17** shows the Resulting curvature measured as the distance from a ruler of 0.5 m for different cradle settings.

Table 17: Resulting curvature for different cradle settings

Cradle setting	- 1mm	Basic	+ 1mm
Deviation from ruler (mm)	13,6	8,2	3,0

Varying the gap setting

In these simulations the cradle setting 3 mm was used. The gap setting was then decreased with 1-3 mm. A decreased gap will increase the strain introduced in the leveller. Reduced gaps results in a compressive strain state after levelling, see **Fig. 138**.

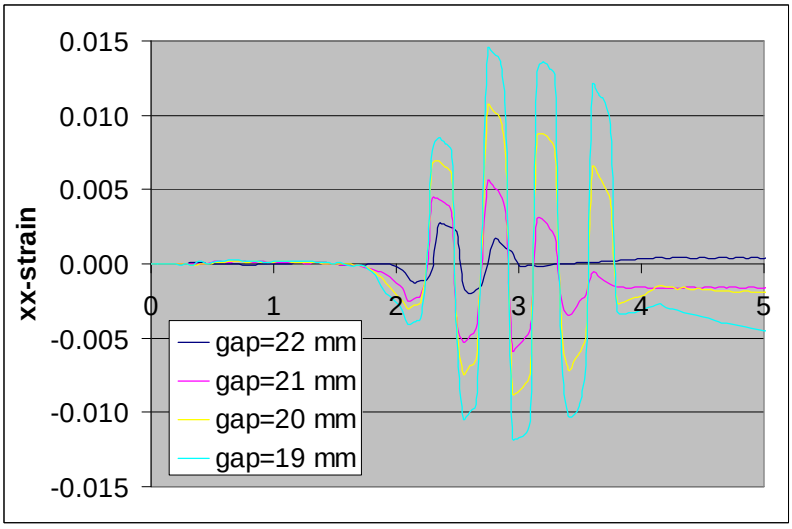


Fig. 138: Calculated lengthwise strain in each bend for different gap settings

Fig. 139 shows the lengthwise stress in each bend for different gap settings. For the smallest gap setting the remaining stress state is tensile.

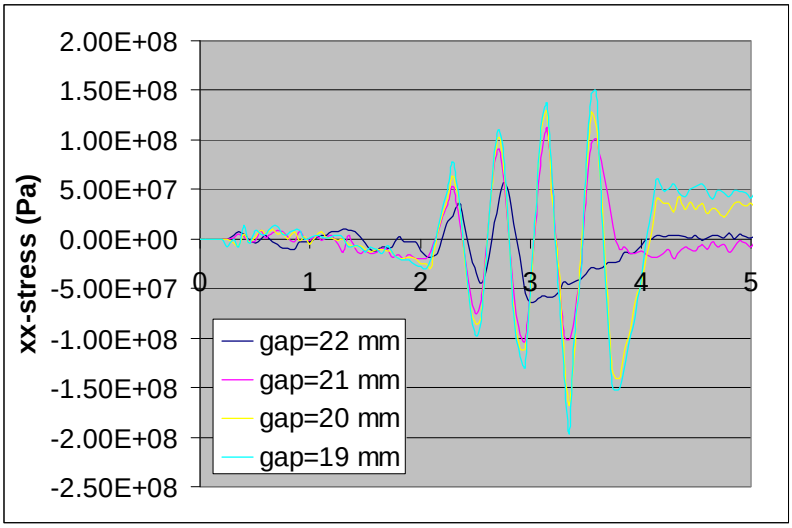


Fig. 139: Calculated stress in each bend for different gap settings

In **Fig. 140** the influence of gap setting variations on exit curvature is shown graphically. Already a gap decrease of 1mm changes the sign of the curvature.

Table 18 summarises the resulting curvature measured as the distance from a ruler of 0.5 m for different gap settings.

Table 18: Resulting curvature for different gap settings

Gap setting (mm)	19	20	21	22
Deviation from ruler (mm)	72	30	21	11

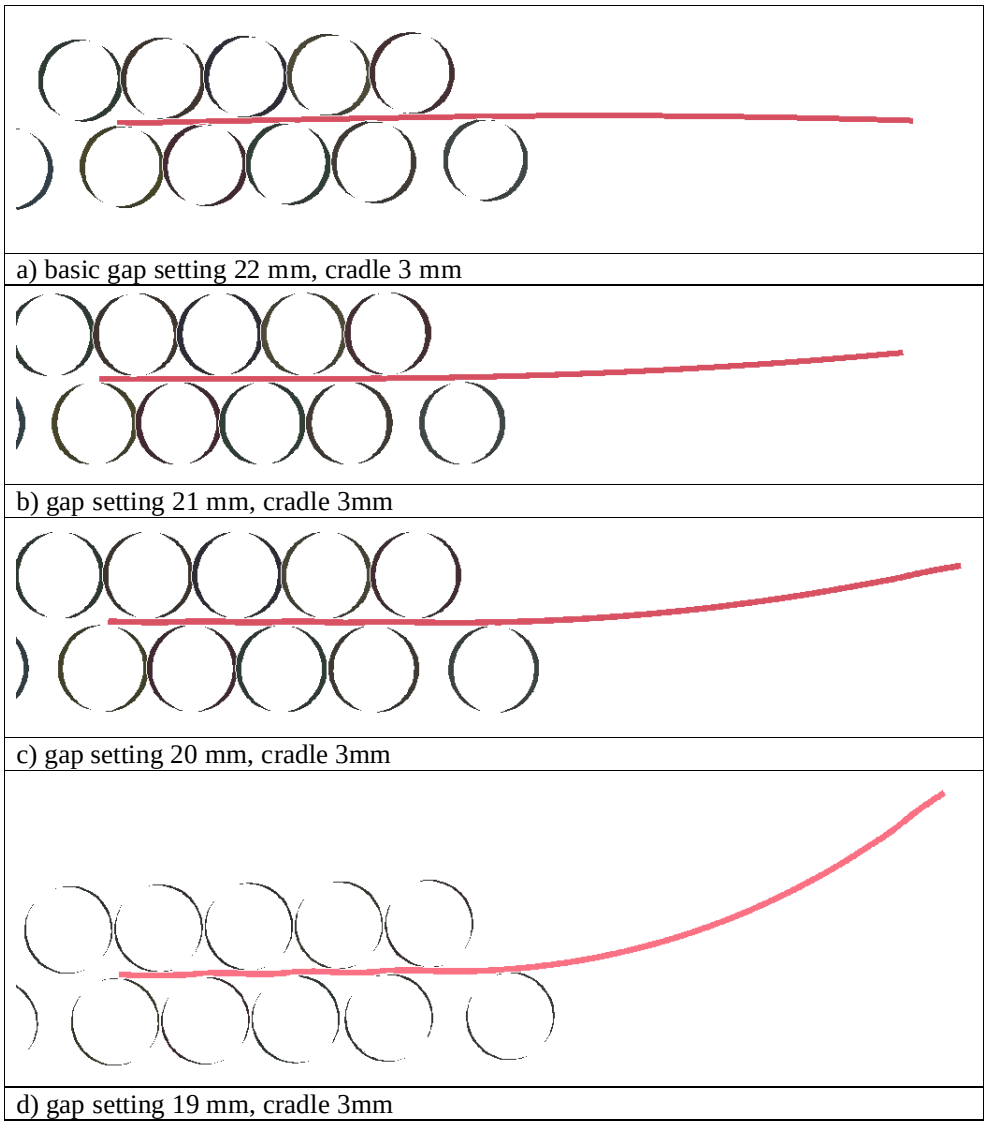


Fig. 140: Calculated curvature after the leveller for different gap settings

Comparison of shape after levelling using isotropic and kinematic hardening

The deformation principle in levelling is bending and unbending which cause the material to elongate and compress repeatedly. Therefore both isotropic hardening and a mixed model based on 50% isotropic and 50% kinematic hardening were utilised. In these calculations the impact of isotropic hardening and the mixed hardening model gives only small differences in the shape after levelling see **Fig. 141**. No gravity effect is applied in the model. Note that there is a small difference in the length of the plate that has exited the mill.

The calculated variation in longitudinal stress between the two models is very small as shown in **Fig. 142**.

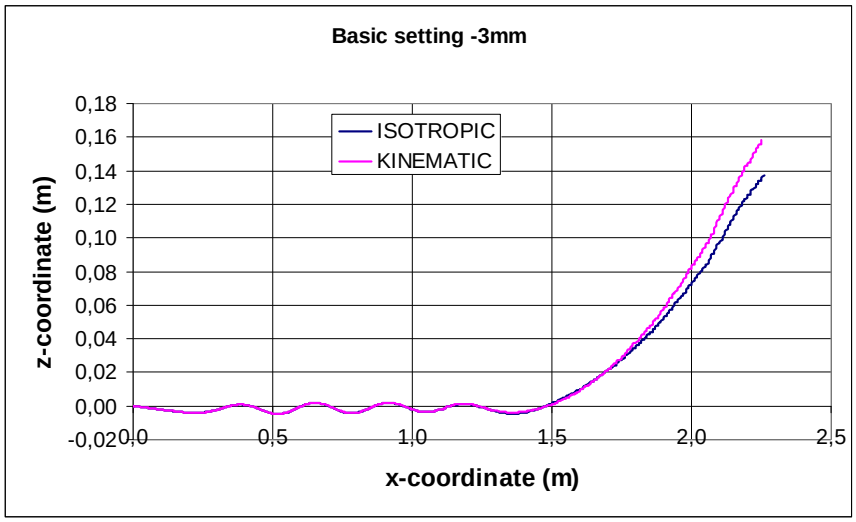


Fig. 141: Plate shape for the increased deformation of 3 mm

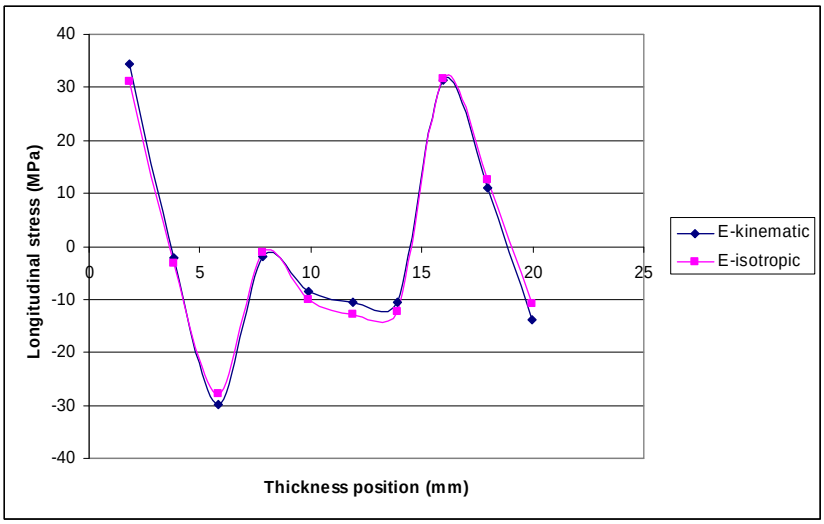


Fig. 142: Comparison of the final stress distribution with different models

Varying the E-modulus

The E-modulus in hot state is difficult to determine in experiments. Therefore the influence of a variation in E-modulus was tested in the simulations. The E-modulus strongly influence the spring back after bending and the results show that a larger Young's modulus gives a higher remaining plastic deformation. This effect is illustrated in Fig. 143.

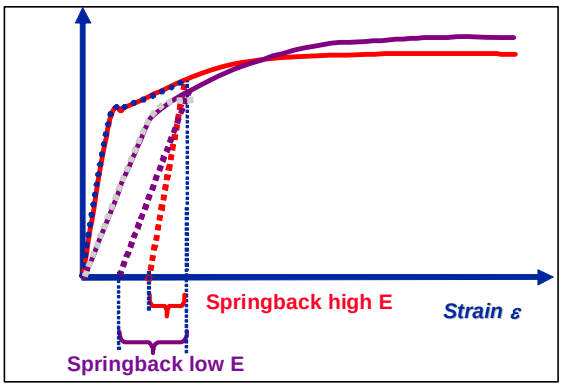


Fig. 143: Influence on plastic strain a variation in E-modulus

In the simulations the E-modulus at 900 °C was assumed to be E=1.04E11 N/m2. For comparison half this value and the double value was tested in simulations. The results show that a higher E-module gives larger strains. **Fig. 144** shows the strain increment for each bending during levelling.

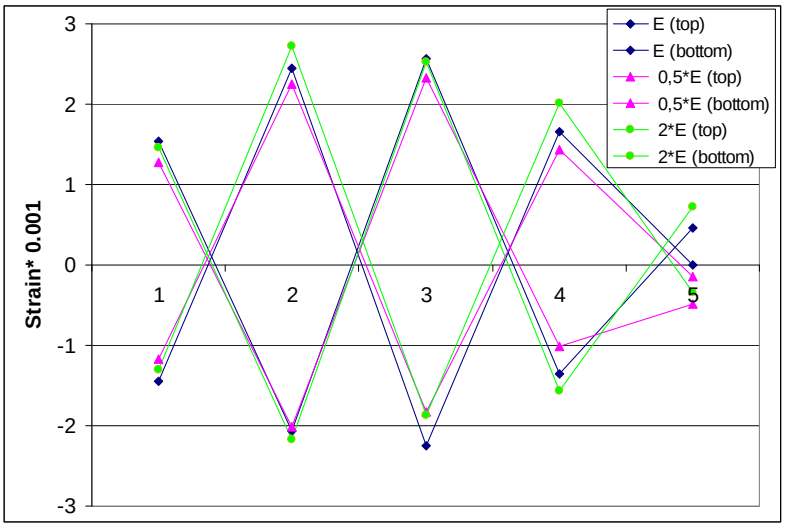


Fig. 144: Calculated strain of top and bottom surface in each bend for different values of E- modulus

Influence of density in the FE-simulations

Contrary to MSC.Marc, which is an implicit code, LS-dyna uses explicit time integration. The implicit method is unconditionally stable meaning that there is no limited time step for achieving a stable solution. On the other hand the explicit method is conditionally stable with a restriction in size of the largest possible time step. The stability condition is

$$\Delta t \propto \frac{L}{\sqrt{\frac{E}{\rho}}}$$

where L is the characteristic element length, E is the Young's modulus and ρ is the density. One way to speed up the calculations when using the explicit time scheme is therefore to increase the density. A consequence of increasing the density is that the dynamic forces in the model are increased in the same amount. This could lead to a solution that does not reflect the real behaviour. It is therefore of great importance to evaluate the dynamic forces and look for unwanted behaviour. In the end the use of so-called mass scaling is experience based and it is up to the user to scale the density without influencing the accuracy of the solution to such an extent that it could be considered as unreliable and unrealistic. FE-codes based on explicit time integration has shown to be a good method for solving complex forming simulations where high levels of deformations are present and a large number of elements are used. In these calculations the density was increased 100 times. The results were compared with calculations made using 10 times the density and showed that the influence of the change in density is very small.

Task 4.3: First model validation and further extension & adaptation of models by Corus

Verification of Plate Path/Curvature

To test the validity of the assumptions used within the '1st/2nd order' modelling approaches outlined above, the predicted plate path has been compared with measured data generated during the trials performed in WP 4.1 (obtained by pixel analysis of digital photographs of plates within the pilot leveller), and with corresponding finite element (FE) model output. The analytical models were run assuming elastic-perfectly plastic material behaviour (this closely matches the uniaxial stress-strain data at the levels of strain encountered during levelling), the FE analysis included a nonlinear isotropic/kinematic work hardening model, based on appropriate cyclic test data obtained.

Measured / predicted plate trajectories, contact point positions and plate curvatures are given for trial plate 'ADR42' (gauge 3 mm, grade S355) in **Fig. 145**, **Fig. 146** and **Fig. 147** respectively. Predictions were obtained using the 2D 1st order analytical model (1D model results very similar), the 2nd order

analytical model described in the previous section, and a 2D FE model (**Fig. 148**) developed using the commercial package ABAQUS/Standard (incorporating the same material properties, and using plane strain reduced integration elements to represent the plate).

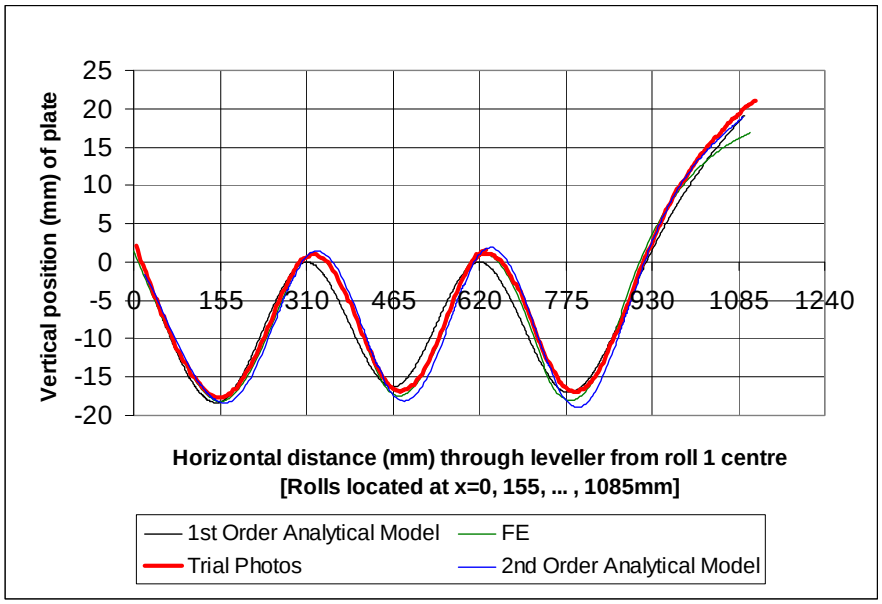


Fig. 145: Comparison of measured and predicted plate trajectory within pilot leveller, for sample 'ADR42' (gauge 3 mm, grade S355)

[Pilot leveller rolls arranged to simulate conditions in a parallel-nested leveller equipped with 7 main rolls and an exit breast roll]

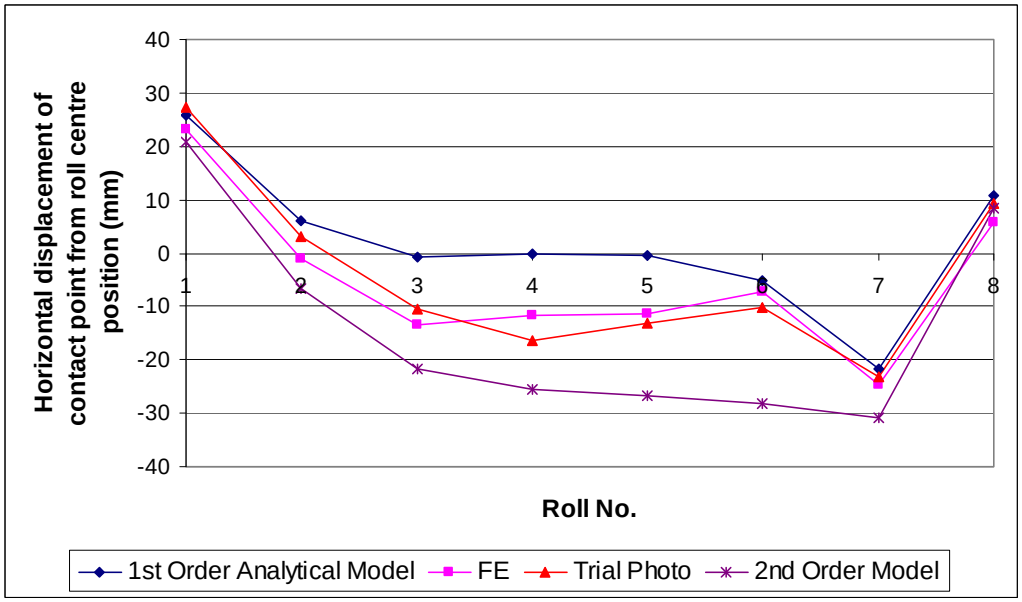


Fig. 146: Comparison of measured and predicted displacement of roll/plate contact points from roll centre positions, for sample 'ADR42' (gauge 3 mm, grade S355)

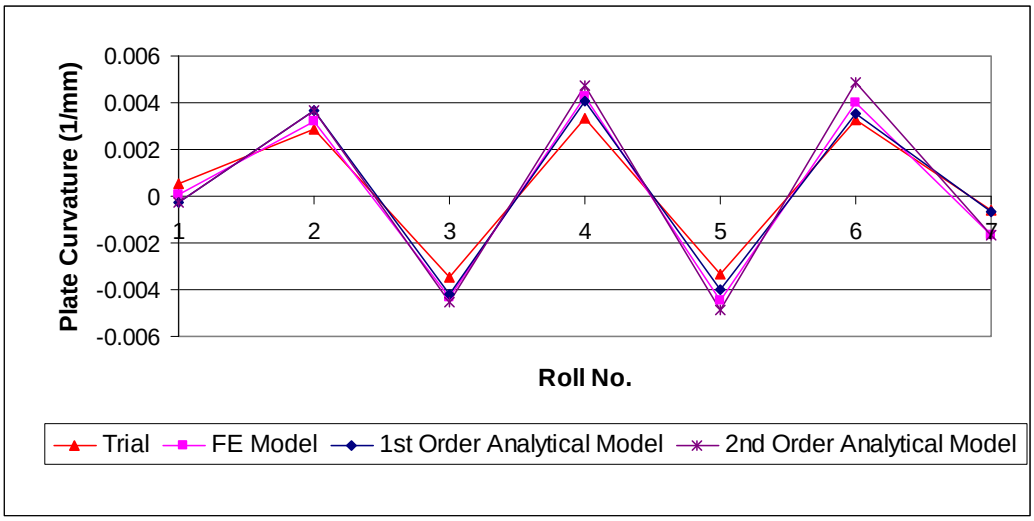


Fig. 147: Comparison of measured and predicted plate curvatures at roll positions, for sample 'ADR42' (gauge 3 mm, grade S355)

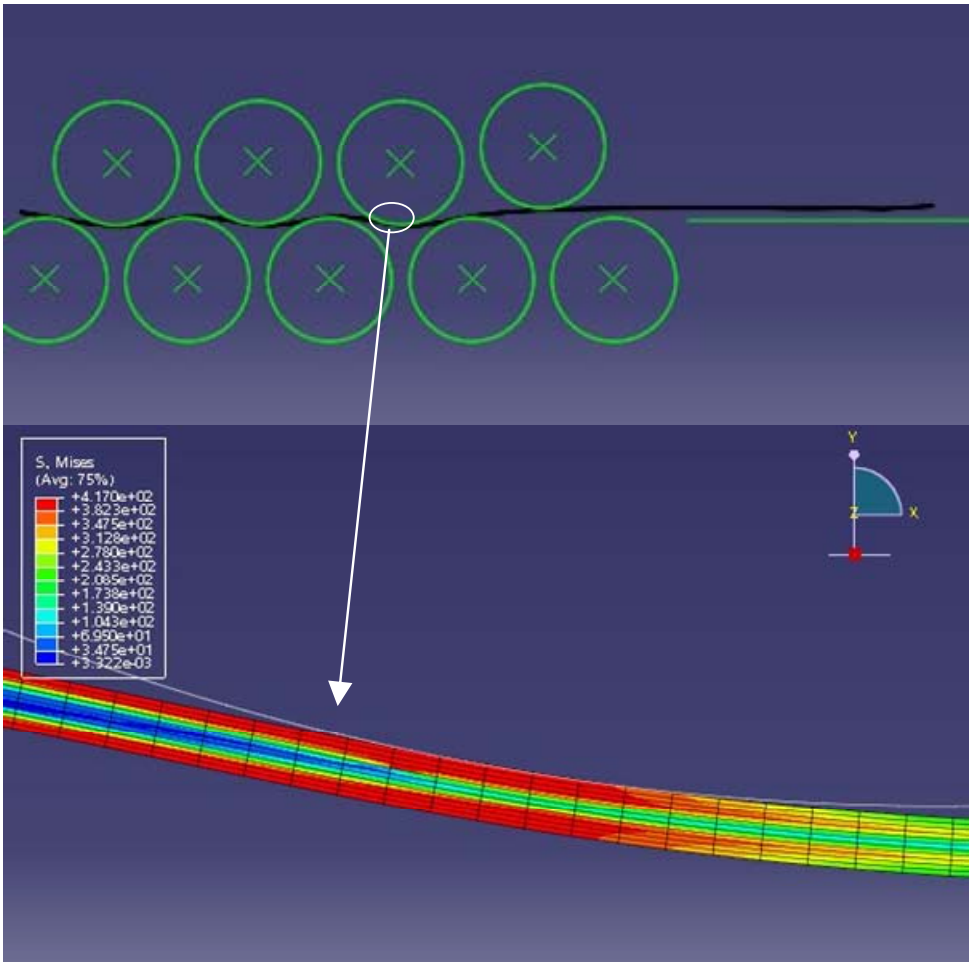


Fig. 148: FE model of roller levelling , for sample 'ADR42' (gauge 3 mm, grade S355)

[Plate modelled using plane strain reduced integration elements]

Results for the 1st order analytical and FE models indicate close agreement of measured/predicted plate trajectories around main rolls 1, 2, 6, and 7 & the breast roll. The FE model and trial results indicate a greater deviation of contact points and trajectory peaks/troughs from the roll centre positions than are predicted using the 1st order analytical model, whilst the 2nd order model indicates an even greater degree of off-centre roll contact. Plate curvatures predicted by FE and the analytical models are similar (the FE model predicts curvatures part-way between those generated by the 1st & 2nd order models), and

slightly higher than the measured values (by about 10 to 30%). Similar sets of results were obtained for other plate samples (**Fig. 149**).

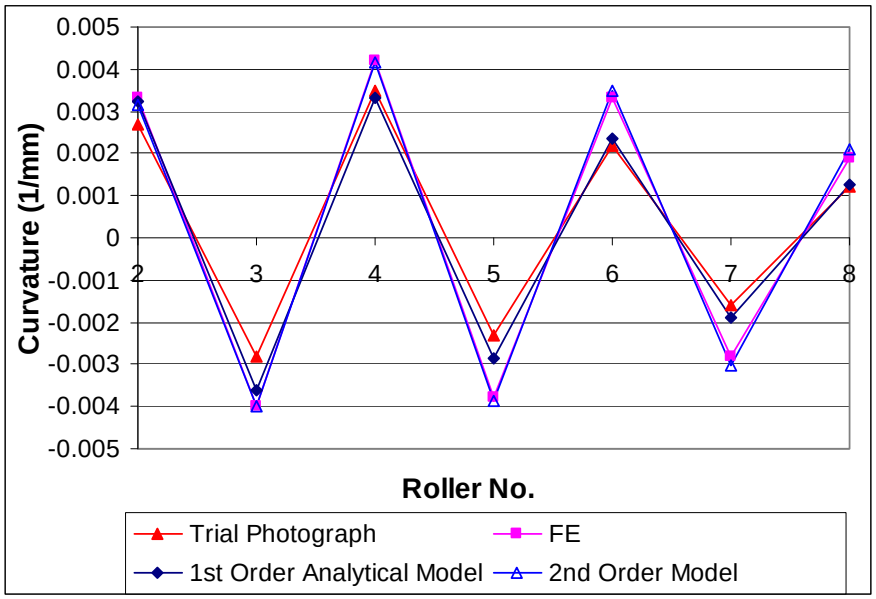


Fig. 149: Comparison of measured and predicted plate curvatures at roll positions, for sample 'SH20' (gauge 3 mm, grade S275)

The results indicate that the 1st order analytical model is capable of accurately predicting the plate trajectory in the initial and final 2 bending triangles, but appears to underestimate the deviation of the contact points from the dead-centre position in the middle triangles. The 1st order analytical model's predictions of plate curvature in each triangle show close agreement with experimental results and appear to be as accurate as those obtained using the FE approach. Application of the 2nd order model did not appear to give any improvement in the accuracy of curvature/path predictions. The level of curvature generated at each bending triangle is the critical factor governing the evolving stress-condition and exit bow of the plate.

Verification of Exit Bow Predictions

The analytical models were used to simulate the levelling of all the plate samples processed in the trials under WP 4.1, incorporating the 'real' penetration-settings recorded in the loaded condition, the measured sample gauge/length, and the appropriate yield strength data [samples of coil-sourced laser cut strip, of grades S275, S355 and S460, were used. Test certificates were obtained for each grade]. As previous studies have indicated that the Bauschinger effect can be neglected when considering the levelling of carbon steel [24], and the uniaxial stress-strain data show minimal work hardening for the levels of strain generated during the process, elastic-perfectly plastic material behaviour was assumed within the simulations.

Results indicate good overall agreement between exit longbow predicted by the 1st order model and measured data, with correlation coefficients of 88% and 80% obtained for parallel nest and tilting nest leveller configurations respectively (**Fig. 150**). Comparison of measurements and 2nd order model predictions gives correlation coefficients of 72% and 82% for the two leveller configurations. In general, the 1st/2nd order models appear to slightly under/overestimate the sensitivity of exit bow to product/processing conditions. On the basis of faster run time and marginally more accurate predictions, the 1st order model was adopted for general use, including the analyses reported under WP4.4 below.

Trends observed during the trials were generally reproducible in model results, even if the precise bow values were not the same (e.g. dependence of exit bow on breast roll offset – **Fig. 151**). The model therefore appears to be a suitable tool for rapid analysis of the levelling process, establishing appropriate settings and key process-sensitivities for a range of different levellers. With a CPU time at or below 0.05s, the 1D/1st order model is suitable for application within control software.

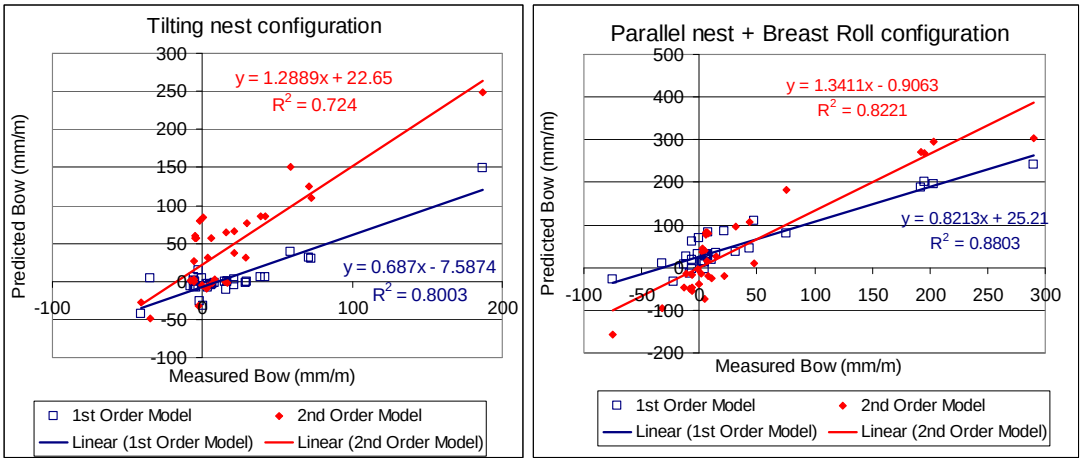


Fig. 150: Comparison of plate exit longbow measured during pilot leveller trials with corresponding 1st & 2nd order analytical model predictions

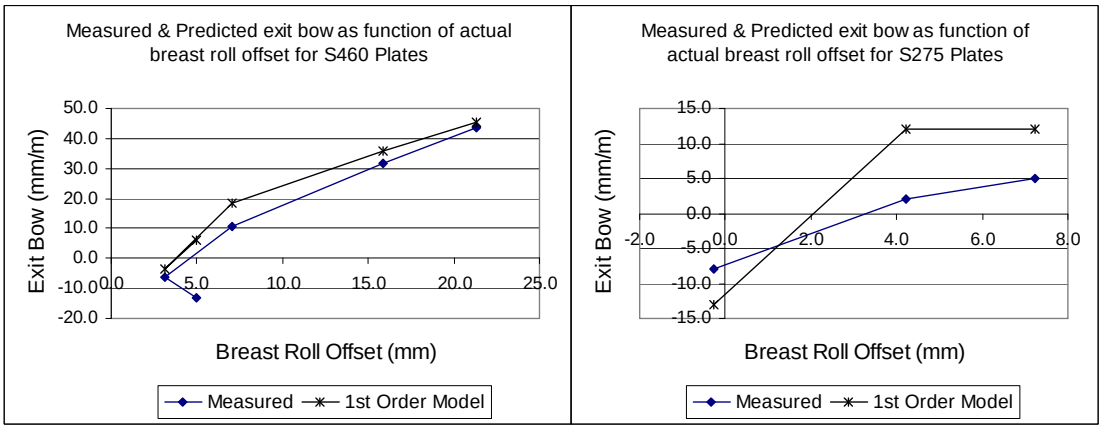


Fig. 151: Measured and predicted variation of exit longbow with breast roll offset

Task 4.4: Model based development of best set-up for levelling and final validation of models & set-up strategies

Assessment of the effects of variations in incoming plate condition and settings applied to leveller rolls by Corus

An assessment of the effects of variations in incoming plate condition and settings applied to leveller rolls has been undertaken, using the analytical models developed under WP4.2. Whilst finite element models allow a more detailed process simulation, run times of several hours make detailed sensitivity analyses/assessment of alternative levelling strategies inconvenient, given the large number of runs required. The spreadsheet user interface (**Fig. 114**) is sufficiently flexible to allow simulation of most common roller leveller configurations.

Roller leveller work roll configuration and settings strategy

For simplicity a simple tilting nest nine-roll leveller (four over five work rolls) of dimensions illustrated in **Fig. 152** has been simulated to test the effect of plate gauge and yield strength errors as well as the effect of first work roll gap plasticity levels using this analytical model. In this work roll configuration, the centres of the work rolls are fixed in line in each of the work roll nests (upper and lower work roll nest) and only the position of the upper work roll nest can be adjusted by tilting it, whilst the lower work roll nest is fixed. This is a very common configuration and is relatively easily engineered.

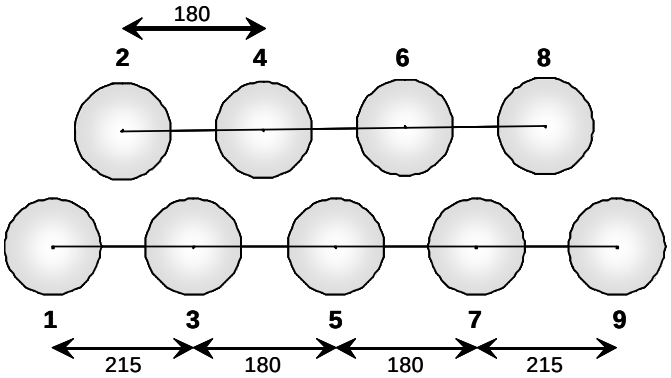


Fig. 152: The configuration of work rolls fixed in upper and lower nests of a tilting nest roller leveller

For this study, the strategy has been to apply settings for the model runs that ensure that the plastic strain imposed by work roll #8 is more than zero so that all of the seven work roll bending triangles apply work to the plate and act to affect its unloaded curvature. That is to say, the work roll gap setting at the last work roll bending triangle (work rolls #7, #8 & #9) is always set smaller than the nominal gauge of the plate in order to effect some plastic strain in it.

The model was run for plate of nominal gauges, 8, 14, 20 and 30 mm covering the majority of the range commonly produced in Scunthorpe Heavy Plate Mill, and for nominal yield strengths 300 N/mm^2 and 500 N/mm^2 to achieve a nominal plasticity of approximately 80% (α=8) i.e. an overstretch of 5 in the plate in process; the exit gap to achieve close to zero exit curvature (< 0.2 mm/m plate bow) was determined by iteration in the spreadsheet with the condition that the plasticity imposed at work roll 8 must be greater than zero. These base cases (**Table 19**) were then used to test the effect of changes in gauge and yield on the output bow of the plate for these base case settings. Variations in gauge up to ±1 mm and in yield strength up to ±100 N/mm^2 were tested. Arbitrarily the acceptable output plate bow was set at ±3.0 mm/m.

Table 19: Base cases used to test the effect of process variances

Gauge (mm)	Yield (N/mm^2)	Output Bow mm/m	1st triangle gap (mm)	Last triangle gap (mm)
8	300	0.0035	2.72	7.06
14	300	0.0023	10.98	14.84
20	300	0.0055	17.89	20.58
30	300	0.0077	28.59	29.75
8	500	0.0079	-0.81	6.41
14	500	0.0023	8.97	13.10
20	500	-0.0023	16.48	20.25
30	500	-0.0093	27.65	30.17

Pattern of plate plasticity through the roller leveller

To set the work roll gaps in a roller leveller to achieve a flat output plate the minimum information required is the plate gauge and its yield strength and some model or strategy to calculate settings appropriate for that roller leveller. The most common strategy is to set the gap in the first work roll triangle to achieve a plasticity, f in excess of 60% (overstretch value, U of 2.5) so that the majority of the thickness of the plate has been plastically deformed and to apply a sufficient level of strain sufficient to override inherent plate shape or curvature. For plates, shape is not often severe and this degree of plasticity may be sufficient but if there is severe shape as might sometimes occur in thinner gauge plates (< 7 mm), or in coil strip, greater plasticity's or overstretch values might be required, up to about 85% (overstretch value, U of 6.7).

We can consider the roller levelling process to consist of a series of alternately positive and negative three point bends (not necessarily symmetrical) of the plate in process in a succession of work roll bending triangles with progressive reduction of bending curvature through the machine. The plate surface in contact with the work rolls is plastically compressed and the opposite surface equally plastically stretched. Normally (without externally applied tension) the centre plane of the plate is the

neutral plane enduring no net stress and at some distance from the neutral plane where the yield stress of the material is exceeded it becomes plastic. A fraction of the plate thickness, f has been plastically strained.

By definition the overstretch value, U is the ratio of the surface strain (ε_s) to the yield strain (ε_y)

i.e. $$U = \varepsilon_s/\varepsilon_y \quad (22)$$

The fraction thickness of plate made plastic, f (plasticity) has the following relationship with overstretch value, U:

$$U = 1/(1-f) \quad (23)$$

In the earlier work roll triangles the plasticity's and bending curvatures are high, progressively decreasing towards the exit work roll triangle, where the gap is set to achieve a flat output plate; in a simple tilting nest roller leveller the work gaps in intermediate work roll triangles are determined by the setting of the first and last work roll gap.

Fig. 153 illustrates the pattern of plasticity generated in the plate at each work roll of the nine roll tilting nest leveller set to produce a flat output plate with every work roll applying some plasticity to the plate. Model results show that the higher the plasticity in the plate at the first work roll triangle then the higher the plasticity necessary at the last work roll triangle to achieve a flat output plate; this can be as high as 60%.

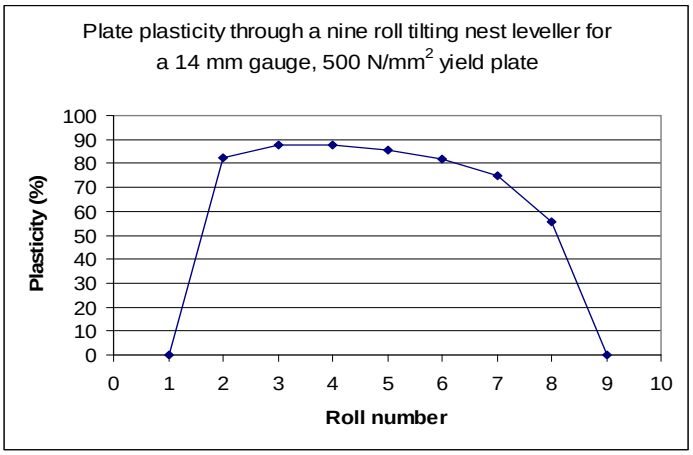


Fig. 153: Variation of fraction thickness of plate yielded through a nine-roll tilting nest leveller

This pattern is characteristic of a leveller with upper and lower work rolls nested (work roll centres on a common plane in each nest).

This high level of plasticity in the later work roll triangles also implies a high level of through-thickness residual stress fluctuation close to the plate surface. If the plasticity/overstretch in the later work roll triangles can be reduced then so will the amplitude of through-thickness residual stress fluctuation in the layers close to the plate surface. This might be achieved by utilising a large number of work rolls or by independent adjustment of the work roll gap in each work roll bending triangle. Thus, high levels of plasticity can be applied in the early work roll triangles to remove severe shape whilst imposing low levels of plasticity in the later work roll triangles which affect residual stress levels in the sub-surface layers.

Applying a polynomial equation to symmetrical three-point bending of plate or strip [14], [25], the maximum curvature, C imparted is given by:

$$C = 16p/L^2 \quad (24)$$

where p is the maximum deflection of the plate or strip and L is the pitch of the lower contact points (**Fig. 154**).

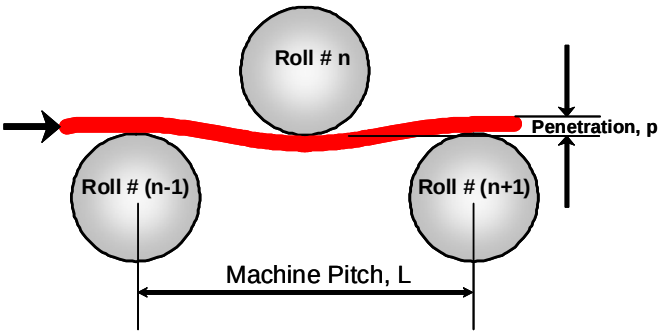


Fig. 154: Symmetrical bending of plate in a work roll triangle

For plate or strip bending in a roller leveller it can be shown that the expression [15] relating work roll penetration into the plate, p, plate yield strength, σ_y, work roll pitch, L, plate thickness, t, and fraction of the plate thickness made plastic, f, is:

$$p = [\sigma_y L^2]/[\alpha E t(1-f)] \quad (25)$$

or

$$p = [\sigma_y L^2 U]/[\alpha E t] \quad (26)$$

Where E is the Young's modulus of elasticity, U is the overstretch applied to the plate and α is a term related to the maximum curvature of the plate in the three point bend.

For a symmetrical bend the value of α is 8 [14], but in practice this is never the case and higher values are encountered.

The effect of inherent plate bow on the roller levelling process

The effect of pre-existing plate bow on the output plate bow was tested for 14 mm gauge plate of 500 N/mm^2 yield strength for a range of first work roll bending triangle plasticity's (Fig. 155).

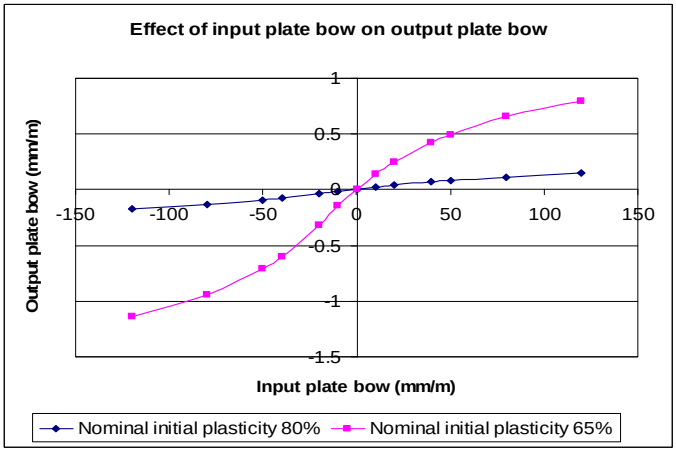


Fig. 155: The effect of pre-existing plate bow on output plate flatness (14 mm gauge, 500 N/mm^2 yield)

The effect was very small and insignificant especially for the settings employing higher imposed plasticity's, showing that the roller levelling process is very robust if the machine is correctly set for the processed plate gauge and yield strength. This observation is in agreement with observations and conclusions of Smith [24] and it is concluded that provided the plasticity in the plate imposed in the earliest work roll bending triangles exceeds 60% the roller levelling process is insensitive to incoming plate curvature. Smith [24] showed that this was true even for coil strip where variations in incoming strip curvature are much greater than those encountered in reversing mill plate.

The effect of deviations from the specified plate gauge on roller levelling performance

Smith [24] has already reported the cyclic variation of plate or strip exit curvature with exit gap setting and discussed the need for operators to find the "sweet point" where the exit gap setting produces a flat output plate. There can be several settings for which flat output may be obtained but for most of these at least one or more of the upper work rolls in the leveller are imposing only elastic or zero strain in the plate in process. Smith discussed the concepts of "convergence point", "zero points", cross over points"

and “the last effective bend”. In order to avoid the effect of the last effective bend in this study, leveller settings have been used for the base cases that ensure all of the upper work rolls are imposing some degree of plastic bending of the stock in process by setting the exit work roll gap to less than plate gauge. An oscillatory variation of exit plate bow with gauge variation around the base case gauge value was observed in models run results as illustrated by the graph in **Fig. 156**.

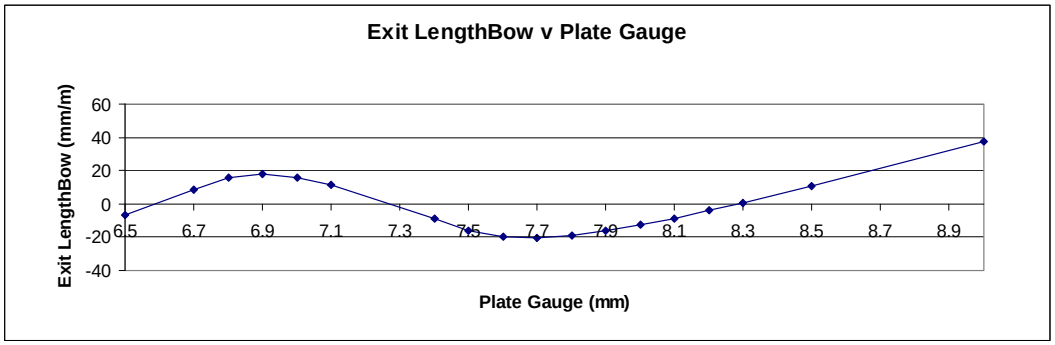


Fig. 156: Variation of output plate bow with change in plate gauge (8 mm, 300 N/mm^2)

The plastic strain imposed in the plate in the latter work rolls of the nine-roll leveller are shown in the graph in **Fig. 157**.

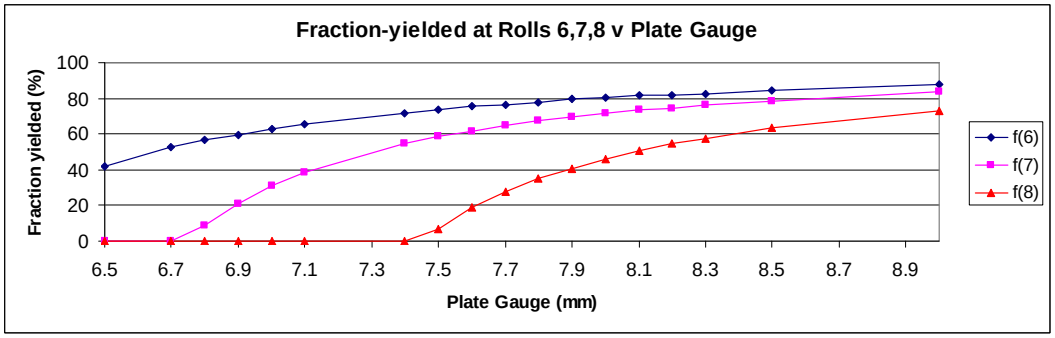


Fig. 157: Variation of fraction thickness of plate yielded at work rolls #6, #7 and #8 with plate gauge (8 mm, 300 N/mm^2)

In **Fig. 156** it can be seen that the oscillatory change of output plate bow occurs at plate gauges less than the nominal (base case) gauge for which the machine has been set to achieve a flat output plate and at gauges above this the curvature of the plate becomes increasingly positive with increase in gauge. This effect can be understood by referring to the work roll configuration illustrated in **Fig. 152** and to the plate bending line generated by this work roll configuration implied by the pattern of plastic work illustrated in **Fig. 153**. As the gauge increases above the gauge for which the machine has been set, so the penetration of the work rolls into the plate increases and work roll #8 applies an increasingly positive bend. As the gauge decreases below the gauge for which the machine was set, so the penetration of the work rolls into the plate decreases so that the last active triangle of work rolls moves upstream in the machine. The output plate curvature is determined by the sense of bending and degree of plasticity imposed by the last active work roll triangle.

Similar results to those illustrated in **Fig. 156** were observed in model run results for 14 mm, 20 mm and 30 mm gauge plate and gauge errors/variations about the nominated value.

In the graph of **Fig. 156** the gradient of the exit bow with gauge depends on which work roll bending triangle is the last to impose significant plastic strain (> ~ 20%). For a nine-roll leveller with substantial plastic strain imposed at work roll #8 (the last work roll bending triangle), the variation of output plate bow with gauge and yield will follow the expected pattern (a positive bend/bow). However if the last plastic strain induced in the plate is at work roll #7, then the gradient of the graph will change to a negative value because the sense of bending is reversed (negative). This reversing pattern repeats as the last active work roll bending triangle moves upstream in the leveller (to work rolls #6, #5, #4 etc).

Fig. 158 shows the effect of gauge variation on output plate bow using a strategy of ensuring plastic strain in the plate at every upper work roll for a leveller set to output flat plate of 14 mm gauge and yield strength 500 N/mm^2 (base case setting). This plot also demonstrates the effect of decreasing plate gauge on the number of active work roll triangles which produces an oscillatory change in output plate bow with decreasing gauge below the base case setting.

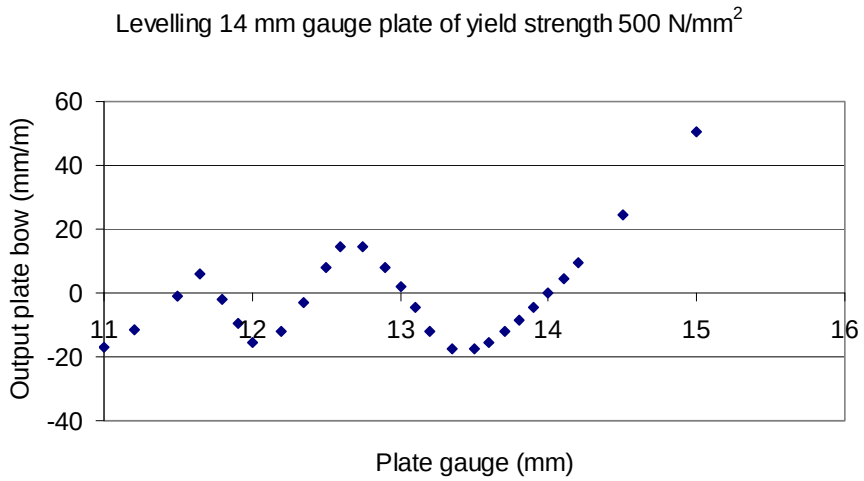


Fig. 158: Effect of changing plate gauge from the base case value on output plate bow

Data in **Table 20** show the effect of plasticity level imposed at work roll #2 on output plate bow as the plate gauge departs from the base case value (14 mm) for a material yield strength of 500 N/mm^2.

Table 20: The effect of imposed plasticity level on output plate bow for a range of deviations from nominal gauge

	Bow at various gauges (mm/m) for various plasticity levels (f) imposed at work roll #2									
	f	**13**	**13.25**	**13.5**	**13.75**	**14**	**14.25**	**14.5**	**14.75**	**15**
Plasticity (%)	**50**	1.30	1.57	-4.02	-7.13	0.01	10.78	22.97	35.77	48.87
	55	-1.56	2.96	-5.60	-7.50	-0.01	10.88	23.12	35.96	49.03
	60	-2.69	3.44	-7.42	-7.94	0.01	11.06	23.35	36.20	49.28
	65	1.02	2.59	-9.50	-8.41	0.07	11.31	23.68	36.54	49.62
	70	7.18	-0.09	-11.82	-9.01	0.00	11.48	23.92	36.81	49.89
	75	8.17	-5.57	-14.46	-9.71	0.00	11.68	24.20	37.11	50.20
	80	2.13	-14.83	-17.39	-10.48	0.00	11.97	24.59	37.53	50.60
	85	-14.37	-24.43	-20.51	-11.33	0.00	12.28	25.02	37.96	51.01

Although the effect of plasticity level is small especially at positive departures from base case gauge (14 mm) the output plate bow is very sensitive to departures from nominal gauge for all the levels of plasticity imposed at work roll #2. The effect appears worse for positive departures from the base case where the output plate bow progressively increases, but at negative departures from base case gauge the effect is smaller and oscillatory with gauge change. A deviation from the specified plate gauge of only 0.1 mm can increase the output plate bow beyond the acceptable range (±3 mm/m).

The effect of deviations from the specified plate yield strength on roller levelling performance

The change in output bow with deviation from the nominal plate yield strength followed a steady slope of constant gradient and no oscillatory pattern of behaviour was observed within the ranges of yield strength examined.

It can be seen from **Table 21** that even with substantial yield errors of 30 to 50 N/mm^2 the output plate bow remains within acceptable limits (±3 mm/m). The effect of yield errors is greater for negative deviations from the base case.

Table 21: Effect of yield variation on the levelling of 14 mm gauge plate of nominal yield strength 500 N/mm^2

		Output variation with yield strength (mm/m) for various plasticity levels (f) imposed at work roll #2										
	f	400	430	450	480	490	500	510	520	550	570	600
Plasticity	50	8.81	5.95	4.15	1.60	0.79	0.01	-0.74	-1.47	-3.50	-4.71	-6.32
	55	8.92	6.03	4.20	1.61	0.79	-0.01	-0.78	-1.54	-3.63	-4.89	-6.57
	60	9.12	6.19	4.32	1.67	0.82	0.01	-0.79	-1.56	-3.74	-5.06	-6.83
	65	9.40	6.42	4.51	1.78	0.92	0.07	-0.76	-1.56	-3.84	-5.23	-7.12
	70	9.60	6.56	4.61	1.81	0.92	0.04	-0.82	-1.66	-4.04	-5.52	-7.55
	75	9.84	6.73	4.74	1.84	0.91	0.00	-0.90	-1.78	-4.30	-5.87	-8.08
	80	10.21	7.01	4.95	1.94	0.96	0.00	-0.94	-1.87	-4.55	-6.26	-8.68
	85	10.65	7.35	5.20	2.05	1.02	0.00	-1.01	-1.99	-4.90	-6.76	-9.45

For the roller leveller settings strategy employed in this study where all the work roll triangles are active, within limits, the effect of plasticity level imposed at work roll #2 on output plate bow is small and would not by itself be a factor in determining roller leveller settings strategy except to apply sufficient strain to remove plate bow or shape or to minimise internal through-thickness residual stress fluctuations.

The sensitivity of output bow to last triangle setting

For a tilting nest leveller the model results show that for a given first work gap setting (work roll #2) the output plate bow is extremely sensitive to the setting of the gap in the last work roll triangle (work roll #8). **Fig. 159** shows the variation in output plate bow with gap setting for the last work roll bending triangle for a 14 mm gauge plate of 500 N/mm^2 yield strength and a nominal plasticity imposed in the plate at the first work roll triangle of 80%.

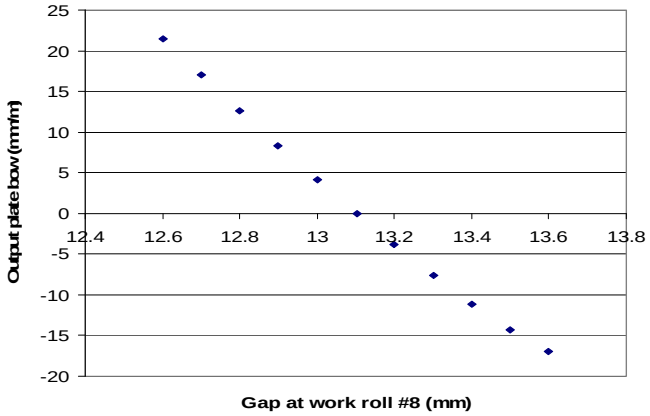


Fig. 159: Variation of output plate bow with work roll exit gap

(gauge = 14 mm, yield strength = 500 N/mm2, plasticity at work roll #2 = 80%)

For the 14 mm gauge plate with a nominal plasticity of 80% imposed in the first work roll triangle a deviation of only 0.1 mm outside the ideal value changes the output plate bow by more than ±3 mm/m for both material yield strengths tested (300 N/mm^2 and 500 N/mm^2). This was observed also for levels of plasticity imposed in the plate at the first bending triangle of 55% to 80%. This sensitivity can be appreciated by examination of the form of Equation (25) where the penetration, p is related to the level of plasticity, f imposed in the plate in the following manner:

$$p \quad \infty \quad 1/(1-f)$$

i.e. at lower values of plasticity, f very small changes in penetration effect large changes in plasticity, f.

It can also be deduced from equation (25) that increasing the work roll pitch, L would reduce the sensitivity of output plate curvature to the applied work roll penetration into the plate , p. However there are practical limits to the work roll pitch that can be used. A larger pitch might be built into the last work roll triangle but to allow for reverse processing of plates this would also be required in the first work roll triangle for simplicity of operation.

Roller levellers with independent adjustment of individual work roll heights

If a roller leveller is configured so that the upper work roll heights can be independently adjusted, then this extra degree of freedom makes it possible to rapidly decrease the bending curvatures and plasticity

levels imposed in the plate as it travels towards the exit of the leveller. Thus very high levels of plastic strain necessary to override curvature or shape inherent from upstream processing can be applied in the early work roll bending triangles, whilst rapidly reducing bending curvature and plastic strain to low levels within only a few downstream work roll triangles. The small curvatures applied in the later work roll bending triangles would have an effect similar to use of a large number of work rolls in a conventional tilting nest leveller with the accompanying advantages [25] and would reduce the extent of the residual stress fluctuations that occur in the through thickness layers close to the plate surface. This would possibly have advantages for end users who might machine the plate surfaces. A comparison of through thickness residual stress patterns that might be expected for a nine-roll tilting nest leveller and a nine-roll leveller with independently adjustable upper work rolls is illustrated schematically below in **Fig. 160**.

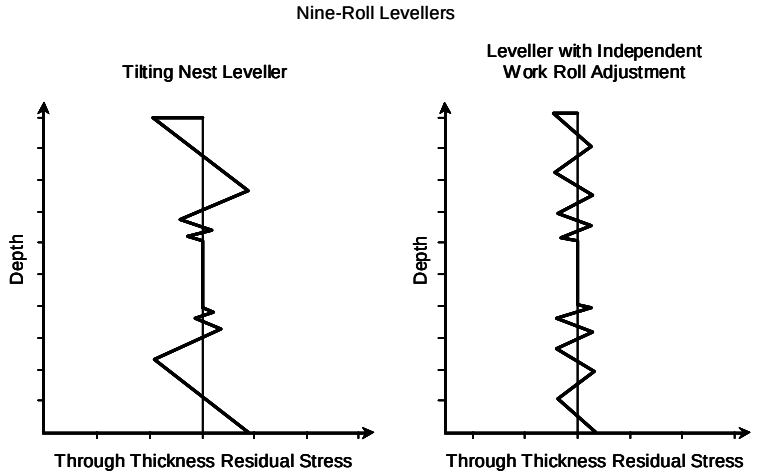


Fig. 160: Through thickness residual stress patterns for a nine-roll conventional tilting nest leveller and a leveller with independently adjustable work rolls

The sensitivity of the output plate bow to leveller exit work roll gap setting and plate gauge might also be reduced in such a leveller because of the reduced plate curvatures near the leveller exit.

Application of the analytical model to a nine-roll leveller configured to allow independent setting of each work roll has shown that adjustment of the last lower work roll (work roll #9) over a range of more than 0.7 mm (for a 14 mm gauge plate of 500 N/mm^2 yield strength) results in output plate bows within the ±3 mm/m acceptable range making adjustment of this roll a useful tactic in achieving flat output plate.

Assessment of the effects of variations in incoming plate condition and settings applied to leveller rolls by Ruukki

At **Ruukki**, plates are levelled in hot conditions as previously described in a 5 over 6 leveller. Different dimensions and settings of the leveller see **Fig. 161**, have been investigated in industrial trials and using 3D modelling. The incoming and outgoing flatness error has been manually evaluated during the trials.

Two types of defects have been studied, the first one with edge waviness and the second one with crossbow. In **Table 22** result from two of the levelling trials is presented. For the first trial only one pass was needed, whereas two passes were necessary for trial no. 2. However, only the first pass is presented in table 1 below, since only the first pass was considered in the FE-analysis. The settings are described in **Fig. 161**.

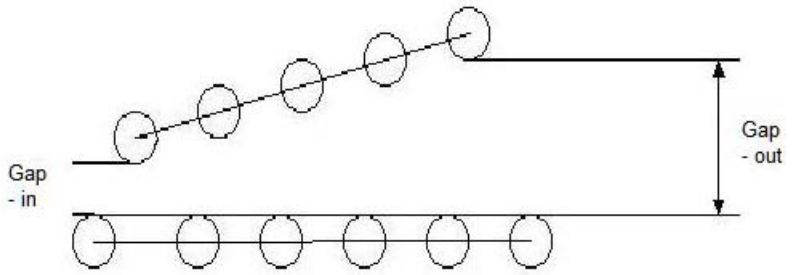


Fig. 161: Hot plate leveller at Ruukki, Definition of gap settings

Table 22: Levelling trials (All dimensions in mm)

Trial no.	Thick-ness	Plate ordered width	Defect type	Amplitude of defect before levelling	Amplitude of defect after levelling	Rolling end tempe-rature	Gap value (in)	Gap value (out)	Bending
1	5.10	3000	Edge Waviness	40	0.0	940	0.64 0.40	6.58 6.75	0.10
2	12.25	2500	Crossbow	10	-*	994	9.72 9.24	1.75 1.74	1.34

* No measurements after only the first pass.

3D modelling of the levelling process

So far the levelling process has been described with 2D models assuming plain strain condition (No straining across the plate). However the deformation state is 3 dimensional and for achieving reliable results all dimensions have to be considered.

Furthermore the previous presented models had no initial defects. In the 3D models those initial defects have been taken into consideration and the models are no longer perfectly flat. Note, that no residual stresses are implemented, which might be questionable. However no measurements are available to either confirm or reject the presence of any residuals stresses.

Due to the number of elements needed, LS-DYNA has been used to achieve reasonable computational times. Instead of using a number of solid elements as in previous 2D-models for the describing the thickness variations, the plates in both trials were discretised with eight-node solid (thick) shell element. The number of through shell thickness integration points was set to five. An isotropic piecewise linear plasticity model and the yield criterion according to von Mises have been used. No heat transfers between the plate and the rolls or the surrounding air have been considered. The simulations were therefore only mechanical analyses. The rolls were assumed to be rigid bodies with a Coulomb friction coefficient of 0.3. Due to the symmetry in the transversal direction only half of the plate had to be considered in the 3D model.

In **Fig. 162**, the plate with edge waviness together with rolls belonging to the roller-table at the inlet side are shown. The model has been reflected in the direction of its symmetry. The plate is friction-driven through the leveller.

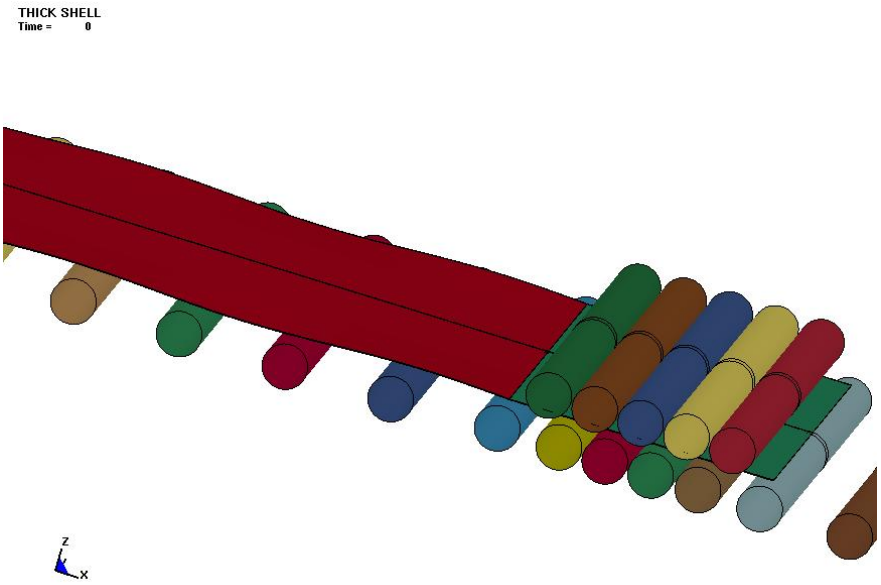


Fig. 162: FE-model of the hot-leveller where the incoming plate has a flatness defect (edge waviness)

Flatness

A common measure to evaluate the flatness of a sheet or a plate is the so-called I-unit. The unit is expressed in the form

$$I = \frac{\Delta L}{\lambda} 10^5$$

where ΔL is the difference between the longest and shortest ribbon across the width of the plate and λ is the wavelength.

Resolution of mesh

During the levelling process it is the small variations in deformation through the thickness and across the plate that levels the defected plate. Typically, some parts of the plate only achieve elastic straining while other parts are deformed plastically as shown earlier. For obtaining a correct description of the levelling process the size of the elements has to be small enough to resolve these small variations. Therefore a coarse grid, an intermediate and a fine grid have been studied for investigating the influence of the element size. Note that only trial no. 2 (crossbow) has been considered.

Mass scaling

As already mentioned, one way to speed up the calculations is to utilise mass-scaling. For trial no. 2 three different sizes of the time step have been used, one small step, one intermediate step (approx. same size as in trial no. 1) and one large step. The amount of kinetic energy was compared to the internal energy (elastic strain energy and work done in plastic deformation) in order to put the choice of time step into perspective. To summarise what mentioned above, simulations according to **Table 23** have been performed.

Table 23: Summary of performed simulations

Simulation no.	Defect	Mesh	No. of elements	Timestep	Timestep [ms]
1	Edge waviness	Intermediate	12500	Intermediate	12
2	Crossbow	Intermediate	14080	Intermediate	15
3	Crossbow	Fine	56320	Intermediate	15
4	Crossbow	Coarse	3520	Intermediate	15
5	Crossbow	Intermediate	14080	Small	4.7
6	Crossbow	Intermediate	14080	Large	47

Result and discussion

The evaluated flatness measure I-unit for the simulations is shown in **Table 24**. Notice that no value was evaluated for simulation no. 4 (crossbow - coarse mesh) since the mesh become too coarse for resolving the small variations in deformation. Except for simulation no. 4 all simulations resulted in very low I-unit values and hence the levelled plates can be considered as flat.

As already mentioned the coarse mesh resulted in ski-ending which was not the case for the intermediate mesh and fine mesh. Based on the I-unit, which became equal for simulation no. 2 (intermediate mesh) and. 3 (fine mesh), the resolution of intermediate mesh is sufficient for characterising the deformation behaviour of the plate during levelling.

The final investigation regarding the influence of the size of the time step clearly showed how the ratio between kinetic energy and internal energy increased as the time step grow as a consequence of enhanced mass (See simulation no. 4 to 6.). The ratio for the final simulation with the largest time step also achieved a value above what could be accepted. However, the other five simulations got kinetic energies, which could be considered as small compared to the internal energies. In **Fig. 163** and **Fig. 164** the effective plastic strain and longitudinal plastic strain for simulation no. 1 (edge waviness) are depicted. As expected the largest effective strain appears at the edges. Another interesting result is that the edges are compressed in the longitudinal direction, see **Fig. 164**.

Regarding the crossbow case, the effective plastic strain is relatively evenly distributed along the plate, see **Fig. 165**. Finally **Fig. 166** shows the plastic strain in the longitudinal direction. Some tendencies except that the strain values seem relatively homogeneously distributed all over the plate are hard to detect.

Table 24: Results from performed simulations

Simulation no.	Defect	I-unit	Mesh	Timestep	$\frac{\text{Kinetic energy}}{\text{Peak internal energy}}$
1	Edge waviness	5	Intermediate	Intermediate	-
2	Crossbow	4	Intermediate	Intermediate	7 %
3	Crossbow	4	Fine	Intermediate	9 %
4	Crossbow	-	Coarse	Intermediate	10 %
5	Crossbow	7	Intermediate	Small	5 %
6	Crossbow	6	Intermediate	Large	32 %

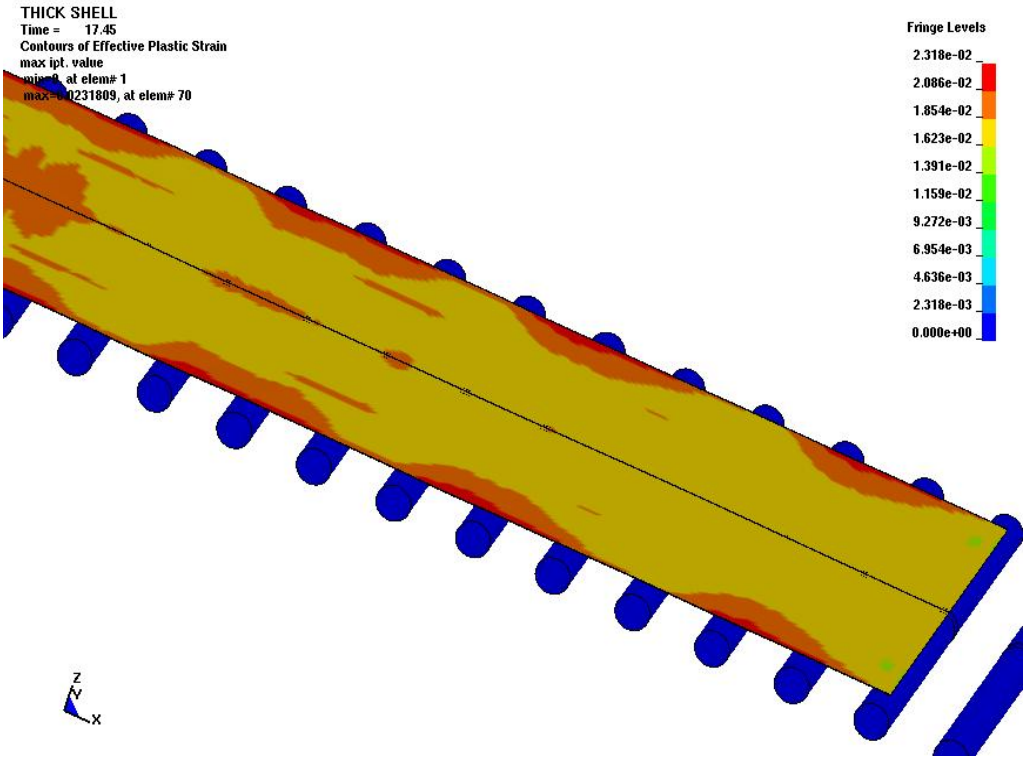


Fig. 163: Trial no. 1. Effective plastic strain after levelling

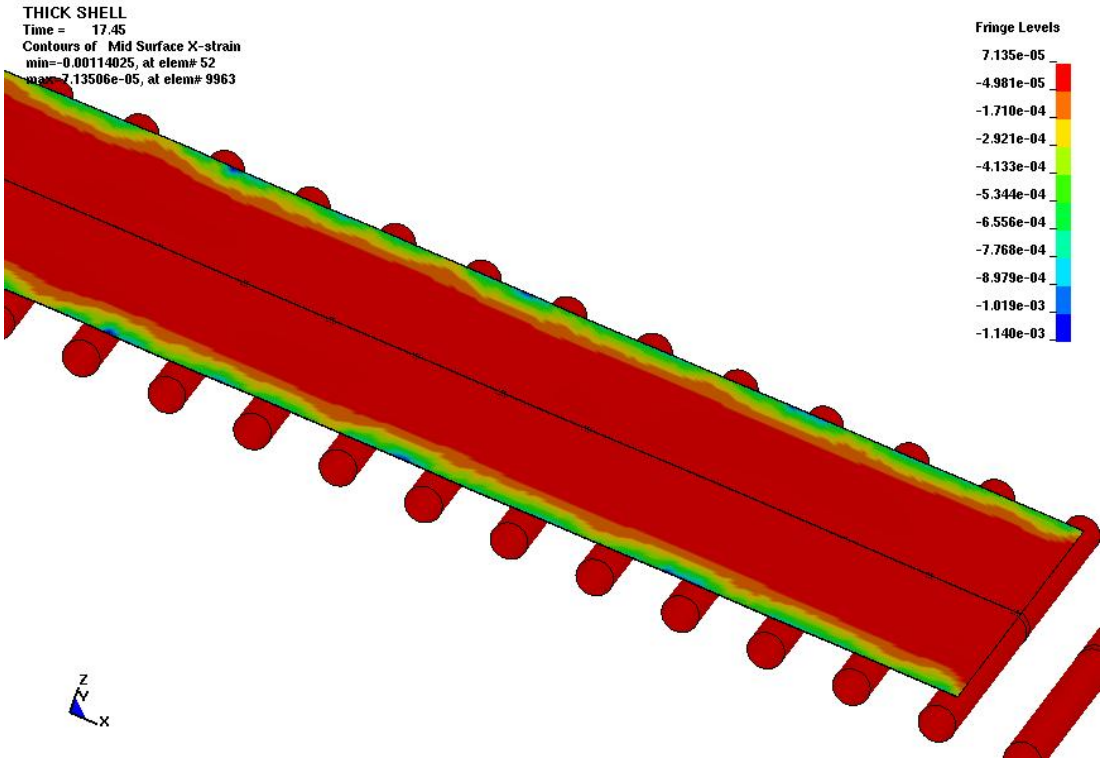


Fig. 164: Trial no. 1. Longitudinal plastic strain at the mid-surface after levelling.

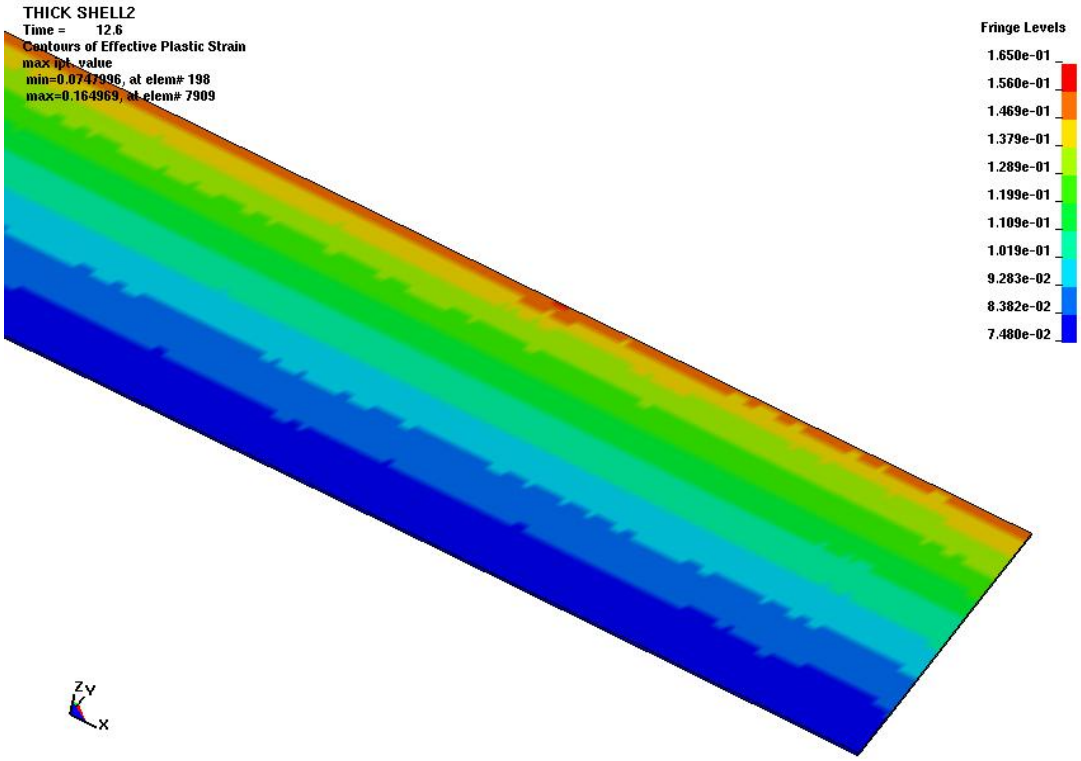


Fig. 165: Trial no. 2. Effective plastic strain after levelling. Half-symmetry.

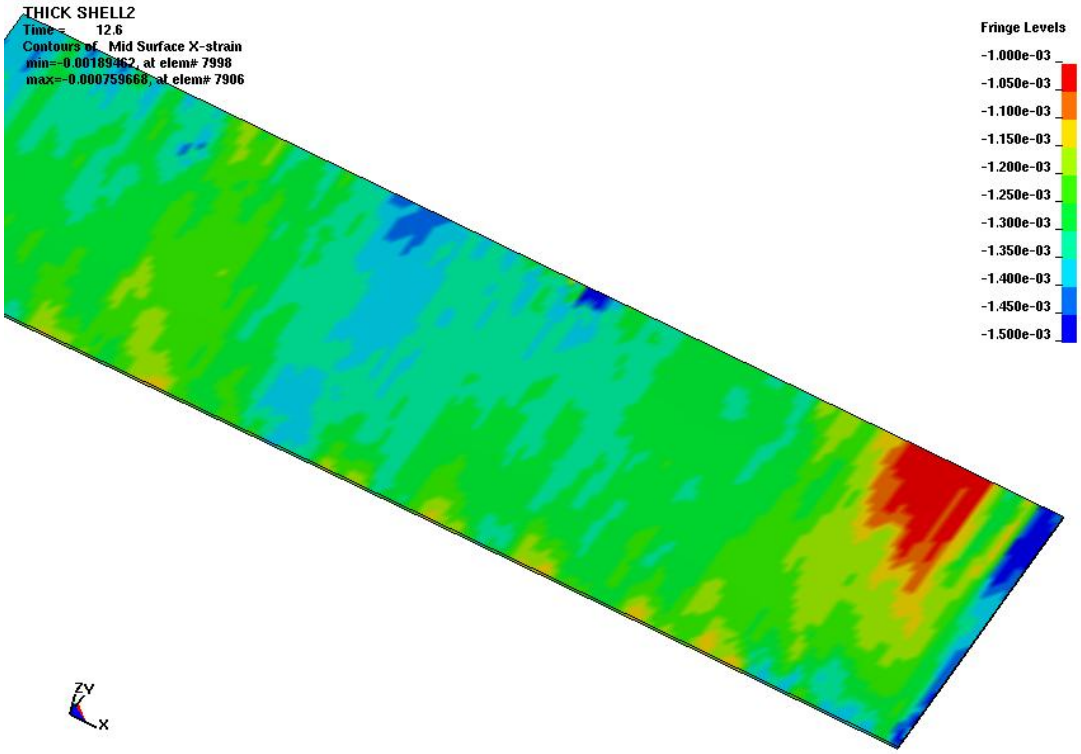


Fig. 166: Trial no. 2. Longitudinal plastic strain at the mid-surface after levelling. Half-symmetry

Task 4.5: Levelling model and set-up rules for global line application

The hot leveller at the **TKS HPM** is equipped for manual and automatic operation. Respectively, the adjustments (**Fig. 167**) of the leveller can be prompted by the operator (**Fig. 168**) or are performed by a levelling model, which requires the following input data:

- Strength of the material,
- Measured temperatures at entry and exit side of the leveller,
- Actual thickness,
- Plate width and
- Information about flatness, visually assessed by the operator (**Fig. 169**).

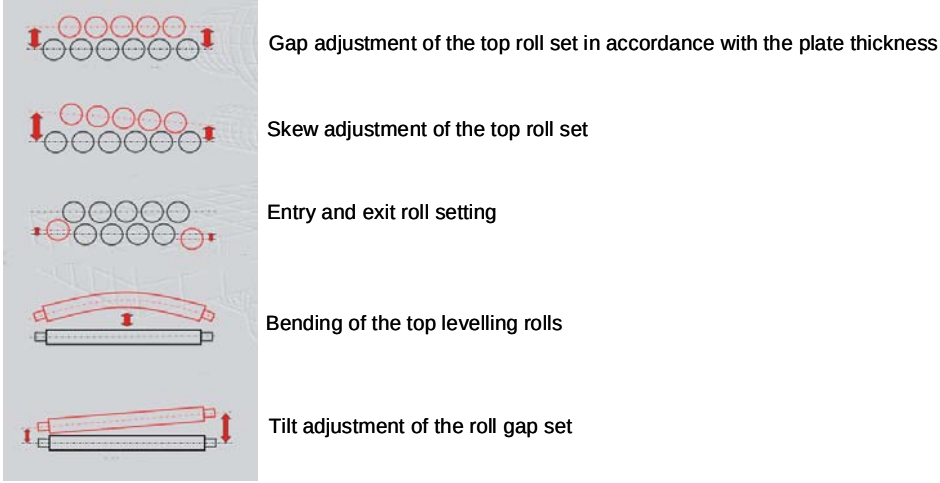


Fig. 167: Adjustments of the hot leveller

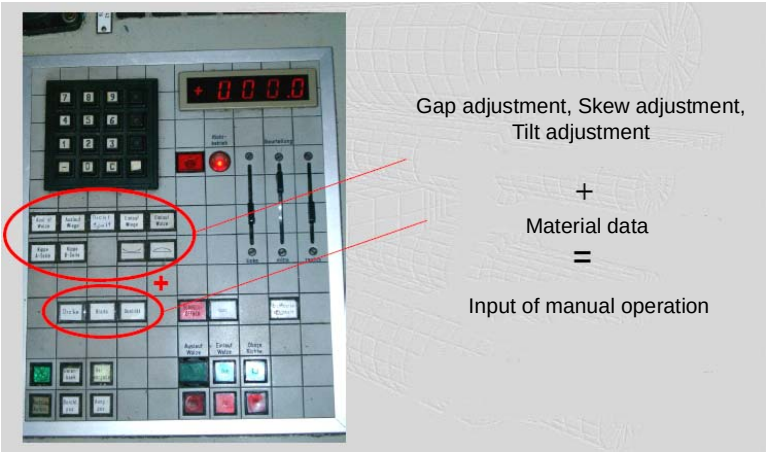


Fig. 168: Control panel of the hot leveller

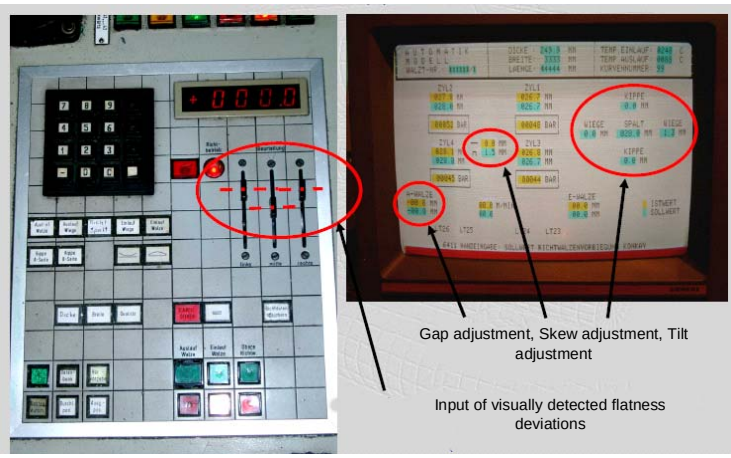


Fig. 169: Input of flatness characteristics, visually assessed by the operator

The visual assessment of the flatness by the operator has an important significance within the above described operating procedure. Therefore the actuations of the operator were compared with the measured flatness.

Fig. 170 and **Fig. 171** represent a demonstration of the measured flatness by use of the TopPlan® system in contrast to the visually assessed flatness profile performed by the operators of the levelling plant. The diagrams refer to two thickness ranges, that is for **Fig. 170** (3mm =< D < 10mm) and for Fig. 171 (10 mm <= D < 20mm). Both Figures show the measured parabolic flatness range in I-units versus the visually assessed flatness profile by the operators. Apart from a few flatness values the visually assessed flatness rates concentrate on values of approximately minus 2 %.

The comparison of both diagrams clarify that the actual flatness situation is not evaluated correctly by the operators which consequently leads to a non optimal adjustment of the levelling plant.

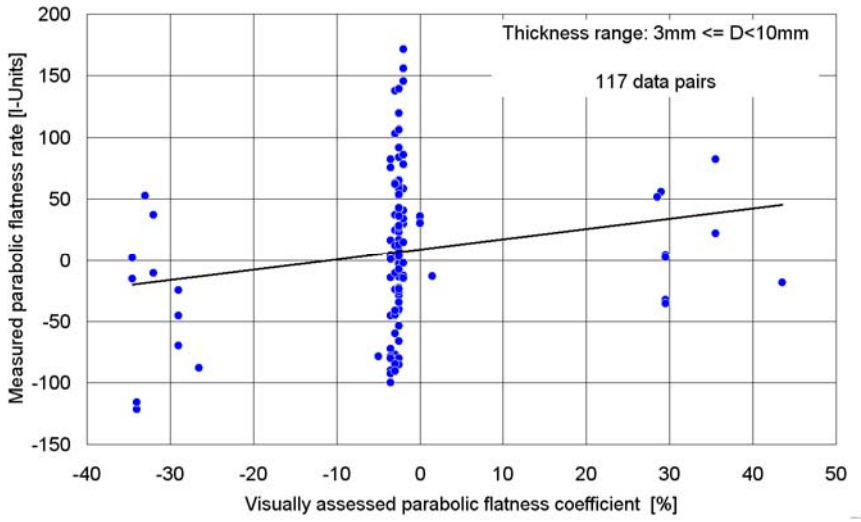


Fig. 170: Comparison of measured and visually assed flatness

(parabolic flatness coefficient)

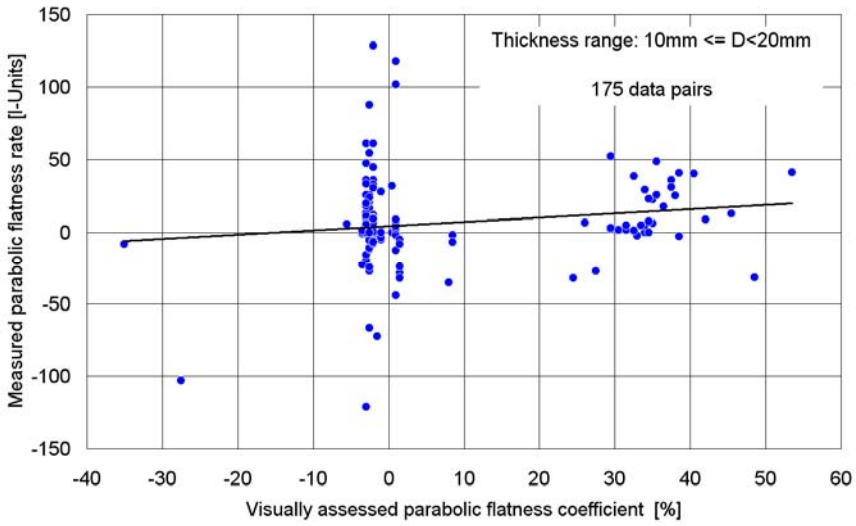


Fig. 171: Comparison of measured and visually assed flatness

(parabolic flatness coefficient)

These investigations demonstrate that an installation of a flatness measuring system on levelling plants is required, in order to perform an optimal leveller adjustment carried out by the operators or by an automatic control system based on the measured flatness profile [26], [27].

Fig. 172 shows the bock diagram of an advanced automatic leveller control system. The main components are

- Flatness measurement systems at the entry and exit side of the leveller,
- Model based controller for foreword control,
- Self learning adaptation module to minimise deviations of model calculations.

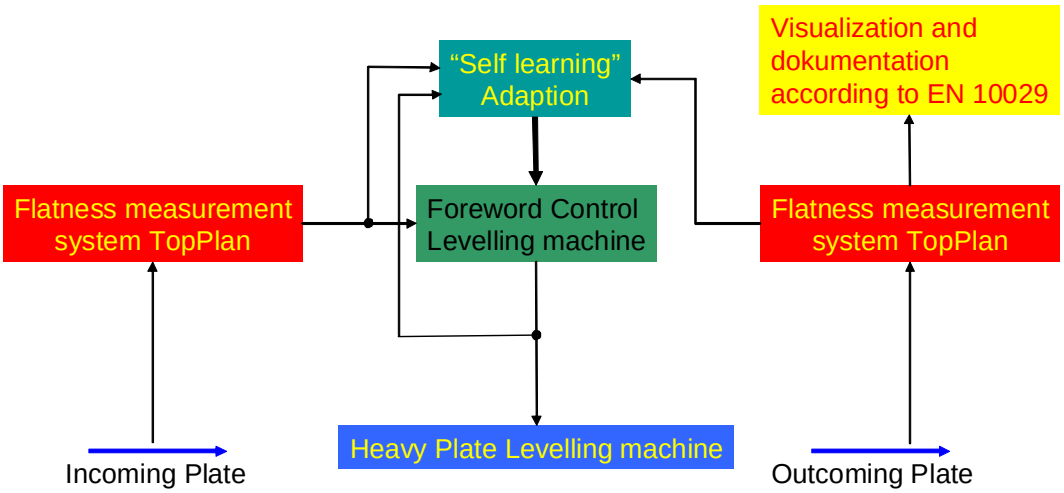


Fig. 172: Block diagram of a leveller control system

WP 5: Global Through-process Flatness Predictor and Coordinated Optimiser

To predict the final flatness of a plate one has to know on which process route the plate will be passed through the different manufacturing processes. An analysis of the process route frequency has been made based on the data stored in the plant database (**Fig. 173**) for the **TKS HPM**. The analysis covered the period between 02.02.2009 and 14.04.2009 where exploitable data of about 5400 plates were available.

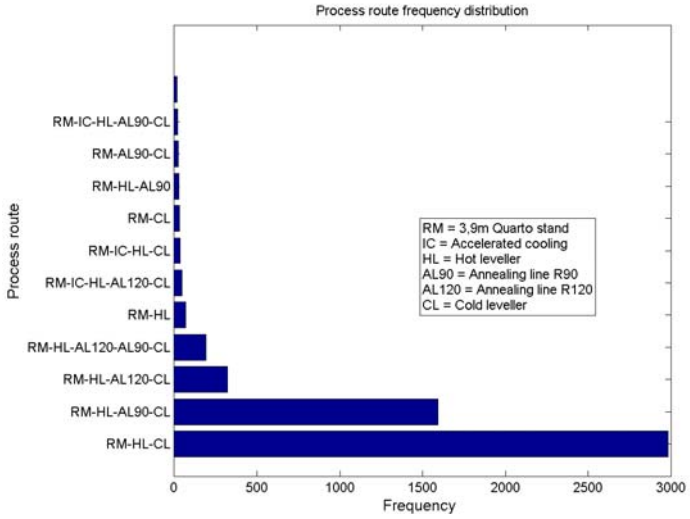


Fig. 173: Frequency distribution of the different process routes in the FKS HPM

The majority of plates is manufactured on the "direct" process route:

- hot rolling (RM)→hot levelling (HL)→cold levelling.

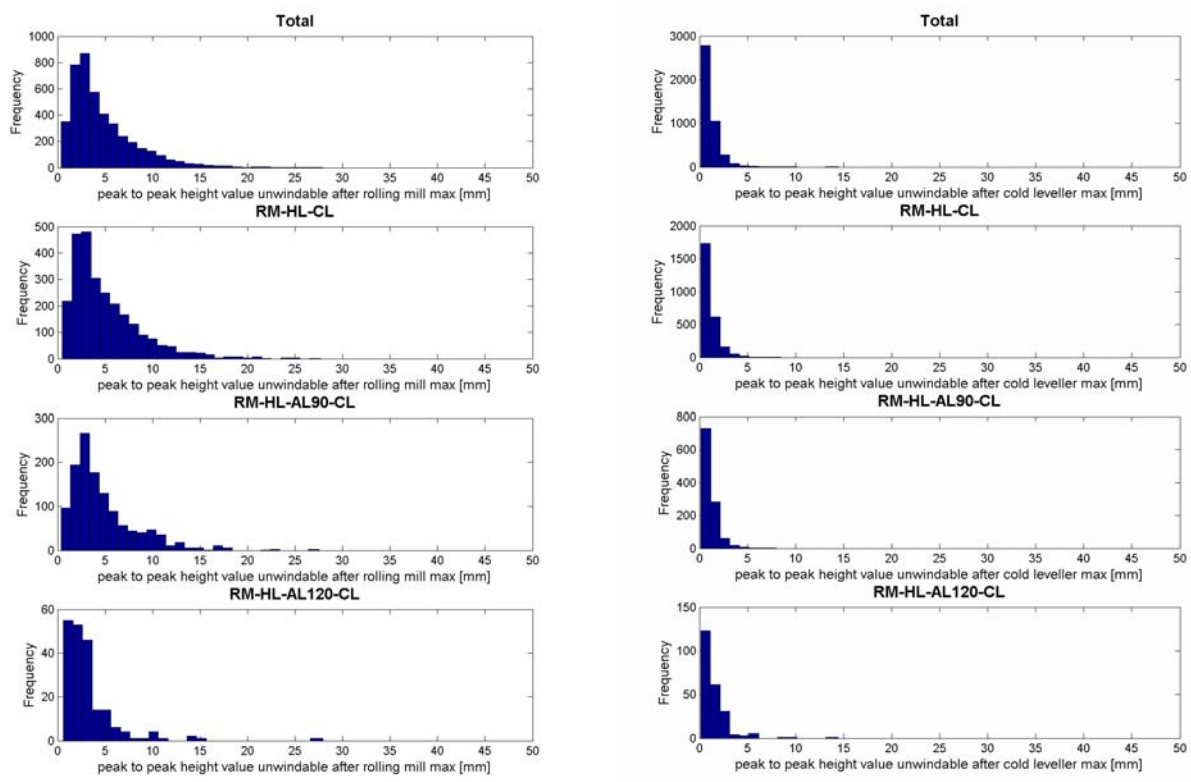
Other important process routes include annealing processes:

- hot rolling (RM)→hot levelling (HL)→annealing line (AL90)→cold levelling,
- hot rolling (RM)→hot levelling (HL)→annealing line (AL120)→cold levelling,
- hot rolling (RM)→hot levelling (HL) →annealing line (AL90)→annealing line (AL120)→cold levelling.

All other process routes have a marginal amount, even in sum.

In the next step one has to analyse the flatness evolution of plates according to the main process routes. **Fig. 174** and **Fig. 175** show the frequency distribution of flatness defects characterised by the peak to peak height value of the unwindable part and of the non unwindable part. (The peak to peak height value is a sharper criterion compared to EN 10029). In both cases the flatness conditions after hot rolling are compared with the conditions after cold levelling. Flatness measurements are only available at these two areas.

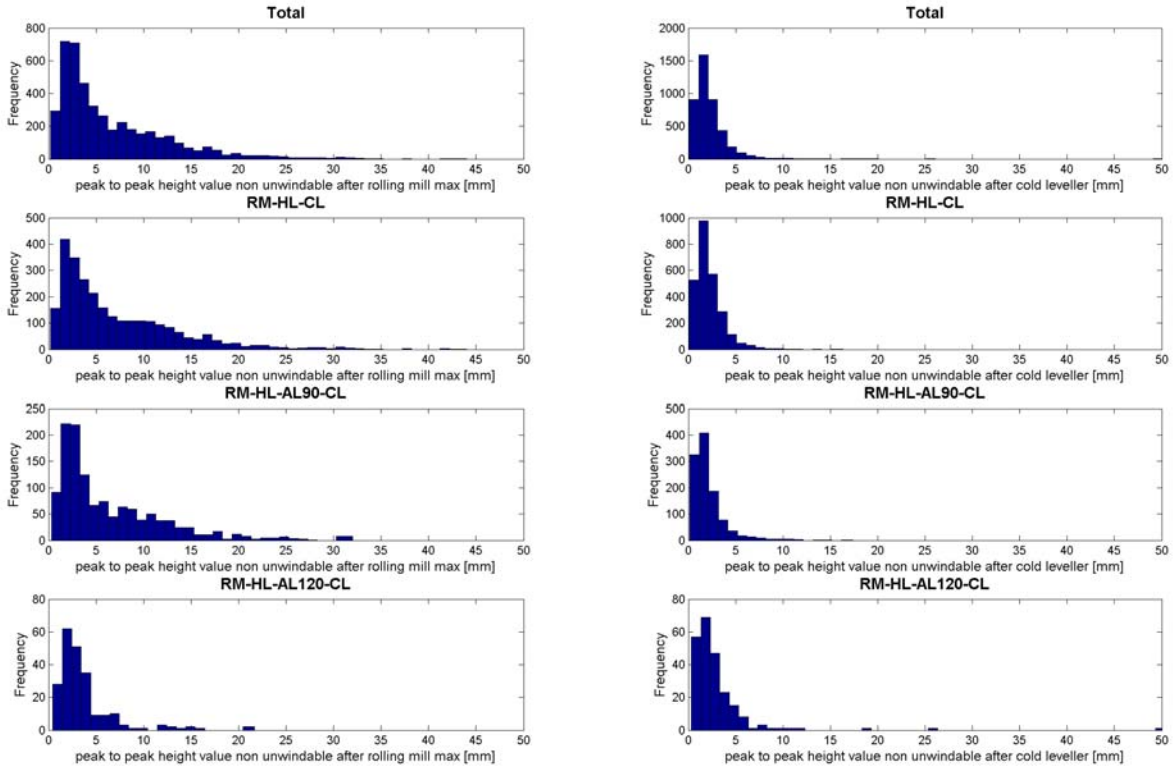
The evaluations show that in total (upper part of figures) the peak to peak height value on an average is diminished from 4 mm to 2 mm for the unwindable part of flatness defects as well as for the non unwindable part of flatness defects. The reduction of flatness defects is nearly independent from the considered process route.



a) b)

Fig. 174: Frequency distribution of peak to peak height value of the unwindable part of flatness defects

a) after rolling mill, b) after cold leveller



a) b)

Fig. 175: Frequency distribution of peak to peak height value of the <u>non</u> unwindable part of flatness defects

a) after rolling mill, b) after cold leveller

A further analysis, taking into account a more detailed characterisation of flatness, has been done. For this purpose the measured flatness, described by the distribution of elongation across the plate width, has been evaluated by the procedure of orthogonal decomposition. This decomposition determines the coefficients of an orthogonal polynomial which is equivalent to the common distribution of elongation. The coefficient c_2 represents the parabolic fraction which indicates the existence of edge waves or centre buckles respectively (**Fig. 176**). The interpretation of results of a smaller sample is explained schematically in **Fig. 177**.

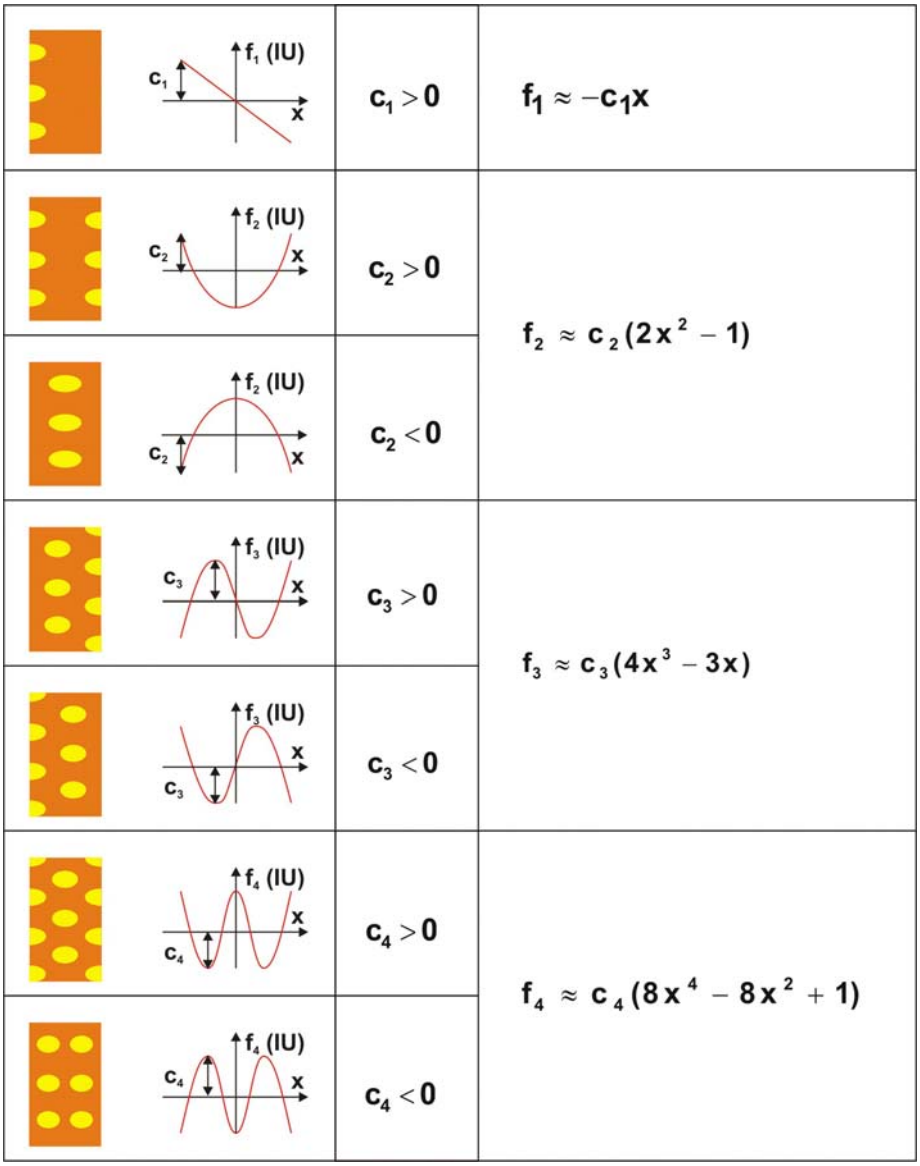


Fig. 176: Coefficients of an orthogonal polynomial

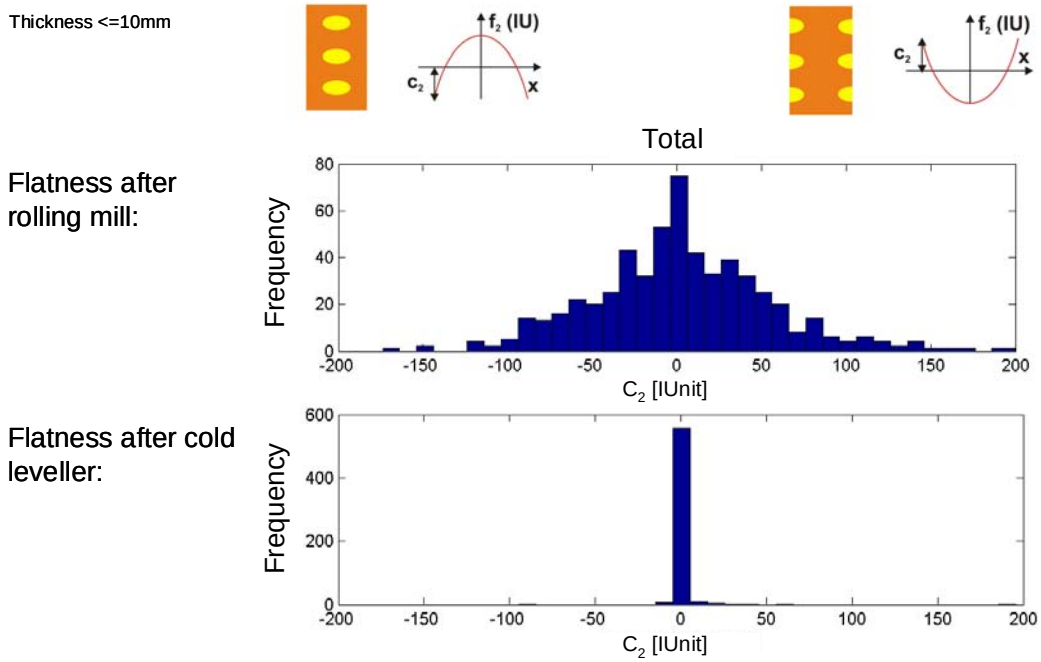
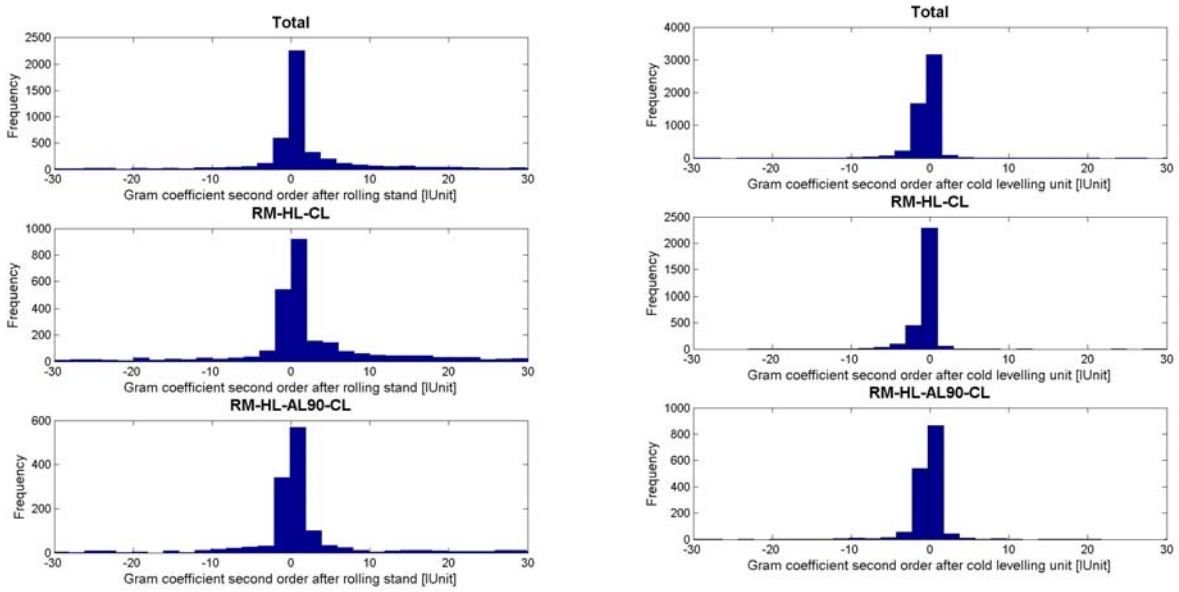


Fig. 177: Interpretation of results of a smaller sample



a) b)

Fig. 178: Orthogonal coefficients (2nd order) of the distribution of elongation

a) after rolling mill; b) after cold leveller (all thicknesses)

As to be seen in **Fig. 178** flatness deviations generated in the rolling stand are eliminated by the subsequent processes mainly by the hot and cold levelling. These processes are controlled locally and have in sum sufficient results.

Furthermore it has to be confirmed that flatness defects are not passed through the processing chain. This is the main reason which makes it impossible to create global flatness predictions and coordinated optimisations. A fundamental prerequisite for global flatness control is that various inputs (e,g. changes of rolling process) would have a strongly correlated impact on final flatness. However, this correlations could not been identified on the basis of the comprehensive process data analysis.

Therefore the development and implementation of the “Global Through-process Flatness Predictor and Coordinated Optimiser” is obsolete by physical reasons.

Nevertheless process optimisations are possible with respect to avoid especially disturbances caused by flatness defects. Using the installed flatness measurement optimisations of the rolling schedule (off-line) as well as of the hot levelling process is possible. The strategy and the data flow are depicted in **Fig. 179**.

This proposal is know to TKS. As the realisation requires a detailed insight the specific knowhow of TKS especially concerning material data further details have to be kept confidential.

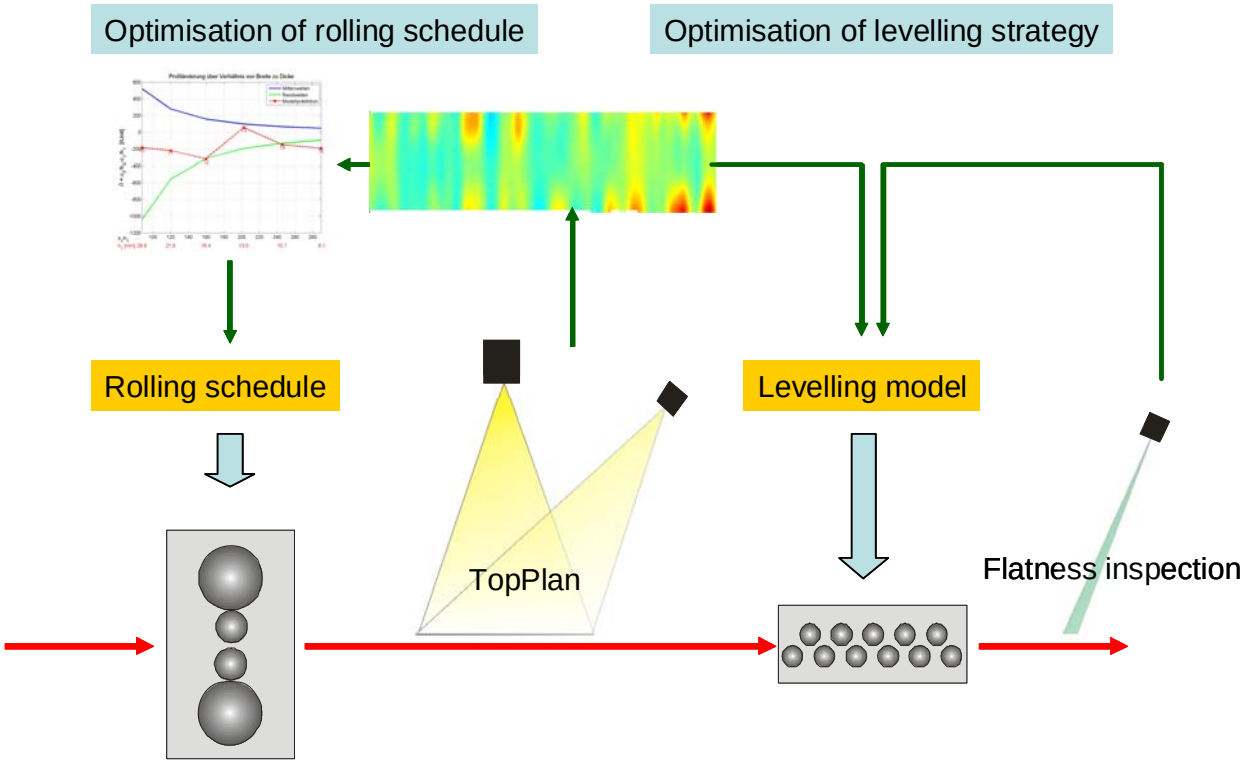


Fig. 179: Strategy and the data flow to optimise the rolling schedule and the hot levelling process

2.4 Conclusions

- The development and implementation of the "Global Through-process Flatness Predictor and Coordinated Optimiser" is obsolete by physical reasons.
- Strategies to locally optimise
  - the rolling schedule,
  - the hot and cold levelling processes,
  - the cooling and stacking process inclusive quenching

  have been investigated.

2.5 Exploitation and impact of the research results

The results are directly exploited by the involved industrial partners (TKS, Rautaruukki). Furthermore publications are planned.

List of Tables and Figures

Table 1: Flatness rejects classified according to the plate thickness, width and length 29
Table 2: Relevant process-/plant variables 31
Table 3: Flatness specifications according to EN 10029 32
Table 4: Variables used in the analyses (partial) 39
Table 5: Snapshot of flatness measurements for a rolled plate with no hot levelling 40
Table 6: Correlation analyses (partial) 43
Table 7: Extended set of variables 58
Table 8: Highest correlations 59
Table 9: Set of parameters 81
Table 10: Leveller-settings and measured exit bow for strip samples processed using the standard '4 over 5 roll' configuration 93
Table 11: Leveller-settings and measured exit bow for strip samples processed using the '3 over 4 plus exit breast roll' configuration 93
Table 12: Experimental data 97
Table 13: Trial schedule and measured values 98
Table 14: Results from FE-simulations on 3-roll bending. Marc default data. 109
Table 15: Results from FE-simulations on 5-roll bending. 111
Table 16: Measured and calculated tip deflection 112
Table 17: Resulting curvature for different cradle settings 116
Table 18: Resulting curvature for different gap settings 117
Table 19: Base cases used to test the effect of process variances 125
Table 20: The effect of imposed plasticity level on output plate bow for a range of deviations from nominal gauge 129
Table 21: Effect of yield variation on the levelling of 14 mm gauge plate of nominal yield strength 500 N/mm^2 130
Table 22: Levelling trials (All dimensions in mm) 132
Table 23: Summary of performed simulations 134
Table 24: Results from performed simulations 134
Table 25: Attenuation table of the filter wheel 9
Table 26: Table roller eccentricity measurements near the USF gauge location 24

Fig. 1: Networked process stages and line coordinated approach with quality data input and the main objectives indicated 5
Fig. 2: Functionality of the system 7
Fig. 3: ArcelorMittal's Spain HPM layout 20
Fig. 4: Layout of the plate rolling plant, RUUKKI 21
Fig. 5: Layout of the cooling and cutting, RUUKKI 21
Fig. 6: HPM layout of TKS 22
Fig. 7: HPM layout of Corus Scunthorpe 23
Fig. 8: Schematic installation of the measuring system at the ArcelorMittal Spain HPM 23
Fig. 9: TopPlan® installation at Ruukki's plate mill 24
Fig. 10: TopPlan® installation at the HPM of TKS 25
Fig. 11: Projection of the stripe pattern on the hot plate surface during the measurement 25
Fig. 12: TopPlan® display screen at the pulpit of the rolling operators 26
Fig. 13:Flatness measurement system (supplier NOKRA) 26
Fig. 14: Exemplary representation of the strip topography after the rolling 27
Fig. 15: Plate topography behind the cold levelling machine 27
Fig. 16: Amount of flatness rejections 30
Fig. 17: Quality assurance system for documenting the final flatness 30
Fig. 18: Max. flatness deviation for TM-rolled plates (measuring length 1m) 31
Fig. 19: Ruler assessment according to EN 10029 32
Fig. 20: Operating image of the flatness measuring system 33
Fig. 21: Approach to characterise the plate flatness 34
Fig. 22: Substantial process steps of rolling heavy plates 34
Fig. 23: General functionality of the system 35
Fig. 24: Integration of the process signal data collection system into the existing network 36
Fig. 25: Configuration for the database 37
Fig. 26: Flatness and gauge profile of plate WW963 (3.15 m wide plate, 10 mm gauge) 40
Fig. 27: Example of flatness map generated from manual measurements on 3.4 m by 6 mm plate 41
Fig. 28: Histogram STARTTEMP 42
Fig. 29: Quartile matrix - ROLLMODE 42
Fig. 30: Rolling loads on the finishing stand for plate number NZ653 43
Fig. 31: Finishing load lines for plate number NZ653 44
Fig. 32: Strip flatness dead band [4] 45
Fig. 33: Shohet and Townsend flatness calculation for plate number NZ653 45
Fig. 34: Rolling loads on the finishing stand for plate number RA991 46
Fig. 35: Shohet and Townsend flatness calculation for plate number RA991 46
Fig. 36: Rolling loads on the finishing stand for plate number RA875 47

Fig. 37: Shohet and Townsend flatness calculation for plate number RA875 47

Fig. 38: Data flow and modules of the stand deflection model 47

Fig. 39: Comparison of the Shohet and Townsend flatness calculation with the measured flatness before the hot leveller for plate number 70569 (scale of pseudo-colours in mm at the right) 48

Fig. 40: Comparison of the Shohet and Townsend flatness calculation with the measured flatness before the hot leveller for plate number 82487 49

Fig. 41: Comparison of the Shohet and Townsend flatness calculation with the measured flatness before the hot leveller for plate number 86606 49

Fig. 42: Comparison of the Shohet and Townsend flatness calculation with the measured flatness before the hot leveller for plate number 82475 50

Fig. 43: Comparison of the Shohet and Townsend flatness calculation with the measured flatness before the hot leveller for plate number 84487 50

Fig. 44: Comparison of the Shohet and Townsend flatness calculation with the measured flatness before the hot leveller for plate number 82393 51

Fig. 45: Comparison of the Shohet and Townsend flatness calculation with the measured flatness before the hot leveller for plate number 85149 51

Fig. 46: Comparison of the Shohet and Townsend flatness calculation with the measured flatness before the hot leveller for plate number 85145 52

Fig. 47: Pass schedule philosophy and influence of CORRF0 53

Fig. 48: Schematic functionality of rolling strategy 32 54

Fig. 49: Corrections on CORRF0 and CORRFLAST Vs plate number for the work roll pair 54

Fig. 50: Correlation matrix 55

Fig. 51: Measured Vs predicted rolling forces at each pass 55

Fig. 52: Plates rolled with the work roll pair 224-225 and CORRFLAST=3 56

Fig. 53: Calculated and real forces for the 16 passes of plate 168297 56

Fig. 54: Plates rolled with the work roll pair 224-225 and CORRFLAST=9 to 9.5 57

Fig. 55: Plates rolled with the work roll pair 280-281 and CORRFLAST=3 57

Fig. 56: Influence of the work rolls on forces distribution 57

Fig. 57: Correlation matrix 59

Fig. 58: Comparison of actual pass sequence with Scheduler prediction for plate RA300 [Plate dimensions: gauge 9 mm, width 3.2 m, CMn grade] 60

Fig. 59: Comparison of actual pass sequence with Scheduler prediction for plate NZ653 [Plate dimensions: gauge 10 mm, width 3.15 m, CMnNb grade] 60

Fig. 60: Comparison of actual pass sequence with Scheduler prediction for plate RA875 [Plate dimensions: gauge 8 mm, width 3 m] 61

Fig. 61: Comparison of Shohet and Townsend flatness calculations for plate RA875 61

Fig. 62: Comparison of actual pass sequence with Scheduler prediction for plate RA703 [Plate dimensions: gauge 6.5 mm, width 3.2 m] 61

Fig. 63: Comparison of Shohet and Townsend flatness calculations for plate RA703 62

Fig. 64: Comparison of actual pass sequence with Scheduler prediction for plate RA991 [Plate dimensions: gauge 10 mm, width 3.4 m] 62

Fig. 65: Comparison of Shohet and Townsend flatness calculations for plate RA991 63

Fig. 66: View from the hot leveller exit roller table of the LSL cooling bank 64

Fig. 67: Temperature-time trace of a 12 mm gauge plate in the LSL after hot levelling 65

Fig. 68: Yield strength variation with temperature for common grades of plain carbon structural steel 66

Fig. 69: Local distortion retained in a cold plate caused by a misplaced push-dog whilst the plate was hot and allowed to cooled to temperatures below 400 °C (a) Damaged plate on skid rails; (b) Damaged plate on the top of the pile 66

Fig. 70: View of cooling bank no. 2 from the hot leveller entry/exit roller table..... 67

Fig. 71: View of the HSL hot leveller exit roller table, and cooling banks no. 3 and no. 4 68

Fig. 72: Photograph of the final stack. In front one can see the aligned edges of the heavy plates (foot end of the plates) 69

Fig. 73: Thermocouple position (top view)..... 69

Fig. 74: Photograph of the stack with thermocouples 70

Fig. 75: Thermograph image of the foot end of the stack after positioning of heavy plate No. 6 on top the first layer of thermocouples..... 70

Fig. 76: Thermograph image of the completed stack from the same angle of view as in Fig. 72..... 71

Fig. 77: Thermograph image of the long side of the completed stack 71

Fig. 78: Measured temperature vs. time (Ch 4, middle of the stack) 71

Fig. 79: Example of plate temperature measurement after mill 72

Fig. 80: Example of plate temperature measurement after mill when there are big skidmarks in the plate 72

Fig. 81: Example of plate temperature measurement after mill when there is no skidmarks in the plate73

Fig. 82: Longitudinal temperature profile of 15 mm plate cooled with laminar cooling system 74

Fig. 83: Thermal camera picture of 15 mm plate cooled with laminar cooling system (same plate)..... 74

Fig. 84:15 mm plate after cooling and hot levelling Transversal flatness avg 1,8 mm/m Longitudinal flatness avg 1,7 mm/m..... 74

Fig. 85: Another 15 mm plate after cooling and hot levelling Transversal flatness avg 2,3 mm/m Longitudinal flatness avg 1,9 mm/m 75

Fig. 86: Main menu of the user interface 76

Fig. 87: Data input section for the quenching part 76

Fig. 88: Presentation of results calculated with Steeltemp. 77

Fig. 89: Temperature field (top) and the temperature gradient (bottom) 82

Fig. 90:Temperature field (top) and the temperature gradient (bottom) 82

Fig. 91: Temperature field (top) and the temperature gradient (bottom) 83

Fig. 92: Temperature field (top) and the temperature gradient (bottom) 83

Fig. 93: User Interface of the cooling simulation module..... 84

Fig. 94: Model with locked displacements (left) and close-up showing element-structure (right)..... 85

Fig. 95: Heat exchange coefficient as applied in the analysis..... 86

Fig. 96: Metallurgical diagram derived from the CCT-diagram for steel grade 18CD4 86

Fig. 97: Temperature in the cross-section of the plate after 5,5sec and 22sec respectively (upper left corner) 87

Fig. 98: Bainite content after 5,5sec and 22sec respectively..... 87

Fig. 99: Martensite content after 5,5sec and 22sec respectively 88

Fig. 100: Displacement in thickness direction after 5,5 sec and 22 sec respectively 88

Fig. 101: Stress in the x-direction (lengthwise) after 5,5sec and 22sec respectively Stresses with positive sign are tensile. 89

Fig. 102: Pilot leveller with rolls arranged in the ‘tilting nest’ configuration 91

Fig. 103: Rearrangement of pilot leveller rolls to simulate conditions in a parallel-nested leveller equipped with an exit breast roll. 91

Fig. 104: Position transducers monitoring deflection of rolls under load 91

Fig. 105: Measurement of plate bow 92

Fig. 106: Path of plate (sample 'SH20') through leveller, with 9 roll contact points indicated 92

Fig. 107: Hot levelling machine at Ruukki heavy plate mill 95

Fig. 108: Left side of leveller with laser unit mounted on the upper frame and the reflecting surface on the lower frame 95

Fig. 109: Deflection at the entry- and exit side of the leveller 96

Fig. 110: Hot levelling trials: 3-roll levelling (left) and 5-roll levelling (right). 96

Fig. 111: Design of tools for hot bending trials. The left tool is moving vertically and the right tool is fixed 97

Fig. 112: Hot bending trials in the pilot-plant forging press at MEFOS 98

Fig. 113: Forces and bending moments acting on a plate during levelling [Force F_i exerted on plate by work roll i, at contact points (X_i,Y_i). Breast roll acts as an additional roll if plate significantly turned up at exit] 99

Fig. 114: Spreadsheet-based user interface for analytical levelling model 100

Fig. 115: External moment Mout due to unsupported length of beam downstream of leveller 100

Fig. 116: Contact conditions between plate and top/bottom rolls [R_{exp}=’Expanded roll radius’ = roll radius + 0.5*plate gauge] 101

Fig. 117: Initial estimation of plate path through 9-roll leveller. 102

Fig. 118: Evaluation of work done to plate by calculation of area traced out by bending moment-curvature graph during successive bending triangles 104

Fig. 119: Reduction in plate longbow using exit breast roll 105

Fig. 120: Isotropic hardening rule, uniaxial test 108

Fig. 121: Combined hardening model - uniaxial tension 108

Fig. 122: Application of the Chaboche model. Cyclic hardening under multiple cyclic loading (left) and Bauschinger effect (right) 109

Fig. 123: FE-simulations 3-roll bending. 850 °C 109

Fig. 124: Results from FE-simulation of 5-roll bending. Isotropic material model. Temperature 850 °C 110

Fig. 125: Results from FE-simulation of 5-roll bending. Yield criterion according to Chaboche. Temperature 850 °C 110

Fig. 126: Single bending model of trial No 4 (left) and when reverse bending was applied in trial No 5 (right) 111

Fig. 127: Calculated plastic strain for the second bend 111

Fig. 128: Flow stress curve used in the simulations 112

Fig. 129: Hot plate leveller at Ruukki. Definitions of cradle and gap settings 112

Fig. 130: FE-Model of the Ruukki leveller. Ten solid brick elements over the plate thickness 113

Fig. 131: Stress in the longitudinal direction 113
Fig. 132: Stress distribution through the plate thickness 113
Fig. 133: Development of effective plastic strain during levelling 114
Fig. 134: Strain distribution through the plate thickness at different positions during levelling 114
Fig. 135: Distribution of accumulated plastic strains for different cradle settings. Plate thickness 20.2 mm 115
Fig. 136: Strain history for all elements cross the plate thickness as the plate passes through the leveller 115
Fig. 137: Maximum total strain reached in each bend for different cradle settings for elements on the top and bottom surface in the plate 116
Fig. 138: Calculated lengthwise strain in each bend for different gap settings 116
Fig. 139: Calculated stress in each bend for different gap settings 117
Fig. 140: Calculated curvature after the leveller for different gap settings 118
Fig. 141: Plate shape for the increased deformation of 3 mm 119
Fig. 142: Comparison of the final stress distribution with different models 119
Fig. 143: Influence on plastic strain a variation in E-modulus 119
Fig. 144: Calculated strain of top and bottom surface in each bend for different values of E- modulus 120
Fig. 145: Comparison of measured and predicted plate trajectory within pilot leveller, for sample 'ADR42' (gauge 3 mm, grade S355) 121
Fig. 146: Comparison of measured and predicted displacement of roll/plate contact points from roll centre positions, for sample 'ADR42' (gauge 3 mm, grade S355) 121
Fig. 147: Comparison of measured and predicted plate curvatures at roll positions, for sample 'ADR42' (gauge 3 mm, grade S355) 122
Fig. 148: FE model of roller levelling , for sample 'ADR42' (gauge 3 mm, grade S355) 122
Fig. 149: Comparison of measured and predicted plate curvatures at roll positions, for sample 'SH20' (gauge 3 mm, grade S275) 123
Fig. 150: Comparison of plate exit longbow measured during pilot leveller trials with corresponding 1st & 2nd order analytical model predictions 124
Fig. 151: Measured and predicted variation of exit longbow with breast roll offset 124
Fig. 152: The configuration of work rolls fixed in upper and lower nests of a tilting nest roller leveller 125
Fig. 153: Variation of fraction thickness of plate yielded through a nine-roll tilting nest leveller 126
Fig. 154: Symmetrical bending of plate in a work roll triangle 127
Fig. 155: The effect of pre-existing plate bow on output plate flatness (14 mm gauge, 500 N/mm^2 yield) 127
Fig. 156: Variation of output plate bow with change in plate gauge (8 mm, 300 N/mm^2) 128
Fig. 157: Variation of fraction thickness of plate yielded at work rolls #6, #7 and #8 with plate gauge (8 mm, 300 N/mm^2) 128
Fig. 158: Effect of changing plate gauge from the base case value on output plate bow 129
Fig. 159: Variation of output plate bow with work roll exit gap 130
Fig. 160: Through thickness residual stress patterns for a nine-roll conventional tilting nest leveller and a leveller with independently adjustable work rolls 131

Fig. 161: Hot plate leveller at Ruukki, Definition of gap settings 132
Fig. 162: FE-model of the hot-leveller where the incoming plate has a flatness defect (edge waviness) 133
Fig. 163: Trial no. 1. Effective plastic strain after levelling 135
Fig. 164: Trial no. 1. Longitudinal plastic strain at the mid-surface after levelling. 135
Fig. 165: Trial no. 2. Effective plastic strain after levelling. Half-symmetry. 136
Fig. 166: Trial no. 2. Longitudinal plastic strain at the mid-surface after levelling. Half-symmetry 136
Fig. 167: Adjustments of the hot leveller 137
Fig. 168: Control panel of the hot leveller 137
Fig. 169: Input of flatness characteristics, visually assessed by the operator 138
Fig. 170: Comparison of measured and visually assed flatness 138
Fig. 171: Comparison of measured and visually assed flatness 139
Fig. 172: Block diagram of a leveller control system 139
Fig. 173: Frequency distribution of the different process routes in the FKS HPM 140
Fig. 174: Frequency distribution of peak to peak height value of the unwindable part of flatness defects 141
Fig. 175: Frequency distribution of peak to peak height value of the non unwindable part of flatness defects 141
Fig. 176: Coefficients of an orthogonal polynomial 142
Fig. 177: Interpretation of results of a smaller sample 143
Fig. 178: Orthogonal coefficients (2^{nd} order) of the distribution of elongation 143
Fig. 179: Strategy and the data flow to optimise the rolling schedule and the hot levelling process 144
Fig. 180: Lab prototype and test plate A1
Fig. 181: Configuration of the measuring system A2
Fig. 182: Images seen by the camera and extracted from the top laser A3
Fig. 183: Dimensions of the industrial prototype A3
Fig. 184: Field of vision of the three lasers by the matrix CCD camera A4
Fig. 185: Procedures used to link the successive plate scans A4
Fig. 186: Example of a 3D plate image A5
Fig. 187: Images captured by the camera and 2D & 3D reconstruction A6
Fig. 188: Schematic installation of the measuring system A6
Fig. 189: Measuring head showing the processor (left) camera (centre) and power supply and lasers control cards (right) A7
Fig. 190: Closed measuring head installed in the mill with water jackets and water and air connections A7
Fig. 191: Image seen by the camera, in normal B/W vision A8
Fig. 192: Width measurement without (left) and with infrared filter (right) A8
Fig. 193: Green laser A8
Fig. 194: Neutral density filter wheel A9
Fig. 195: Scheme of the trial A9
Fig. 196: Components used in tests A10

Fig. 197: Effect of the angle in laser lines A10
Fig. 198: Effect of the angle in interferential filters A10
Fig. 199: Results obtained with an interferential filter with a higher centre wavelength than the laser . A11
Fig. 200: Test result: Image with the aperture opened A11
Fig. 201: Results obtained with infrared filter A12
Fig. 202: Course of the measured gray values along the centre of different samples A12
Fig. 203: Laser enclosure A13
Fig. 204: Laser operation scheme A13
Fig. 205: Comparison of width evaluation methods A14
Fig. 206: Comparison of width evaluation methods at lower plate temperature A15
Fig. 207: Detection of plate edges applying higher weights of gradients A16
Fig. 208: Detection of plate edges applying higher weights of gradients A17
Fig. 209: Detection of plate edges applying higher weights of gradients at extreme temperatures A18
Fig. 210: Simple model to calculate the coordinates z, x from u (row in the camera) A19
Fig. 211: Correlation images A19
Fig. 212: Scheme of calibration system A20
Fig. 213: Microsonic type mic+35 analogue ultrasonic transducer A20
Fig. 214: Principle of measurement using ultrasonic flatness gauge A21
Fig. 215: Schematic of USF Gauge measuring and logging arrangement A21
Fig. 216: Ultrasonic transducer carrying beam located on Scunthorpe Light Shear Line A22
Fig. 217: Detail of beam support A22
Fig. 218: Manual measurements of plate flatness using a 1 m straight edge A23
Fig. 219: Manually generated flatness map for plate number MS790 ..... A23
Fig. 220: Flatness map generated from USF gauge data for plate number MS790 ..... A24

List of References

[1] Ashton, D. A. et al: “Closed loop automatic shape and residual stress control during levelling.” ECSC contract number 7210.PA-D/339, March 2006

[2] Bogdanoff, A., Müller, U., Wolff, A., Nilsson, A. and A. Richardson, “Reduction of Shape Defects and Yield Losses by Advanced Online-Adaptation of Control Systems and New Operating Strategies in Heavy Plate Rolling Mills.” RFSR – CT – 2003 – 00039

[3] Williams A et al, ‘Scunthorpe plate mill through process flatness audit’, Research Report, Reference Source Number 144854, November 2008

[4] Ginzburg, V. B., Ballas, R.: “Flat Rolling Fundamentals.” Marcel Dekker INC., 2000.

[5] Shohet K N and Townsend N A, ‘Flatness control in plate rolling’, Journal of the Iron and Steel Institute, October 1971

[6] Somers, R. R., et al, “Verification and Application of a Model for Predicting Hot Strip Profile, Crown and Flatness,” AISE Year Book, 1984, pp. 441-450.

[7] Beaverstock R, Carey H, Martin I, Parker S, Richardson A, ‘Modelling of processing and finalproperties of reversing mill plate’, Steel Rolling Conference, Paris, 19-21 June 2006

[8] Ryalls S, ‘Setting up the prototype ultrasonic flatness gauge’, Short Note, Reference Source Number 134919, January 2008

[9] Irastorza L, Giusti J, Eberwein K, and Kirsch H-J: Metec Congress 94, Proceedings of 6th International Rolling Conference, Dusseldorf 20-22 June 1994, Vol. 2, pp106-110, “Modelization of flatness evolution during cooling and levelling of plates as a base for production design.”

[10] Leden, B: “STEELTEMP - A program for temperature analysis in steel plants”,Scandinavian Journal of Metallurgy, 15 (1986), pp. 215-223.

[11] Nilsson A.: “FE-simulation of the hot flattening process.” MEFOS-report 2007.

[12] MSC.Marc Volume A “Theory and user information”.

[13] Chaboche, J.L.: “Constitutive Equations for Cyclic Plasticity and Cyclic Viscoplasticity”, International Journal of Plasticity, Vol.5, pp. 247-302, 1989.

[14] Smith B E, Abbott C W, & Pooni B S, "Studies of straightening and levelling operations for plate and section products", EUR 10711 EN, 1987

[15] Beveridge D R, Henderson S, Neuschuetz E, Muecke G. and Pera J-O, "Optimisation of plate and strip processing to meet high customer demands", EUR 20211 EN, 2002

[16] Beveridge D, Henderson S, et al, “The theory and practice of coil plate levelling – recent experience”, Corus RD&T Internal Report 116587, 2001

[17] Toose E M, “TRL: Tension and Roller Levelling Model”, Corus Internal Report No. 105881, 2001

[18] Morley A, “Strength of materials”, 11th Edition, Longmans, Green and Co., 1954.

[19] Batty F A and Lawson K T, “Heavy plate levellers”, Journal of the Iron and Steel Institute, November 1965, pp1115-1128

[20] Beveridge D R, “Discussion of the calculation of torques during roller levelling”, Corus RD&T Internal Report 117659, 2000

[21] Wang N, “Preliminary findings using an Analytical Tension Levelling Model”, Corus RD&T Internal Report 118120, 1998

[22] Owen D R J and Hinton E, “Finite elements in plasticity: theory and practice”, Pineridge Press Limited, Swansea, UK, 1980

[23] Misaka Y and Masui T, “Shape correction of steel strip by tension leveller”, Transactions ISIJ, Vol. 18, 1978, pp475-484

[24] Smith R P, “Modeling plastic strain during cold leveling of steel plates”, Proceedings of the Annual Convention and Iron & Steel Exposition, Ohio, 27th September 1999, AISE Pittsburgh PA.

[25] Bourgon J-Y, Guillard O, Guillardeau B, Eberwein K and Bouillot M: Metec Congress 94, Proceedings of 6th International Rolling Conference, Düsseldorf 20-22 June 1994, Vol. 2, pp112-119, “Modeling of leveling process and applications to heavy plate mills and strip finishing mills”

[26] Jelali, M., Müller, U., Wolff, A. a. W. Ungerer: “Advanced control strategies for rolling mills.”, MPT International 3/2001.

[27] Jelali, M., Müller, U., Wolff, A., Ungerer, W. and G. Thiemann: “Advanced measurement and flatness control for hot strip mills.”, ATS International Steelmaking Conference, Paris, December 2001.

Appendices

Development, construction and installation in the plate mill of a new measuring system based on artificial vision for plate shape, flatness and turn up/down of the head end

A new measuring system has been developed by integrating existing knowledge of ArcelorMittal Spain gained from developing previous measuring systems, specially width measuring gages, strip head end shape determination and camber. Hardware foreseen was the use of a single CCD camera with a double array, one matrix and another lineal. This camera has different regions of interest (ROI) defined at the matrix CCD with intrinsic triangulation functionality. Three laser lines would be projected on the plate for triangulation purposes. A commercial PC mini ITX type would be used to run the system software.

Techniques foreseen for the development of the system were triangulation (for flatness and sky end effect) and artificial vision (for width, camber and rectangularity). The measuring system was installed at the exit of the hot leveller to measure flatness, width, length, camber and ski effect under real operating conditions.

The construction of the system started with a prototype that was tested in lab conditions where different processing algorithms were developed, **Fig. 180**. The most difficult task was to design an accurate processing application that avoids the random jumps of the plate in the rolling mill.

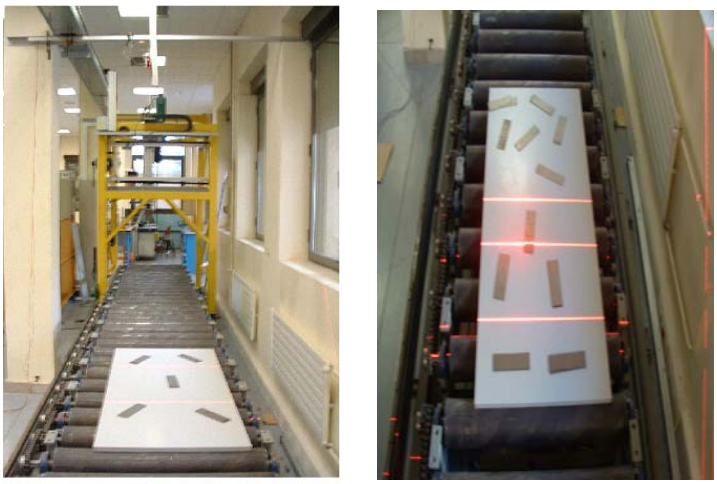


Fig. 180: Lab prototype and test plate

After validation of the reliability of the device, the next task was to design a robust enclosure that resists the hostile environment of the HPM using compressed air and a water circuit for cooling down the system. Another difficulty was to determinate the most appropriate light for the lasers due to the self-radiation of the hot plates that overlap the laser light. Because of this fact different trial were done with different lighting configurations. And finally to obtain the measurement results a suitable calibration was required using very sophisticate algorithms.

The camera used is an IVP-RANGER with a double CCD array, one matrix and another linear. The matrix array has an interference filter in order to see only the lasers, thus it will be used for measuring flatness, front edge bending and camber. The linear array will be used for width and front end rectangularity measurement.

The hardware of the multi-measuring system consists of the following components:

- A CCD double array camera IVP-Ranger C55 3D Multiscan 1536x512 + 3072x1 pixels, with appropriated optics (Pentax 12.5mm, F1.4) and accessories,
- Three laser markers that will generate three parallel lines on the plate,
- A image acquisition card Coreco X64-CL Express 85MHz, 32MB RAM, double channel,

- A PC Mini ITX Commell, mother board LV 673 with PCI Express, processor Intel Pentium M750, 1.86 GHz, 533 Mhz FSB, 512 MB RAM DDR2 533 Mhz, HD 120 GB, appropriate for rack mounting and

- A monitor TFT 17".

A preliminary and very rudimentary laboratory prototype was installed to gain knowledge about the performances of the camera and suitability for this use. **Fig. 181** and **Fig. 182** show this preliminary installation and an example of how the camera sees the small pieces placed on the plate and information extracted from the top laser.

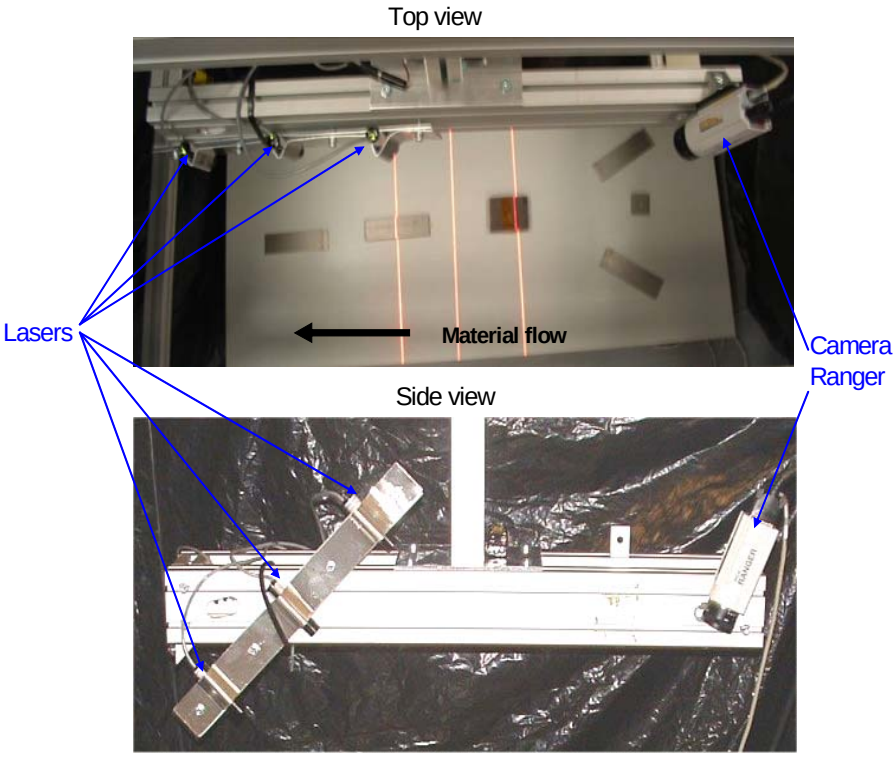


Fig. 181: Configuration of the measuring system

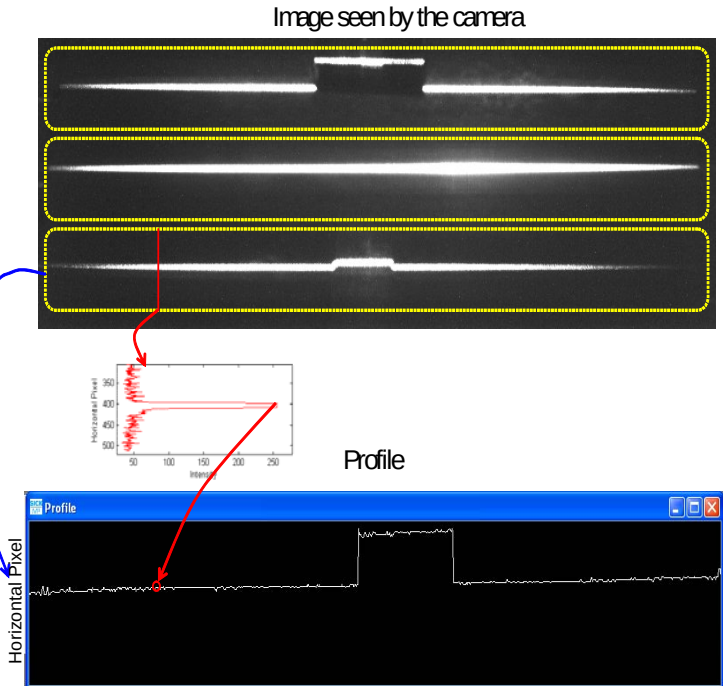


Fig. 182: Images seen by the camera and extracted from the top laser

After this preliminary test a laboratory the prototype was designed and installed in lab for developing and testing the system under conditions similar to the final installation in the HPM. The first task was to define the location of the system in the mill and the dimensions, length of plate to be seen, height of the system over the plate, etc. The defined dimensions are shown in **Fig. 183**.

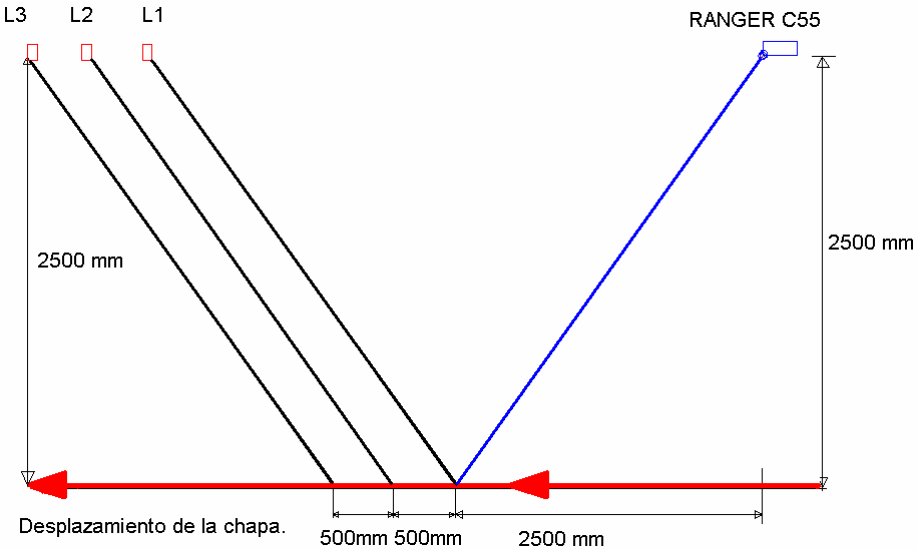


Fig. 183: Dimensions of the industrial prototype

According to those dimensions, a lab prototype was installed, **Fig. 180**.

Calculations were made to determine the range of view of the three lasers in the three regions of interest (ROI) of the camera as a function of the plate height. Results showed that laser L3 will be seen between lines 0-200, laser two between lines 210-380 and laser one between lines 400-512. If plate height exceeds 210 mm the image of laser L1 will be lost and if it reaches 250 mm laser L3 will be seen in the zone of laser L2 and laser L2 in the zone of laser L3. That means that the maximum admissible plate height will be 200 mm, which was considered enough for this application. **Fig. 184** shows graphically these results.

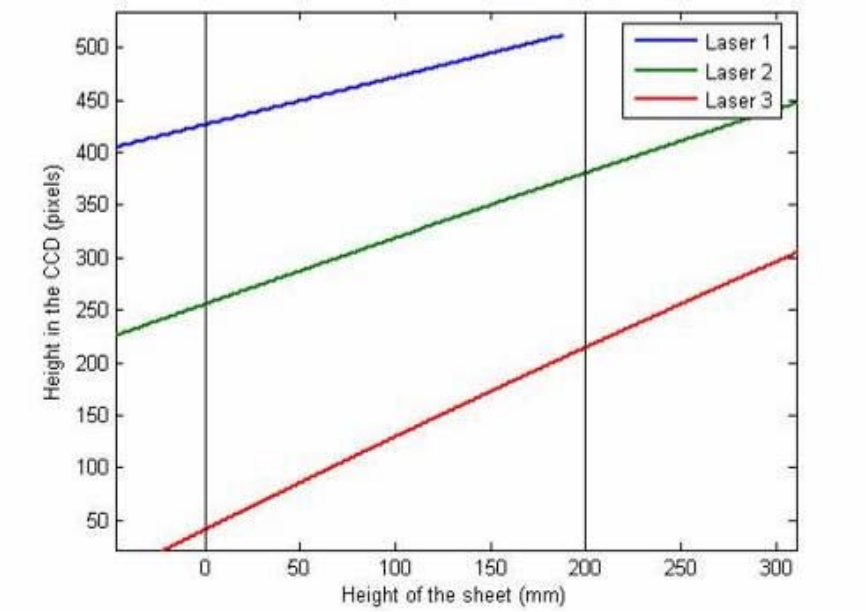


Fig. 184: Field of vision of the three lasers by the matrix CCD camera

Other steps of development were the adaptation of filters appropriate to eliminate noise in the images, the elimination of trending in the images of the lines (caused by the effect of the angle of the camera respect the horizontal that makes that the laser lines appear as no parallel), the elimination of the effect of the perspective that makes that lines closer to the camera to be seen larger, and the calibration of the relationship pixels to millimetres.

The plate is continuously scanned by the camera as it passes under the laser markers. Link of the samples done by the CCD matrix is done by means of two procedures represented in **Fig. 185**, one is considering that the angle defined by the tree lasers on the plate do not change as the plate moves, and the other considering that the relative plate heights defined by the lasers do not change as the plate moves.

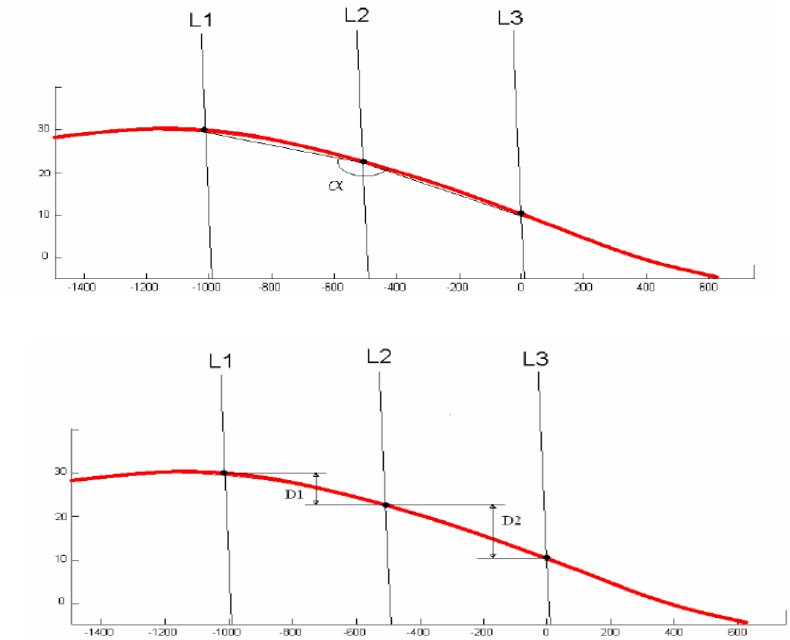


Fig. 185: Procedures used to link the successive plate scans

For each plate, passing under the measuring system, a complete scan, full length and width, is taken by the measuring system. The software generates a virtual 3D-image of the plate shape in the memory of the system. This image is correctly calibrated to represent the real shape of the plate. Later, the measuring software modules apply different criteria to extract the required information according to standard quality

rules (as an example, use of rulers of one and/or two meters to measure the flatness). **Fig. 186** is a representation of the type of image obtained.

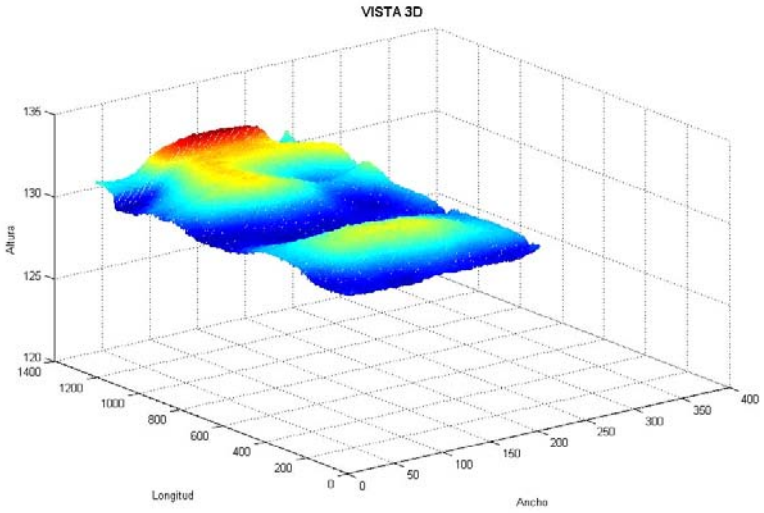


Fig. 186: Example of a 3D plate image

The software for image data capture, data extraction and generation 3D-images was developed. The process followed is:

- Light of the lasers on the plate is captured by the three ROI's of the CCD camera,
- Signals are filtered for suppression of noise,
- Pixel information are converted into metric information by using the calibration values,
- Measurements by the three ROI's of the CCD camera are integrated to an unique image,
- Real dimensions are extracted from this image and calculations of edges and flatness are done.

Fig. 187 shows a graphical example as how the software works when inspecting a real flat plate with some artificial irregularities created by means of several objects of different dimensions on it. The upper three images show the view of each ROI of the camera when the plate passes under the system. The colour code used gives an idea of their height. The fourth image shows a 2D reconstruction of the plate by integration of the three previous images and using the same colour code. Finally the bottom image gives the 3D reconstruction of the complete object.

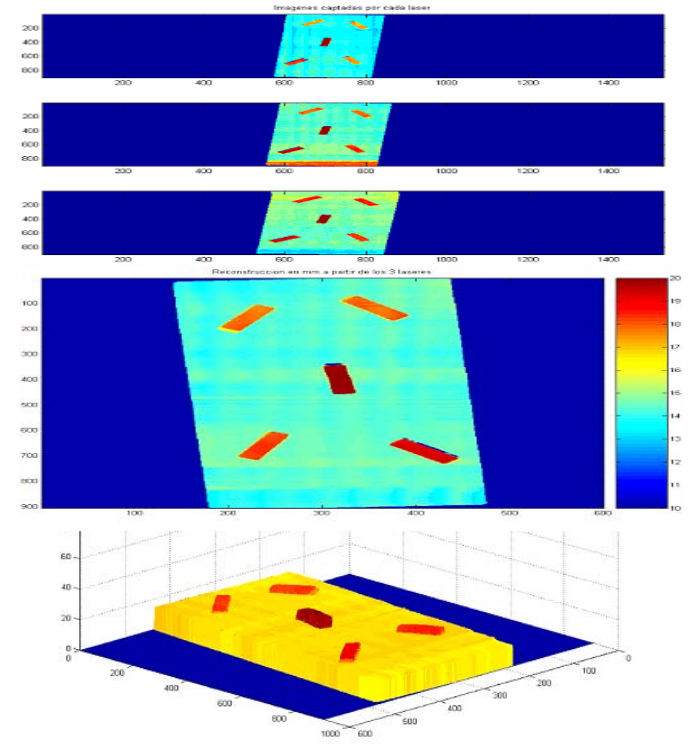


Fig. 187: Images captured by the camera and 2D & 3D reconstruction

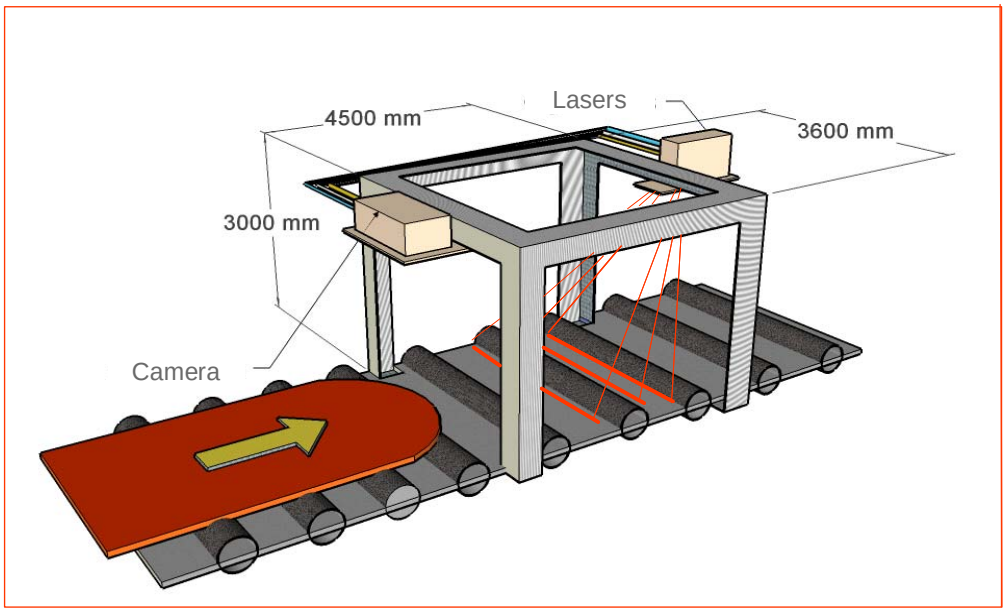


Fig. 188: Schematic installation of the measuring system

After certification of the reliability of the solution in the lab, the final installation in the plant started. The first task was to design a robust mechanical structure to support the measurement system without vibrations and being aware of the hostile environment of the factory with high levels of temperature and dirtiness. To meet this requirements a compressed air and water system was implemented to cool down the device.

The two modules, the Ranger camera and the three laser markers, were installed on a mechanical structure over the plate mill at the exit of the hot leveller. **Fig. 188** is a schematic representation of the installation done and distances between different components.

The measuring head containing the camera and the pre-processor was installed in a metallic box with water jackets attached around and pressurized air to keep clean the optics. **Fig. 189** and **Fig. 190** show the inside of the box and the box with the water jackets and heat shielding.

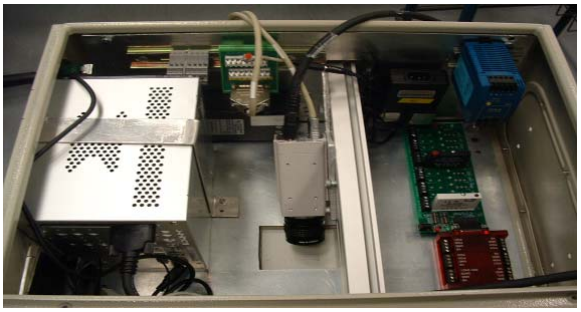


Fig. 189: Measuring head showing the processor (left) camera (centre) and power supply and lasers control cards (right)



Fig. 190: Closed measuring head installed in the mill with water jackets and water and air connections

The measuring system receives analogue signals of plate speed from the mill drive automation (used for linking the images) and hot plate presence next to the measuring system (used for turning ON the lasers when the plate approaches in order to increase the lasers life and also for safety reasons). Additionally, the system is interfaced by Ethernet TCP/IP to the process automation to receive plate identification and other characteristics and send results of the measurements.

After the system was calibrated in the mill a problem arose when trying to measure the hot plate: the infrared filter installed to reduce the amount of IR light received by the camera attenuated also the laser lines seen by the camera on the plate and this caused that most of the measurements were incorrect. This is due to the low power of the lasers (100 mW) selected to make them harmless for people. Same lasers are being used without visibility problems in other applications for hot strip in the hot strip mill for narrower material but here the material width is twice larger and this decreases the intensity of the laser lines. **Fig. 191** is an example in normal B/W vision of the camera, where the three laser marks of 660 nm and 100 mW cannot be seen, the aperture of the optics was near its minimum opening trying to avoid the saturation of the image and the sampling time 1 ms.

Fig. 192 shows the signals of the width measuring software that uses the infrared radiation emitted by the plate, at the left side the signal without application of a filter and at the right with application of a filter, where the plate edges are not detected.

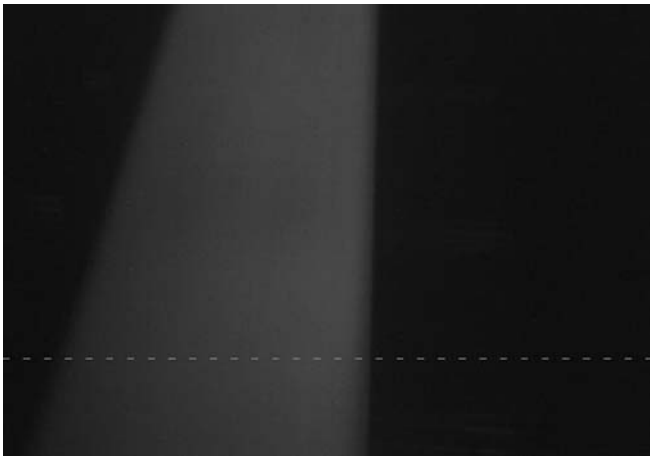


Fig. 191: Image seen by the camera, in normal B/W vision

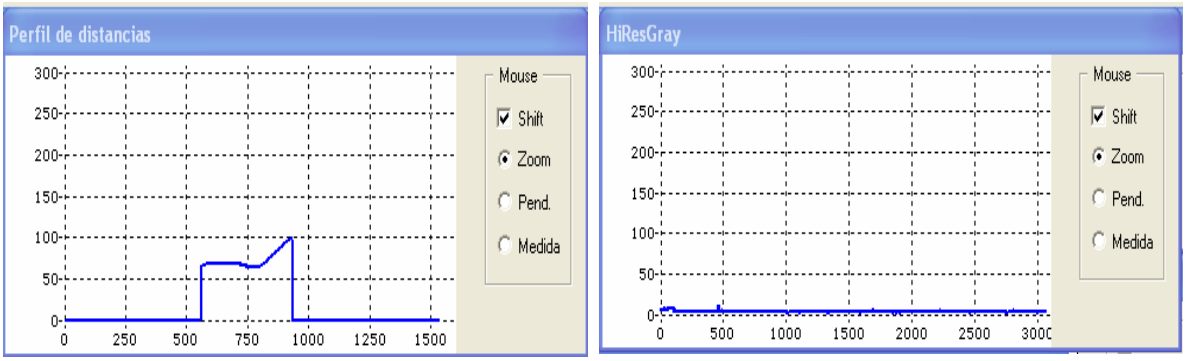


Fig. 192: Width measurement without (left) and with infrared filter (right)

Several tests were done to overcome these problems. Two lasers, one of red light and 500 mW power and another of green light and 1 W power, were applied. In consideration of the fact that this laser power is harmful for people, different attenuation filters were also tested on site to determine the minimum power required to gain better results. Next these tests are explained.

Illumination:

For these tests, a green laser LaserGlow 532 nm 1000 mW (**Fig. 193**) and a neutral density filter wheel Thorlabs NDC-100S-4M (**Fig. 194**) have been purchased.



Fig. 193: Green laser



Fig. 194: Neutral density filter wheel

Because the potential danger of a laser of this characteristic in direct or reflected contact (it is a IV category laser), the first objective was to determinate the minimum work power to distinguish the laser line in work conditions. This test (**Fig. 195**) consisted in modifying the position of the filter wheel, so that the optic density that the laser was crossing, was different and therefore also the output power.

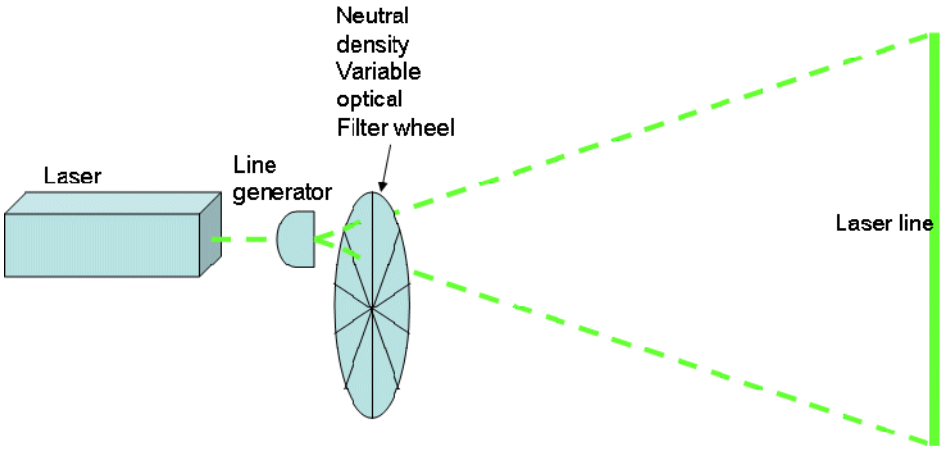


Fig. 195: Scheme of the trial

Table 25 shows the attenuation produced by the filter wheel.

Table 25: Attenuation table of the filter wheel

Position	Optic Density (OD)	% transmission $T = 10^{-OD}$
0	0.04	91.2
1	0.1	79.4
2	0.2	63.1
3	0.3	50.1
4	0.4	39.8
5	0.5	31.6
6	0.6	25.1
7	1.0	10.0
8	2.0	1.0
9	3.0	0.1

All the components were assembled in a box with heat protection, **Fig. 196**.

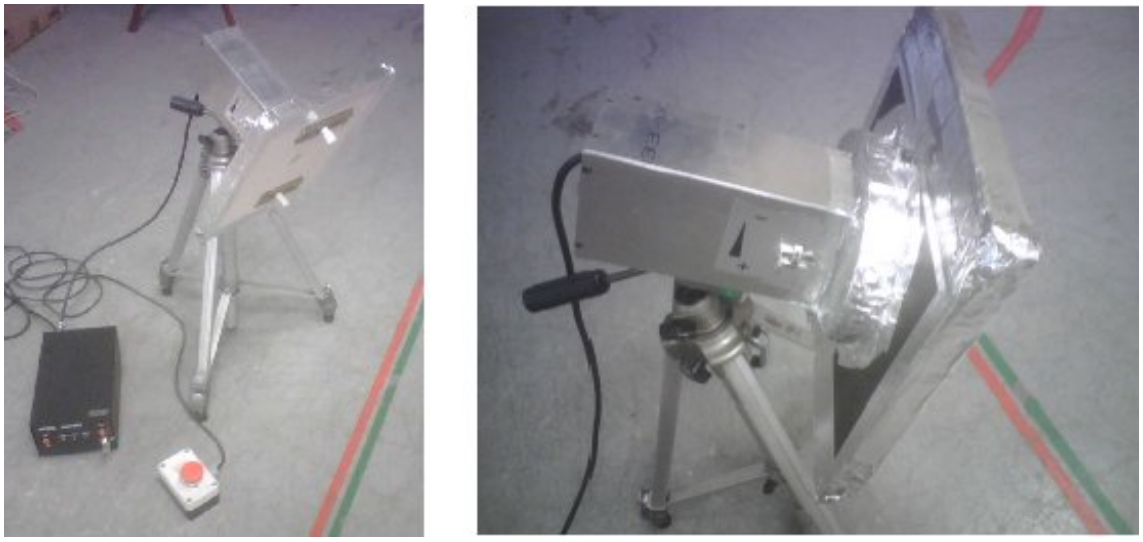


Fig. 196: Components used in tests

Visualization:

To emphasize the laser from the background, it an interferential filter of 542 nm FWHM 27 nm has been used in front of the camera, that should only permit to pass the wavelength of the laser.

The wavelength of the filter is a little bit higher than the wavelength of the laser in order to obtain a greater uniformity, below this phenomenon is explained more in detail. If a laser line is observed with a camera aligned with the laser, the centre of the line is observed with an angle of 0º and the extremes with a greater angle, obtaining a weaker in the sensor. This fact is represented in **Fig. 197**.

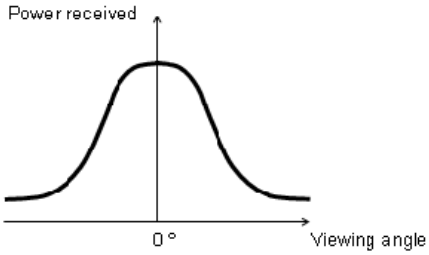


Fig. 197: Effect of the angle in laser lines

Interferential filter is also affected by the viewing angle, being its cut-off wavelength (λ) lower when the angle is greater. When λ moves away from laser wavelength, the percentage of light, that passes the filter, decreases, therefore if the filter cut-off wavelength were the same of the laser wavelength, the signal in the extremes would be lower because the angle, **Fig. 198**.

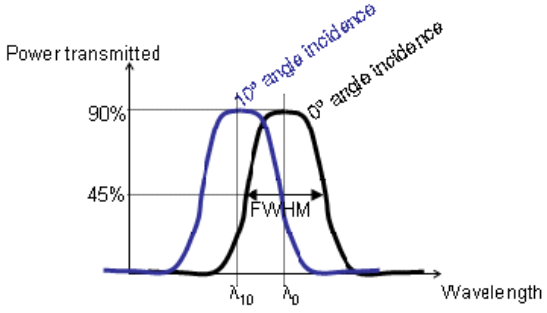


Fig. 198: Effect of the angle in interferential filters

The application of a filter with the same centre wavelength as the laser and the decrease of power due to the angle causes, if the camera is aligned with the laser, that the centre would be very bright (camera saturation) and the extremes would not be well observed. This would produce a loss of information.

Using an interferential filter with a higher centre wavelength than the laser (542 nm of the filter and 532 nm of the laser) a lower light transmission at 0º and higher in the extremes will be obtained. The result will be a more uniform line. **Fig. 199** show the results obtained with this configuration. The great uniformity achieved with previous method can be observed.

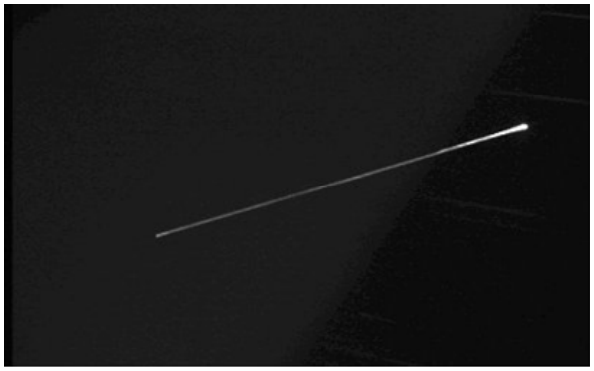
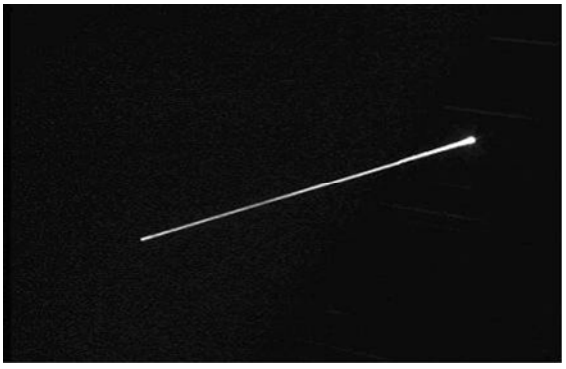
Filter position nº7 (10% transmission, output power 100mW) Camera aperture: F#18 (closed)	Filter position nº5 (31% transmission, output power 310mW) Camera aperture: F#18 (closed) (plate colder)
	

Fig. 199: Results obtained with an interferential filter with a higher centre wavelength than the laser

In these cases aperture needs to be closed in order to avoid the saturation produced to the infrared emissivity of the heat plate. In **Fig. 200** it is well observed what happens if the aperture is opened.



Fig. 200: Test result: Image with the aperture opened

An infrared filter was also tested. The objective was to increase the laser light captured, opening slightly the camera aperture.

Filter position nº7 (10% transmission, output power 100mW)
Camera aperture: F#4 Infrared filter

Filter position nº5 (31% transmission, output power 310mW)
Camera aperture: F#4 Infrared filter.

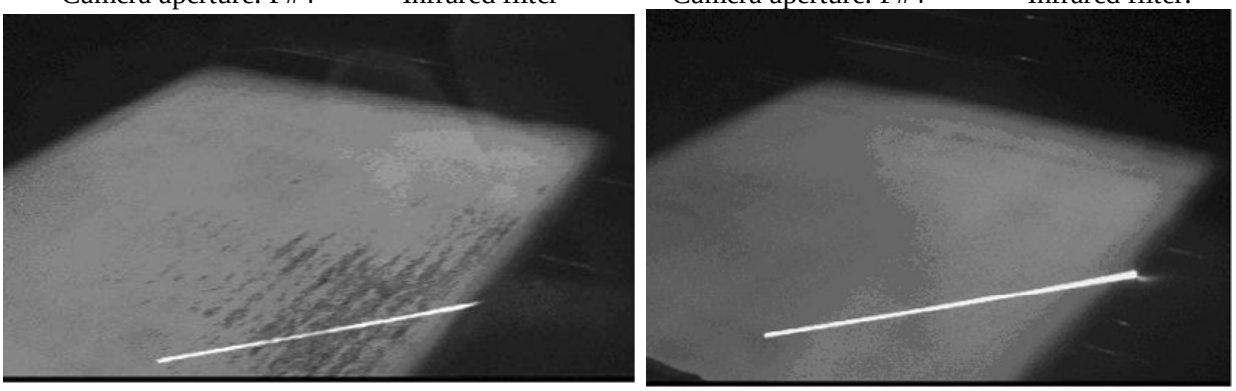


Fig. 201: Results obtained with infrared filter

To compare the results in **Fig. 202** the course of the measured gray values along the centre of different samples are shown.

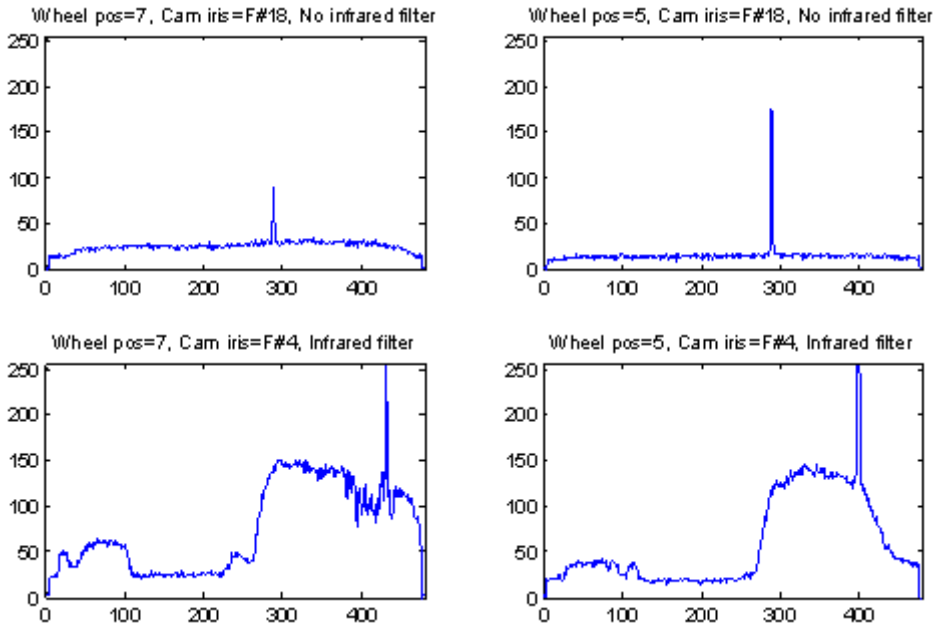


Fig. 202: Course of the measured gray values along the centre of different samples

The laser line is perfectly seen in all cases, with infrared filter and without it. But when the plate is cold, its limits are not well defined if infrared filter is not used. This would not permit to use the linear sensor of the camera to measure the width with double precision.

Nevertheless, using the infrared filter and opening the aperture of the camera, more luminance is acquired by the sensor and consequently, the laser and the plate are perfectly defined. This way it is possible to use properly the laser with less power. Besides, without infrared light, less heat is received by the device.

In conclusion, after these tests and taking into account the changeable conditions in the facility (distances, integration time, specular reflectivity, illumination, etc.) the best option is to use a laser of 200 mW and 532 nm (class III-b), interferential filter of 542 nm and an infrared filter.

An industrial enclosure was developed and tested for the application of a green laser, **Fig. 203**.

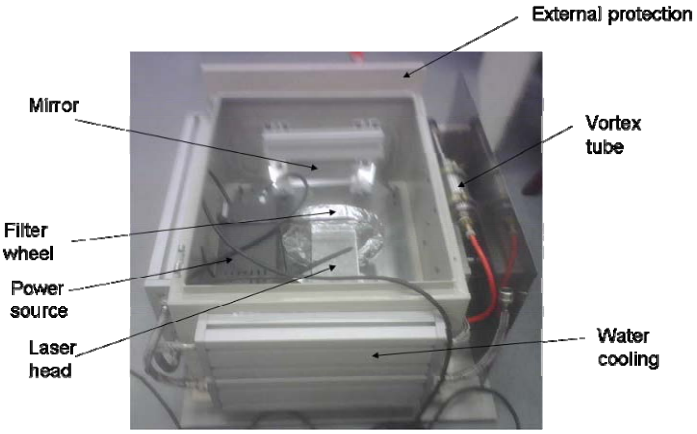


Fig. 203: Laser enclosure

An external protective shield reduces the radiation to the internal box. Two types of cooling have been provided for the box: water based cooling for the external part, and internal cold air injection by means of a Vortex tube. The system completes internally with an external infrared reflecting window and an internal infrared transmitting mirror that allows an easier setup (see **Fig. 204**).

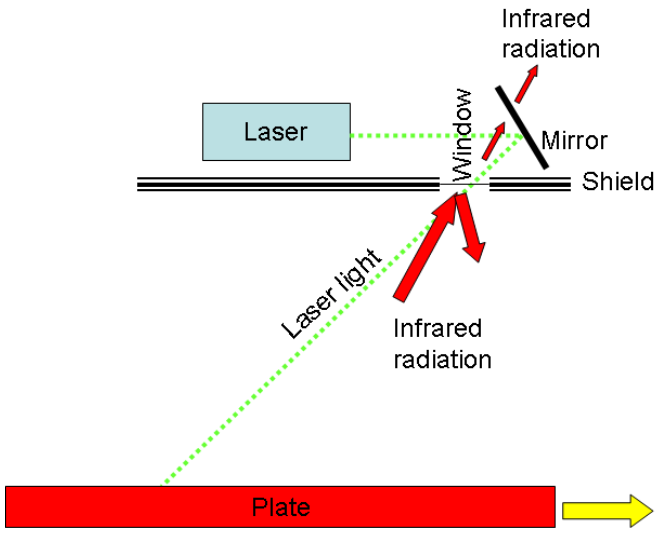
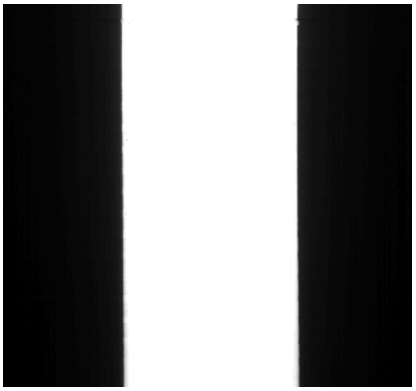


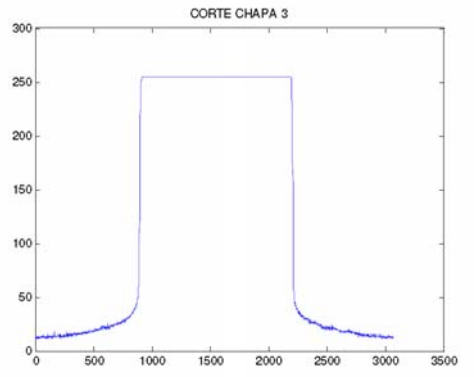
Fig. 204: Laser operation scheme

In the next step, the software tool to use the plate emissivity and the double precision CCD array of the camera to obtain the width, length and head & tail end shape was modified.

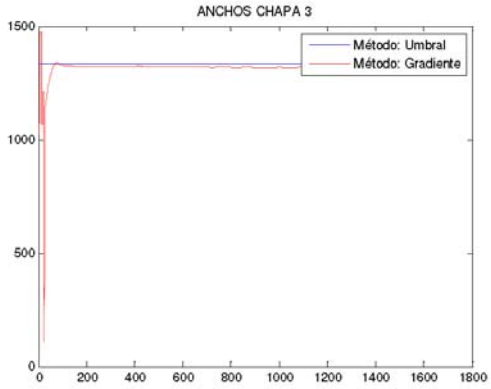
In a first approach, the gradient of the gray value course captured by the camera was calculated to obtain the edges. But since the temperature differs in each pass of the plate, the code used was modified applying a dynamic threshold to determine the position of the plate edges. In **Fig. 205** the differences between both methods are shown.



Picture capture by the camera (1600 x 3024)



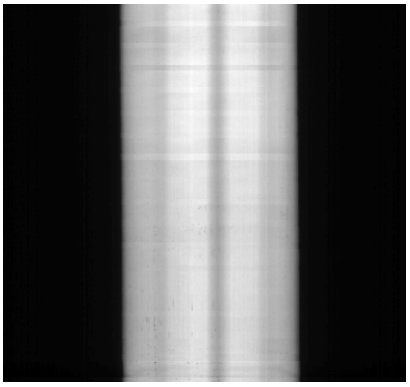
Profile of emissivity capture by the camera



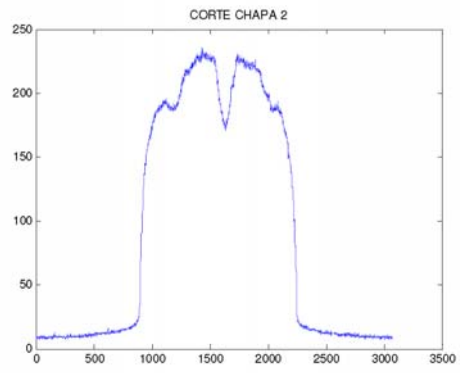
Width evaluation using both methods (gradient in red and threshold in blue)

Fig. 205: Comparison of width evaluation methods

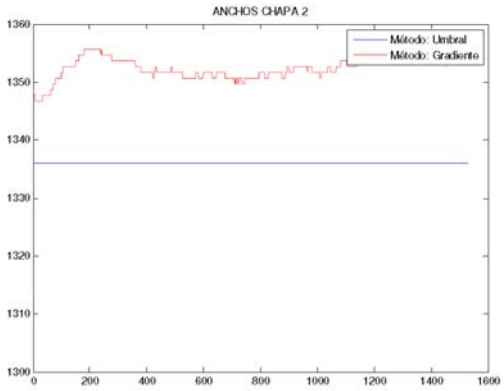
As shown in **Fig. 205**, the threshold method provides a more uniform graph corresponding with reality. When the temperature of the plate is lower, the emissivity acquired by the camera is also lower. In this case, gradient method is clearly worse than threshold method as shown in **Fig. 206**.



Picture capture by the camera (1600 x 3024)



Profile of emissivity capture by the camera



Width evaluation using both methods (gradient in red and threshold in blue)

Fig. 206: Comparison of width evaluation methods at lower plate temperature

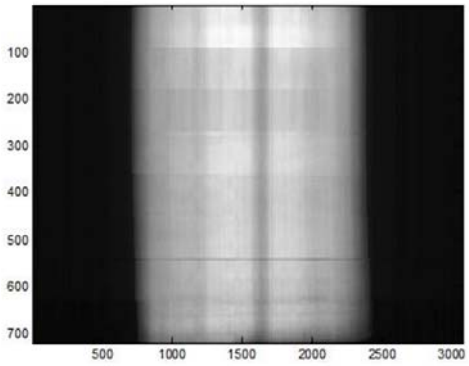
The threshold method was implemented and the software was working as expected. But these initial algorithms turned out to be too simple for the large variation of conditions that occur (different temperatures, materials and surface aspect).

Two more algorithms have been developed and tested to optimise edge detection, based on: maximum of gradient and splines. In the first case, the algorithm looks for the maximum of the gradient with several specific characteristics that have shown to improve the results:

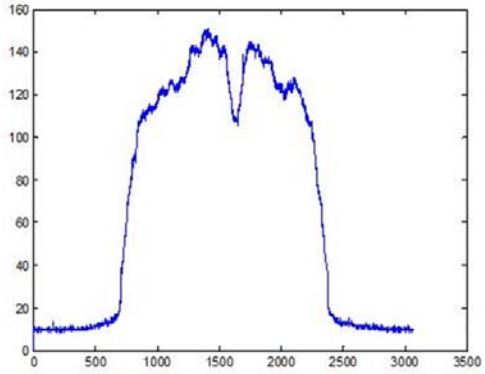
- Pre-filtering with median filter,
- Give higher weights to gradients with lower intensity values,
- Look for centre of gradient by means of seeking the maximum of the second order polynomial.

Fig. 207 and **Fig. 208** show the results obtained with these algorithms for two extreme cases: Case I / lower temperature and Case II / higher temperature.

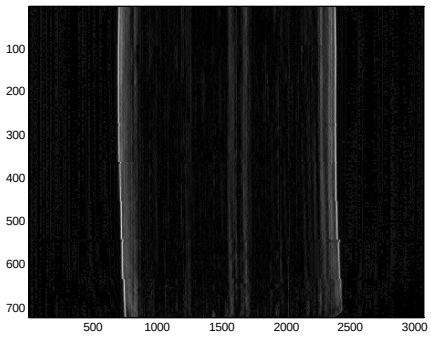
Case I:



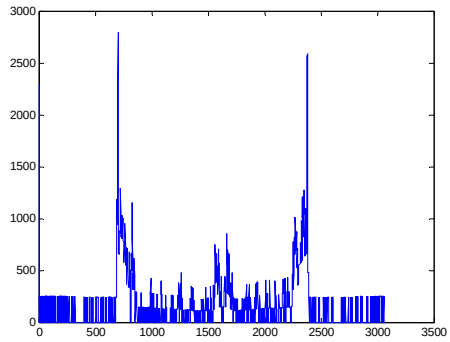
Original image



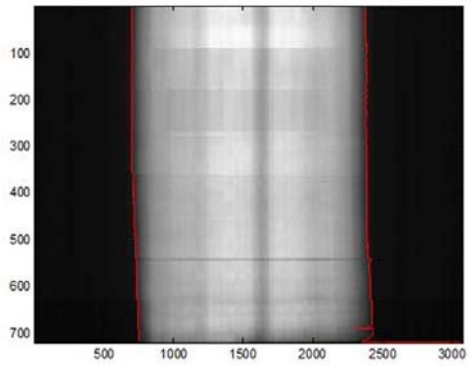
Profile of emissivity capture by the camera



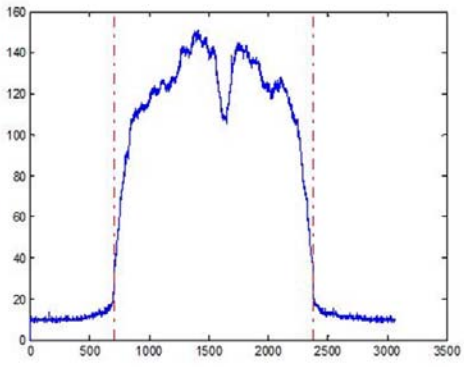
Application of higher weights to gradients



Gradient of profile of emissivity



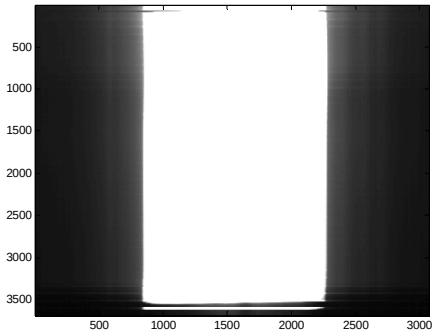
Detection of plate edges



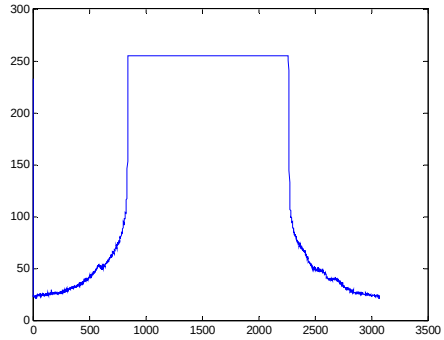
Threshold and profile of emissivity

Fig. 207: Detection of plate edges applying higher weights of gradients

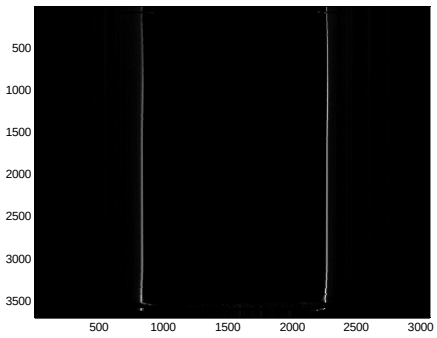
Case II:



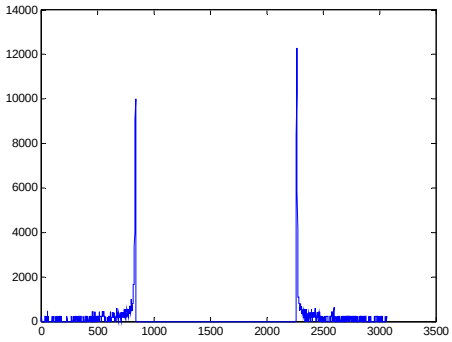
Original image



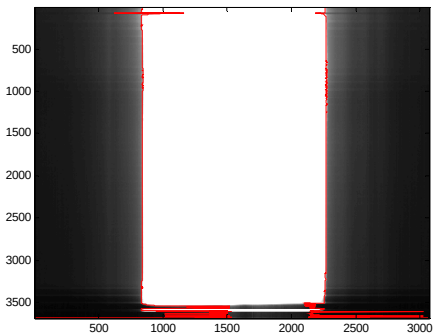
Profile of emissivity capture by the camera



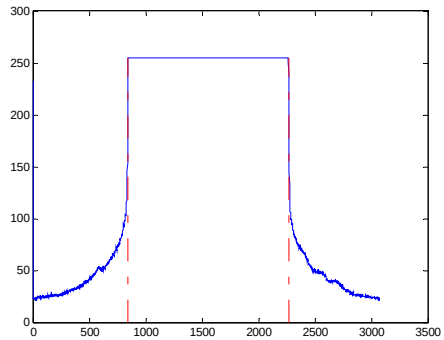
Application of higher weights to gradients



Gradient of profile of emissivity



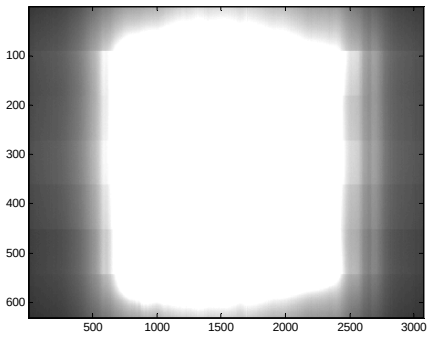
Detection of plate edges



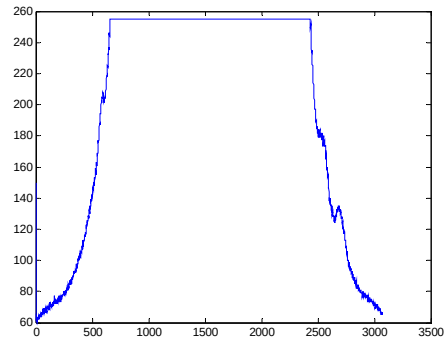
Threshold and profile of emissivity

Fig. 208: Detection of plate edges applying higher weights of gradients

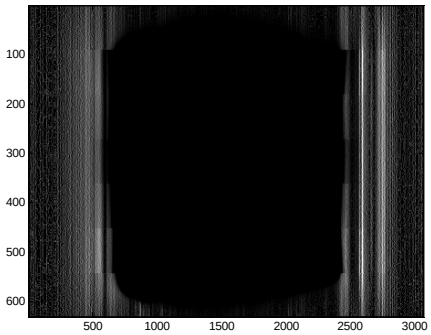
Another problem arises because of the high temperature difference between the different passes: it is not possible to use a unique integration time that is valid for all the cases (**Fig. 209**).



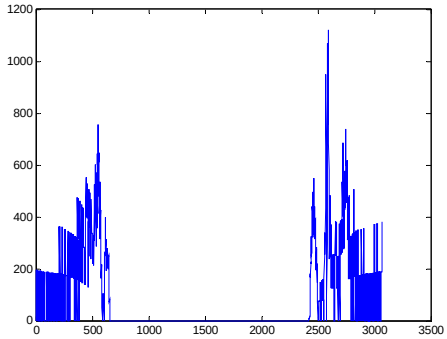
Original image



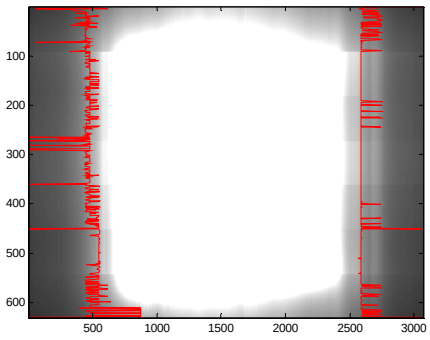
Profile of emissivity capture by the camera



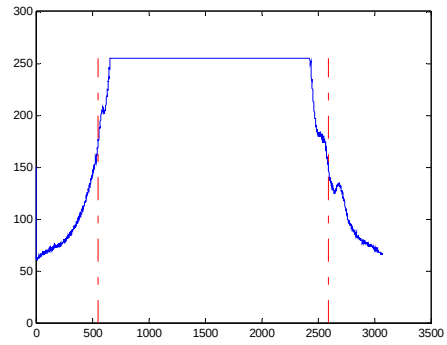
Application of higher weights to gradients



Gradient of profile of emissivity



Detection of plate edges



Threshold and profile of emissivity

Fig. 209: Detection of plate edges applying higher weights of gradients at extreme temperatures

An algorithm was developed for automatic recalculation of the integration time based on previous images. After each image is acquired, the number of saturated pixels and the trend in both sides of the image are calculated. If the number of saturated pixels exceeds a minimum threshold and the trend of the sides of the image (that should be constant dark) is high, then the integration time is reduced. If the maximum of the image is far from saturation, the integration time is incremented.

This algorithm was tested, and implemented in the final application, and the systemE is at this moment providing very accurate measurements in real time under real operating conditions.

The next task is the calibration of the system in the line. Accurate calibration of these large systems is a difficult task. Simplified models with very few parameters and known equations are generally used for calibration, so very few calibration points generate enough information to recover this small number of parameters. In these cases, the system setup is prepared by means of accurate positioning of the different elements in order to match the simplified model.

For triangulation, the simplified model implies that the laser line is perfectly parallel to the rows of the camera chip for a horizontal flat sheet (see **Fig. 210**). In this case, the model enabling to recover 3D coordinates is simple and has few parameters (α, β, xF, yF,xL). The calibration can be done using a few points.

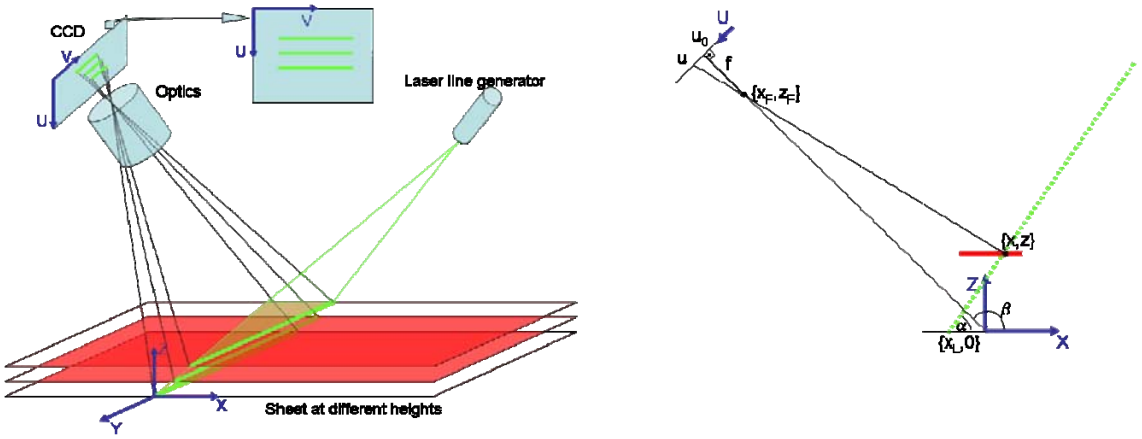


Fig. 210: Simple model to calculate the coordinates z, x from u (row in the camera)

In large systems for industrial plants, it's very difficult to realize a system with sufficient accuracy to use such a simplified model. The axis of freedom needed for alignment should be implemented with mechanical elements that do not behave robustly in case of vibrations and thermal changes.

In place of that, a robust system is preferred, even if not perfectly aligned. In that case, calibration becomes a more difficult task, as the model becomes 3D and many new parameters arise. The calibration of all these parameters becomes complex and many accurate calibration data are needed.

A different approach for the calibration of such system has been developed. In spite of having a mathematical model for which parameters are estimated through calibration, two sets of 2D data (YZ and UV) are used to provide a conversion between both grids, and interpolation based methods are used to recover YZ data given UV values. This method also includes non-linearity due to the lens aperture that is more difficult to integrate in a calibration from mathematical model. An approximation of X data is easily obtained from an estimation of angle α, **Fig. 211**.

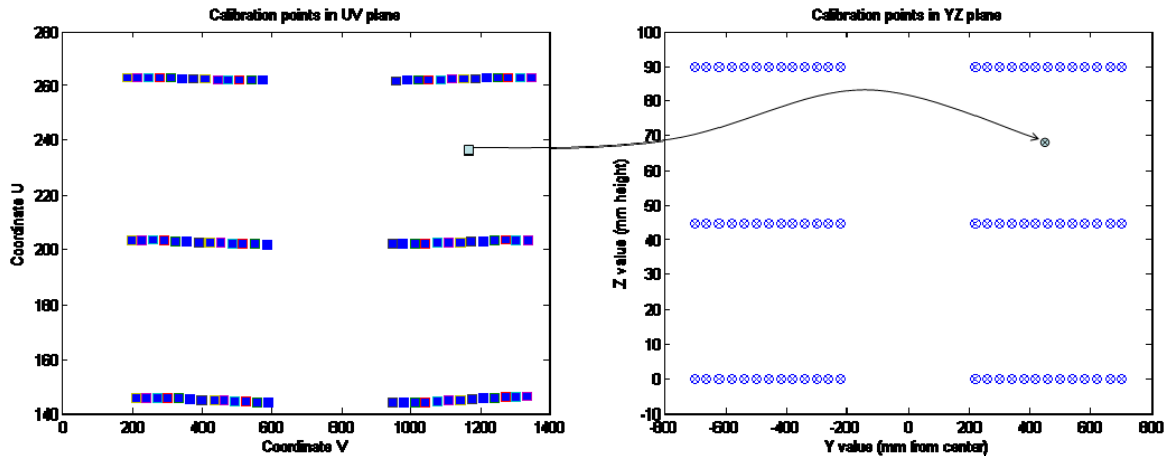


Fig. 211: Correlation images

As interpolation method, biharmonic splines have been selected as they seem to fit better regarding the nonlinearities of the system. Given the two sets of calibration points, biharmonic splines interpolation method enables to easily obtain a matrix that allows converting data from one set to the other, based on an

interpolation in which the weight of each calibration point is inversely proportional to its distance to the desired point.

Another challenge for the calibration of these large systems is the calibration setup. Usual triangulation systems are manufactured in the lab, where all the parameters can be easily tested and supposed not to change in plant conditions. Very large triangulation systems, as the one proposed, have to be installed and calibrated in the plant.

For that purpose, a calibration piece covering the full range of the product in width, and the possible heights has to be installed in the measuring zone, images have to be acquired, and the YZ and UV points have to be matched for calibration.

For this purpose, a solution based on a small and robust chariot that carries a calibration sheet has been designed and constructed (see **Fig. 212**). The scissor type elevation provides smooth and robust setup for height calibration. The chariot can be translated over a longitudinal path of any size, by means of a rack-pinion displacement mechanism. An encoder is placed in one of the articulation of the scissor to measure the height, and a potentiometer is used to measure the displacement. This displacement system is fully controlled by the computer that synchronizes the acquisition of the calibration points with the YZ position of the chariot.

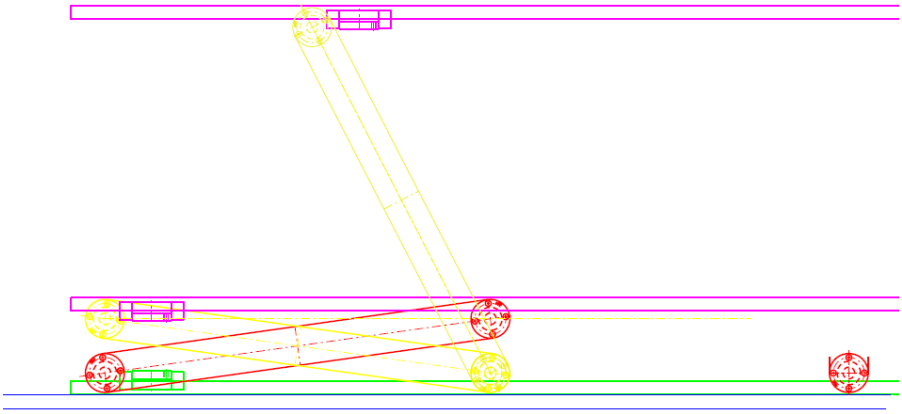


Fig. 212: Scheme of calibration system

Flatness measurement system, based upon an array of ultrasonic transducers

The prototype Ultrasonic Flatness (USF) Gauge consisted primarily of a set of eleven Microsonic analogue ultrasonic transducers (type mic+35), mounted in a carrier beam that spanned 4 m across the width of the roller table. The transducers have a nominal operating range of 60 to 350 mm and a maximum range of 600 mm. The carrier beam was clamped at a fixed height above the roller table and each of the transducers measures the distance between itself and the plate surface as it passes beneath. The transducer itself is shown in **Fig. 213** while the measuring arrangement is presented in **Fig. 214**.



Fig. 213: Microsonic type mic+35 analogue ultrasonic transducer

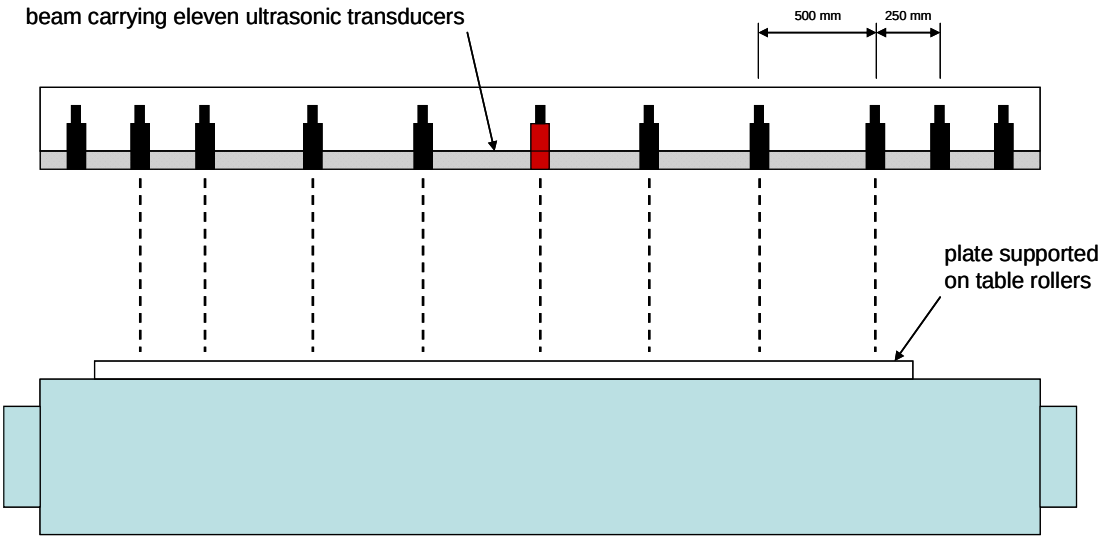


Fig. 214: Principle of measurement using ultrasonic flatness gauge

The transducers were connected to a data logger which was in turn linked to a PC located in a cabin close to the process line. An encoder was fitted to one of the roller table drives to provide plate length information and this was also connected to the data logger. The arrangement can be simply represented by **Fig. 215**.

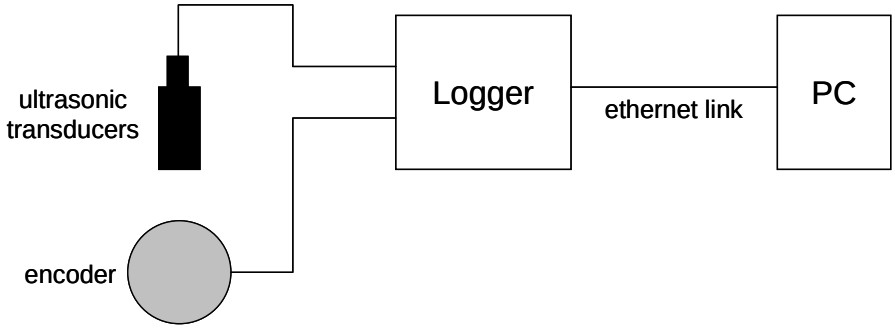


Fig. 215: Schematic of USF Gauge measuring and logging arrangement

The central transducer of the eleven (number 6 and highlighted in red in **Fig. 214**) has two outputs. It has an analogue output, similar to the other ten transducers, which carries the signal for the distance between itself and the plate surface. However, it also has a switched output, which is either on or off depending on whether or not a plate is present under the gauge. When a plate arrives under the gauge, the switched output triggers the encoder and it starts to 'count'. Once the plate has passed and it is no longer present under the gauge, the switched output from the triggering transducer turns 'off' and the encoder signal is returned to zero. The total count from the encoder while the plate passes through is a measure of the plate length, and therefore the information received from all of the ultrasonic gauges is associated with a position along the length of the plate.

In order for the correct plate position (height above the roller table) at up to eleven points across the plate width to be recorded, a calibration procedure was performed. The signal from each transducer in turn was calibrated, as well as that from the encoder. Additionally, the switched output from the triggering transducer was set up to recognise whether or not there was a plate under the gauge.

A Data logger was used to process and record the signals from both the transducers and the encoder and the signals to this logger were calibrated. The carrier beam is shown in its location on the Light Shear Line in **Fig. 216**. Note that there are two support arms welded to the bridge, one at each end. The beam was bolted to these two supports as shown in **Fig. 217**.



Fig. 216: Ultrasonic transducer carrying beam located on Scunthorpe Light Shear Line



Fig. 217: Detail of beam support

Once installed, the next stage was to calibrate the component parts of the ultrasonic flatness (USF) gauge - the ultrasonic transducers themselves, the encoder, and the signals logged to the PC via the data logger. This calibration was done manually, using MDF boards of various thickness placed on the roller table for the ultrasonic transducers, and by rotating the encoder by hand. A number of plates were then monitored to check that the system was operating correctly and producing sensible measurements.

The data logger output indicated that the system was indeed operating correctly. However, this output simply provided a measurement of plate distance from each transducer, and did not give a measurement

that could be easily interpreted as plate flatness. It was possible to create a flatness map from the logged file by importing it into an Excel spreadsheet, but this map would only be available after the plate had been processed, and was fairly labour intensive. For a flatness map to be viewed as the plate is processed, further development of previously written software [1] was necessary. This software basically takes the transducer signals from the data logging system, and produces a flatness map which is generated automatically as the plate passes under the USF gauge.

The next step was to validate the measurements made by the USF gauge with some manual plate measurements. Each plate to be checked was lifted off the cooling bank, and allowed to cool. Its flatness was measured manually while lying on the mill floor using a purpose made 1 m straight edge fitted with a DTI. The readings were taken as shown in **Fig. 218**.

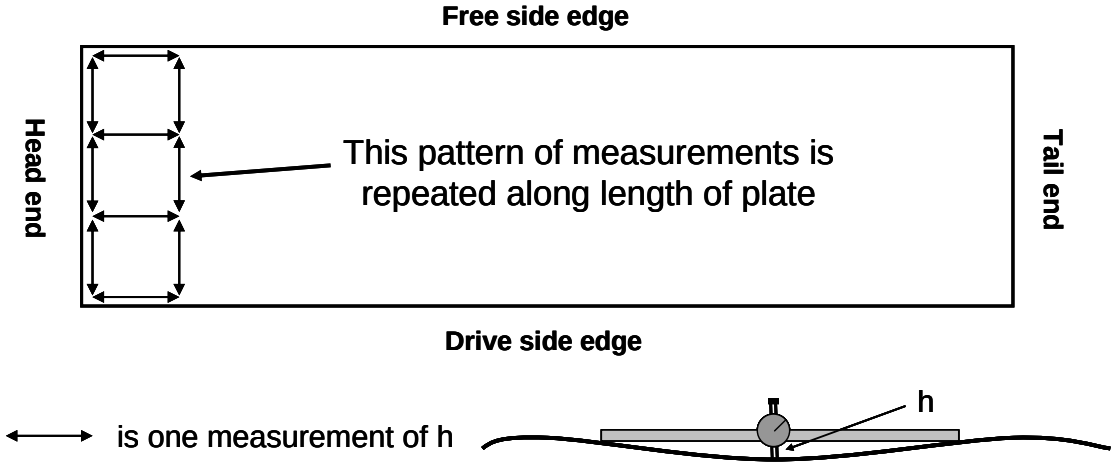


Fig. 218: Manual measurements of plate flatness using a 1 m straight edge

The height measurements taken were converted into a flatness map, an example of which is shown in **Fig. 219**. The x-axis is the plate length in metres, and the y-axis represents the plate width in millimetres. The map itself comprises of wave height measurements in millimetres per metre length (mm/m) and each colour represents a wave height band of 3 mm/m. It is still important to note that the plates were measured when placed upon the mill floor, which is itself, far from level and flat. However, even allowing for this fact, it is reasonable to state that the flatness map for this particular plate (MS790) indicates a good flatness with height variations for the majority of the plate surface being less than 3 mm/m.

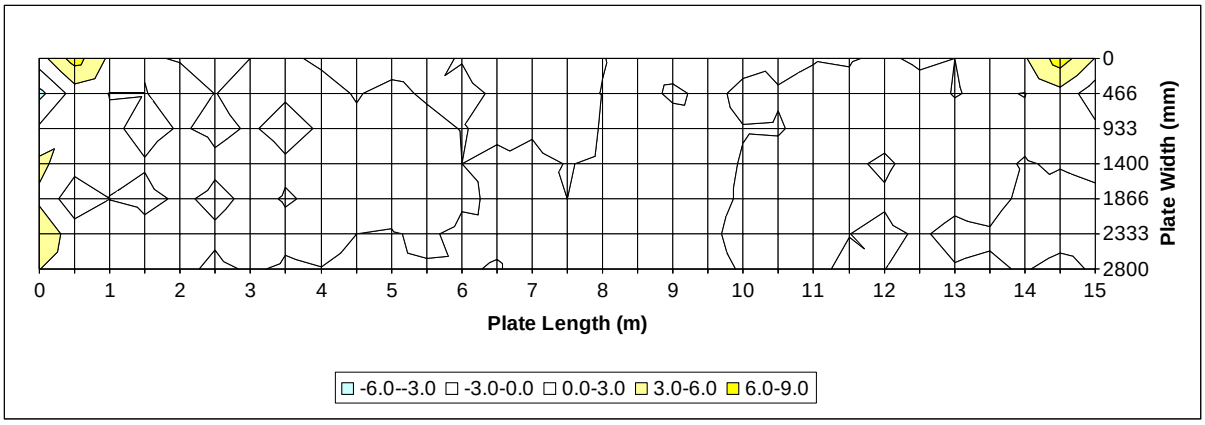


Fig. 219: Manually generated flatness map for plate number MS790

Each plate was then put back on the Light Shear Line roller table and run under the USF gauge three times. A flatness map was generated for each forward pass of the plate under the gauge. Encouragement was taken from the fact that all three measurements on each plate were similar, thus showing good repeatability. However, the correlation between the manual measurements and those generated from the USF gauge measurements was not particularly good. It was possible to determine the difference between

a flat plate and a wavy plate using the gauge, but quantifying the flatness of each plate was not possible. The main problem seemed to be the condition of the roller table on which the plates were supported as they passed under the USF gauge.

Fig. 220 shows the flatness map generated from the USF gauge measurements for plate number MS790. This map is slightly different from that of **Fig. 219** because the height measurements are in mm and not mm/m. When measured manually, this plate was flat, with the vast majority of the plate surface height variation being within 3 mm/m. The flatness map for the same plate generated from data logged by the gauge showed a repeating wave of height between 5 and 10 mm along the entire length of the plate. The pitch of this wave was approximately equal to one table roller circumference, and was thought to be caused by one or more of the rollers being eccentric. This effect was noted on the other plates measured as well.

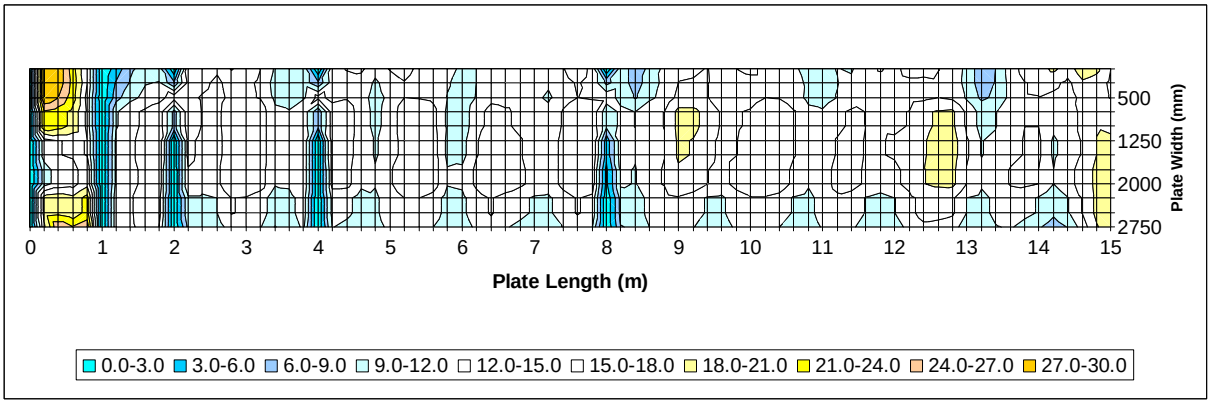


Fig. 220: Flatness map generated from USF gauge data for plate number MS790

Following on from this, a video was taken that clearly illustrated the plate bouncing significantly as it moved under the USF gauge, and the eccentricity of the rollers immediately upstream from and downstream of the USF gauge was measured using a DTI. The results are shown below in **Table 26**.

Table 26: Table roller eccentricity measurements near the USF gauge location

Roll Number	Eccentricity (mm)
-3	9.1
-2	No measurement
-1	5.1
+1	9.3
+2	10.3
+3	5.7

Roll number refers to the position of the roller relative to the USF gauge so for example -1 refers to the roll immediately upstream from the gauge, whereas +2 refers to the second roller downstream of the gauge. The eccentricity of each roller was interpreted as the difference between the maximum and minimum values displayed by the DTI and it was only possible to measure on the free side of the roller table. It is likely that the degree of eccentricity varies across the width of each roller, however, access to the drive side with the roller table not immobilised was difficult.

The obvious conclusion from the measurements is that these levels of roller eccentricity are responsible for the poor correlation between USF gauge generated flatness maps and those produced from manual measurements. The magnitudes of the repeating wave heights mentioned earlier are consistent with those eccentricity values of **Table 26**.

During these measurements, it was also noted that the roller closest to the gauge (+1 in Table 2) was not being driven but was only turned by the plate passing down the table. This fact, combined with the belief that rollers -1, -2, and -3 are driven as part of a bank of rollers that is separate from rollers +1, +2, and +3, means that the combined effect of the eccentric rollers on the vertical position of a plate under the gauge,

is not consistent. This fact meant that subsequent attempts to correct for the table roller eccentricity, by manually adjusting the flatness data, were not successful.

It was always anticipated that the flatness of the plate front and back ends would be difficult to measure because of bounce on the roller table. However, the magnitude and range of roller eccentricities measured were not anticipated and it is unlikely that any flatness measurement device would work completely satisfactorily on this roller table in its present condition.

A somewhat different issue was the damage sustained by the prototype gauge during two separate incidents, in spite of the care taken to site the USF gauge where it was considered highly unlikely to be struck by a plate. Repairs to the gauge were necessary after the first incident, and before it could be used again it had to be recalibrated by following the set procedure [8]. After the second incident, the USF gauge was made safe and taken out of operation.

It had been hoped that the correlation between the two sets of measurements (manual and automatic) would provide confidence in the USF gauge and would enable many plate flatness measurements to be taken. However, the damage sustained to the USF gauge, together with the difficulties in using it for anything other than a broad indicator of flatness, meant that the decision was reluctantly taken to not pursue automatic flatness measurement any further at that stage. Instead, flatness measurements would be made manually and a brief meeting was held at Scunthorpe Plate Mill to discuss how these measurements were to be coordinated.

European Commission

EUR 25852 — Optimisation of final plate flatness by set-up coordination for subsequent manufacturing process (FinalPlateFlatness)

Luxembourg: Publications Office of the European Union

2013 — 179 pp. — 21 × 29.7 cm

ISBN 978-92-79-28902-6
doi:10.2777/63845

HOW TO OBTAIN EU PUBLICATIONS

Free publications:

- via EU Bookshop (http://bookshop.europa.eu);
- at the European Union's representations or delegations. You can obtain their contact details on the Internet (http://ec.europa.eu) or by sending a fax to +352 2929-42758.

Priced publications:

- via EU Bookshop (http://bookshop.europa.eu).

Priced subscriptions (e.g. annual series of the *Official Journal of the European Union* and reports of cases before the Court of Justice of the European Union):

- via one of the sales agents of the Publications Office of the European Union (http://publications.europa.eu/others/agents/index_en.htm).

KI-NA-25852-EN-N

Nowadays the flatness performance of plate manufacturing lines is still tackled in terms of enhanced local flatness of the plates in the line. The aims of this project had been to optimise local flatness approaches and to progress from this basis by taking the flatness requirements of the subsequent production quantitatively into account in form of a co-ordinated flatness set-up system.

This system should integrate all sub models including models of transfer conditions from process stage to process stage and perform a line through process flatness prediction. Based on this a line set-up optimiser connecting local stage rules by a line optimisation strategy should generate the best fitting actions relevant to the evolution of flatness.

The plate processing comprises rolling, cooling, hot and cold levelling quenching and stacking, whereas the process stages in each individual process route may differ, being product related. The development, enhancement and extension of process models to predict the flatness produced at each processing stage in dependence of plate data, entry flatness, main process characteristics and set-up values have been investigated comprehensively.

Analyses of the gained plate flatness in the various process routes showed that the reduction / evolution of flatness defects is nearly independent from the considered process route. Furthermore it has to be confirmed that flatness defects are not passed through the processing chain. This is the main reason which makes it impossible to create global flatness predictions and coordinated optimisations. As a fundamental prerequisite for global flatness control is that various inputs (e.g. changes of rolling process) would have a strongly correlated impact on final flatness. However, this correlations could not been identified on the basis of the comprehensive process data analysis.

Therefore the development and implementation of the “Global Through-process Flatness Predictor and Coordinated Optimiser” is obsolete by physical reasons.

Studies and reports

Publications Office

ISBN 978-92-79-28902-6

doi:10.2777/63845